UNDERSTANDING THE INTERFACE INTERACTIONS BETWEEN BIOLOGICAL MOLECULES AND PRECIOUS METAL NANOPARTICLES

BY

MAKGOBA MALESELA WALTER

A THESIS SUBMITTED IN ACCORDANCE WITH THE FULFILLMENT OF THE REQUIREMENTS FOR THE DEGREE OF

DOCTOR OF PHILOSOPHY
IN

PHYSICS

FACULTY OF SCIENCE AND AGRICULTURE

UNIVERSITY OF LIMPOPO

TURFLOOP CAMPUS

2024

SUPERVISOR: Prof T.E MOSUANG

CO-SUPERVISORS: Prof L.M SIKHWIVHILU (MINTEK)

: Dr N MHLANGA (MINTEK)

DECLARATION

I declare that this thesis: "**Understanding the interface interactions between biological molecules and precious metal nanoparticles**", hereby submitted to the University of Limpopo for the degree Doctor of Philosophy has not been previously submitted before by myself or any individual for a degree at this university or any other institutions. This is purely my hard earn work and dedication, and all the corresponding and utilised sources have been fully recognised.

MAKGOBA MALESELA WALTER

Signature 

Date 14 February 2025

ACKNOWLEDGMENTS

My appreciation goes to my supervisor, Prof TE Mosuang, co-supervisors Prof LM Sikhwivhilu and Dr N Mhlanga, their fellow collaborators Dr MA Mahladisa, Dr MG Matshaba, Dr M Gandamipfa, for their unconditional support and guidance throughout my research journey. Their guidance resulted in ensuring that I complete my research without any major complications or extreme delays. I would also like to thank my parents (Mr Lesetja Makgoba and Mrs Diphala Makgoba), my brothers (Matukela and Matsebe Makgoba) and my sisters (Grace and Meriam Makgoba) for their support during this research journey. Special thanks goes to the University of Limpopo and MINTEK for financial support and access to experimental component equipment. Much recognition and appreciation also goes to the Centre for High Performance Computing (CHPC) for computational resources. Lastly, I would like to thank myself for never giving up even under extreme pressure and overwhelming situations. Overall, I would like to thank God for seeing me through this journey without any health and mental complications.

Abstract

Interface interactions of Au- and Ag-nanoparticles with fibrin protein molecules have been investigated using both computational and experimental approaches. Computational approach used Monte Carlo, density functional theory, and classical molecular dynamics simulations. Sampling of Au(19)/Ag(19), Au(38)/Ag(38), Au(55)/Ag(55), and Au(79)/Ag(79) nanospheres against different possible combinations of 1, 2, 3, and 4-fibrin protein chains were explored for possible Au/Ag-nanosphere+fibrin corona formations. Negative adsorption energies were recorded for some possible Au(19)/Ag(19)+1, 2, 3, and 4-fibrin; Au(38)/Ag(38)+1, 2, 3, and 4-fibrin; Au(55)/Ag(55)+1, 2, 3, and 4-firbin; and Au(79)/Ag(79)+1, 2, 3, and 4-fibrin corona complexes. Au(55)+1, 2, 3, and 4-fibrin corona complexes recorded the most energetically stable adsorption energies of -2.99, -2.73 and -3.00 eV. Similarly, Ag(55)+1, 2, 3, and 4-fibrin corona complexes also recorded the most energetically stable adsorption energies of -2.99, -2.72 and -3.27 eV. Radial distribution functions approximations showed Au-H having the shortest bond lengths of 2.37, 2.47, 2.57, and 2.37 Å respectively relative to Au(19), Au(38), Au(55), and Au(79) nanospheres. Likewise, Ag-H registered the shortest bond lengths of 2.11, 2.45, 2.57, 2.47 Å respectively relative to Ag(19), Ag(38), Ag(55), and Ag(79) nanospheres. Mean square displacements and diffusion coefficients constant hint on H, C, N, and O functional group atoms having good diffusion probabilities onto Au- and Ag-nanospheres. H, C, and N functional group atoms recorded the highest diffusion coefficient constants onto the Au(55) nanosphere whilst H, C, N, and O functional group atoms further recorded the highest diffusion coefficient constants onto the Ag(79) nanosphere. Mülliken charges analysis lead to either enhanced negative or positive charges onto specified carbon (C1, C2, and C3) atoms after Au-nanosphere+fibrin or Ag-nanosphere+firbin

corona formations. Radius of gyration further suggest a tighter packing on the adsorption of fibrin molecules onto Au(38)/Ag(38), Au(55)/Ag(55), and Au(79)/Ag(79) nanospheres in the following preference: Au(79)/Ag(79) > Au(55)/Ag(55) > Au(38)/Ag(38).

Experimentally, Au- and Ag-nanoparticles were synthesised using sodium citrate induced method, thereafter, conjugated with fibrin proteins for adsorption studies. Average spherical diameter sizes 11, 18, 45 and 50 nm of Au-nanoparticles and 12, 14, and 26 nm of Ag-nanoparticles were considered for the conjugation process. Possible adsorption and formation of Au/Ag-nanoparticle+fibrin protein corona complexes were verified using UV-vis and FTIR spectroscopies, Zeta potential, and TEM imaging. UV-vis blue shift was observed on fibrin conjugated Au-nanoparticles relative to the unconjugated Au-nanoparticles, confirming the formation of Au/Ag-nanoparticle+fibrin protein corona complexes. FTIR spectra provided a trace of possible fibrin functional group atoms bonding with Au- and Ag-nanoparticles surface atoms in the possible formation of Au/Ag-nanoparticle+fibrin protein corona complexes. TEM imaging was also utilised to observe and estimate nanoparticles distribution and sizes chronologically. Unconjugated Au-nanoparticles materialise as agglomerates of nano-clusters whilst fibrin conjugated Au-nanoparticles appear as dispersed individual random nanoparticles. On the other hand, unconjugated Ag-nanoparticles occur as scattered irregular individual nanoparticles which agglomerate into nano-clusters upon conjugation with fibrin protein molecules.

Research publications

- Malesela Makgoba, Thuto Mosuang, Abram Mahladisa, Malili Matshaba, Lucky Sikhwivhilu, and Tebogo Mokhena, *Au- and Ag-nanoparticles interaction with fibrin protein molecules*, MATEC Web of Conferences 388, 07006 (2023); DOI: https://doi.org/10.1051/matecconf/202338807006.
- MW Makgoba, MA Mahladisa, MG Matshaba, M Gandamipfa, N Mhlanga, T Mokhena, LM Sikhwivhilu, TE Mosuang; *"Binding nature of fibrin molecules onto Au_{92} and Ag_{92} nanoparticles*"; Proceedings of the 66th Annual Conference of the South African Institute of Physics (SAIP2023).
- MW Makgoba, TE Mosuang, MA Mahladisa, MG Matshaba, RR Maphanga, N Mhlanga, T Mokhena; *"Structural stability of some gold (Au) and silver (Ag) nanoparticles*."; Proceedings of the 66th Annual Conference of the South African Institute of Physics (SAIP2022).

Conference presentations and attendance

- MW Makgoba, MA Mahladisa, M Matshaba, LM Sikhwivhilu, N Mhlanga, T Mokhena, TE Mosuang, "*Adsorption studies of fibrin protein onto Au- and Ag-nanoparticles*"; 2024 Annual Nanotechnology Conference, European Nanoscience and Nanotechnology, (NANOMAT2024), Vienna, Austria*,* 25 - 28 August 2024.
- Malesela Makgoba, Thuto Mosuang, Abram Mahladisa, Malili Matshaba, Lucky Sikhwivhilu, and Tebogo Mokhena, *"Au- and Ag-nanoparticles interaction with fibrin protein molecules"*; RAPDASA-RobMech-PRASA-AMI Annual Conference – 2023, 30 October - 2 November 2023.
- MW Makgoba, MA Mahladisa, MG Matshaba, M Gandamipfa, N Mhlanga, T Mokhena, LM Sikhwivhilu, TE Mosuang; *"Binding nature of fibrin molecules onto Au_{92} and Ag_{92} nanoparticles*"; 66th Annual Conference of the South African Institute of Physics (SAIP2023), 3-7 July 2023.
- MW Makgoba, TE Mosuang, MA Mahladisa, MG Matshaba, RR Maphanga, N Mhlanga, T Mokhena, "*Modelling of the interaction of Ag-nanoparticles with biological molecules*; 15th CHPC National Conference, CSIR, 30 November – 02 December 2022.

- MW Makgoba, TE Mosuang, MA Mahladisa, MG Matshaba, RR Maphanga, N Mhlanga, T Mokhena, *"Modelling of the interaction of Au-nanoparticles with biological molecules*; 12th Faculty of Science and Agriculture Postgraduate Research Day, University of Limpopo, 21 – 23 September 2022.
- MW Makgoba, TE Mosuang, MA Mahladisa, MG Matshaba, RR Maphanga, N Mhlanga, T Mokhena; *"Structural stability of some gold (Au) and silver (Ag) nanoparticles*."; 66th Annual Conference of the South African Institute of Physics (SAIP2022), 4-8 July 2022.
- MW Makgoba, TE Mosuang, MA Mahladisa, MG Matshaba, RR Maphanga, G Ndlovu, "*Most probable nanospheres in the gold nanoparticles modelling*; 14th CHPC National Conference, CSIR, 01 – 03 December 2021.

CONTENTS

List of Figures

List of Tables

CHAPTER 1

Introduction

1.1 Foreword

Nanoparticles are widely used and applied in nanomedicine as drug carriers as well as medical imaging, due to their small size and vast peculiar properties [1, 2]. There are couple main procedures that are known to be utilised in nanomedicinal drug distribution. The first option being the incorporation of drugs with appropriate nanoparticle to dispatch at the intended area of target, the other option being to put the drug in the inner part of the nanoparticle for a later release at the intended area of interest [3, 4].

Under normal circumstances, when drugs are developed, they are firstly tested on some live animals, before they can be recommended or administered to humans. This approach is deemed important as it gives researchers enough time to uncover possible toxic effects which may be linked with such drugs [5]. Even though animal testing procedure is currently the most acknowledged and considered strategic procedure for checking the effects of new drugs, it is still expensive, time consuming, ethically problematic, malicious, and highly controversial practice [6, 7]. One possible deflection instead of harsh animal-based testing is the establishment of civilised, computer-based models and simulations [8, 9]. In this manner, it is put forward that the successful perusal of such models and simulations could lead to the ultimate repealing of the testing of new drugs on animal species practice. Such humanised and alternative approaches may be cost effective on research time, in the process also hindering the slaughter of animals.

Normally, when nanoparticles infiltrate the physiological fluids, certain proteins get adsorbed on the nanoparticle's surfaces. This reduces the free energy of the nanoparticles [10, 11], and in the process forming 'nanoparticle+protein' corona complexes [12, 13]. Upon entering the biological fluid environment, the nanoparticle surfaces spontaneously induce the adsorption of biomolecules in the neighbourhood, specifically protein molecules resulting in the creation of the nanoparticle+protein coronas. Thus far, the actual challenge is that within the nanoparticle+protein corona, possible alteration of the nanomaterial's structure and the protein molecules and properties [14, 15], make the corona complex arrival at the target site uncertain. Thus, the mechanism of interface interaction between the surface functionality of the nanoparticles in relation to the adsorbed protein molecules remains unclear.

Again, the biological responsiveness of the various types of nanoparticles is highly controlled by the sturdiness of the nanoparticle+protein corona complex [16]. Hence, the binding of the protein molecules onto the nanoparticle might result in some configurational readjustment, which may in turn change the conformal structure and the functioning of the said protein molecules [16]. Research studies by Galloway [17] and Karlsson [18], have indicated that some of the nanoparticles can alter the configuration structure of biological molecules; as a result, leading to the altered purpose or just disordered form of functional expectations. Such a disordered effect on the functionality outcomes can be classified as nano-toxicity [17, 19].

Some determinants responsible for configurational alteration in the protein molecules include surface charge, shape, size and the kind of the nanomaterial [3]. As the purpose (activity) rely on the configuration of a certain given protein species, major alterations in the structure may cause inactivity of some protein species, which in the

meantime could be referred to as the afore-mentioned nano-toxicity [3]. It is quite vital on the utilisation of some nanomaterials, that the existence of nanoparticles shouldn't change the structure of a given protein molecular species, as every molecular function is associated with its corresponding structure. Otherwise, actual origins of nanoparticle's toxicity remain indistinct. Some related studies by Zhang *et al.* [20] suggested an oxidative stress as the ultimate source for metal-rooted nanoparticle toxicity.

Such concerning and informative issues may be addressed appropriately by a combination of experimental and computational investigations. Experimental techniques allow the ability to interpret mechanism of interaction at the macroscopic level while computational approaches assist in understanding the origins or mechanisms behind concerned interactions at atomic and electronic level [21, 22]. As such, Suvarna *et al.* [23] showed the influence of nanoparticle size on the structural geometry as well as the role of albumin protein molecules, where the conformational changes of the structure of protein molecules is highlighted. On the other hand, Tavanti *et al.* [24] shed some light on the interaction of standard blood protein molecules with some gold (Au) nanoparticles, where no dramatic alterations in the structure of the protein molecules were exhibited.

Consequently, there is an astounding lack of knowledge and comprehension of the physico-chemical features of nanoparticles inside the biological environment [25]. As such, clinical transferal and favourable outcomes of nanoparticles would rely on essential interactions with protein molecules, including other biomolecules in human or even other animal cells. A good information on nanoparticle+protein interaction could pave the way to a clarified knowledge on nanoparticle-cell interactions which in

turn may lead to administering safe nanomedicines. In this project, different spherical sizes of Au and Ag-nanoparticles have been considered. Such nanoparticle sizes were subjected to possible interaction with varying concentrations of fibrin protein molecules for possible Au-nanoparticle+fibrin and Ag-nanoparticle+fibrin protein coronas. In any case, fibrin protein molecule which is a derivative of fibrinogen has been identified as an emerging and promising protein species suitable for biomedical applications [27].The interaction of Au- and Ag-nanoparticles with fibrin molecules have been probed through both computational modelling and experimental techniques, where the stability and interface interactions have been analysed, contrasted, and related based on energetics, binding tightness, and diffusivity.

1.2. Purpose of the study

1.2.1. Aim

The aim of the study is to optimise the interface binding and stability of the nanoparticle+protein corona using both computational and experimental techniques.

1.2.2. Objectives

The objectives of the study were:

(i) to construct optimal Au- and Ag-nanoparticles structures by calculating their energetics to yield optimal systems.

(ii) to model nanoparticle+protein corona complex molecule structures and energetics.

(iii) to model interfacial interaction mechanisms between various metal nanoparticles and protein molecules using both molecular dynamics and density functional theory methods.

(iv) to calculate thermodynamic and electronic properties of the nanoparticle+protein corona complexes.

(v) to prepare nanoparticle+protein corona by means of the incubation technique.

(vi) to characterise nanoparticle+protein corona through different experimental techniques.

1.3. Outline

The thesis has been arranged in the following manner: the next chapter concentrates on the literature review of some precious metal nanoparticles and their potential interaction with biological molecules. Chapter 3 discusses the computational and experimental methods used in this study. Concerning computational studies; density functional theory (DFT), Monte Carlo adsorption study, and molecular dynamic (MD) simulations were initiated. Regarding experimental studies, experimental characterisation approaches such as, X-ray Diffraction (XRD), Ultraviolet Visible-spectroscopy (UV), Fourier Transmittance Infrared (FTIR) spectroscopy, zeta potential and Transmittance Electron Microscopy (TEM) have been utilised.

Chapters 4 and 5 deal with computational results. In particular, Chapter 4 discusses interface interaction of Au-nanospheres with fibrin protein molecules while Chapter 5 is focused on the interface interaction of Ag-nanospheres with fibrin protein molecules. Lastly, Chapter 6 discusses experimental based results. A discussion of the synthesised Au- and Ag-nanoparticles before and after conjugation with the fibrin protein is highlighted herein.

Chapter 7 concludes the findings of this research project. A summary of all the findings, the work done, and achievements are highlighted herein.

CHAPTER 2

Precious metal nanoparticles interaction with some biological molecules

2.1. Overview

Apart from application in various human working implements and decorations, modern medicine has identified precious metals as possible route to assist in curing some human diseases and injuries. Such medicinal use may include pacemakers, substitutional bone, cartilage and muscular tissues. At nanoscale, precious metals which includes zinc (Zn), nickel (Ni), copper (Cu), silver (Ag), platinum (Pt) and gold (Au) etc have potential to be utilised in medical imaging, and drug delivery in human body systems [26, 28-34]. Such modern medical applications often referred to as biomedicine are informed by the metal nanoparticle's unique physical-chemical properties, such as chemical surface functionalisation, optical response and electronic characteristics [26, 30]. Moreover, these fascinating properties are mainly attributed to the electron’s density distribution on the metal along the nanoparticle surface. But the shape as well as the size of the metal nanomaterials involved which can be regulated during the synthesis process may also play a crucial role [30, 35, 36].

Various theories and synthesis methods have been developed and implemented with evolving times for the continuous improvement of the metal nanomaterials quality [37, 38]. Up to this moment, metal nanoparticles synthesis methods can be manipulated to conform to different structural morphologies which include but not limited to metal nanospheres [39-41], nanowires [42, 41], nanoshells [43, 41], nanocubes [44, 41], nanoflowers [45, 41], nanotriangles [46, 41], and nanorods [47, 41]. Figure 2.1 further highlights some of the possible visual shapes of identified precious metal nanoparticles which could be acquired by means of assorted synthetic procedures.

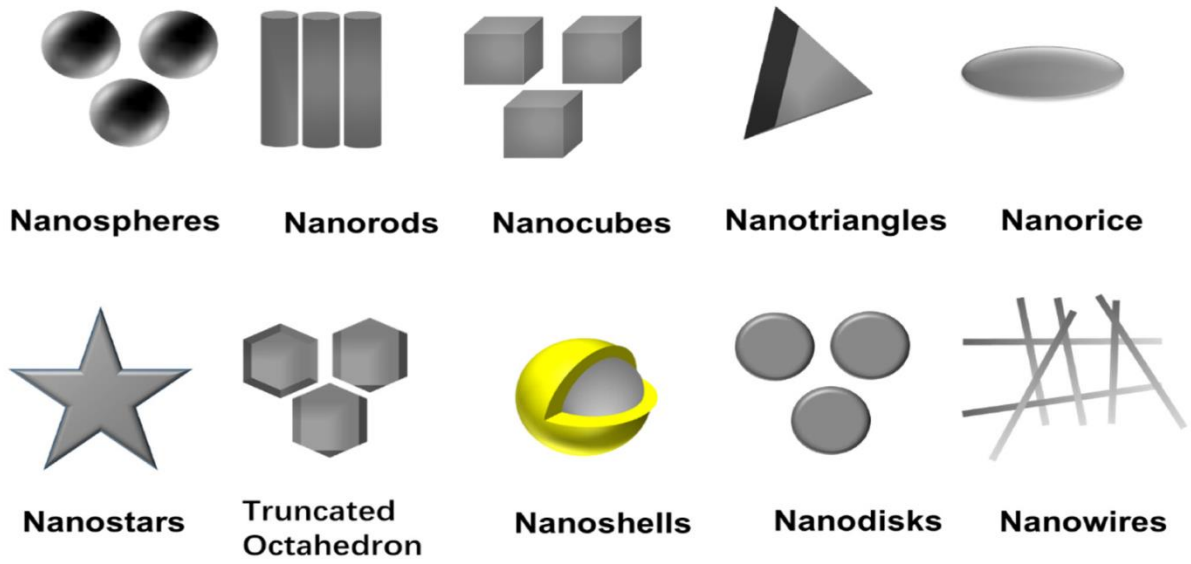

Figure 2.1: Some possible shape morphologies of the precious metallic nanoparticles [41].

But, according to Faraday [37], despite all the improvements and modifications carried out, nearly all gold (Au) nanostructures synthesised via wet-chemical methods tend to adopt thermodynamically stable face-centred cubic (FCC) crystallographic phase. Chronologically, silver (Ag) nanomaterials synthesised under chemical methods also follow the FCC crystal structure [48, 49].

Monopoli *et al.* [11] and Nel *et al.* [10] elaborated that when gold nanoparticles encounter physiological fluids or biological molecules, certain protein molecules are adsorbed on the nanoparticle's surfaces. In this instance, the accumulation of protein molecules on the gold nanomaterials to create relevant coronas is evident [12, 13]. Similarly, Tomak *et al.* [50] has shown that the facets of silver nanomaterials are instantly decorated by a layer of protein molecules, which can be regarded as protein corona, after being introduced into biological environment.

Specifically, 'nanoparticle+protein corona' is an atomistic level coating of some protein molecules from the surrounding protein-fluid medium on the nanoparticle's surface. When this nanoparticle+protein corona gets formed; alteration in size, shape and

interfacial composition of the nanoparticle may occur, giving the nanoparticle a physiological appearance that differ from its original method of synthesis [12]. As highlighted by Pinals *et al.* [51], the development of the nanoparticle+protein corona may result in the limitations on the functionality of the original nanoparticle in the biological/physiological environment concerning bio-distribution and toxicity. Moreover, regarding the created interfacial composition of the nanoparticle+protein coronas, functionality may be related to toxicity or nontoxicity consequences. Thus far, with excellent knowledge of the functional groups available when protein molecules encounter metal nanoparticles, researchers may understand what brings about toxicity and non-toxicity during the drug delivery process. Such understanding may further lead to substantial reduction of the toxic effects at the same time beneficial nanoparticle+protein coronas may be realised [52]. Satisfactorily, the nanoparticle+protein corona can also be manipulated to reduce the toxicity effects in the biological/physiological systems.

This chapter explores how precious metal nanoparticles, especially Au- and Ag-nanomaterials interrelate with some protein species within human cells for possible safe nanomedicine applications. Suggested working mechanism of interaction between Au/Ag-nanomaterials and protein molecules in order to produce corresponding nanoparticle+protein coronas have been presented. Possible energies involved when Au- and Ag-nanomaterials interact with protein molecules functional groups on generation of nanoparticle+protein coronas have also been presented. Electrons sharing model which might occur between Au/Ag-nanoparticles atoms and protein molecules functional groups atoms leading to the nanoparticle+protein coronas have also been presented. Lastly, insights on possible consideration of Au- and Ag-nanoparticles in nanomedicine administration are also suggested.

2.2. The structure of some precious metal nanoparticles and protein molecule(s)

2.2.1. Precious metal nanoparticles

Most precious metal nanoparticles can be obtained through electro-physical and chemical methods [53]. Electro-physical methods are based on subdividing of the bulk materials, by mechanical crushing or pulverisation followed by vapour condensation. In the chemical methods, fabrication of nanoparticles occurs directly from the liquid phase solution, influenced by various factors which include temperature, pressure, time as well as mixing modes [53].

Precious metal nanomaterials such as gold copper (Cu), nickel (Ni), iron (Fe), palladium (Pd), gold (Au), platinum (Pt), and silver (Ag) etc have been synthesised as outlined in the literature using chemical and physical methods to attain the required morphology of interest [37, 41, 61-63]. In addition, biosynthesis of precious metals such as zinc (Zn), magnesium (Mg) and titanium (Ti) nanoparticles through an eco-friendly approach using fungus has also been outlined by Raliya *et al.* [64]. Shape guided fabrication of metal nanomaterials has further been emphasised, envisioned, and elaborated by Xia *et al.* [36].

Sainath *et al*. [65], considered classical molecular dynamics simulations to model successful transformation of bulk body centred cubic (BCC) iron (Fe) to essential Fe nanowires. Such Fe nanowires, Lin *et al*. [66, 67] hinted that they can be experimentally fabricated by reducing iron (II) chloride ($FeCl_2$) in a high magnetic field environment. Besides, atomistic calculations of Xu *et al*. [68] established that bulk BCC tungsten (W) can be transformed into BCC W nanowires. Likewise, Vaddiraju *et al*. [69] further confirmed using experimental vapor phase methods that such W nanowires are possible to synthesise. Both Fe and W are known to have space group

of *Im-3m* as well as their lattice constants of $a_{\mathrm{Fe}} = 2.8665\ \text{Å}$ and $a_{\mathrm{W}} = 3.1652\ \text{Å}$ respectively [86, 88, 89]. Planes such as (110), (200), (211) and (220) are often used for the identification of per synthesised BCC iron and tungsten nanowires as highlighted in Table 2.1 [66, 69]. What is more, Fe nanowires have been used in human cell-type specific multimodal therapy [70]. Basically, some important key factors such as space group, lattice constants and especially indexed planes, tend to play a major role in the identification of a nanomaterial. As such, Table 2.1 shows some other synthesised Fe nanomaterials such as BCC Fe nanotubes and spherical Fe nanoparticles with their corresponding space group of *Im-3m* as well as their calculated lattice constants of $a_{\mathrm{Fe}} = 2.8664\ \text{Å}$ and $a_{\mathrm{Fe}} = 2.8650\ \text{Å}$ respectively, along with their favourable planes.

Researchers such as O'Shea *et al.* [71] have considered density functional theory (DFT) to model bulk crystal structure of hexagonal closed packed (HCP) cobalt (Co). Farkaš *et al.* [72] modelled both HCP bulk cobalt and its transformation to HCP nanoparticles using density functional theory with reference to possible biomedical applications. Synthesis of some HCP nanoparticles such as HCP cobalt nanocubes and HCP zinc nanowires have also been demonstrated in the literature [73, 74, 75]. Gräf *et al.* [73] studies outlined how HCP cobalt nanocubes can be synthesised through thermal decomposition of the precursor material di-cobalt octa-carbonyl. In another paper, Chen *et al*. [74] have shown that HCP zinc nanowires can be synthesised through boiling a combination of boron and zinc oxide (ZnO) powders in the presence of nitrogen atmosphere. Both cobalt and zinc are known to have space group of *P63/mmc* and lattice constants of $a_{\mathrm{Co}} = 2.5071\ \text{Å}$, $c_{\mathrm{Co}} = 4.0686\ \text{Å}$ and $a_{\mathrm{Zn}} = 2.6650\ \text{Å}$ $c_{\mathrm{Zn}} = 4.9470\ \text{Å}$ respectively [86, 89, 90]. Planes such as (100), (002), (101), (102), (110) and (112) are also utilised for the identification of such synthesised HCP

cobalt nanocubes and zinc nanowires as in Table 2.1 [73, 74]. Most zinc nanowires are often covered with an oxide layer [75]. Hong *et al.* [76] has further demonstrated that ZnO nanowires can be employed for cancer targeted optical imaging. The study by Rauwel *et al.* [77] has also demonstrated the feasibility and relevance of cobalt nanoparticles for applications in nanomedicine photo-therapy, hyperthermia and even stem cell production. At nanoscale, some synthesised Co (Co nanotubes) and Zn (Zn nanowires/nanocables) conform to HCP crystal structure of space group *P63/mmc* with lattice constants $a_{\mathrm{Co}} = 2.5140$ and $c_{\mathrm{Co}} = 4.1050$ Å and $a_{\mathrm{Zn}} = 2.6620$ and $c_{\mathrm{Zn}} = 4.9450$ Å respectively as exhibited in Table 2.1 along with their favourable planes.

In other other papers, Hollec *et al*. [78], considered molecular mechanics (MM) and *ab initio* simulations to model successful transformation of bulk face centred cubic (FCC) gold (Au) to essential Au nanocubes and nanospheres. Huang *et al*. [79] validated that Au nanocubes can be experimentally fabricated by electrochemical techniques utilising a surfactant solution and acetone. In addition, Inoue *et al*. [80] further confirmed using hexadecyltrimethylammonium (CTA(+)) chloride (CTAC) and CTA(+) bromide (CTAB) solutions that Au nanospheres are possible to be synthesised. Some indexed planes such as (111), (200), (220) and (111), (200), (220), (311), (222) have also been used for the identification of some synthesised FCC Au nanocubes and nanospheres respectively as in Table 2.1 [79, 80]. Au nanocubes have been identified for use in cell imaging and photothermal therapy [81]. Huang *et al*. [82] have further shown that Au nanospheres provide a modern distinct agents for prospective in vivo photothermal cancer treatment.

Some precious metals undergo structural transformation at different temperatures. Iron for instance, transform to FCC above 912 °C and back to BCC at temperatures above 1400 °C [83]. Similarly, hexagonal closed packed to face centred cubic phase

change in cobalt takes place at temperatures above 450 °C [72, 84]. This implies that most of the precious metals may exist in various phases depending on the method of synthesis and temperature. A crucial issue is at which stable crystal phase are such precious metal nanoparticles utilised for biomedical applications.

In this study, a focus is on the FCC structured Au- and Ag-nanospheres. Using computational modelling Au and Ag unit cells may be periodically repeated in three dimensions to yield any intended supercell formations. Alternatively, bulk Au and Ag can be scaled down to any preferred nanoscale shapes and sizes; nanospheres, nanorods, nanotubes, and nanocubes. As reported in literature [36, 54, 55], physical and chemical properties of gold and silver can be customised using architectural control of size and shape. Faraday [37] synthesised the first colloidal Au-nanoparticles by means of phosphorus based reducing agents. This led to the development of many kinds of synthetic methods such as seed growth [56-58], surfactant-mediated synthesis [59] and aluminium anodic oxide templated growth [60]. Different synthesis procedures lead to tunable and well-defined structural features of Au-nanomaterials. Corresponding morphologies of Ag-nanomaterials with peculiar properties are known to be fabricated through different methods including physical, chemical and biological methods. Biological methods are more favored compared to other methods [41]. A review by Zhang *et al*. [41] demonstrated the utilisation of biological materials, which includes enzymes, bacteria, fungi and plant extracts, to generate Ag-nanoparticles as other available options to usual physical and chemical approaches. Accordingly, at nanoscale, Au and Ag still conform to FCC crystal structure of space group *Fm-3m* with lattice constants $a_{\mathrm{Au}} = 4.0762\ \text{Å}$ and $a_{\mathrm{Ag}} = 4.0860\ \text{Å}$ respectively as laid out in Table 2.1 for Au and Ag spherical nanoparticles. These dimensions lead to unit cell

volumes of 67.90 $Å^3$ and 68.40 $Å^3$ respectively for gold and silver nanomaterials [85, 87].

In summary, Table 2.1 shows some of the possible synthesised BCC, HCP and FCC precious nanomaterials along with their space group, their associated possible lattice constants and their corresponding favourable planes.

Table 2.1: Some precious metal nanoparticles crystal structures, lattice parameters and favourable planes.

		Precious metal	Space group	Lattice parameters (Å)	Favourable planes
Nanoparticle crystal symmetry	FCC	Ag nanorods [91]	*Fm-3m*	$a = b = c =$ 4.0780	(111), (200), (220)
		Ag spherical nanoparticles [92]	*Fm-3m*	$a = b = c =$ 4.086	(111), (200), (220), (311), (222)
		Au spherical nanoparticles [93]	*Fm-3m*	$a = b = c =$ 4.0762	(111), (200), (220), (311), (222)
		Au nanocubes [79]	*Fm-3m*	$a = b = c =$ 4.0680	(111), (200), (220)
		Fe nanotubes [94, 95]	*Im-3m*	$a = b = c =$ 2.8627/ 2.8664	(110), (200), (211)
		Fe nanowires [66]	*Im-3m*	_	(110), (200), (211), (220)

	BCC	W nanowires [69]	*Im-3m*	_	(110), (200), (211), (220)
		Fe spherical nanoparticles [96]	*Im-3m*	$a = b = c =$ 2.8650	(110), (200), (211)
	HCP	Co nanocubes [73]	*P63/mmc*	_	(100), (002), (101), (102), (110), (112)
		Co nanotubes [95, 97]	*P63/mmc*	$a = b =$ 2.5140 $c =$ 4.1050	(100), (101), (110)
		Zn Nanocables/nanowires [98]	*P63/mmc*	$a = b =$2.6620 $c =$ 4.9450	(100), (101), (110)

2.2.2 Some protein species molecules

Animal based biological molecules or specifically protein species which have been found in literature to interact or even adsorb onto surfaces of metal nanoparticles includes but not limited to fibrinogen [99], proline [100, 101] and cysteine [102].

Proline ($C_5H_9NO_2$) and cysteine ($C_3H_7NO_2S$) protein species contain functional group atoms which are related closely with those found in the fibrinogen and fibrin protein molecules [103, 104]. Their functional groups involve hydrogen, nitrogen, oxygen, and sulphur. Typical chemical formula structures are presented courtesy of https://pubchem.ncb.nlm.nih.gov/compound in Figure 2.3. In the same order, molecular weights are 115.13 g/mol and 121.16 g/mol respectively [103, 104]. Proline species has hydrogen bond donor and acceptor counts of 2 and 3 respectively, whilst

those of the cysteine species being 3 and 4 in turn [103, 104]. Table 2.2 further shows a comparison of some basic measured bond lengths within the structure of proline ($C_5H_9NO_2$) and cysteine ($C_3H_7NO_2S$) for C-H, C-C, C-S, C-N, N-H and C-O bonds obtained in the literature [105, 106], in comparison with those obtained from the fibrin ($C_5H_{11}N_3O_2$) in the current study (to be emphasised again in later chapter 4), hence there is no known literature of the fibrin bond lengths currently reported. The fibrin bond lengths are in accordance with the bond stretching of proline and cysteine.

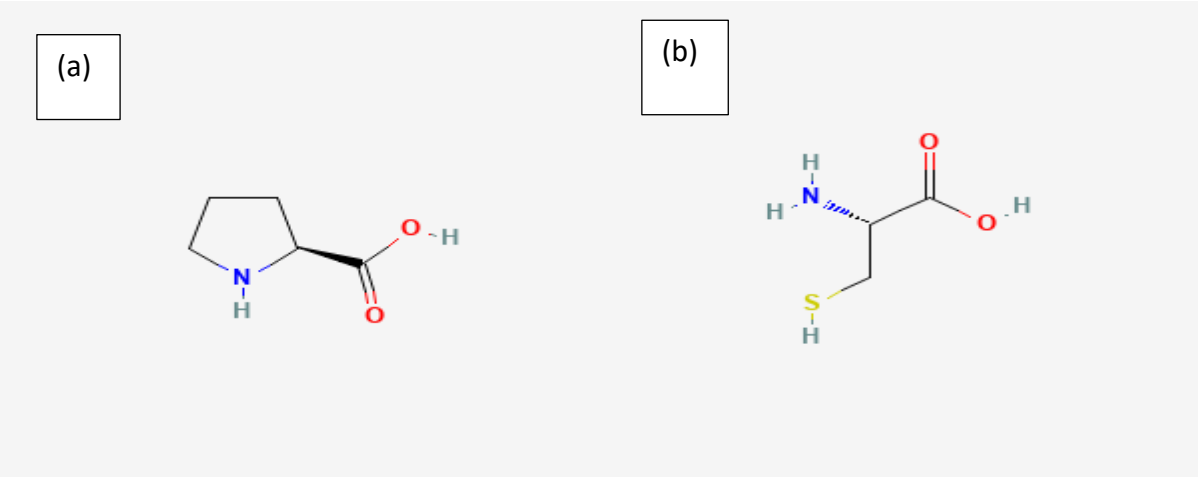

Figure 2.2: (a) Proline [103], Functional atoms: Carbon (C), nitrogen (N), oxygen (O), and hydrogen (H). (b) Cysteine [104], Functional atoms: Carbon (C), nitrogen (N), oxygen (O), hydrogen (H) and sulphur (S). Courtesy of https://pubchem.ncb.nlm.nih.gov/compound.

Table 2.2: A comparison of some basic measured bond lengths in Angstroms (Å) within the structure of proline ($C_5H_9NO_2$) and cysteine for C-H, C-C, C-S, C-N, N-H and C-O bonds attained as per the literature with that of fibrin ($C_5H_{11}N_3O_2$) protein in this study.

	Bond Lengths (Å)		
	Fibrin (This work)	Cysteine [105]	Proline [106]
C-H	1.0903	1.080	1.090, 1.100
C-O	1.2385	1.239, 1.254	1.210, 1.360
C-C	1.5345	1.578, 1.531	1.540, 1.530
C-N	1.4168	1.500, 1.484	1.470, 1.480
N-H	1.0210	1.00, 0.990	1.010, 1.020
S-H	_	1.325, 1.340	_
C-S	_	1.834, 1.819	_

A study based on electronic structure theory of proline protein species binding onto gold nano-clusters was conducted by Rai *et al.* [100]. In the study, effective interaction between proline and gold nano-clusters occurs through Au-N and Au-O bonding as well as the noncovalent Au and O-H or N-H reaction. In this scenario, a natural bond orbital interpretation suggests a charge distribution which occurs in the interaction of proline as a donor and the gold nano-cluster as an acceptor. In anyway, the entire proline + gold nano-cluster interaction is partially covalent. Karmakar *et al*. [101] have also reported how proline functionalised gold nanoparticles (Pro-AuNPs) affect the strength of electric signals in kinetics of egg albumin lysozymes.

Moreover, theoretical investigation on the attachment of thiol-containing cysteine amino acids on the surfaces of silver nano-clusters via cluster model was performed by Nhat *et al*. [107]. Cysteine protein molecules interact with Ag nano-clusters preferably through their thiol (-SH), carboxylic (-COOH), and amine ($-NH_2$) electron rich functional groups. In acidic and gaseous conditions, cysteine species prefers attaching on Ag nano-clusters through the nitrogen (N) atom of the associated amine functional group. In a watery solution, cysteine exist in deprotonated form, as such the sulphur (S) atom of the thiol group end up being the favoured attachment spot. Literature studies by Adnan *et al*. [102] have identified cysteine functionalised Ag-nanoparticles as potential colorimetric probes for enzyme free detection of blood glucose levels.

Fibrin protein molecule species are regarded as insoluble type of protein species which are produced in response to bleeding and are major components of blood clots. Fibrin protein molecules (later referred to as just fibrin(s)) are tough protein-based substance arranged in long fibrous chains. These protein species materialise from fibrinogens, some soluble protein species that exist within blood plasma while being fabricated by the liver, as their main source of production [108-111]. Structural information of protein molecules with fibrin(s) in particular are of interest when exploring the interfacial interactions of Au- and Ag-nanoparticles with protein molecules. The molecular formula of the basic fibrin is $C_5H_{11}N_3O_2$. A simple basic fibrin molecule chain is presented in Figure 2.4.

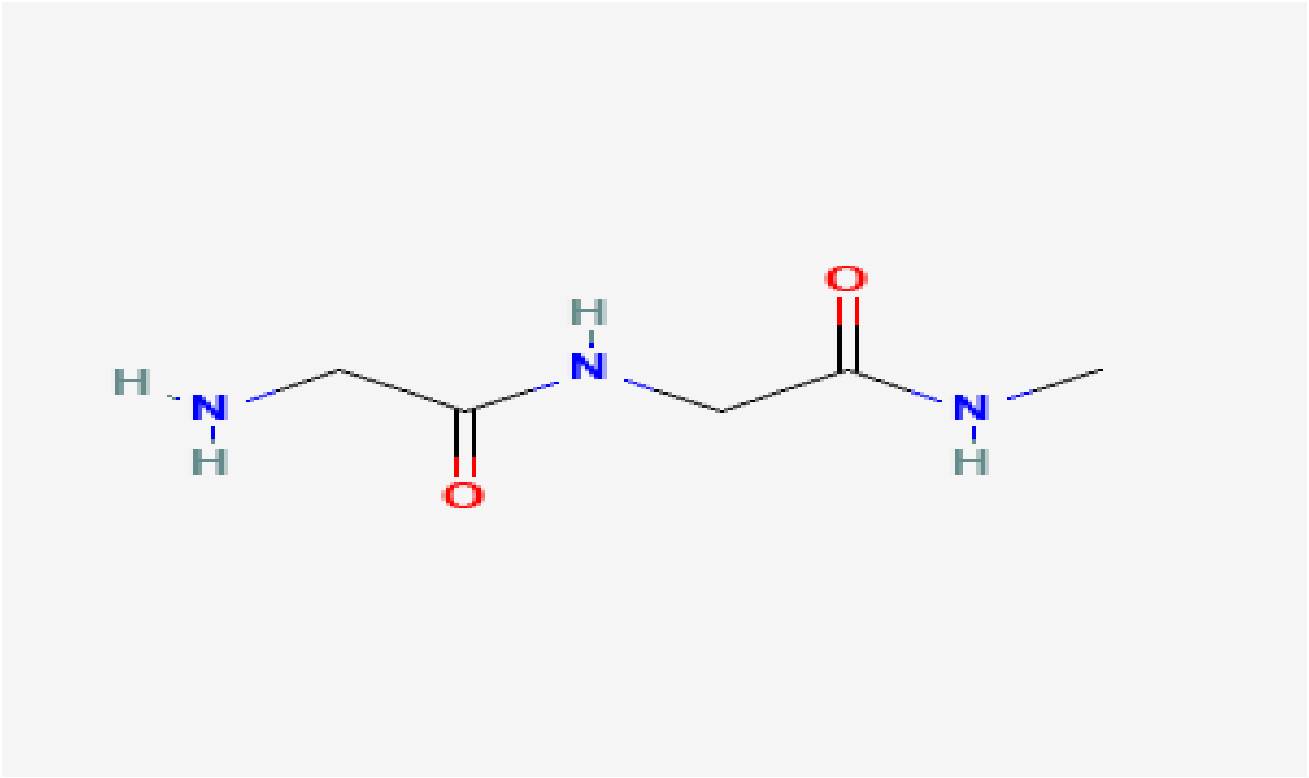

Figure 2.3: Chemical structure of fibrin molecule [112].

A simple fibrin molecule (Figure 2.4) is made up of five carbon (C), three nitrogen (N), two oxygen (O), and eleven hydrogen atoms. Breaking the structure into functional groups formations, it consists of one $–CH_3$, two $–CH_2$, two –CO, two –NH, and one $–NH_2$. As such, the molecular weight of the basic fibrin molecule is 145.16 g/mol with hydrogen bond acceptor count of three (3) and hydrogen bond donor count of three (3) [112]. The functional groups contained in the fibrin molecule are suitable for the interaction with a variety of metal nanoparticles surface atoms. Fibrin molecules are also classified as peptides [112], meaning their chains or concentration can be replicated into more chains or specifically two (2), three (3), and four (4) fibrin molecules chains and more.

For further insight, protein molecules (proteins are a string/chain of amino acids) are regarded as organic materials composed of hydrogen (H), nitrogen (N), carbon (C),

oxygen (O) and in some other cases sulphur (S) atoms [113]. Protein molecular species behaviour which includes interactions and dynamics depend on the specified protein's physico-chemical characteristics, even while executing intense and elegant functions *in vivo* [113]. Hence, knowledge of diverse protein molecular features is generally contemplated to be quite helpful when analysing and trying to understand protein species.

Some of the basic properties of protein molecules includes molecular weight (MW), hydrophobicity, and isoelectric point (*p*I) as stated in the literature [113, 114]. Tomii [113] and independently Wang and Tang [114] emphasise a particular protein species molecular weight as the total of the constituent protein's amino acids molecular weights. A knowledge of a protein species molecular weight is vital when preparing and choosing techniques used in classifying and purifying processes. An isoelectric point refers to the pH value attained when a protein species exhibits a zero net charge. Different protein species display different *p*I values regulated by the kind and quantity of constituent amino acids. As the last point, protein species also demonstrate hydrophobic and polar charged residues. The quantity of hydrophobic residues assists when classifying protein species, as membrane protein species usually have more hydrophobic residues compared to other protein species.

It is also known that fibrin individually or coupled with other associated biomaterials, has been utilised essentially as a biological scaffold for stem or primary cells to regenerate ocular tissue, ligaments, skin, liver, tendons, nervous tissue, bone, and cardiac tissue [108, 115]. As such, interaction of gold (Au)- and silver (Ag)-nanomaterials with fibrin protein molecules are of interest, particularly the interface region may hold the key on how the Au-nanoparticle+fibrin and Ag-nanoparticle+fibrin coronas materialise or do not materialise.

2.3. Impact of precious metal nanoparticles in nanomedicine

Even though metal nanoparticles exhibit auspicious characteristics as potential therapeutic candidates for biomedical administration, so far, the quantity of nanoparticles which have been recognised for clinical implementation is still quite small. This is mostly because there is inadequate comprehension and management of the nanoparticle's interaction with biological environments [116-118]. Nowadays due to different available industries, exploration mining goes with the release of toxic chemicals which contain small amounts of precious elemental Au, Ag, Ni, or even Pt residues into the environment. Chances of living organisms being exposed to or being in contact with gold (Au) and silver (Au) nanoparticles either directly or indirectly is greatly exacerbated [119-121]. Such human practices have resulted in major health and safety concerns [119-121].

On the other hand, the potential biomedical benefits of gold and silver nanoparticles have led to the toxicological study being of significant attraction from the clinical viewpoint [118, 120, 121]. Over the years, many studies have accomplished better comprehension into Au/Ag nanoparticles-protein complexes, and endlessly trying to improve and comprehend the characteristics of bio-nanoconjugates and the outcomes of Au- and Ag-nanoparticles in biological systems [122-125, 121, 126]. Most biomedical employment of Au- and Ag-nanoparticles depend on protein molecular species which covalently adsorb on their surfaces [126, 127]. As already emphasised, the overall character of Au/Ag nanoparticle+protein complexes may rely on the kind of the protein molecular species and most importantly the features of the Au/Ag nanoparticles which includes size, the surface charge and the nanoparticle morphology [126, 128].

Precious gold (Au) and silver (Ag) nanomaterials under certain given conditions may serve as excellent candidates for protein molecules immobilisation [129-133]. Through immobilisation, some cell based toxic reaction which may lead to tumors or cell death may be overcome. So, these nanoparticles can easily react with the amino and thiol groups of some protein species leading to the creation of the nanoparticle+protein corona. Furthermore, these nanomaterials synthesis methods can be manipulated through shapes and sizes in order to conform to a preferred protein molecular species adsorption.

Protein immobilisation is regarded as the attachment of protein species onto the facet of nanoparticles, which may result in the reduction or loss of mobility in the cellular system [134]. The manner in which protein molecules are immobilised will dictate or govern the properties of the nanoparticles. Immobilisation of proteins onto the surface of nanoparticles could occur through physical or covalent immobilisation. In the case of physical immobilisation, protein molecules can get attached on surfaces through polar interactions, hydrophobic interactions, ionic bonds and intermolecular forces. On the other hand, covalent immobilisation involves protein molecules binding covalently by means of valence electrons to the surface of the nanoparticles via reachable functional groups of vulnerable amino acid molecules [134]. As such, a comparatively stable method of protein immobilisation is to conjugate a protein to the nanoparticles surface through covalent bonding [134].

The atomic composition and chemical response at the surface of these Au- and Ag-nanoparticles contributes a lot in the fabrication, fate, as well as the modulation of the nanoparticle+protein coronas. These dynamic processes affect the nanoparticle's structure and activity, profoundly [135]. Adsorption of protein molecules in their native configuration or compelling them to alter their configuration after attachment onto

nanoparticles could result in an effective nanomedicine product or a toxic nanoparticle. Existing data [136 –141] indicates that the acknowledged kinds of nanoparticles for nanomedicine application is quite low, which implies that more investigations aligned with biomedical applications need to be carried out. This is blamed on the lack of comprehension and regulation of the nanoparticle's interactions with physiological environments. This only proves that a better understanding of how metal nanoparticles react when subjected to biological molecules is required to fulfil the ever-growing need of nanoparticles in the biomedical field.

However, only few of the metal nanoparticles under development have been processed into successful nano-medicinal applications [142]. Ethical issues involving in vivo may be associated with experiential delays towards successful applications [142]. When administered through *in vivo*, metal nanoparticles come into contact with complex and peculiar biological fluids (possessing different pH levels), plentiful biomolecules and immune cells, which in turn impacts the bio-distribution, metabolism, cellular internalisation, as well as toxicity of administrated nanoparticles [142].

2.4. Formation of the metal nanoparticle + protein corona complexes

Conventionally, metal nanoparticles are introduced into the human blood system by injection [143-146]. In the blood system, such nanoparticles find themselves in the pool of various protein molecule species. As such a possible competing interaction among protein molecule species and the nanoparticles ensues. Upon this competition, any possible 'nanoparticle+protein corona' complex may materialise. Such probable nanoparticle+protein corona depends on the surface charge, shape, density, size, and surface atomic distribution of the primary nanomaterial. On the protein molecule side, the helix chain length, type and number of the functional groups involved contributes a lot to the nanoparticle+protein corona complex formation. A possibility of the

dissociation of the nanoparticle into constituent atoms or ions due to this interaction must also not be ruled out. Such interactions may lead to the creation of the nanoparticle+protein corona or just dissociation of metal nanoparticles [147, 148]. Another objective in this study is a clarified injection of nanoparticles into the human blood environment (*in vitro*) process. Such enlightenment could limit the direct experimental analysis on live animals (i.e., *in vivo*).

A review by Bal *et al.* [149] has shown that human serum albumin (HSA) is a predominant physiological transporter of the precious metal ions such as Cu^{2+} and Zn^{2+} in the associated bloodstream. It was also stated that its attachment to metals such as Ni^{2+}, Co^{2+}, or Cd^{2+} can take place *in vivo*, but is only of toxicological importance. In this moment, human serum albumin is classified as one of the dominant targets as well as the widely studied binding protein species for metallo-drugs based on complexes with Au, Pt and V. In the review of Bal *et al.* [149] , it has been shown that metals which include Cu, Zn, Co, Cd, Pt, Hg, Fe, Ni, Au, and V can successfully interact with human serum albumin (HAS) which could result easily in the potential metal nanoparticle+protein corona complexes.

The significance of metal ions in the behaviour of bovine serum albumin (BSA) in the biological systems has been illustrated by Jing *et al.* [150], focusing on comprehending the interactions between the metal ions which include Fe^{2+}, Fe^{3+} and Cu^{2+} with bovine serum albumin (BSA) molecules. The results divulged that the incorporation of Fe^{3+}, Fe^{2+}, and Cu^{2+} ions alter the tertiary structure of BSA molecules and exposes the aromatic heterocyclic hydrophobic group of BSA amino acid residues. The incorporation of Fe^{3+} and Cu^{2+} ions result in increased viscosity and decreased intensity of the water peak in the BSA solution. Also, Fe^{3+} and Cu^{2+} ions were found to visibly enhance the α-helix to β-sheet transfiguration of bovine serum albumin

molecules because of the lowered disulphide bond sturdiness. The introduction of Cu^{2+} ions promote the assemblage of bovine serum albumin molecules. The overall research study suggests that different metal ions can successfully interact with protein molecules in a peculiar manner resulting in nanoparticle+protein corona complexes.

One peculiar process is followed in the generation of the nanoparticle+protein corona, where the nanoparticles are usually introduced into a protein source medium such as human blood plasma (HBP). Metal nanoparticles are first synthesised by any preferred method and thereafter introduced into a particular protein source medium. This is followed by incubation for a certain amount of time, and eventually regained through centrifugation, magnetic force or chromatographic techniques [148, 151-153]. Several washing procedures may be considered to remove excessive unbound protein molecules. In turn, the nanoparticles of focus might be covered with tightly bound protein molecules in what is referred to as ‘hard corona’. In addition to this a so called ‘soft corona’ is also present as the secondary layer of protein molecules which are loosely bound to the nanoparticle’s surfaces [148, 152, 153].

Consequently, the character of the soft corona is however receiving scrutiny as it is still considered to be very complex and may be governed by some factors which includes shear force in a breathing life form [151]. Otherwise, reports suggests that hard corona proteins command the biological behaviour of a nanoparticle [148, 151, 153]. It is basically clear that the hard corona signifies a tightly bound layer of protein molecules, driven by high affinity toward the surface of the nanoparticles. While, the soft corona, signifies a less tightly bound layer of proteins, exhibiting low affinity to the nanoparticles surface and simply a high exchange rate with other protein molecules [148, 153, 154].

A standard analysis on time reliant adsorption mechanism and separate protein corona foundation was pursued by Sasidharan *et al*. [155], in which 40 nm sized Au- and Ag-nanoparticles were coated with citrate and lipoic acid. Such Au- and Ag-nanoparticles were exposed to three major protein species, which include human serum albumin (I), fibrinogen and immunoglobulin G (IgG) at their physiological concentrations for 24 hours. In this case, time evaluation data in the range of 0 hours, 6 hours, 12 hours including 24 hours indicate that regardless of the surface chemistry, instant and eminent attachment of I and IgG created coronas on citrate as well as lipoic acid decorated gold (Au)- and silver (Ag)-nanoparticles bringing about an enlargement in size, with no aggregation/agglomeration over the cause of 24 hours at a body temperature of 37°C. Fibrinogen invoked agglomeration instantaneously upon contact with the nanoparticles. Such interesting discoveries points out that regardless of the nanoparticle surface chemistry, corona protein molecules at their physiological concentrations tend to interact differently. In this case, nanoparticle+I and nanoparticle+IgG coronas adsorbed strongly while keeping both individual Au- and Ag-nanoparticles well dispersed, whilst fibrinogen caused what could be classified as rapid, strong and irreversible nanoparticles cluster agglomeration.

Researchers such as Casals *et al*. [156] established that the size enlargement of Au nanoparticles was reversible upon incubation for a brief duration of time, particularly in complete cell culture medium. Whilst prolonged incubation (approximately 48 hours) established hard corona as the nanoparticle size gets bigger from 10 nm to 16 nm. Whereas Maiorano *et al.* [157] as well highlighted that the enlargement of hydrokinetic diameters of 3 Au nanoparticles differed in size after incubation with 10% fetal bovine serum. Correspondingly, a contemporary study presented an in-depth run-through of size enlargement and charge lowering of Au nanoparticles decorated with citrate in

dissimilar sizes, subsequent their subjection to cell culture medium until 48 hours [158].

Likewise, Tomak *et al.* [50] has investigated the development of the silver nanoparticle protein corona upon subjection to cell culture media comprising of 10 % fetal bovine serum (FBS). In this manner, different parameters that could affect nanoparticle-protein corona complex were probed, this includes incubation time, cell culture medium, and incubation temperature. Their findings revealed that the physiological environment directly affects protein corona formation on nanoparticle. To be specific, incubation condition-dependent differences in the amounts of bound proteins were noted. Further on, the mean diameter of Ag-nanoparticles was found to increase from 50 nm to 75 nm after 24 h incubation in FBS supplemented cell culture medium. As a results, it was concluded that the average increase in the particle size affirmed the existence of a protein layer circulating Ag-nanoparticles. In this instance, more proteins were adsorbed on Ag-nanoparticles when the incubation time was prolonged. In anyway, protein corona encrusted Ag-nanoparticles were established to have more negative charge values as distinguished to pure Ag-nanoparticles. Prolonged incubation time emanated in more negative charge values at neutral pH (7.3), highlighting the significance of protein exposure in modulating electrostatic interactions.

The properties of metal nanoparticles due to their synthetic procedure such as size [157-160], surface charge [161, 162], and hydrophobicity [163, 164] influence the overall resultant of the protein corona. As such, nanoparticles with higher hydrophobicity adsorb more proteins with higher affinity [163]. On the contrary, the shape of the nanoparticles also influences protein corona formation, and it is

recommended that highly complex surfaces exhibit the adsorption of large amount of proteins [165].

Different nanoparticles shapes such as nanospheres, nanorods and nanostars tend to adsorb different amounts of proteins. Although it is not clear on how this comes about, a study showed that the amount of the protein adsorbed by the Au nanorods was the highest as compared to Au nanospheres and Au nanostars [166]. It is clear that different morphologies adsorb different number/amount of proteins. In any case, Wang *et al.* [167], emphasised that a positively charged Au nanorods adsorbed more serum species type of protein molecules than negatively charged Au nanospheres.

Moreover, Ashkarran *et al.* [168] conducted a study on hard and soft corona repercussions, with the aid of probing the interrelation of 4 various Ag nanomaterials morphologies (which includes nanotriangle, nanosphere, nano-cube and nanowire) with fetal bovine serum (FBS). Their results revealed that the protein coronas possess dissimilar concentrations and configurations relying on the nanoparticle morphology, signifying the fact that nanoparticle-protein interrelations are morphology reliant. In anyway, it is important to state that not only the curvature effects vary for different nanoparticle shapes, but also the arrangement of the atoms on the associated surfaces, resulting in various surface energies for every unique morphology, that may contribute to the protein adsorption.

Interestingly, the size of Au-and Ag-nanoparticles can also influence the amount of protein molecules adsorbed onto the nanoparticle surface. As such, it has been shown that Au-nanoparticles with large surface areas have greater capability of binding to plasma type protein molecules. Meanwhile, Au-nanoparticles with compromised surface areas tend to adsorb fewer protein molecules on their surfaces [167, 169].

Correspondingly, in some interesting study [148], it was validated that the interaction of Au-nanoparticles (10.02±0.91 nm), Ag-nanoparticles (9.73±1.70 nm) and Pt-nanoparticles (2.40 ± 0.30 nm) with human serum endure the resultant of a protein corona surrounding the nanoparticle, this was observed in all the cases. The resultant of this protein corona depends on the configuration of the nanoparticle as well as its size. As a result, it was noted that smaller nanoparticles (2.40± 0.30 nm Pt-nanoparticles) exhibit lower protein adsorption (198 proteins) as compared to larger nanoparticles which exhibit more protein adsorption (10.02±0.91 nm Au-nanoparticles and 9.73±1.70 nm Ag-nanoparticles) (215 proteins).

Larceda *et al*. [170] studies observed that for some species, adsorbed protein molecules undergo conformational changes which is followed by continued enrichment of the adsorbed protein molecule layers. It was further shown that the binding capacity of Au-nanoparticles to some protein, specifically fibrinogen, becomes greater when the size of Au-nanoparticles increases [171]. Deng *et.al* [171] suggested that larger Au-nanoparticles have higher protein adsorption than smaller Au-nanoparticles, and this is due to the fact that smaller Au-nanoparticles have elevated curvature that lessens the protein binding affinity [169].

In most cases, research studies include nanoparticles that are mainly bigger than the size of the corresponding proteins, in which the nanoparticles can be observed as the carrier of protein cargo. As such, Glancy *et al.* [172] showed that when human serum proteins are incubated with nanoparticles of an average diameter of 10 nm, the nanoparticles start to behave as the cargo instead of the carrier in the nanoparticle-protein corona formation process. In other words, if the nanoparticle is larger than the protein, then the nanoparticle will behave as the protein carrier. Meanwhile, if the

protein is larger than the nanoparticle, then the protein will act as the carrier of the nanoparticle.

Hydrophobicity of Au- and Ag-nanoparticles are important characteristics to control the configuration and amount of protein adsorption [173]. Hydrophobicity usually describes the ability of a surface to repel water molecules. Studies also shows that hydrophobic nanoparticles can also adsorb more proteins from plasma [174, 175]. Therefore, lower surface hydrophobicity can reduce plasma protein adsorption. As a results, protein corona formation may change the hydrophobicity of nanoparticles. In the meantime, hydrophobicity of nanoparticles may determine the nature of protein corona [175, 176]. A review by Fratoddi *et al.* [173] has emphasised that hydrophobic ligands happen to be appropriate for bio-medical functions, usually in amalgamation with hydrophilic ligands, particularly in the occasion of Au-nanoparticles, providing the Au-nanoparticles with that satisfying potential theragnostic features. Also, Ag-nanoparticles stabilised with hydrophobic ligands have been broadly explored for their existence as effectual growth inhibitors against several micro-organisms and after to be utilised in nanomedicine.

The other important aspect is the surface charge to mediate cytotoxicity of Au- and Ag-nanoparticles. In this instance, charge is often tangled when it comes to toxicity as exhibited through research conducted by Goodman *et al.* [177]. Their findings illustrated and concluded that positively charged nanoparticles were found to be extremely toxic than negatively charged nanoparticles. This can be due to the factuality that positively charged nanoparticles are less biocompatible within cells as compared to negatively charged particles which are more biocompatible within cells. However, in other cases, the smaller nanoparticles which are negatively charged seems to have the greatest adsorption pace and the broadest organ dissemination

[178,179]. Onwards, the cytotoxicity of the Au and Ag nanorods were found to depend on the polarity of the surface charge as outlined by Kuo *et al.* [180]. As such, the nanorod surface with the positively charged amino end group was established to be the slightest toxic whilst the nanorod surface with the negatively charged carboxylic acid end group established the greatest cell death. For emphasis, the functionalised nanorods proved to be much toxic as compared to the serum decorated nanorods.

Reports also shows that refinement of nanoparticle surface's charge can also affect protein binding capabilities [181,182]. Hence, it has been highlighted that the surface of a nanoparticles possessing zero charge binds fewer proteins as compared to the surfaces of positively charged nanoparticles (NH_2 functionalised), and negatively charged nanoparticles (COOH functionalised) [176-179, 181-183]. In this way, the surface refinement could provide sufficient total charges on the Au- and Ag-nanoparticles surfaces, which in this case cause electrostatic attraction to the differently charged functionalities in protein molecules.

Some recent report exhibited that the configurational change of fibrinogen can intentionally be influenced by the surface characteristics of Au-nanoparticles [181]. Consequently, negatively charged Au-nanoparticles, as compared to the neutral/positively charged Au-nanoparticles, were demonstrated to attach fibrinogen in a position that caused cytokine discharge in human monocytic THP-1 cells *in vitro* [181]. From physics point of view, it can be concluded that negative charges in Au-nanoparticles were attracted to positive charges in fibrinogen, which can be regarded as electrostatic attraction where like charges repel one another and unlike charges or opposite charges attracts one another.

Interestingly, the interaction mechanism of Au-nanoparticles with proteins may results in the alteration of the native features of both nanoparticles and proteins. Importantly, the interactivity can influence several biological variations, inclusive of the structure of adsorbed proteins as well as aggregation of proteins. As such, in a process whereby fibrinogen interrelate with Au-nanoparticles decorated with poly (acrylic acid), the fibrinogen tends to unravel and reveal its corresponding cryptic peptide [184], which can be classified as electrostatic attraction where fibrinogen charges become attracted to Au-nanoparticles charges or charges in the Au-nanoparticles.

Still on electrostatics interaction, Eigenheer *et al*. [185] highlighted a technique whereby mass spectrometry proteomics was initiated to regulate protein corona inhabitants as well as quantification of protein enhancement on the surfaces of various Ag-nanoparticle [this includes negatively charged nanoparticles covered with citrate (10 and 100 nm) and positively charged nanoparticles covered with polyethyleneimine (100 nm)] in the physiological systems or conditions. Onwards, the protein coronas of negatively charged nanoparticles covered with citrate (10 nm) were differentiated to positively charged nanoparticles covered with polyethyleneimine (10 nm) and negatively charged nanoparticles covered with citrate (100 nm) in order to investigate the significant of size and surface charge. On the bright sight, the findings from the protein corona concentration experimentations plainly demonstrated that the charge on the surface of the Ag-nanoparticles contributed more to corona fabrication as compared to their size. Therefore, there was an elevation in the majority of negatively charged proteins that attached to positively charged Ag-nanoparticles as compared to the 10 and 100 nm negatively charged Ag-nanoparticles. In the meantime, there was a twofold reduction in the anionic proteins that were attached to 10 nm (34 %) and 100 nm negatively charged Ag-nanoparticles (20 %), as compared to positively

charged Ag-nanoparticles (71 %). Such informative findings clearly shows that electrostatics is one of the main determinant factors involved in the regulation of protein molecules affinity for Ag-nanoparticles or any other associated metallic nanoparticles.

2.5. Interface interaction of gold (Au) and silver (Ag) nanoparticles with protein molecules

Studies suggest that the nanoparticle+protein corona can be categorised via two forms: soft and hard nanoparticle+protein corona depending on how the protein molecules respond to the nanoparticle surface area [186]. As discussed earlier in section 2.4, the soft nanoparticle+protein corona is generated when the low affinity protein molecules interact positively with the metal nanoparticle of interest. Such low affinity protein molecules are naturally loosely bound amongst one another but have the possibility of engaging in exchange interactions with other biomolecules within a given plasma solution spontaneously. On the other hand, the hard nanoparticle+protein corona materialises from the high affinity protein molecules which become strongly adsorbed on the metal nanoparticles surface as can be seen in Figure 2.5 [11, 163]. Plainly, the high affinity protein molecules provide a primary layer around the metal nanoparticle, whilst the low affinity protein molecules wrap up a second layer above the high affinity hard corona protein molecules. This implies, the high affinity protein molecules interact more easily with the nanoparticle surface as compared to low affinity protein molecules, hence they are primary and strongly adsorbed onto the surface. It must be noted that the most abundant protein species are readily attached onto the surface of the metal nanoparticles at the early stages of the creation of the nanoparticle+protein corona, but as time goes, they get replaced by high affinity protein molecules. This phenomenon in which a pool of different protein

molecular species compete for interaction with the exposed metal nanoparticles is classified as the *Vroman effect* [187].

Processes which include physical and chemical adsorptions come into play during the creation of this nanoparticle+protein coronas. In the meantime, coordination, electrostatic interactions, hydrogen bonding, hydrophobic interactions and van der Waals forces tend to contribute a lot when it comes to initiating the attachment of protein molecules on to nanoparticle's surfaces [188-191]. For example, when protein molecular species such as BSA encounters Au- and Ag-nanoparticles, the disulphide bonds of BSA binds on the surface of Au- and Ag-nanoparticles through Au-S and Ag-S bonds respectively [189, 192].

Initial findings on the interrelation of metal nanoparticles and plasma protein molecules were started in the years: 1996 to 2000 [193-195]. But the research group of Cedervall [196] was the first to introduce the nanoparticle+protein corona complex concept. Figure 2.5 provides a visual demonstration of the nanoparticle+protein corona complex notion. It can be seen how the hard and soft nanoparticle+protein coronas constitute a primary layer of protein molecules followed by a secondary layer dispersed around the nanoparticle surface.

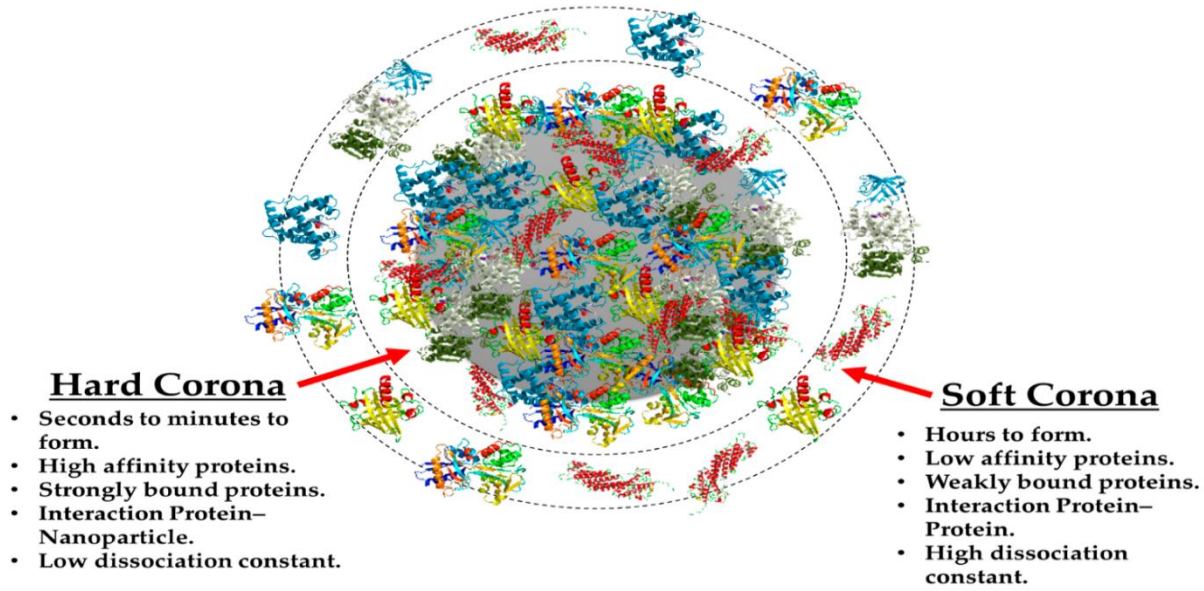

Figure 2.4: Visual demonstration of the nanoparticle+protein corona complex [186].

With reference to the gold nanoparticles, some experiments have shown that the protein species: fibrinogen, immunoglobulin G (Ig-G), human serum albumin (HAS), and apolipoprotein A1 (ApoA1) give rise to hard nanoparticle+protein coronas. The order of affinity for the hard corona on these protein species is ApoA1 > fibrinogen = HAS > Ig-G [197, 198]. This suggest the strength of fibrinogen and human serum binding on the Au-nanoparticles is equal. Apolipoprotein A1 acquire highest binding strength whilst immunoglobulin possess the lowest.

Literature studies of Duran *et al.* [199] have illustrated some possible interactions between Ag-nanoparticles and different protein species to explain how Ag-nanoparticle+protein corona complexes might get formed. Ag-nanoparticles could interact easily with protein molecules of bovine and human serum albumin, tubulin and ubiquitin type, resulting in single molecule Ag-nanoparticle+protein coronas. In other instances, Ag-nanoparticles could also interact with protein molecules of yeast extract as well as fetal bovine serum resulting in complex Ag-nanoparticle+protein coronas. Hence, it is evident that dissimilar protein species may generate a

nanoparticle+protein corona complex which correlates to the surface curvature and size of the Ag-nanoparticles.

To better understand the distribution of the protein molecules onto the surface of nanoparticles, Lu *et al.* [14] investigated apolipoprotein and human serum albumin that were attached on Au nanosheets and graphene surfaces. Their results of the investigation showed that the secondary structures and bondable stability of protein molecules can be moderated by the quantity and positions of hydroxyl (-OH) groups attached on the nanosheets surfaces. Depending on the environment, reports further suggest that the methyl ($-CH_3$) groups may strengthen the binding between the peptide chains and the Au nanoclusters [200].

In other cases, ubiquitin which is consider as a smaller cysteine-free protein species binds to citrate-decorated gold-nanoparticles mostly through small domains of the non-electrostatic interactions, like hydrogen bonds, in which the -NH group attaches to the carboxyl (-COOH) group of the citrate surface on the nanoparticles. In this way, the -NH group is basically bonded the carboxylate group of the citrate through the hydrogen bond. In other words, the H and N directly interact with the Au-nanoparticles as well as the citrate. This interaction is further revealed and evaluated in detail by experimental (i.e. nuclear magnetic resonance and circular dichroism) and computational techniques such as Brownian dynamics, ab initio quantum mechanics and classical molecular dynamics [201]. The entire configuration of ubiquitin is highly close-packed and strongly hydrogen-bonded. On the experimental point of view, research findings have deduced that ubiquitin institute a hard corona onto the Au-nanoparticles surfaces [201].

Buglak *et al.* [202] have also shown that biological molecules such as cysteine, aspartic acid, glutamic acid, arginine and tyrosine can effortlessly get attached to the facets of Ag nanomaterials. In such reactions, tyrosine, aspartic acid, and cysteine possessing deprotonated side chains display the greatest binding energy out of all other associated biomolecules. The study has shown that binding could occur through Ag-O, Ag-N, Ag-H and Ag-S bonds, depending on the type of biological molecule or protein/ammino acids. This simply confirms that different protein species or biological molecules bind differently to the nanoparticle's surfaces, depending on the various atoms or functional groups possessed by a given protein species.

In some peculiar cases, the amide I region (i.e. NH_3) resulting from a C=O stretching mode has been broadly utilised for the recognition of protein secondary structure [203]. Hence, the average shape and maximum of the amide I band can be utilised to attain the disorganisation of the protein after its attachment onto the nanoparticle surfaces. Whereas the binding of protein molecules to plane surfaces frequently instigates crucial modifications in secondary structure, the higher curvature of nanomaterials can assist protein molecules to maintain their primary structure. Even though the protein molecules can maintain majority of their original structure subsequent to adsorption onto the nanomaterial surface, in other situations, the thermodynamic sturdiness of the protein molecule may be lowered, influencing the protein molecule to be quite sensitive to chemical denaturants like urea [204]. It was also shown that in the existence of gold nanoparticles, bovine serum albumin (BSA) exhibits a decrease in α-helical structure as well as major enlargement in sheet and turn structures [205]. Structural alterations come about because of the inherent features of the protein molecules merged with the characteristics of the nanoparticles, which includes surface curvature as well as surface chemistry [204]. Research findings on the interrelation

between colloidal Ag-nanoparticles with bovine serum albumin have been recently reported [206]. The results showed that the bovine serum albumin binding on the surface averted the Ag-nanoparticles from agglomerating in solutions of pH higher than 5. Otherwise, modifications in bovine serum albumin configurational structure after its interrelation with Ag-nanoparticles was evident at a basic pH level. Consequently, extra observations were that the agglomeration of the Ag-nanoparticles hindered their intake in cellular environment which also limits their applicability as bio-probes.

A study by Nhat *et al.* [107] illustrated that in extreme acidic environments and vacuum, cysteine molecules like to bind on silver nano-clusters through the amine functional group (-NH_2). However, the thiolate functional group (-SH) appears to be the best favourable and active binding position, in an aqueous solution. Cysteine compatibility of silver nano-clusters is highly affected in various conditions, as such the following trend is suggested; aqueous solution> vacuum> acidic solution, which is also greatly reliant on the cluster size.

Adsorption of amino acids such as cysteine and glycine onto Au and Ag nano-clusters was also investigated and validated by Pakiari *et al.* [207]. The work demonstrates that the interrelation of amino acids (the building block of proteins) with Au and Ag nanoclusters is ruled by 2 main bonding features: (i) conventional S-Au/Ag, O-Au/Ag, and N-Au/Ag bonds and (ii) nonconventional O-H…..Au/Ag and N-H…..Au/Ag hydrogen bonds. Similar bond types have been seen in complexes containing anionic, cationic, and neutral amino acids. In other studies, Li *et al.* [208] further showed the possibility of the emergence of an Ag-nanoparticles+apolipoprotein bio-corona at low-lying ion concentrations, in which citrate-decorated Ag nanoparticles (negatively charged) were interacting with 15 apolipoproteins.

The importance of examining adsorption energies involved when protein molecules adsorbed onto the nanoparticles have been emphasised in the literature [202, 209]. In this manner, the adsorption/binding energies were further investigated for the protein molecules adsorbed onto Au-nanoparticles [209]. Correspondingly so, the binding energies were calculated for a variety of plasma protein molecules and amino acids, which includes immunoglobulin A, E, and G (IgA, IgE, and IgG), HSA, hemoglobin, transferrin (TF), and myoglobin, which in this case assist with the prediction of their adsorption capabilities to various sized Au-nanoparticles [209]. Even in the case of Ag-nanoparticles, adsorption energies were further investigated for the adsorption of deprotonated glutamic acid, aspartic acid, tyrosine, and cysteine onto Ag-nanoparticles to assess their binding affinity [202].

Until this point, nanoparticle composition [210, 211], hydrophobicity [212], temperature, pH extent, and existence of functional groups [213] have been demonstrated to perturb protein molecules binding capabilities onto the surface of the nanoparticles. Deposition of nanoparticles specifically in an in vitro subjection environment has also been suggested in some way to impact cellular interrelations [214]. In addition, HSA is recognised as the superabundant protein species for nanoparticles with unique morphologies such as star shapes, rod shapes and spherical shapes [156, 165]. Specifically, protein molecules that could be identified within the nanoparticle+protein corona with different abundance includes proteins of the complement system, vitronectin, and albumin.

Researchers Piella *et al.* [215] examined the interrelation of citrate-stabilised Au-nanoparticles with protein molecules in the size trend: 3.5 - 150 nm and discovered that the broadness and compactness of the nanoparticle+protein coronas formed were highly reliant on the size of the nanoparticles. As a result, the nanoparticle size can be

controlled by a variety of methods of transfiguration. This includes generation of an imperfect corona, development of an almost single-density nanoparticle+protein corona coating, and generation of a multicoating (hard and soft) corona. As a final point, the transportation of protein molecules in a nanoparticle+protein corona configuration could be regarded as safe and could also lead into reduction of potential nanoparticle toxicity.

Likewise, Shannahan *et al.* [216] discovered that citrate decorated silver nanoparticles can easily establish nanoparticle+protein coronas when interacting with high-density lipoprotein (HDL), bovine serum albumin (BSA), and human serum albumin (HSA). In this way, the formation of nanoparticle+protein coronas with HDL, BSA, and HSA resulted in the increase of the hydrokinetic sizes of the Ag-nanoparticles. The incorporation of BSA and HSA decreased the disintegration of Ag-nanoparticles. Meanwhile, the incorporation of HDL increased the disintegration of Ag-nanoparticles. The researchers (Shannahan *et al*. [216]) highlighted that this took place due to the decrease in the zeta potential of the high-density lipoprotein+Ag-nanoparticles in contrast to bovine serum albumin and human serum albumin.

2.6. Characterisation techniques used on metal nanoparticle+protein corona complexes

As of to date, different and unique techniques that could be initiated for an in-depth analysis of metal nanoparticle+protein corona have been explored, with some techniques rendered somehow complicated. Hence, it is recommended that choosing a suitable technique is very significant and vital for a specific nanoparticle+protein corona analysis. In this regard, several unique and interesting techniques for analysing nanoparticle+protein corona have been reported and reviewed in several publications [217-220]. Some structural evolution analysis of protein molecules adsorbed onto

metal nanoparticles surfaces can be scrutinised via methodological approaches which includes Fourier transform infrared (FTIR) [221], Raman spectroscopy, nuclear magnetic resonance (NMR), and X-ray crystallography (XRD) [222].

But experimental techniques such as NMR and XRD are generally not preferred even though being utilised in the study of nanoparticles and protein molecules as the preparation of nanoparticle+protein complexes are somehow complicated and such techniques have limitations [189, 217]. Parameter measurements from these methods are also time consuming and expensive to carry out [189, 217]. To overcome such limitations, some improved and recommended approaches involve X-Ray absorption near-edge structure (XANES) [189, 223] and surface-enhanced Raman scattering (SERS) [217, 224]. SERS is mainly utilised progressively for molecular imaging of animal and plant cells. In any case, SERS evaluates the enhanced Raman scattering of molecules attached on metal surfaces. Hence, SERS is responsive enough to trace and observe individual nanoparticles. XANES can provide the chemical composition of the protein molecules. In this way, physical and chemical adsorption of protein molecules onto precious metal nanoparticles surfaces can be investigated satisfactorily [189, 223].

FTIR [221] and Raman spectroscopy [222] have been considered for the monitoring of the secondary structure of protein molecules bonded onto nanoparticles. Atomic structures of nanoparticle+protein corona can be analysed using XRD crystallography technique. Ultraviolet-visible (UV-vis) spectroscopy [225, 226] can provide rapid measurements for the establishment of the quantity of adsorbed protein molecules. NMR provides surface chemistry characterisation. However, as already highlighted, appropriate nanoparticle+protein samples suitable for NMR and XRD characterisation are complex, expensive, and take time to prepare [217].

Other utilised techniques, includes dynamic light scattering (DLS) which has been openly initiated to characterise general nanoparticle+protein interrelations. The technique could divulge possible variations on nanoparticle surface charges and size distribution [227]. The process of adsorption of protein molecules onto nanoparticle surfaces may influence dimensional increase of the nanoparticle's size. As such, researchers have demonstrated DLS as a dominant technique for detecting and observing the adsorption of protein molecules onto metal nanoparticles [228-233].

Information on nanoparticle+protein corona in aqueous solution indistinguishable to biological environment can be attained via NMR techniques [234, 235]. However, NMR has protein molecules size restrictions [236]. Even better, techniques such as X-ray photoelectron spectroscopy (XPS) have been adopted to resolve such limitations. XPS is regarded as a spectroscopic technique with surface susceptibility that could quantifiably evaluate surface composition of any metal nanoparticle and give an approximate on the denseness of nanoparticle+proteins as well as the quantity of protein molecules on the surface of the nanoparticles [237, 238]. In this manner, XPS can give an approximation of thickness of protein molecular layers around a given nanoparticle. Konduru *et al.* [239] achieved the relative quantification of different protein molecules forming Au-nanoparticle+protein corona by using gel-based densitometry. In addition, Cui *et al*. [240] employed DLS for quantification, however, this technique possesses insufficient sensitivity for low-lying quantity of protein molecules being adsorbed onto the Au-nanoparticles.

Some of the standard methodological procedures that could reveal data about variations in hydrodynamic sizes of Au- and Ag-nanoparticles after corona fabrication involves differential centrifugal sedimentation (DCS) [242], ultracentrifugation [241], and flow field flow fractionation (AF4) and others [243, 244]. As a result, AF4

assembles a wide dynamic range of size separation that is specifically crucial for isolating big protein molecules from nanoparticle+protein conjugates by size [245]. Basically, amalgamation of this technique alongside DLS could provide further precise size quantification of possible Au- and Ag-nanoparticle+protein corona complexes.

Methodological approaches which include scanning electron microscopy (SEM) and transmission electron microscopy (TEM) are of major interest in the characterisation of nanoparticle+protein coronas. SEM can be used to examine the shape, length and composition of the protein molecules adsorbed on the surface of the metal nanomaterials [133]. The matrix morphology and possible agglomerations of nanoparticle+protein complexes can be investigated using the TEM [246].

2.6.1. Enhanced stability of protein molecules

The toxicity of nanoparticle+protein corona may be related with the protein helices loss of its functional group form which may also lead to the possible change in the expected activity of the protein molecule species upon binding with the nanoparticle. However, potential constructive processes with rewarding outcomes which involve extended life span may be expected from this upshot. Envisaged stabilising of certain enzymes for extended life span can be directly linked to them binding to the nanoparticles. Studies by Palocci *et al*. [247] have found that such enzymes binding to nanoparticles enhances activity and selection compared to those attached to ordinary carriers.

Another fact to note; nanoparticles adsorption may also increase thermal, pH stability as well as well-defined enantiomers on a particular certain protein molecule species. Asuri *et a*l. [248] have further demonstrated that a spherical C60 fullerene surface enhances the half-life of the enzyme, soybean peroxidase by 2.5-fold higher than when adsorbed on the flat pristine graphite flakes. When compared to the ordinary

free enzyme, the one adsorbed on the spherical carbon become 13-fold higher on the half-life. Such observations of elongating the life span have been recorded with silica and Au-nanoparticles.

2.7. Interaction energy involved on the nanoparticle + protein corona generation

When metal nanoparticles interact with protein molecules to form a nanoparticle+protein corona complex, the following interaction energies are assumed:

(a) Van der Waals site-site Lennard Jones energy (E_{LJ})

(b) Metal-adsorbate Coulomb interaction energy (E_{CI})

(c) Delsovation energy of the metal (E_{DE}^{m})

(d) Desolvation energy of the protein (E_{DE}^{p})

The Coulomb electrostatic term arises from the surface metal electron density and the polarisation of the functional groups in the vicinity of the metal surface. For example: -CH covalently bonded functional group will be polarised such that the H atom adopt the positive charge, and the C base adopt the negative charge. A situation manifests such that the strongest binding energy is associated with the number of functional groups bonded to the metal nanoparticle surface. Studies by Brancolini *et al*. [249] argue that the bonding locations on the nanoparticle surface are not necessarily created as a result of some functional groups having high affinity to some precious metal bonding. Nonetheless, any functional group within the precious metal electron charge density field acquire induced polarisation which facilitate the nanoparticle and protein molecule bonding.

The assumption is that the metal nanoparticles (MNPs) are very large when compared to the interacting protein molecules. Consider a scenario of Au-nanoparticles (AuNPs) with 12 nm diameter interacting with a protein molecule of 3 nm length. To a good

approximation: AuNP >> protein molecule. As such it is quite convincing to further approximate the AuNP surface to a flat surface with reference to the tiny protein molecule.

So, at a face value, such AuNPs and protein molecules interactions could be grouped into two portions: *Physical and Chemical adsorptions*. The physical adsorptions could be described using the van der Waals, Lennard-Jones and metal-adsorbate Coulomb energies. The chemical adsorptions are described based on the metal and protein molecule valence electrons sharing dissolvation energies.

2.7.1. Physical adsorption

Physical adsorption is contemplated as the easiest immobilisation method, in which biomolecules are attached to the metal nanoparticles surfaces through weak van der Waals forces [240, 250, 251]. In simple terms, physical adsorption refers to the consequences of a proportionally infirm solid-gas interaction [251]. Such physical affinity results from non-specific, proportionally weak van der Waal's forces [251]. Physically adsorbed biomolecules can easily diffuse through the surface of the adsorbent without being bound to a particular position on the surface [251], in this case, being only weakly bound. As such, metal nanoparticles surfaces are often enhanced with electrolytes, like sodium citrate, to improve their dispersibility. In the process, the surface adjustment produces sufficient net charges on the metal nanoparticles, which in turn generates electrostatic attraction to the oppositely charged functional groups in protein molecules [250, 252].

It is in this regard that, recognition of the forces presiding over the binding of metal nanoparticle surfaces and protein molecules is vital for better comprehension and

forecasting a given metal nanoparticle to protein/biological molecules adsorption selectivity as well as for estimating protein binding propensities [250, 253].

In other studies, a ProMetCS model [253-255] was initiated to enumerate the Au metal nanoparticle - protein molecule interaction forces. In such model, the energy function is made up of 2 significant terms: the electrostatic interaction energy (because of metal polarisation) and the non-polar interaction energy. The electrostatic interaction energy consists of the Coulombic interaction, the electrostatic protein and metal dissipation terms. Meanwhile, the non-polar interaction energy consists of Lennard-Jones (van der Waals and weak chemical interactions) and non-polar dissipation terms.

The metal nanoparticle-protein interaction energy function, E, which includes solvent effects, is described in the ProMetCS model as the summation of three separate contributions [254, 255], as shown in equation 2.1:

$$E = E_{\mathrm{LJ}} + E_{\mathrm{EP}} + E_{\mathrm{dissip}} \qquad (2.1)$$

Herein, the E_{LJ} energy term describes non-polar, Lennard-Jones (LJ), van der Waals, and weak chemical interactions between a metal nanoparticle surface and a protein molecule. So, E_{LJ} is parametrised to reproduce experimental binding properties of gold nanoparticles and small organic molecules [254]. Also, E_{EP} is the metal nanoparticle-protein molecule electrostatic potential (EP) interaction free energy in an aqueous solvent. In special cases, E_{EP} also includes the energy due to the electrostatic interaction between the charges in the protein binding site and the interfacial water potential on the metal nanoparticle surface.

Lastly, E_{dissip} describes dissipation effects (dissip). Therefore, the free energy change arises from protein – water molecules, solid nanoparticle surface – water molecules, and water – water molecules interactions.

As a result, the dissipation effects can be further split into two separate components as shown in equation 2.2, which includes the dissipation energy of the protein molecules, $E^{\mathrm{p}}_{\mathrm{dissip}}$ and the dissipation energy of the metal nanoparticle surface, $E^{\mathrm{m}}_{\mathrm{dissip}}$

$$E_{\mathrm{dissip}} = E^{\mathrm{p}}_{\mathrm{dissip}} + E^{\mathrm{m}}_{\mathrm{dissip}} \qquad (2.2)$$

The first expression on the right, $E^{\mathrm{p}}_{\mathrm{dissip,}}$ the non-polar (or hydrophobic) protein molecule dissipation energy, is the free energy change of the protein – water molecules system that arises from the replacement of the protein – water molecule interface in the region of the adsorption site by a protein - vacuum interface. The second term, $E^{\mathrm{m}}_{\mathrm{dissip}}$, represents effects arising from the partial replacement of the metal hydration shell by a protein molecule adsorption site [254].

In the case of Ag-nanoparticles – protein molecules interaction, a novel Coarse-Grained Nanoparticle-Protein Hamiltonian was considered by Li *et al.* [208] for the modelling of AgNPs with apolipoprotein molecules. In addition to natural contact interaction, each AgNP and apolipoprotein molecule interaction consisted of two (2) additional sets of interactions: (a) excluded volume (*EV*) and (b) electrostatic interactions (*elec*):

$$H_{long} = H_{NC} + H_{EV} + H_{elec} \qquad (2.3)$$

where H_{NC} represents the native structure. In this representation, each AgNP bead has excluded volume interactions with each apolipoprotein bead:

$$H_{EV} = \sum_{i,j}^{Protein-nanoparticle} \left(\frac{\sigma}{r_{i,j}}\right)^{12} \quad (2.4)$$

where r_{ij} is the distance between two interacting beads and σ is set to 3.8 Å.

Also, the negatively charged Ag-nanoparticle bead, which models a citrate-coated Ag-nanoparticle, has electrostatic interactions (H_{elec}) with the charged apolipoprotein residues. To maximize the bio-corona formation, only electrostatic interactions which involve positively charged residues are considered. The electrostatic interactions between the protein and nanoparticle beads are represented by the Debye-Huckel potential:

$$H_{elec} = \sum_{i,j}^{Protein-nanoparticle} \frac{z_i z_j e^2}{4\pi\epsilon_0 \varepsilon_r r} e^{-\frac{r}{l_D}} \quad (2.5)$$

The Debye length, l_D, is tuned to reflect the changes in ion concentration, z is the charge between interacting beads, and r is the distance between them.

2.7.1.1. Dynamic binding – *Vroman effect*

A dynamic binding occurs when a nanoparticle immersed in a biological or physiological fluid is in contact with a complex mixture of protein molecules, lipids and salts [256]. In this situation a number of protein molecules species will be competing in the early binding interaction process. As the time progresses, certain protein molecular species with less concentration but higher binding probability emerge and come into the picture. As such, the overall process is not an equilibrium one, but a dynamic competitive process [257, 258].

Due to the dynamic nature of the nanoparticle – protein molecule interaction, a protein species that was bound earlier on may still be displaced by the latter competing protein molecule. The assumption that protein molecules with longer helices will have several

functional groups which interact independently with the nanoparticles is also considered. In such a situation, protein species may end up binding irreversibly onto the nanoparticle's surfaces. The opposite is also true, that protein species with shorter chains will have fewer functional groups which suggest a possible adsorption and desorption as single unit [257].

2.7.2. Chemical adsorption

On chemical adsorption, the aim is to discuss borders on how peripheral atoms of the protein molecules functional groups interact with the surface atoms of the metal nanoparticles. Such interactions may be described by strong covalent, ionic, or hydrogen bonding depending on the actual nature of factors contributing to the bond [259].

Interestingly, with regard to better understanding the dispersion of the protein molecules onto the surface of various nanoparticles, Lu *et al.* [14] investigated HSA and apolipoprotein (APO) that were attached to graphene and Au nanosheets. The results show the binding sturdiness and secondary structures of protein molecules could be regulated by the number and positions of hydroxyl (-OH) groups that were attached on the nanosheet surface.

It is also highlighted that in some instances, the methyl ($-CH_3$) groups tend to intensify the binding between peptides and Au clusters [200]. A study also showed that the surface chemistry of laser-ablated metal nanoparticles such as Ag-nanoparticles can be governed by negatively charged functionalities like OH^- and O^- [260]. Furthermore, the surface of the modelled carbon nanotubes (CNTs) was reportedly modified into -COOH, -OH, and $-NH_2$. Hence, the -OH modification was intended to examine the effect of the hydrogen bonding donor or acceptor [261].

For further illustration, a hydrogen bond can be described as bringing an acceptor and a donor group together. Specifically, depending on a given environment the functional groups –COOH or $–NH_2$ may act as acceptors whilst the Au atoms with π electrons on the surface of the nanoparticles act as donors. A possible interaction can be given by:

$$-\mathrm{COOH}^{+} + \mathrm{Au}^{-} \longrightarrow -\mathrm{COOH} \cdots \mathrm{Au}$$

and

$$-\mathrm{NH}_2^{+} + \mathrm{Au}^{-} \longrightarrow -\mathrm{NH}_2 \cdots \mathrm{Au}$$

Such bonding between protein molecules and nanoparticles may provide answers to the origins of the hard nanoparticle+protein coronas [261].

Lastly, the gold-cysteine bond formation has been extensively studied and as a result, the effects of infirm interactions on AuNP – protein molecule binding are thus far vague and inadequately perceived due to experimental restrictions in disclosing the binding dynamics, the adsorption configurations and positioning of a protein/peptide molecule [253, 262].

On the contrary, full theoretical research was conducted on a narrative bioactive molecule 2-(3-bromobenzoyl)-*N*-methylhydrazine-1-carboxamide (BMC), whereby its adsorption onto Ag_6 was deeply investigated [263]. Subsequent adsorption with Ag_6, the bond lengths of BMC molecule exhibit distinctions. Majority of the other bond lengths also illustrate variations following adsorption with Ag_6 and all these reveal interaction with metal and adsorption mechanism classified as chemisorption. The binding points are greater for Ag_6 - BMC and hence the Ag_6 configuration an optimistic possible nanomedicine constituent. Subsequent to the adsorption with Ag_6 cluster, the Mulliken charges of BMC molecule exhibit variations which confirms the charge transfer which leads to chemisorption of BMC with Ag_6. Most of the atoms show

notable charge variations due to interaction with Ag_6 cluster. In simple terms, the Mulliken charges of BMC becomes less negative subsequent to adsorption, in the process validating, charge distribution interaction, enhanced bioactivity of BMC-Ag_3 complex and chemisorption activity.

2.8. Potential challenges and projections on nanoparticle+protein corona

Apparently, metal nanoparticles toxicity or non-toxicity may be aligned with the possible form of the nanoparticle+protein corona. Some studies [199, 215], suggest toxicity of nanoparticle+protein corona originating from the protein molecules loss of helicity, which in turn could lead to change in expected activity of a given protein molecules species upon binding with the nanoparticles. Other studies [205, 206], suggest the formation of nanoparticle+protein coronas leads to extended life span of some protein species. Nanoparticle sizes and shapes may also affect activity and life span of some protein species.

The ultimate objective on successful nanomedicinal drug delivery is the ability to identify particular protein species adsorbed on the precious metal nanoparticles, the life span of the protein species attached on the metal nanoparticles, the possible evolution of the attached protein molecules. Such research information is quite vital with useful implications in the design of safe biomedical applications nanomedicine. A good information on nanoparticle – protein interface interaction could pave the way to a clarified knowledge on nanoparticle – cell as well as cell membrane interactions which in turn may lead to administering safe nanomedicines.

How hard and soft nanoparticle+protein corona complex materialise is another research avenue which still require further interrogation.

CHAPTER 3

Methodology, characterisation and analytical procedures

Both computational and experimental approaches have been utilised to comprehend the stability of the Au- and Ag-nanoparticles, fibrin protein molecules, and the possible nanoparticle+protein corona interactions. Computational approaches assisted with the understanding of atomistic and electronic level interactions between the nanoparticles and the fibrin protein molecules. Experimental based blending and measurements were further used to compare and contrast for possible formation of nanoparticle+protein corona complexes.

3.1. Computational method

3.1.1. Molecular dynamics (MD)

The classical molecular dynamics (MD) approach, employing Leapfrog Verlet (LF) algorithm to integrate the equations of motion was chosen in this study. Specifically, MD is the most favoured computational technique which explore the physical mobility of atoms and molecules [264, 265]. This computational technique can can simulate nanoparticles in sheets or aggregates, in the process revealing various significant details such as optical, electrical, and sensing capabilities that may not be accessible experimentally [264, 265]. Particularly, DL_POLY [266] software was utilised to execute the MD simulations because of its effectiveness in handling the potentials and structural models expended in this work. Gold (Au) and silver (Ag) bulk supercells with 4000 atoms each were explored at 0 K and 100 K in an *NVT* Evans ensemble, in which *N* denotes the number of particles, the volume of the system is represented by *V* at a specific temperature *T*. The equilibrium structures of the supercells with 4000 atoms were attained at known equilibrium lattice parameters for bulk Au and Ag systems

respectively. The Au- and Ag-nanoparticles each of 2067 atoms were then extracted from the equilibrated bulk supercells for ultimate nano-level stability analysis.

Classical molecular dynamics emanate from Newton's equations of motion applied on the particles of a given system according to [267]:

$$F = m_i a. \tag{3.1}$$

In equation 3.1, i denotes a specific atom relative to a system of N atoms, m_i is representation of the mass of the i^{th} atom, meanwhile, a is the rate of change of velocity whilst F is the force being employed on i atoms. Classical molecular dynamics is regarded as a deterministic method, whereby if a preliminary set of positions and velocities are recognised, at that moment the overall time evolution of a certain specific system is completely determined [264, 265].

Making use of the potential energy U, forces acting on the atoms can be expressed as the gradient of the potential energy function [267]:

$$F_i = -\nabla U. \tag{3.2}$$

At equilibrium, equations (3.1) and (3.2) become:

$$-\frac{dU}{dr} = m_i \frac{d^2 r}{dt^2}. \tag{3.3}$$

Because of this, Newton's equation of motion correlates the derivative of the potential energy to the variations in position as a function of time [268, 269].

On this account, the Leapfrog Verlet (LF) algorithm is considered when configuring the atomic trajectories by integrating Newton's equations of motion [270, 271]. Consequently, the Leapfrog Verlet is regarded as being one staged as it requires the values of position (r) and force (f) at a certain time (t), and velocity (v) at half a time-

step behind: $t - \frac{1}{2}\Delta t$. The initial approach involves setting or advancing the velocities to $t + \frac{1}{2}\Delta t$. Integration of the force function is also considered to yield:

$$v(t+\tfrac{1}{2})\Delta t \leftarrow v(t-\tfrac{1}{2})\Delta t + \Delta t \frac{f(t)}{m}. \quad (3.4)$$

Based on equation 3.4, m is the mass of a site for every particle in the matrix and Δt denotes the time step. Correspondingly, the representation of the updated positions as a consequence of the new velocities are as follows:

$$r(t+\Delta t) \leftarrow r(t) + \Delta t v(t+\tfrac{1}{2}\Delta t). \quad (3.5)$$

Molecular dynamics simulations tend to desire properties that are time and velocity dependent simultaneously. In the LF algorithm, the velocity at time t is attained from the mean of the velocities at half a time-step on any side of time t:

$$v(t) \leftarrow \tfrac{1}{2}[v(t-\tfrac{1}{2}\Delta t) + v(t+\tfrac{1}{2}\Delta t)]. \quad (3.6)$$

In this manner, distribution of velocities or initial velocities are often ascertained from their casual distribution with their magnitudes abiding to the entailed temperature, corrected in such a way that there is no overall momentum [268, 269].

The propagation of positions and velocities enclosed in the leapfrog algorithm as a function of time are highlighted in Figure 3.1, further elaborating the notion that the positions and velocities in LF are attained at various time steps:

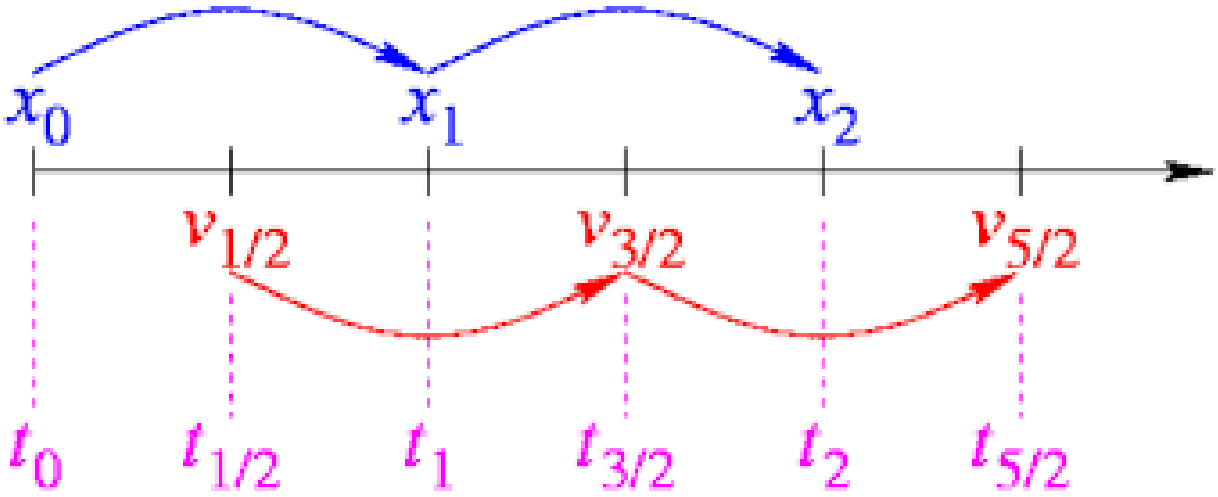

Figure 3.1: Evaluation of time, position, and velocities in Leapfrog Verlet integration method [271].

In Gromacs MD simulations, the LF algorithm is regarded as the conventional MD integrator [272, 273]. Otherwise, this algorithm tends to be stable and works without fault in the matter of short and long-time steps [274]. it is also commended that the time in LF is wonderfully variable and precise [274]. On the interesting part, LF algorithm has the upper hand of being symmetric, in the process, possessing the ability of being time reversible, and avoiding the initialisation problem [275]. In this manner, Leapfrog algorithm can be set in motion at any specific time, at any position, along with any velocities and forces.

Based on the certainty that Leapfrog algorithm is essentially numerical, the validity of this algorithm is usually influenced by variation of the time and spatial steps of this algorithm. Correspondingly, with regard to a situation whereby analytical solutions can be taken into consideration, the reliability of LF can be superb even in the occasion of larger time steps [276]. Lastly, with the LF algorithm, temperature variability is attainable via velocity variation [277].

In summary and for further emphasis, Figure 3.2 illustrates the schematic process followed in MD algorithm [267]. Before initiating a molecular dynamic simulation, a molecular system which consists of all interacting components (such as atoms or molecules) is built. The results of a molecular dynamic simulation provide orientation/path of all n atoms as a function of time, based on which the system's thermodynamic properties, correlation functions, transport properties and so on can be determined.

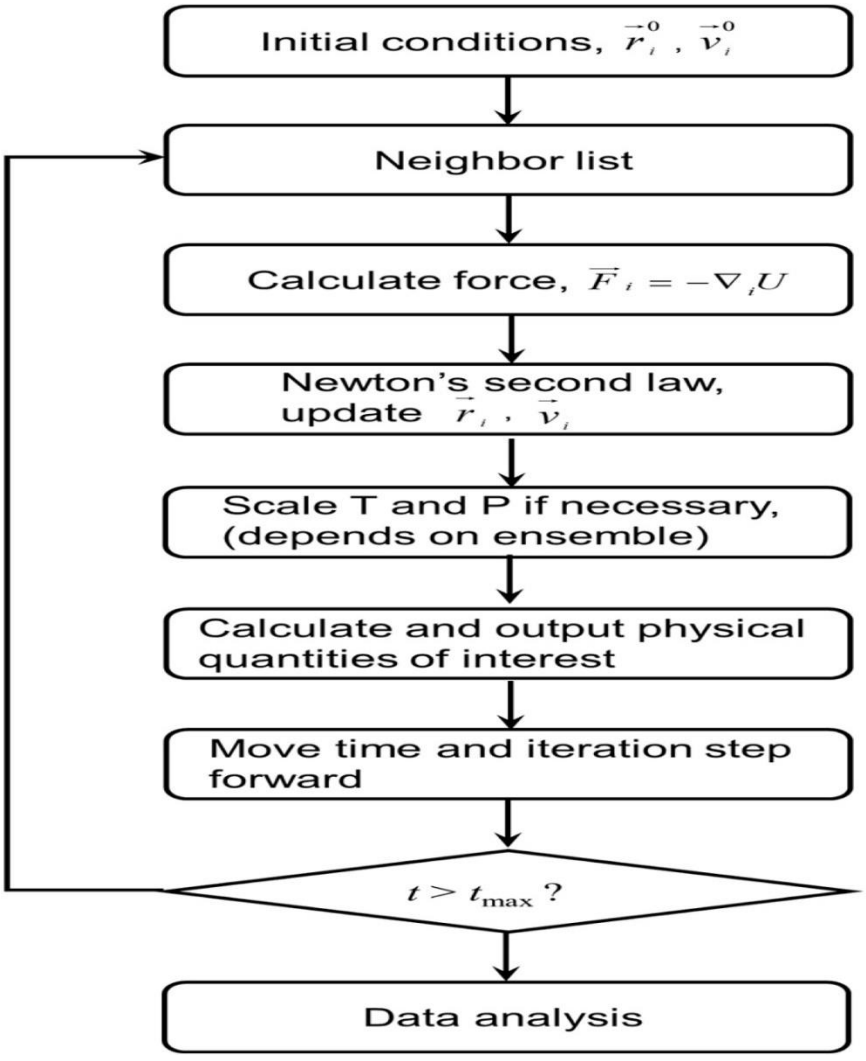

Figure 3.2: Basic schematic representation of MD algorithm steps [267].

3.1.2. Sutton-Chen potential

The many-body Sutton-Chen potentials [278] were employed to model the interactions between Au and Ag bulk and nanoparticle systems. Variation of total energy as a function of temperature were then investigated in both materials' systems. Radial distribution functions (RDFs) were utilised to predict the probable crystal forms of Au and Ag systems at both bulk and nanoscale. While mean square displacements (MSDs) were considered to study the mobility of Au and Ag atoms within their structures.

The Sutton-Chen potential (SC) as proposed by Sutton and Chen [278, 279], can also be regarded as Finnis-Sinclair potentials (FS) with long-range interactions. As a result, this potential combines the perfect description of short-range interactions of the Finnis-Sinclair potential with the van der Waals correction to give more precise narration of the long- range order.

The Sutton-Chen potential energy is described using the expression [278, 279]:

$$E = \varepsilon[\frac{1}{2}\sum_i \sum_{j<i} V(r_{ij)} - c \sum_i \sqrt{\rho_i}] \quad (3.7)$$

where,

$$V(r_{ij)} = (\frac{a}{r_{ij}})^n \quad (3.8)$$

and

$$\rho_i = \sum_{j \neq i} (\frac{a}{r_{ij}})^m. \quad (3.9)$$

Regarding equations 3.7 to 3.9, $V(r)$ describes the repulsive pair interactions, r_{ij} is the distance between atoms i and j, ρ_i is the coordination of i atoms, and ε, C, a, m,

and n all are fitting parameters. These parameters are determined by fitting known experimental values of cohesive energy and crystal lattice parameters.

To be precise, C is a dimensionless parameter, ε is a parameter with the dimensions of energy, a has the dimensions of length, whilst n and m are positive integers such that $n > m$ [278, 279]. The parameters ε, C and a are not independent and can be calculated conveniently using the face-centred cubic lattice symmetry. Exponents n and m are set for simulating various metals by fitting the elastic constants as closely as achievable. For a certain crystal structure, the Sutton-Chen potential is determined by n and m. This is to allow the equilibrium conditions of a given crystal structure to be able to produce a unique C parameter [278, 279].

In this thesis, similar potential parameters as suggested by Sutton and Chen [279] have been considered for both gold and silver metals. Such potential parameters have been shown to produce bulk and surface properties quite accurately as reported in the literature [280-282]. Table 3.1 display such extracted Au and Ag potential parameters used in this write up [279].

Table 3.1: Au and Ag potential parameters as derived by Sutton and Chen [279].

Metal	ε (eV)	n ; m	a (Å)	C
Au	0.012793	10 ; 8	4.08	34.408
Ag	0.002542	12 ; 6	4.09	144.41

The simplicity of the analytic formula of the Sutton-Chen potential makes the potential versatile so that many variants with different sets of parameters have been proposed and have proved to provide correct interpretation of numerous properties of metals as well as their associated alloys [283, 284].

The force on every atom can be noted as the summation of pairwise contributions [279]:

$$F_i = \sum_j F_{ij} \tag{3.10}$$

hence,

$$F_{ij} = \varepsilon[n(\frac{a}{r_{ij}})^n - \frac{Cm}{2}(\rho_i^{-\frac{1}{2}} + \rho_j^{-\frac{1}{2}})(\frac{a}{r_{ij}})^m]\frac{r_{ij}}{r_{ij}^2} \tag{3.11}$$

Similar to equations 3.7, 3.8, and 3.9, herein, r_{ij}, C, ε, m, and n constants hold the same descriptions.

3.1.3. Density functional theory (DFT)

Density functional theory (DFT) was also explored through the Material Studio® 2020 (MS) software package to quantify computational investigations [285]. DFT involves *ab initio* electronic structure calculations on crystals, surfaces, molecules, and atoms, including their interactions [286]. A DMol^3 code [287, 288] enclosed in MS software, was considered for DFT related geometry optimisation calculations. In this approach, fast accurate results whilst maintaining low computational memory and cost is instrumental. DMoL^3 (DFT-based DMol^3 code) is a modelling program or code that utilise density functional theory to model chemical systems and estimate properties of materials both swiftly and precisely [289]. On the bright sight, DMol^3 correlates to a

conventional academic software package which practices DFT method grounded on a numerical basis set.

DMol^3 can be used to study a wide spectrum of systems which include organic and inorganic molecules, also covalent and metallic solids, molecular and ionic crystals, etc by predicting their structural formations, interaction energies, barrier potentials, thermodynamic, dynamic, and optical properties [289]. Most importantly, DMol^3 is appropriate for molecules and 3D periodic solids, but may not function or operate for 1D or 2D periodic structures. In order to simulate such systems, periodic replicas of 3D formations partitioned with vacuum must be created [289]. The code has the capability to perform different tasks which comprise: single-point energy, geometry optimisation, molecular dynamics, transition-state search, transition-state optimisation, reaction path, elastic constants, reaction kinetics, and electron transport calculations [289].

DFT was made possible by Hohenberg and Kohn [290]. As such, Hohenberg and Kohn stated two interesting theorems that paved the way for the implementation of DFT. The two theorems as outlined by Hohenberg and Kohn are [291]:

Theorem 1

The external potential, $V_{ext}(r)$ is a peculiar functional of electron density $n(r)$, possessing a specific association among potential and electron density for a many body system; $V_{ext}(r) \gg n(r)$, whereas this electron density can be initiated to narrate the whole data of the system.

To generate a mathematical analogy, it is assumed that the exterior potentials are $V(r)$ and $V(r')$. The change among these potentials is always the same since the ground

state electron density is comparable in every part of the crystal, specifically, $V(r) - V(r') =$ constant. Based on this theory, electrons move in a field produced by exterior potential V_{ext} and interact with one another in addition to their external potential, and the corresponding Hamiltonian can be expressed as:

$$H = T + V_{ext} + U, \tag{3.12}$$

where T is the kinetic energy of electrons, V_{ext} the external potential and U the Coulomb interaction energy.

Theorem 2

The true ground state density of an electron correlates to the electron density that minimises the overall energy of the functional.

To establish mathematical analogy, let us consider, $n(r)$ the density which corresponds to ground state while $n'(r)$ any other density state of a many-body system. The total energy functional is then given by: $E[n'] > E[n]$.

Onwards, assume that $F[n(r)]$ is a general functional that is valid for fixed electrons at all external potentials. Mathematically this can be expressed as:

$$F[n(r)] = T[(n(r)] + U[(n(r)] \tag{3.13}$$

Even though Hohenberg-Kohn theorems are exact, some shortcomings are noted when applied to real calculations [290]. A many electrons interaction in an external potential (V_{ext}) problem is simplified into a set of self-consistent single particle problem in an external potential (V_{ext}). The total energy functional of the ground state interacting electrons in a fixed potential $v(r)$ is given by:

$$E[n(r)] = V[n] + U[n] + G[n] \tag{3.14}$$

The universal density functional $G[n]$ holds exchange-correlation functional which is:

$$G[n(r)] = T_s[n] + E_{xc}[n] . \quad (3.15)$$

$T_s[n]$ is the kinetic energy of a non-interacting many-body system, $V[n]$ the external potential produced by core electrons having a positive charge, $U[n]$ the Coulomb potential as a result of electron-electron interactions, and finally, $E_{xc}[n]$ is the energy due to exchange-correlation effects [291].

For further clarification, a schematic diagram illustrating the Kohn-Sham mapping of interacting and non-interacting system is shown in Figure 3.3.

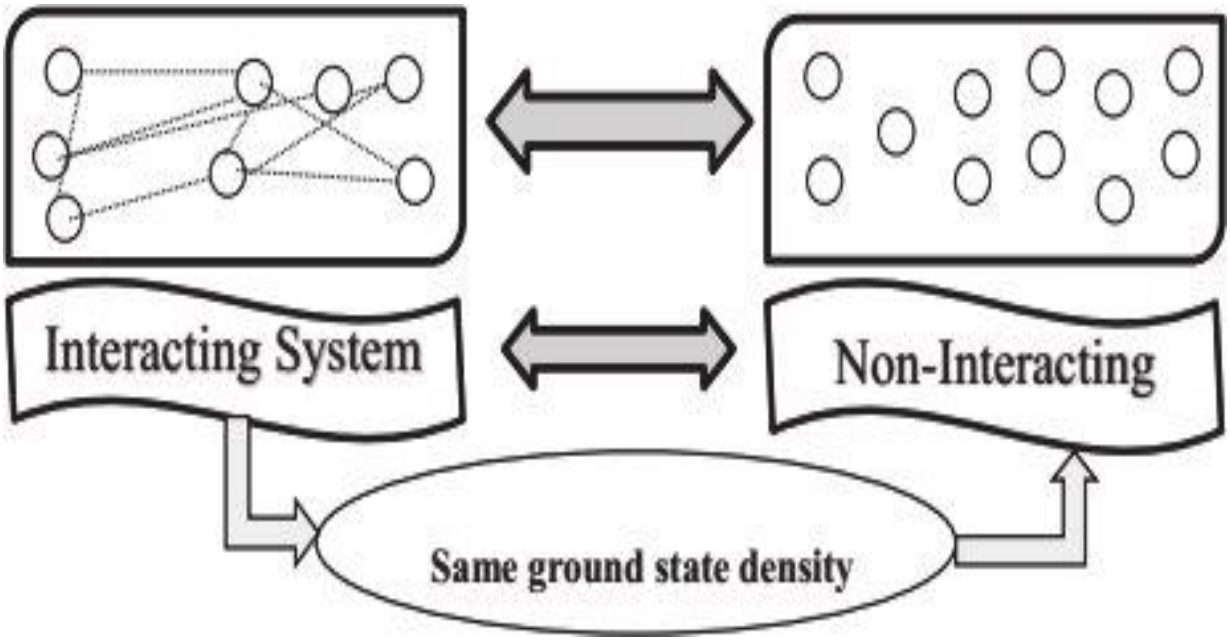

Figure 3.3: Kohn-Sham mapping of interacting and non-interacting system [291].

3.1.4. Local density approximation (LDA) and generalized gradient approximation (GGA).

Common main approximations for the exchange-correlation interactions include local density approximation (LDA) and generalised gradient approximation (GGA). LDA is referred to as one of the first and common approximation for the exchange-correlation interaction [292]. Such approximation assumes that the exchange-correlation energy of the system is equal to the one of a homogeneous electron gas with the density $n(\boldsymbol{r})$. The accurate expression of the exchange-correlation energy functional of such a homogeneous electron gas is:

$$E_{xc}[n] = \int n(\boldsymbol{r})\, \epsilon_{xc}^{hom}[n(\boldsymbol{r})] d\boldsymbol{r}, \tag{3.16}$$

Here, ϵ_{xc}^{hom} is the exchange-correlation energy per electron in a homogeneous electron gas of density n.

The drawbacks of the LDA were amended using the GGA. The GGA takes into account the non-uniform character of the electron density by replacing the ϵ_{xc}^{hom} with a semi-local function which depends on the electron density and the magnitude of the electron density gradient [292]:

$$E_{XC}[n] = \int f\big(n(\boldsymbol{r}), |\nabla n(r)|,\big) dr, \tag{3.17}$$

where the function f is chosen using a set of relevant criteria. Different types of function f have been proposed, but consensus is beginning to develop around several which are qualitatively similar for systems of physical interest.

Accordingly, f is an analytical function which can also be parameterised in different ways, with the most common ones being Perdew-Burke-Ernzerhof (PBE) [293] and the Perdew-Wang (PW) [294] parametrisations.

The GGA was considered during the optimisation of the structures as it has been found to improve the quality of total energies, atomisation energies, energy barriers including structural energy differences [292, 293, 295, 296]. As such, GGA tends to expand and soften the bonds, which is a peculiar effect that leads to the correction and in other cases overcorrection of the LDA prediction [293, 295].

These GGA's have been particularly successful in chemical applications, where they tend to reduce the LDA overestimation of molecular binding energies. In atomic applications, GGA's greatly improve upon the LDA total energy, but improve the first ionisation energy and electron affinity only marginally [296]. In the solid state, the (expanded) GGA lattice constants are sometimes more and sometimes less accurate than those of LDA [295].

On the other hand, with reference to LDA and GGA, which are explicit functionals of the density, meta-GGAs also depend on the Kohn-Sham orbitals [297]. Specifically, meta-GGA functionals depend on the kinetic energy density of the Kohn-Sham orbitals [291]. It is vital to note that one is still in the realm of DFT, since through the Kohn-Sham equations [298], the orbitals are functionals of the Kohn-Sham potential and therefore by virtue of the Hohenberg-Kohn theorem, also functionals of the density. Such orbital functionals or implicit density functionals tend to contribute vastly to a wide field of current dynamic research. The most popular orbital functional is the exact exchange energy functional (E_x^{EXX}) [297]:

$$E_x^{EXX}[n] = -\frac{1}{2} \sum \int d^3r \int d^3r' \times \sum_{ij}^{OCC} \frac{\varphi_{i\sigma}(r)\varphi_{i\sigma}(r\prime)^* \varphi_{j\sigma}(r\prime)\varphi_{j\sigma}(r)^*}{r-r\prime} . \qquad (3.18)$$

The exact exchange Kohn-Sham orbitals are acquired by minimising this same functional (3.18) under the additional constraint that the single particle orbitals arise from a local potential [297].

In addition, another final category of approximations to the exchange-correlation energy are classified or known as hybrid functionals which mix a fraction or portion of exact exchange (E_x^{EXX}) with GGA exchange (E_x^{GGA}) [297],

$$E_x^{HYB}[n] = aE_x^{EXX}[n] + (1-a)E_x^{GGA}[n]. \quad (3.19)$$

Here, a is the mixing parameter. Onwards, this exchange functional is then combined with some GGA for correlation. These hybrid functionals are amazingly popular and successfully applied in quantum chemistry with much less success in solid state physics. As a final point, when considering the addition of an orbital-dependent correlation, this may be reliant on the virtual Kohn-Sham orbitals (double-hybrids) [299].

3.1.5. Monte Carlo adsorption study

Monte Carlo (MC) computations depend on recurrent arbitrary sampling and statistical interpretation to calculate necessary results. These methods are adopted from arbitrary experimental research; these involves the experimental research in which certain outcomes are not clear in particular [300, 301]. As such, each MC simulation begin by establishing a deterministic simulation which strongly imitate the actual situation in any field of research [300, 301]. These simulations are employed to numerically resolve unique multi-dimensional partial differentiation and integration issues. Such methods are also initiated when solving optimisation complications in Operations Research (such optimisation techniques are classified as simulation optimisation) [300, 302-305]. In an attempt to solve integration problems, MC methods

are used to simulate quantum problems that permits a straightforward depiction of many-body effects in the quantum realm, at the consequence of statistical unreliability that can be lowered with prolonged simulation time [300-305].

Such computations usually rely on the total of input variables, which when sort through or integrated through the mathematical equations/expressions in the model, tend to result in a single or multiple outputs. A dramatic scenario of the operation procedure is validated in Figure 3.4.

Figure 3.4: Schematic arithmetic model applied in Monte Carlo simulations [300].

On modelling adsorption of fibrin protein molecules onto Au- and Ag-nanospheres, fibrin molecules were considered as adsorbate and Au- and Ag-nanospheres as substrates. By using the adsorption locator module, single molecule of adsorbate was simultaneously adsorbed onto the Au- and Ag-nanospheres surfaces. In addition, 2, 3 and 4 molecules of fibrin were also applied with respect to imitate the increasing concentration of adsorbates. The adsorption studies were carried out using the Universal Force Field (UFF) along with fine convergence tolerance [306, 307]. Such force fields are considered to be reliably applied in structures containing metal systems [308]. With regard to the energy parameters, group-based and atom-based summation methods were applied to compute the non-bonding electrostatic and van der Waals interactions throughout the Monte Carlo simulations.

Upon adsorption, the structures for Au nanosphere+fibrin molecule and Ag nanosphere+fibrin molecule matrix complexes were then optimised via Dmol^3 code in order to reach their most stable total energy structures. In this content, the single-point

energy of the optimised structures using GGA as parametrised by PBE [293] functional have been calculated, hence, this functionals have been proven to be used in previous DFT studies of gold nanoparticles with biological molecules attached [309]. Double numerical atomic orbital augmented by a polarisation p-function (DNP) basis set [287] were employed to rely on the spin unrestricted calculations. As such, the 0.005 Ha of smearing value was employed in orbital occupation to accelerate the convergence. The maximum iteration for optimisation steps was set at 1000 in order to reach the satisfied convergence level for each complex of Au-nanoparticle and Ag-nanoparticle with fibrin molecules interactions.

3.1.6. Universal force field (UFF)

The UFF is inherently established on the atomic elements, associated hybridisation, together with connectivity. The angular distortion functional configurations in universal force field are selected to be phenomenally practical for enormous amplitude displacements [310]. Universal force field were successfully applied to organic, and inorganic molecules as well as transition metal complexes [310].

Universal force fields describe the bond stretching interactions as either harmonic oscillator [310]:

$$E_R = {}^1\!/_2\, k_{IJ}\, (r - r_{IJ})^2 \tag{3.20}$$

or Morse functions:

$$E_R = D_{IJ}\, [e^{-\alpha(r-r_{IJ})} - 1]^2. \tag{3.21}$$

Here, k_{IJ} denotes the force constant in units of $(\mathrm{kcal/mol})/\mathrm{\AA}^2$, r_{IJ} represent the conventional or native bond length in angstroms (Å), D_{IJ} signifies the bond dissociation energy $(\mathrm{kcal/mol})$.

Morse functions are greatly errorless in their descriptions as they implicitly include harmonic term around equilibrium separation (r_{IJ}) which leads to the finite energy (D_{IJ}) associated with bond breaking [310].

3.1.7. Forcite code

Molecular structures generated using the MC adsorptions were initially optimised using the Forcite code. In this code, COMPASS [311, 312] force fields are considered in order to reach sufficient stability in the preferred conformational forms. COMPASS are well known reliable force fields preferred for most small biological molecules. A self-consistent field iteration for such calculations were set at 10000 cycles. This is to ensure that Au-/Ag-nanoparticles + n-fibrin molecules interactions are able to acquire sufficient, accurate convergence.

Forcite is a code accessible in BIOVIA Materials Studio software [313], a modern and sophisticated standard molecular mechanics (MM) technique, which allows fast computation of energy and dependable geometry optimisation of non-periodic and also periodic molecular systems [314, 315]. A Forcite code can execute a broad spectrum of tasks through classical calculation methods, which includes but not limited to geometry optimisation, dynamical structure evolution etc. The geometry optimisation task of Forcite enables the computation or processing of the structural geometry until it comes to a certain stipulated criteria known as the convergence level [313, 314].

Forcite-Geometry optimisation calculations are based around the force fields type and parameters instituted before running the calculations [314, 315]. In this stance, selecting an acceptable force field is considered as the most significant parts of the calculations. The dynamic structural evolution studies were also employed to investigate molecular interaction between nanoparticles and fibrin molecules.

So far, the Compass Force fields have a wide extent or consideration in covalent molecules which includes many regular organic molecules, small inorganic molecules as well as polymers. The most recent evolution in COMPASS achieved the representation to incorporate inorganic materials such as metals, metal oxides, and metal halides utilising a variety of non-covalent models. The parameterisation of some of these inorganic materials has been achieved [313, 314].

In particular, with regard to organic molecules, the functional configuration of the COMPASS energy proclamation and the valence term parameterisation procedure is [312]:

$$E_{total} = \sum_b [\ k_2((b\ -\ b_0)^2\ +\ k_3((b\ -\ b_0)^3\ +\ k_4((b\ -\ b_0)^4] +$$

$$\sum_\theta [\ k_2(\theta\ -\ \theta_0)^2\ +\ k_3(\theta\ -\ \theta_0)^3\ +\ k_4(\theta\ -\ \theta_0)^4] + \sum_\varphi [k_1(1 - \cos\varphi) +$$

$$k_2(1 - \cos 2\varphi) +\ k_3(1 - \cos 3\varphi)] +\ \sum_\chi k_2(\chi\ -\ \chi_0)^{\ 2} + \sum_{b,b'} k(b\ -$$

$$b_0)(b'\ -\ b_0{}')\ +\ \sum_{b,\theta} k(b\ -\ b_0)(\theta\ -\ \theta_0)\ + \sum_{b,\varphi} (b\ - b_0)\ [k_1\ cos\varphi\ +$$

$$k_2\ cos\ 2\varphi\ +\ k_3\ cos\ 3\varphi]\ +\ \sum_{\theta,\varphi} (\theta\ -\ \theta_0)[k_1\ cos\ \varphi\ +\ k_2\ cos\ 2\varphi\ +$$

$$k_3 \cos 3\varphi] + \sum_{b,\theta} k(b - b_0)(\theta - \theta_0) + \sum_{\theta,\theta',\varphi} k(\theta - \theta_0)(\theta' -$$

$$\theta_0')(\varphi - \varphi_0) + \sum_{ij} \frac{q_i q_j}{r_{ij}} + \sum_{ij} \varepsilon_{ij} [2(\frac{{r_{ij}}^0}{r_{ij}})^9 - 3(\frac{{r_{ij}}^0}{r_{ij}})^6]. \quad (3.22)$$

In equation 3.22, $b, \theta, \varphi,$ and χ represent bond lengths, valence angles, dihedral angles, and Wilson out-of-plane displacements in that order, and the subscript zero is initiated to designate the reference unperturbed values, with the remaining force field parameters designated k_i. The nonbonded interactions are detailed by the last two terms, in which r_{ij} indicates the inter-atomic length, q_i and q_j designates the atomic charges, and ${r_{ij}}^0$ and ε_{ij} are Lennard-Jones parameters.

Simulation procedures are constructed with material software (MS) Amorphous cell. Amorphous cell can be described as a chamber of computational instruments that permit one to establish typical models of complex amorphous systems and to forecast key attributes. As such, the attributes of interest that can be predicted and investigated includes but not limited to chain packing, equation-of-state behaviour, localised chain motions and cohesive energy density [313, 314].

3.2. Experimental method

3.2.1. Reagents used for the synthesis of Au- and Ag-nanoparticles.

Chemical reagents used in this study were purchased from Sigma Aldrich. Such reagents include chloroauric acid ($HAuCl_4$), silver nitrate ($AgNO_3$), and sodium citrate ($C_6H_5Na_3O_7$) as well as protein fibrin powders to implement conjugation process with the synthesised Au- and Ag-nanoparticles.

3.2.2. Synthesis of Au- and Ag-nanoparticles

Gold nanoparticles (AuNPs) were synthesised via seeded growth method [316, 317]. In this method, 150 mL of 2.2 mM sodium citrate was brought to boiling in an Erlenmeyer flask. When the solution was boiling, 1 mL of $HAuCl_4$ 25 mM was introduced in the solution. After a certain period (approximately 1-2 min), the color of the solution turned pink, indicating the formation of AuNPs with average diameter of 11±3.26 nm. Thereafter, the temperature of the solution was decreased to 90 °C. Furthermore, for appropriate growth steps of the nanoparticles, 1 mL of sodium citrate 60 mM and 1 mL of $HAuCl_4$ 25 mM were vigorously added to increase the size of the nanoparticles with each addition leading to an increased size of the nanoparticles. The process of the addition of both sodium citrate and $HAuCl_4$ was repeated after every 30 min, which led to the formation of new nanoparticles with increased average diameter sizes of 18±3.15, 45±12.8 and 50±17.4 nm. The high standard deviation was observed for 45 and 50 nm due to the presence of some few small nanoparticles in the background as the size was increased. This is expected as the capping agent (sodium citrate) attempt to bring smaller nanoparticles together to form larger nanoparticles.

Correspondingly, Ag-nanoparticles (AgNPs) were also synthesised via sodium citrate induced method [318]. In this case, 50 mL of 1 mM $AgNO_3$ was heated to boiling in an Erlenmeyer flask. Subsequently, 5 mL of 1% sodium citrate was then introduced into the solution. In the course of this process, the solution was also periodically heated until a series of color changes were observed; from yellow, brown, until pale brown. The process yielded Ag-nanoparticles with different average diameter sizes of 12±3.49, 14±7.52 and 26±5.83 nm with each phase of color change respectively.

3.2.3. Fibrin protein preparation or dissolution and adsorption

1 gram of fibrin protein was acquired in powdered form from Sigma Aldrich. A concentration of 0193 mg/mL was then prepared by dissolving 0.005 g of this powdered fibrin protein into 25 mL of phosphate buffer saline (PBS) of pH 7.4. The dissolution of fibrin powder into PBS took over 48 hours at 37 °C. Upon preparation of the fibrin concentration solution, the Au- and Ag-nanoparticles were then incubated with fibrin proteins for 12 hours. Prior to incubation processes, the behavior of the nanoparticles in the absence of fibrin was investigated and then adsorption of fibrin onto the nanoparticles was also studied.

3.2.4. Characterisation of Au- and Ag-nanoparticles

For lack of access to advanced XANES, SERS, DCS, AF4, and XPS characterisation equipment, ordinary characterisation machines accessible were resorted to. Characterisation of Au- and Ag-nanoparticles are considered somehow complicated since these nanoparticles were synthesised via citrate induced method. Given that citrate has been used as a capping agent, some citrate related signals maybe noted in the spectroscopic signals analysis. Below, a couple of spectroscopic techniques which assisted on verification and validation of investigated samples are discussed.

3.2.4.1. X-ray diffraction (XRD)

XRD was used to determine the crystal structure of acquired Au- and Ag-nanoparticles. It must be mentioned that nanoparticle+protein corona based XRD characterisation were not made due to alluded limitations highlighted in sub-section 2.6. A unique diffraction pattern gets formed whenever incident X-rays interact with a material of interest [319, 320]. In this way, an ordered atomic arrangement obtained from the scattered X-rays provide the required crystalline structure of a material under

investigation. Specifically, X-ray diffraction pattern of Au- and Ag-nanoparticles were conducted using Empyrean X-Ray diffractometer (Malvern Panalytical).

The crystalline sizes of these Au- and Ag-nanoparticles are calculated using the Debye-Scherrer's equation [321, 322]:

$$D = \frac{K\lambda}{\beta \cos\theta}, \tag{3.23}$$

where D is the crystallite size, λ denotes the X-ray wavelength, β is the full width at half maximum (FWHM) of the diffraction peak, K is the constant (0.9), θ is the diffraction angle at the maximum.

3.2.4.2. Transmission Electron Microscopy (TEM)

A transmission electron microscope (TEM) is a technique with capabilities of atomic-scale chemical and structural characterisation of solid-state material samples [323, 324]. A FEI Tecnai F20 Transmission Electron Microscope (TEM) (Thermo-Fisher Scientific) was used to analyse Au- and Ag-nanoparticles before and after conjugation with the fibrin protein (i.e. conjugated nanoparticle+fibrin corona samples) at a voltage of 200 kV. The Au- and Ag-nanoparticles before and after conjugation with the fibrin protein were further explored potentially at an acceptable scan size. This instrument was used to characterise Au- and Ag-nanoparticles before and after conjugation with the fibrin protein due to its capabilities to be able to view nanomaterials or nanoparticles at an atomistic level. With its advantage of being an atomistic level analyser, the TEM can also be employed for the detection of defects, vacancies and dislocations in some nanomaterials [325, 326]. Interest on the surface morphology and possible atomic distributions of Au- and Ag-nanoparticles before and after mixing with

the fibrin protein was considered. Figure 3.5 below exhibit the conceptual working principle of TEM.

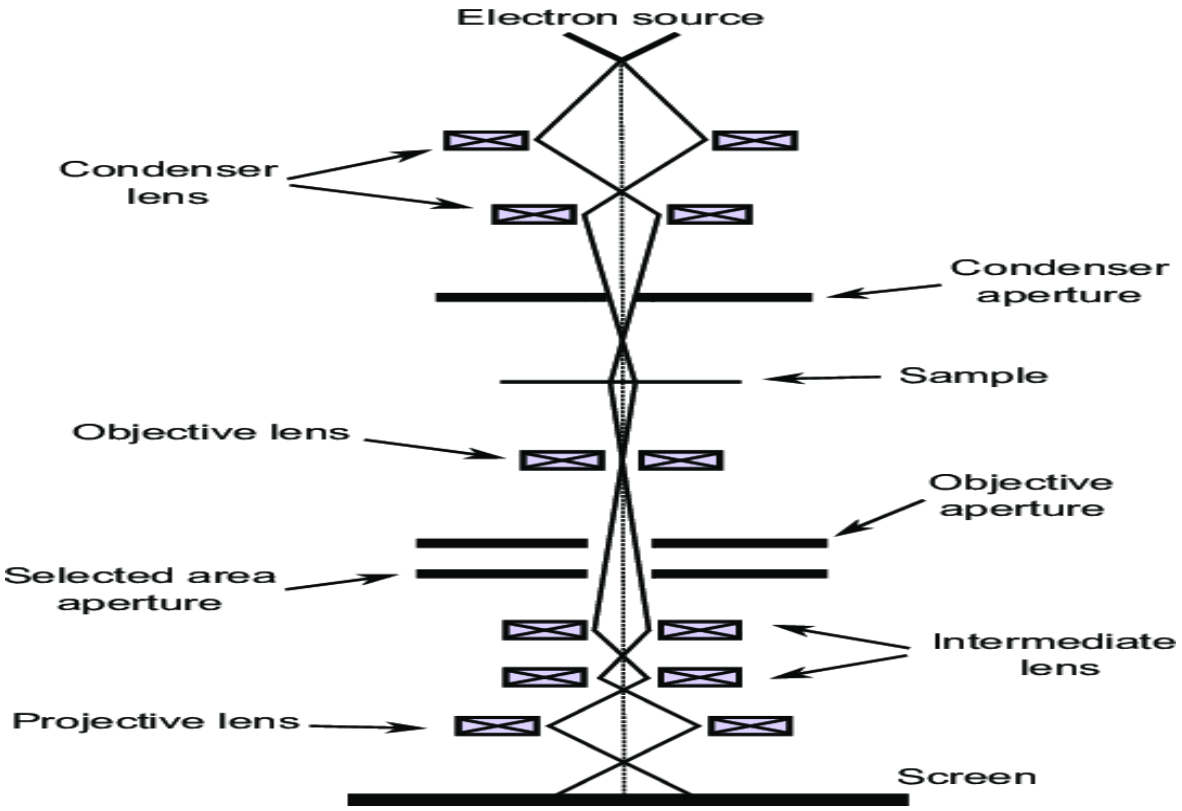

Figure 3.5: Schematic diagram indicating how the TEM produces images [327].

Based on Figure 3.5, electron gun/source is responsible for the release of electrons, which are then allowed to pass through a variety of magnified lenses and apertures. During this process, the electrons wave packets are transmitted through the sample [328]. In any case, the un-scattered electron waves, are also transmitted through the sample, in the process colliding with the fluorescent screen at the bottom of the microscope. Such collisions lead to the generation of the real image of the sample on the screen. Interestingly, regarding image resolution improvement, the voltage of the electron gun can be manipulated in a way that the velocity of the electrons is modified and monitored which in turn results in the improve resolution of the obtained image [329]. For appreciable results concerning resolution of the image in TEM, the samples

are expected to be extremely thin, as this will allow electrons to be transported successfully through the sample. TEM tend to operate at high voltages, approximately 50 to 1000 kV [329, 330]. A voltage of 200 kV which has been used in this research fall within this approximated range.

TEM is based on the gathering of the transferred electrons throughout the sample to reveal valuable data and images regarding the sample under examination. TEM can be adjusted in such a way as to collect signals at the same level of the scanning electron microscopy (SEM) signal generation, depending on the model of TEM [331, 332]. Nevertheless, it is also suggested that TEM can be used to complement crystallographic techniques (such X-ray diffraction), especially it comes to size of the material validations [333-335].

3.2.4.3. UV-vis spectroscopy (UV)

UV-vis spectroscopy is considered as a peculiar mode of analysis that quantify the amount of distinct wavelengths of visible light being transferred through the sample or being adsorbed by the sample in comparison with a reference sample. The amount of visible light being adsorbed is regarded to be regulated by the chemical configuration of the sample. As such, the amount of visible light being adsorbed by the sample will provide information abouts its identity [336].

UV-vis spectroscopy spectrum was adopted to investigate the optical properties of Au- and Ag-nanoparticles and corresponding nanoparticle+fibrin coronas [336, 337]. An absorption spectrum in the range of 250 - 900 nm was adopted for Au- and Ag-nanoparticles before and after conjugation with the fibrin protein to establish the absorption maxima as well as its corresponding plasmon resonance behaviour in relation to the morphology and dimensions of the nanoparticles. Thermo Scientific

Multiskan Go Spectroscopy was utilised to conduct all the quantifications via the cuvette mode (therefore, disposable cuvettes were used).

Somehow, localised surface plasmon resonance of the precious metal nanoparticles is regarded as their valuable property. So, this property becomes apparent when photons of a particular frequency prompt the collective oscillation of conduction electrons on the precious metal nanoparticles' surface, which lead to selective photon absorption, efficient scattering, as well as improved electromagnetic field strength in the vicinity of the nanoparticles [338].

The maximum wavelength (λ_{max}) of the nanoparticles in the UV-visible absorbance spectrum is dictated by the domains encircling the nanoparticles [338, 339]. In this instance, the movement in λ_{max} can be utilised to track modifications in the surface configuration of the nanoparticles. On the other hand, the shifting or the difference in maximum wavelength (λ_{max}), can be used to trace the attachment of biomolecules on the surface of nanoparticles in the UV-visible spectroscopy [338, 340, 341].

For better understanding of how the UV-vis spectroscopy components functions, the working principle of the UV-vis spectroscopy is highlighted in Figure 3.6.

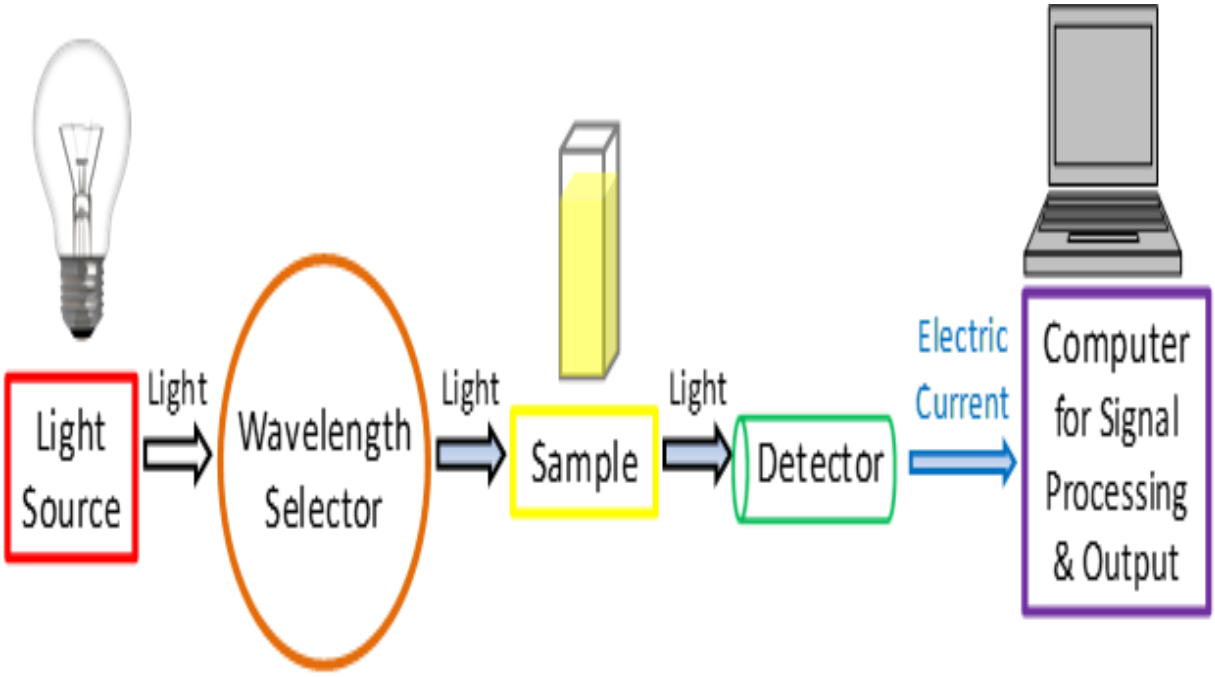

Figure 3.6: A schematic presentation of how UV-Vis spectroscopy operates [342].

With reference to, this scheme, the visible light is always transmitted through the sample no matter which wavelength selector is initiated in the spectroscopy. With regard to sample analysis, a reference sample is quite important, and a cuvette encapsulated with a solvent is employed in the composition of such sample [329]. For clarity, in a situation where a buffered solution contains the sample of interest such as proteins, this simply means that a buffered solution alone without the sample of interest is used as the reference [342].

In general, following the transmission of visible light through the sample, a detector as in Figure 3.6 is utilised to transform the visible light into an interpretable electronic indicator via a digital computer [329, 341]. In this case, the interpretable data appears as the graph of absorbance as a function of wavelength in the UV-vis spectroscopy. Meaning that in the graph, absorbance is presented on the vertical y axis meanwhile wavelength is distributed on the horizontal x axis [329, 341]. At the end, the wavelength correlating to the greatest absorbance of the desired sample is considered

for evaluation [329, 341]. With the aid of ensuring highest sensitivity, since the highest response is achieved for a certain analyte concentration.

3.2.4.4. Fourier Transform Infrared Spectroscopy (FTIR)

FTIR, well-recognised and acceptable approach which characterises bulk and nanoscale materials through fluid medium by identifying relevant functional groups in the sample matrix has also been used. A Perkin Elmer FTIR TWO spectrometer was identified and utilised to probe functional groups available in the citrate immersed with Au- and Ag-nanoparticles as well as conjugated nanoparticle+fibrin corona samples. Consequently, associated structural properties of fibrin protein before and after conjugation with Au- and Ag-nanoparticles were also extracted. For good measurements, the spectral wavenumber range of 400 to 4000 cm^{-1} was initiated. In the process, a total of 1801 scans were achieved at a resolution wavenumber of 4 cm^{-1}. In any case, Figure 3.7 further validates the analytical procedure of the FTIR spectrum:

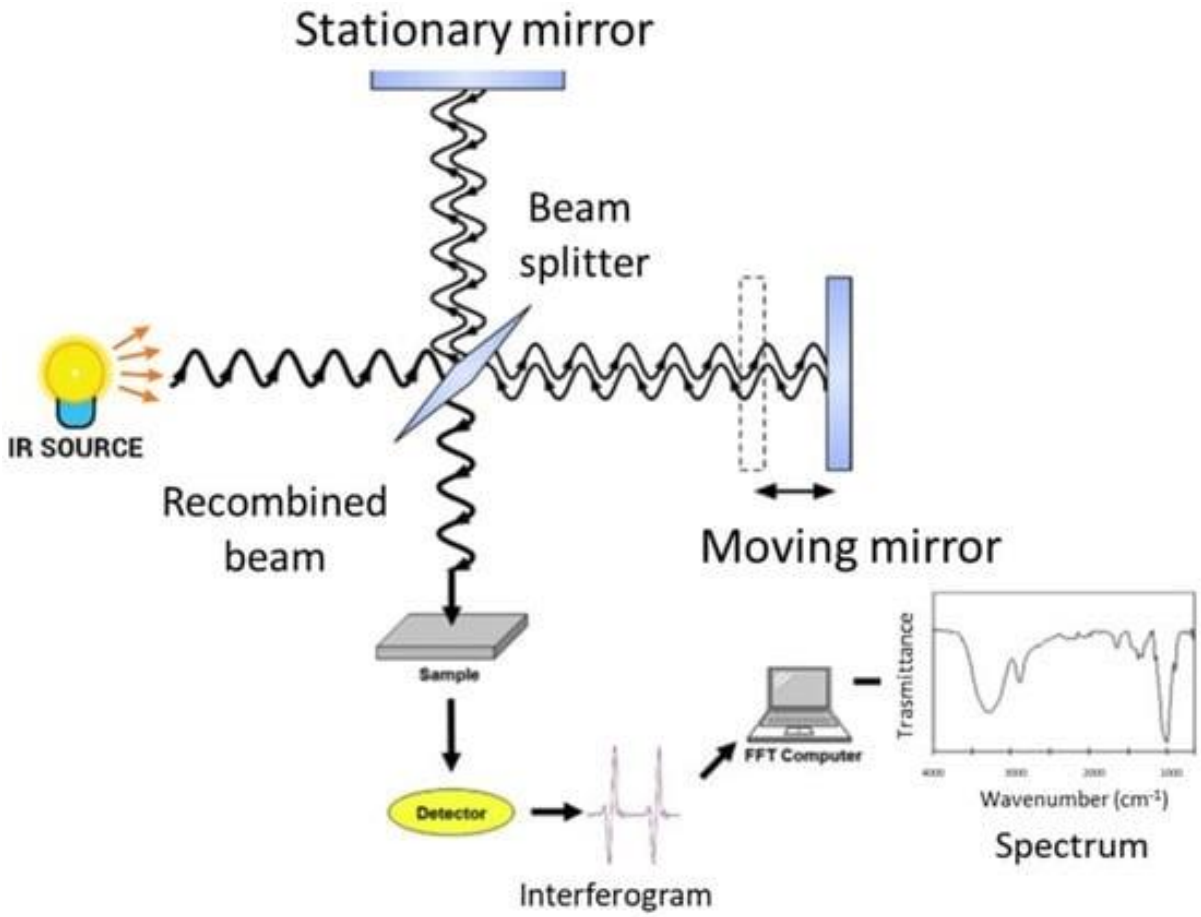

Figure 3.7: A schematic sketch illustrating how the FTIR emits its spectrum [343].

In particular, the FTIR spectroscopy utilises interferometer to monitor the broadband infrared (IR) source. The procedure makes use of the detector to measure the intensity of the reflected light as a function of the lights' wavelength, which becomes the interferogram. As a results, the interferogram is transformed into IR absorption spectrum by a digital computer utilising Fourier transform. Onwards, this spectrum is well noted with % transmittance plotted against wavenumber (cm^{-1}) as illustrated in Figure 3.7 [343-347].

Some studies show that FTIR monitors the absorption of infrared light to certain specific energies that contributes to the excitations of molecules by vibrations [343, 344]. Therefore, this simply implies that FTIR spectra are characteristics of the bonds

in molecules or specifically the quantum harmonic oscillators of bonded structures such as in solid lattices. Basically, this spectrum is applied as an identification or fingerprint which identifies possible impurities, changes, and quality of the associated molecules [348].

As a final point, FTIR spectroscopy specifically regulates the molecular vibrations in molecules. As such, functional groups in a certain material of interest may be linked with characteristic infrared absorption bands. Such bands are known to be associated with the fundamental vibrations of the functional groups in certain materials as outlined in some literature [343, 344, 348, 349].

3.2.4.5. Zeta potential (ZP)

Zeta potential (ZP) measurements are simple, easy and reproducible when averaging or estimating and acquiring particle surface charge. Zeta potentials were examined to trace the charge distributions onto the surface of the nanoparticles before and after adsorption of the fibrin protein molecules [350-352]. Isolated nanoparticles exhibit the lowest negative charge before adsorption which then converts to a higher value after the fibrin protein adsorption.

Au- and Ag-nanoparticles and corresponding nanoparticle+fibrin coronas zeta potentials were physically characterised using Zetasizer in disposable capillary zeta cells at a temperature of 25 °C. Attained zeta potential measurements were averaged from three repeated measurements for informed convincing results.

The zeta potential, also known as electro-kinetic potential, is regarded as the potential at the slipping/shear plane of colloid particles moving in an electric field [353], as shown in Figure 3.8. As such, the electric potential at the surface amounts to work done required to bring a unit positive charge from infinity to the surface of the

nanoparticle at constant speed. In essence, the zeta potential becomes the potential difference between the electric double layer (EDL) of electrophoretic mobile charges and the dispersant layer in the locale of the slipping plane [351].

A charged particle dispersion influences creation of the EDL on the surface [354]. The inner layer consists of ions whose charge opposes that of the primary nanoparticle (Stern layer). Beyond Stern layer, the electrostatic effects due to the surface charge on the particles decrease according to Debye's law [355].

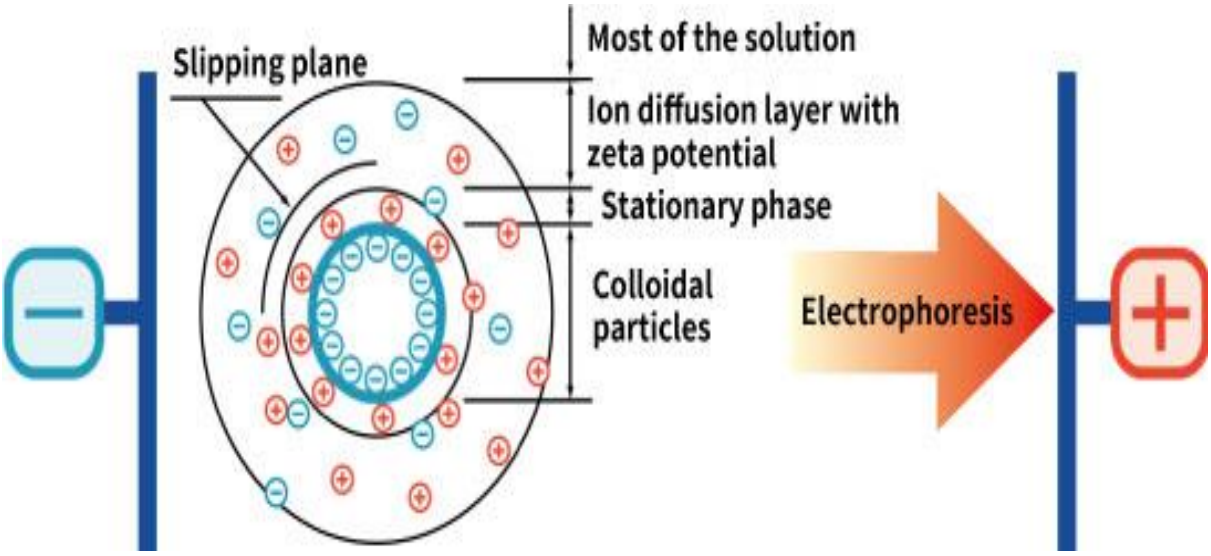

Figure 3.8: Conceptual analysis of the zeta potential [351].

Even though mathematically, electrostatic effects extend towards the infinity, experimentally such effects are only experienced a few nanometres from the nanoparticle surface. Due to the electrostatic field of the charged nanoparticles, a diffuse layer consisting of both same and opposite charged ions/molecules get generated beyond the Stern layer which along with the Stern layer form the EDL as clarified in Figure 3.8. The composition of this diffuse layer is dynamic and varies depending on a variety of factors such as pH, ionic strength, and concentration of the solution therein. In this instance, when an electric field is introduced to such dispersion,

the charged particles move towards the opposite electrode (the process known as electrophoresis) as Figure 3.8 demonstrates. In the diffuse layer there is a hypothetical plane which resonate as the interface between the moving particles and the layer of dispersant around it while electrophoresis continues. Such plane is the characteristic slipping/shear plane meanwhile zeta potential is regarded as potential at this particle-fluid interface [351].

CHAPTER 4

Interface interaction of Au-nanoparticles with fibrin protein molecules

4.1. Introduction

Gold nanoparticles (Au-nanoparticles) are identified as possible metal-based substrates which can be used in some drug delivery processes into human systems [356]. However, there are some reported health-related issues with reference to gold (Au) metal and their related compounds. As such, over-exposure of some human tissues to Au and their related gold compounds may result in increased risk of cancerous and associated diseases damaging the liver, stomach, respiratory tract, and other human organs [357]. This treatise is driven by the fact that if precious metal nanoparticles, say gold could be sited in a cellular physiological fluid, spontaneous interaction with immediate biomolecules including proteins ensues [165, 236].

On the Physics point of view, the successful adsorption process, due to this spontaneous interaction between Au-nanoparticles and protein molecules will result in the reduction of the nanoparticle's free energy. Eventually, this entire process will result in the formation of Au-nanoparticle+protein corona complexes [165, 236]. Au-nanoparticle+protein corona can be described as a single or more layers of a certain protein species molecules around the nanoparticle's spherical surface. Supposedly, upon entering the intercellular plasma environment, the nanoparticles surface simply induces the adsorption on the neighbouring biomolecules, specifically protein molecules, resulting in the formation of the nanoparticle+protein coronas.

Taha *et al.* [358] conducted DFT studies of cyclic glycine-alanine dipeptide attaching/binding onto Au-nanoclusters in the quest of understanding possible interactions occurring between cyclic glycine-alanine dipeptide and gold nanoclusters.

Another investigation by Jahan *et al*. [359] used mesoscopic coarse-grained MD simulations to examine ovispirin-1 and lysozyme protein coronas on pristine Au nanomaterials. The outlined studies included some stability and reliability of the acquired nanoparticle+protein coronas. Such research studies have demonstrated to be quite helpful in describing the possible mechanism of interaction that could be occurring in the biological inter-cellular environment. Despite advancement in the applicability of the nanoparticle+ligands conjugates in health-related applications, their interactions remain not well understood, and it is unclear which amino acids or peptides groups are favoured for binding in a particular protein species. The findings of the DFT study by Buglak *et al.* [360] have exhibited that Au-nanoparticles can interact with the nitrogen, sulphur and oxygen atoms of the amino acid residues through Au-N, Au-S, and Au-O atomic bondings. In other studies, the interaction of proline which is an example of amino acid found in many proteins, with gold atomic clusters have been investigated through DFT, and the corresponding findings indicated that the interactions were sorely via the amide terminal [361]. This simply suggest that different protein species bind differently to the surface of some specific nanoparticles.

Quantitatively, according to Hu *et al.* [362], at nanoscale, the gold samples adopt the face-centred cubic (FCC) phase. In this nano-phase, different thermodynamic properties can be studied well by variation of energy, temperature, and pressure. In most instances, thermodynamic properties of nanoparticles, which includes melting point, Debye temperature and heat conductivity drops as the nanomaterial size decreases [363]. But in this context, the specific heat tends to rise when the size of nanomaterial is reduced. Correspondingly, lowering in melting point while the size of

nanoparticles decreases is associated with a greater quantity of surface atoms which are less bonded to the internal atoms.

In this chapter, a model interaction was designed between different spherical sizes of Au-nanospheres and different chain lengths of fibrin protein molecules. It must also be stated now that for simplicity, Au-nanospheres are associated with experimentally observed Au-nanoparticles. The model made use of an amalgamation of DFT, MC methods, and MD simulations to aid in understanding the interface binding nature and mechanism of fibrin protein molecules onto Au-nanospheres towards Au-nanosphere+fibrin corona formation.

4.2. Modelling of Au-nanospheres and fibrin protein molecules

4.2.1. Modelling of Au-nanospheres.

Spherical Au-nanospheres of 19, 38, 55, and 79 atoms (later referred to chronologically as Au(19), Au(38), Au(55), and Au(79)) were constructed using Material Studio (MS) package [285]. Figure 4.1 (a) illustrates the initial Au(19) (Au-nanosphere with 19 atoms). Triangular pyramidal bonds between adjacent Au atoms assist in tracing the original FCC symmetry of the nanosphere. A corresponding geometrically optimised Au(19) nanosphere is also presented in Figure 4.1 (b).

A choice of 19, 38, 55, and 79 atomic spherical values fall within the structural surface and yet reactive magic numbers of generating stable, improved nanoparticles [364]. Advancing on, all Au-nanospheres models were constructed, thereafter geometrically optimised to obtain relaxed favourable configurational nanospheres for this project. Illustrations of Figure 4.1 (a) and (b) demonstrate how regular, straight lined pyramidal inter Au-Au adjacent bonds transform into curly Au-Au-Au in the middle extreme positioned atomic arrangements after geometric optimisation, depicting acceptable

circumference of spherical symmetry. A similar procedure was followed on the model construction and geometric optimisations of the subsequent Au(38), Au(55), and Au(79) nanospheres.

DMol^3 code as executed in Material Studio, was initiated to carry out all calculations associated with DFT-based geometry optimisations. The generalised gradient approximation (GGA) according to Perdew-Burke-Ernzerhof (PBE) exchange-correlation energy functional was employed for the optimisations [293]. Double numerical atomic orbital augmented plane waves by a polarisation p-function (DNP) basis set [287] were engaged to depend on the spin unrestricted calculations. On the contrary, the maximum value of energy, gradient, and displacement tolerances were set at 'customised' quality which are 1 x 10^{-5} Ha, 2 x 10^{-3} Ha/Å, and 5 x 10^{-3} Å respectively.

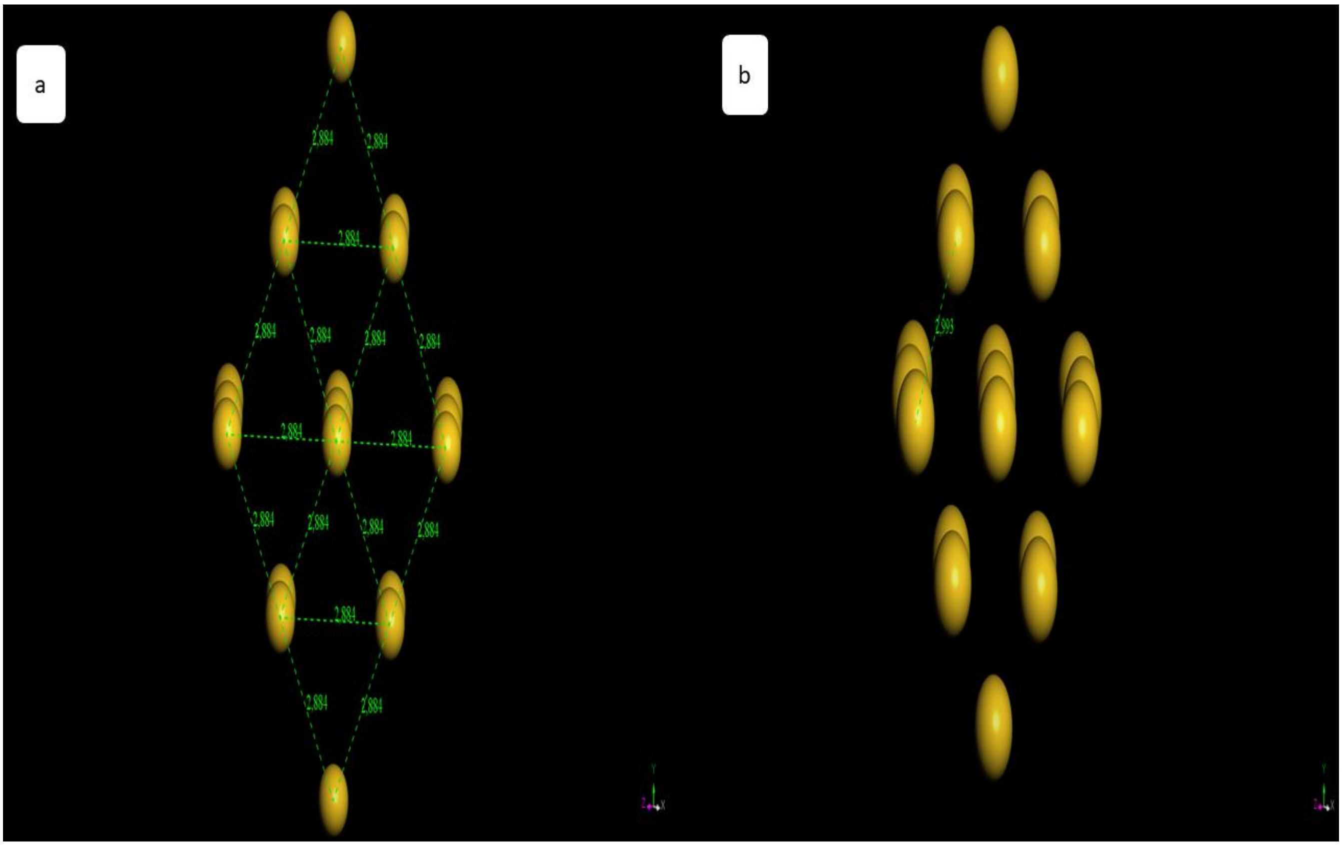

Figure 4.1: (a) A typical initially modelled structure of Au(19)-nanosphere. Triangular dashed lines assist in tracing original conventional FCC character. (b) A typical geometrically optimised Au(19)-nanosphere.

4.2.2 Modelling of fibrin protein molecules

The basic 1-fibrin protein molecule chain has a molecular formula $C_5H_{11}N_3O_2$ [112] whose model is presented in Figure 4.2. As already stated, fibrin protein molecule which is a derivative of fibrinogen has been identified as an emerging and promising protein species suitable for biomedical applications [27].

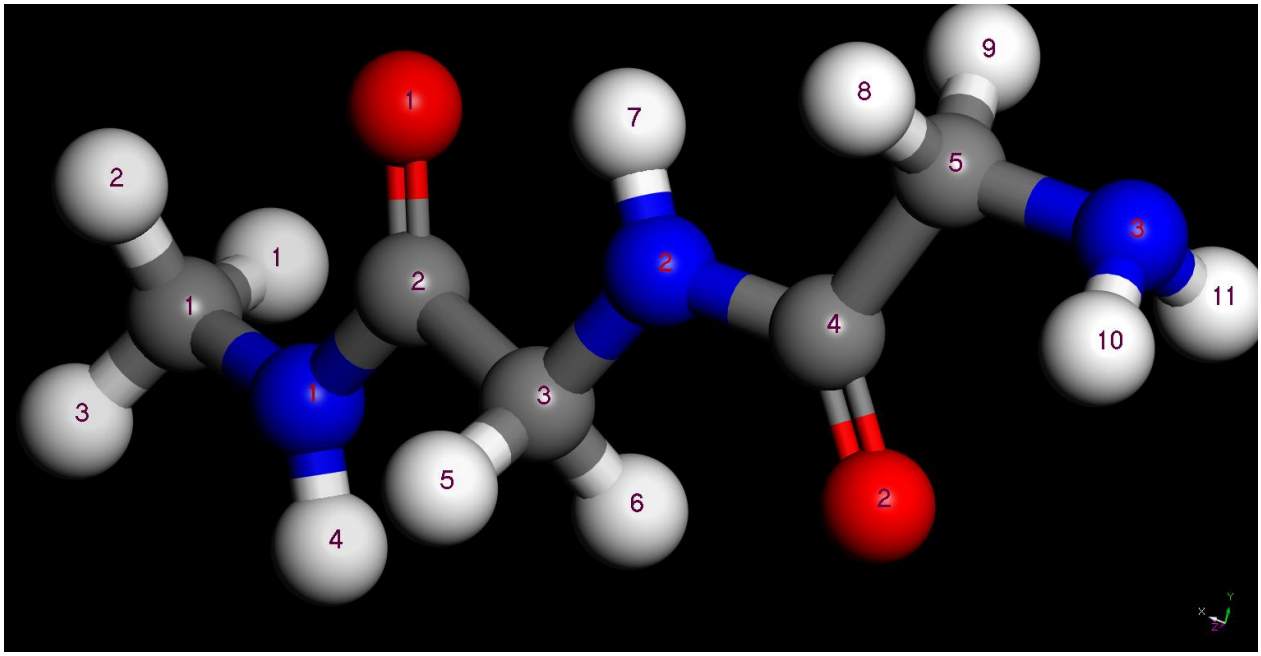

Figure 4.2: A typical structure of 1-fibrin molecule.

A fibrin protein molecule (Figure 4.2) chemical structure consists of 5 carbon (C-grey), 11 hydrogen (H-white), 3 nitrogen (N-blue), and 3 oxygen (O-red) atoms. Inherently, a basic fibrin (thereafter referred to as 1-fibrin) molecule has two -CH_2, two -CO, two -NH, one -NH_2, and one -CH_3 functional groups. Making use of the –NH_2 or –CH_3 side functional groups, extra chains can be added to generate 2, 3, 4, and more sequential fibrin chain molecules. Consequently, a fibrin protein molecule (thereafter will be referred to as just fibrin or fibrin molecule) can also be classified as a peptide [112], meaning a basic single chain can be replicated into more chains or specifically 2-, 3-, and 4-fibrin molecule chains which are considered in this study.

Forging ahead, the structures of the fibrin molecules were firstly optimised individually using $DMol^3$ code in order to reach their most stable energy conformational structures. The bond lengths of the atoms within the basic 1-fibrin molecule were further explored as displayed in Table 4.1 below with reference to their numbering in Figure 4.2. Hence

the measured bond lengths were found to be in good comparison with the expected available values in other different studies [105, 106, 366-368].

Table 4.1: Approximate bond lengths of some CH, CO, NH, CN, CC bonds in Angstroms (Å) within the basic 1-fibrin molecule as per referenced numbering in Figure 4.2.

	Average bond length (Å) (This work)	Literature
C-H	1.0903	1.080 [105], 1.090 [106], 1.097 and 1.110 [366]
C-O	1.2385	1.202 and 1.212 [367], 1.210 [106], 1.239 [105]
N-H	1.021	1.000 [105], 1.020 [368, 106]
C-N	1.4168	1.466 [367], 1.470 [106], 1.484 [105]
C-C	1.5345	1.530 [106], 1.531 [105], 1.532 [367]

With regard to fibrin protein molecules, dissimilar parameters were initiated as compared to the nanoparticles in order to attain correct prediction of the structural and electronic features of the molecules. As a result, dispersion corrected-DFT (DFT-D) was generally utilised to evaluate the molecular properties of fibrin molecules. DFT-D was implemented using DMol^3 alongside generalised GGA functional by PBE and Grimme's empirical dispersion correction [369]. The DFT-D method of Grimme is recommended for modifying the performance of standard DFT, particularly for defining the non-covalent forces, which include van der Waals and hydrogen bonding [369,

370]. For better improvement of the calculations, fine quality of global orbital cut-off was adopted [371]. The maximum of energy, gradient, and displacement tolerances were chosen to be 1 x 10^{-5} Ha, 2 x 10^{-3} Ha/Å, and 5 x 10^{-3} Å, respectively. As such, the 0.005 Ha of smearing value was initiated in orbital occupation to accelerate the convergence.

4.3. Results and discussion

4.3.1. Au-nanosphere + fibrin protein corona complexes

In order to understand the possible nature of interaction between Au-nanoparticles and fibrin molecules, a model interaction between Au(19), Au(38), Au(55), and Au(79) and 1, 2, 3, and 4-fibrin molecules was suggested and developed. In certain studies, such model interaction between nanoparticles and biological molecules, whereby biomolecules end up being attached to nanoparticles surfaces is referred to as docking [372, 373]. In this section, such modelled interaction analysis are discussed based on all possible identified permutations of Au and fibrin molecules.

To further clarify the situation, for the Au-nanospheres, the following sixteen (16) model interactions with fibrin molecules were considered:

Au(19) + 1-fibrin, Au(19) + 2-fibrin, Au(19) + 3-fibrin, and Au(19) + 4-fibrin

Au(38) + 1-fibrin, Au(38) + 2-fibrin, Au(38) + 3-fibrin, and Au(38) + 4-fibrin

Au(55) + 1-fibrin, Au(55) + 2-fibrin, Au(55) + 3-fibrin, and Au(55) + 4-fibrin

Au(79) + 1-fibrin, Au(79) + 2-fibrin, Au(79) + 3-fibrin, and Au(79) + 4-fibrin

Upon adsorption models, the complex structures of Au-nanospheres + n-fibrin molecules (n = 1, 2, 3, and 4) were further optimised via Dmol^3 code to reach their most stable energy structures. Thereafter, single-point energies of the optimised structures using the same approaches discussed in sub-sections 4.2.1 and 4.2.2 were

calculated. Subsequently, the adsorption energies of Au-nanospheres + n-fibrin corona complexes were calculated. A focus was based on those models with the most stable Au-nanosphere+fibrin coronas.

In the first setting, the simulation involved each of the Au(19), Au(38), Au(55), and Au(79) nanospheres interaction with each of the 1, 2, 3, and 4-fibrin molecules. Figure 4.3 presents how Au(55) nanosphere adsorbs the 1, 2, 3, and 4-fibrin molecules respectively after geometrical optimisation. The same scenario was achieved for the Au(19), Au(38), and Au(79) nanospheres adsorption of one-on-one 1, 2, 3 and 4-fibrin molecules after geometrical optimisations. Such adsorption complexes can as well be referred to as nanosphere+fibrin corona complexes. Sequentially, the total energies for the Au-nanospheres adsorption of 1, 2, 3 and 4-fibrin molecules after geometrical optimisations were explored as shown in Figure 4.4. In Figure 4.4, the total energies of the nanosphere+fibrin corona systems were found to decrease with the increasing number of the fibrin chains. Literature works by Carr *et al.* [309] further concurs that the same behaviour of energy was observed for Au-nanoparticles interaction with cysteine protein species. Besides, it is notable that Au(79) interaction with 1, 2, 3, and 4-fibrin experiences the lowest total energies whereas, Au(19) versus 1, 2, 3, and 4-fibrin experiences the highest.

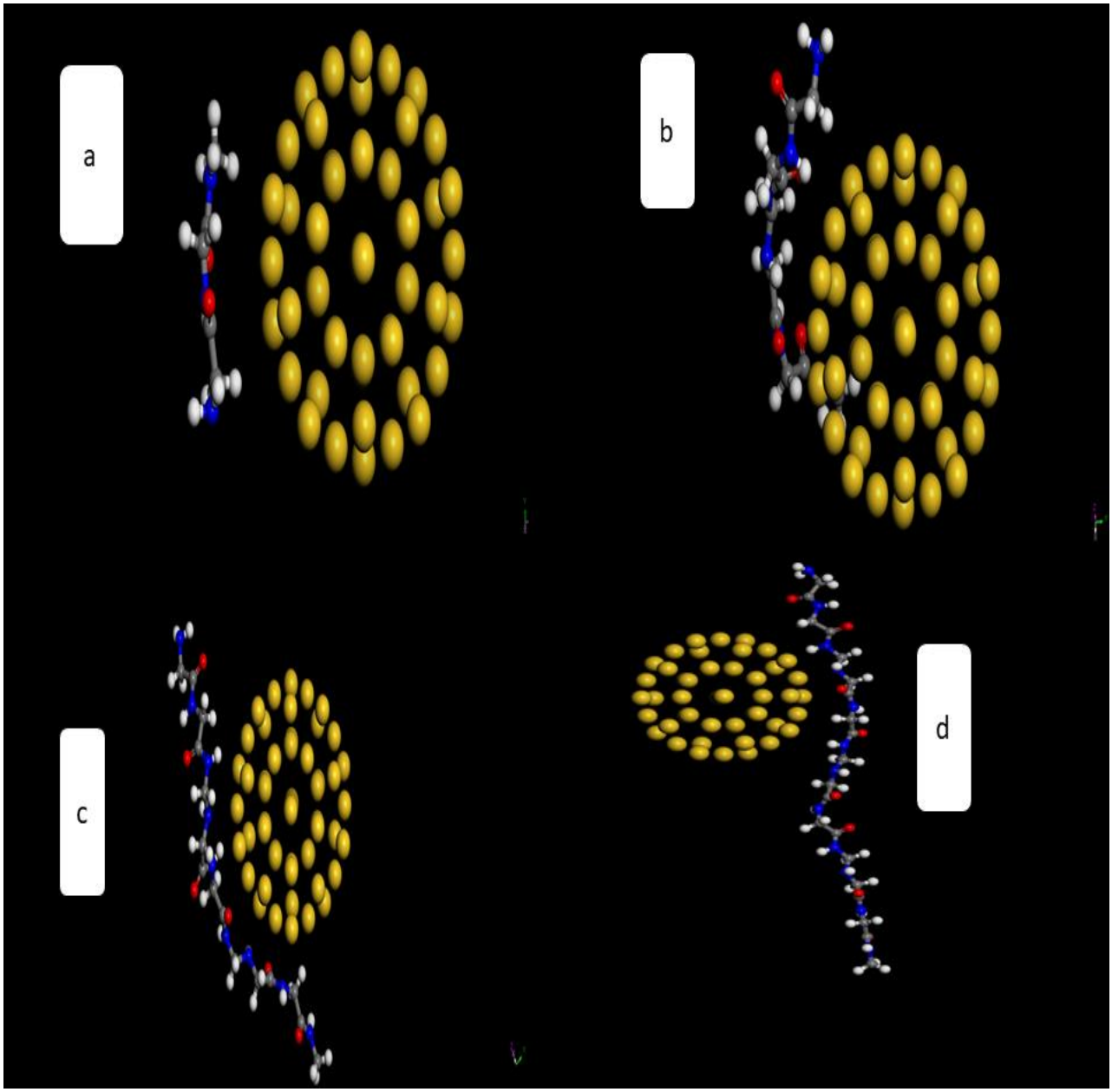

Figure 4.3: 1, 2, 3, and 4-fibrin molecule chains adsorption onto Au(55) nanosphere. The yellow balls represent the Au atoms. The grey, blue, red, and white balls represent the C, N, O, and H atoms respectively in the 1, 2, 3, and 4-fibrin molecules.

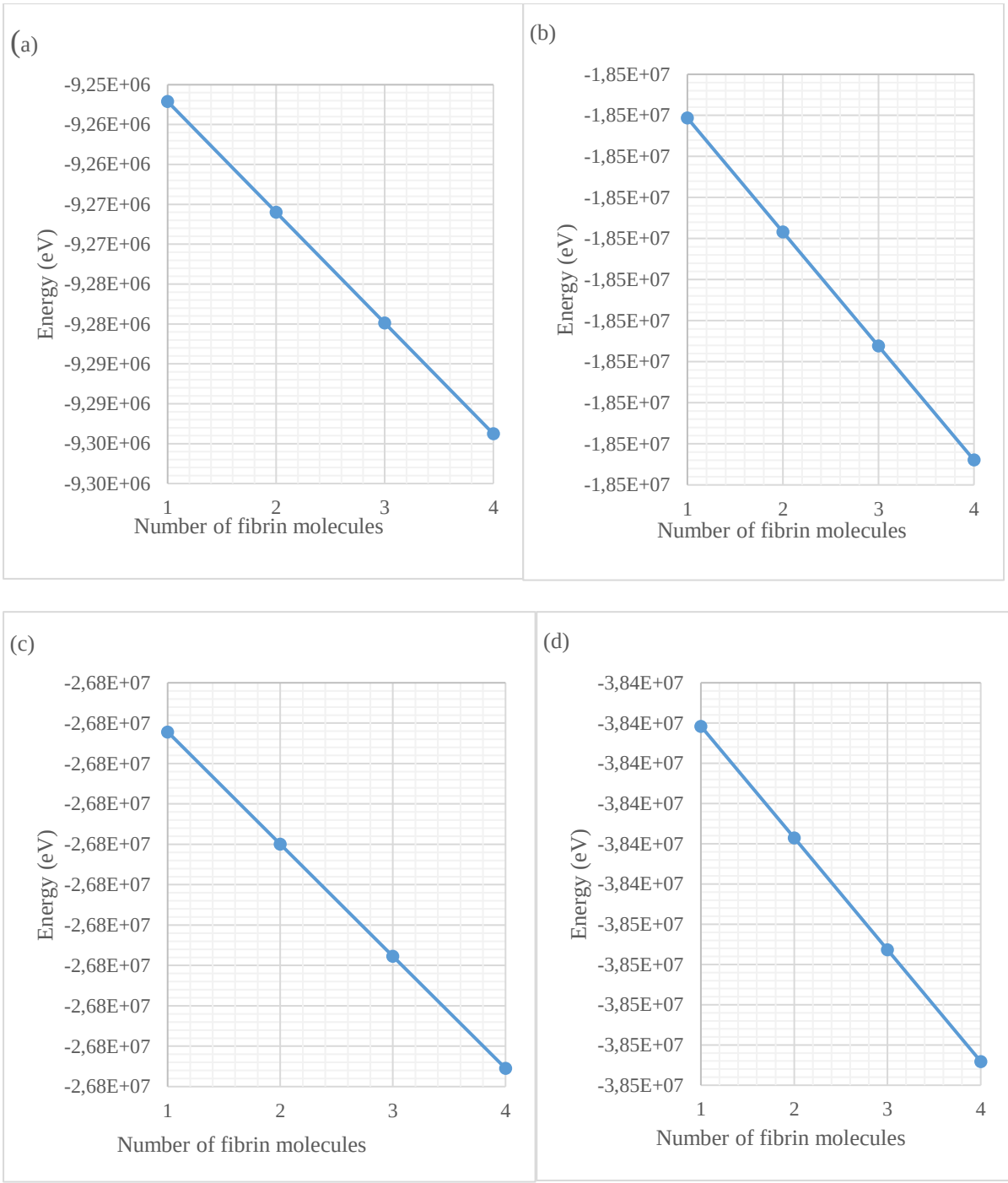

Figure 4.4: Au-nanopshere + n-fibrin corona complex total energies versus n-fibrin molecules (n = 1, 2, 3, and 4). (a) Au(19) + 1, 2, 3, and 4-fibrin total energy versus 1,2,3, and 4-fibrin, (b) Au(38) + 1, 2, 3, and 4-fibrin total energy versus 1,2,3, and 4-fibrin, (c) Au(55) + 1, 2, 3, and 4-fibrin total energy versus 1,2,3, and 4-fibrin, and (d) Au(79)+ 1, 2, 3, and 4-fibrin total energy versus 1,2,3, and 4-fibrin.

4.3.2. Adsorption energies and bond lengths of Au-nanosphere + fibrin corona complexes.

In order to predict possible formation of the nanoparticle+fibrin protein corona complex, the adsorption energy of the systems must also be calculated. The adsorption energy at the interface is given by [309, 358]:

$$E_{Ad} = E_{(ns+fm)} - nE_{fm} - E_{ns}. \qquad (4.1)$$

Here, E_{Ad} is the adsorption energy of the fibrin protein molecules onto the nanosphere surface. $E_{(ns+fm)}$ is the total energy of the nanosphere+fibrin molecule (*ns*+*fm*) corona complex. E_{ns} and E_{fm} are total energies of the nanosphere (*ns*) and fibrin molecule (*fm*) respectively, whilst *n* stands for the number of fibrin molecules present in the nanosphere binding. Based on this equation, a negative adsorption energy indicates that the nanosphere adsorption of fibrin molecule(s) is exothermic resulting in an energetically stable and possible occurrence of the nanosphere+fibrin corona system [154, 309, 358, 374].

Adsorption energies of Au(19), Au(38), Au(55), and Au(79) nanospheres with 1, 2, 3, and 4-fibrin molecules were calculated, thereafter listed in Table 4.2. Negative adsorption energies were obtained for all the Au-nanosphere + *n*-fibrin protein molecules binding possible formations modelled. As per equation (4.1) this suggest that all the nanosphere+fibrin corona complexes presented in Table 4.2 are energetically stable. To quantify this, the energy values further indicate the possible strength of the nanosphere + fibrin corona binding. So, the lowest negative adsorption energy is associated with the most stable nanosphere+fibrin corona complex. Even better, model Au(55) nanosphere interaction with 1, 2, 3, and 4 fibrin molecules recorded the lowest adsorption energies implying the most stable nanosphere+fibrin corona complexes. Surprisingly, a zero adsorption energies were also recorded on the

Au(19) nanosphere interaction with 3 and 4-fibrin species. This could quantify the suggestion that the Au(19) nanosphere may have far smaller surface area due to very few clustered atoms spherical size for possible binding with the 3 and 4-fibrin molecule chains.

To corroborate the adsorption energies, bond lengths were also explored for possible Au-H, Au-O, Au-N and Au-C atomic bonding as itemised in Table 4.3. The arrangement is for Au(19), Au(38), Au(55), and Au(79) nanospheres possible bonding permutations with 1, 2, 3, 4-fibrin molecules. The permutations of the possible bonding assist in recognising which of the bond lengths have the smallest values. Such bond lengths would then suggest the most probable bonding between the Au-nanospheres and the fibrin molecules. Excessively large bond lengths would also suggest unlikely occurrence of the bonding between the specified atomic species. Stable and exothermic energies along with acceptable bond lengths interactions signify that specified nanospheres can successfully transport associated fibrin protein species into cellular environment.

Table 4.2: Adsorption energies (E_{Ad}) of 1, 2, 3, and 4-fibrin molecules onto Au(19), Au(38), Au(55), and Au(79) nanospheres.

E_{Ad}(eV)		1-fibrin	2-fibrin	3-fibrin	4-fibrin
	Au(19) +	-0.27	-0.28	0.0	0.0
	Au(38) +	-0.54	-0.28	-0.81	-0.28
	Au(55) +	-2.99	-2.73	-3.00	-2.73
	Au(79) +	-1.63	-1.37	-1.09	-1.37

For every nanosphere + fibrin possible bonding, as the number of fibrin molecules increase from 1 to 4, bond lengths appear to contract as indicated in Table 4.3. In addition, certain bond lengths decrease with nano spherical size from Au(19) to Au(79).

Table 4.3: Predicted bond lengths in Angstroms (Å) between Au-atoms and specified fibrin molecules atoms. All the nanospheres, Au(19), Au(38), Au(55), and Au(79) against 1, 2, 3, and 4-fibrin molecules have been considered.

		Au(19) +				Au(38) +				Au(55) +				Au(79) +			
		1-fibrin	2-fibrin	3-fibrin	4-fibrin	1-fibrin	2-fibrin	3-fibrin	4-fibrin	1-fibrin	2-fibrin	3-fibrin	4-fibrin	1-fibrin	2-fibrin	3-fibrin	4-fibrin
Bond lengths (Å)	Au-H	3.175	3.434	3.012	2.883	3.317	3.093	3.353	3.003	3.443	2.690	2.979	2.924	2.808	2.799	2.976	3.031
	Au-C	3.893	3.395	3.597	3.144	4.040	3.400	3.334	3.583	4.112	3.546	3.414	3.559	3.427	3.527	3.693	3.692
	Au-N	3.880	3.550	2.778	2.653	3.888	3.862	2.556	3.980	4.059	3.719	2.587	2.697	3.836	2.611	2.873	3.382
	Au-O	4.145	2.525	3.372	2.766	3.737	2.566	3.455	2.706	3.875	2.739	2.768	3.475	2.890	2.643	2.978	2.948

4.3.3. Molecular dynamics (MD) geometrically optimised structure of 1-fibrin molecule adsorbed onto Au-nanospheres

Molecular dynamics (MD); Forcite code [314] was firstly used to geometrically optimise the complex models of Au(19), Au(38), Au(55), and Au(79) nanospheres with 1-fibrin protein species. For a proper representation, a rectangular slab was created around each of the Au-nanosphere + 1-fibrin complexes (i.e. Au(19) + 1-fibrin, Au(38) + 1-fibrin, Au(55) + 1-fibrin, and Au(79) + 1-fibrin). In this way, relaxed minimum energy systems with less uncertainty were attained. The slabs were modelled at room temperature (298 K) under NVT ensemble. A time step of 1.0 fs and total dynamic time of 100.0 ps was set for all the simulation runs. With regard to the thermostat, a Nose technique was applied and the number of simulation steps were 100000. A random value temperature-dependent Gaussian distribution was used to initiate velocities.

The slabs of the simulated geometry optimised Au(19), Au(38), Au(55), and Au(79) nanospheres interactions with 1-fibrin molecule species are presented in Figure 4.5.

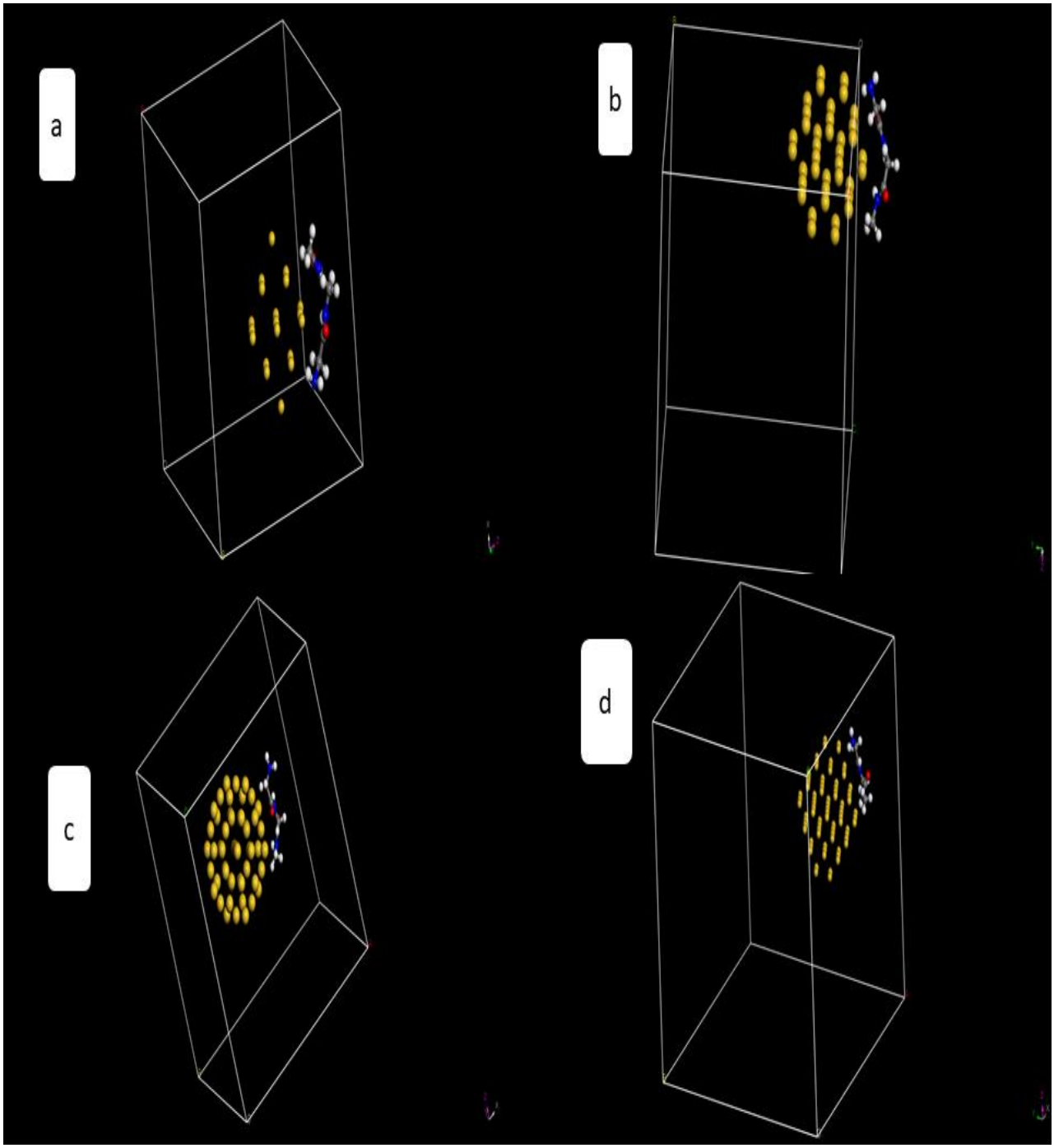

Figure 4.5: MD geometrically optimised models of (a) Au(19) + 1-fibrin, (b) Au(38) + 1-fibrin, (c) Au(55) + 1-fibrin, and (d) Au(79) + 1-fibrin.

4.3.3.1 Radial distribution functions of Au(19) + 1-fibrin, Au(38) + 1-fibrin, Au(55) + 1-fibrin, and Au(79) + 1-fibrin

Radial distribution function (RDF) in each system of particles (atoms) present how density tends to vary as a function of distance with regard to a reference particle (atom). The RDF provide an evaluation of the probability that, if there is an atom at the origin of an arbitrary reference frame, then there will be an atom with its centre located in a spherical shell of infinitesimal thickness at a distance, r, from the reference atom [314]. This simply suggests that the atom at the origin and the atom at distance r may be of different chemical types, such as α and β [314]. In this order, the resulting function can be represented by $g_{\alpha\beta}(r)$. In the nanosphere + fibrin corona complexes, the radial distribution functions (RDFs) which entails the Au-nanosphere surface atoms as reference frame atoms with respect to atoms on the functional groups of the fibrin molecules were plotted. Figures 4.6 – 4.9 displays the said Au(19) + 1-fibrin, Au(38) + 1-fibrin, Au(55) + 1-fibrin, and Au(79) + 1-fibrin RDFs based on reference Au-nanosphere's surface atoms. Intrinsically, making use of the first and second nearest neighbour distances, the most probable Au-H, Au-C, Au-N, and Au-O bonds on the Au-nanosphere + fibrin molecule can be predicted. In this aspect, Table 4.4 sets out the RDFs on the proposed Au-H, Au-C, Au-N, and Au-O first and second nearest neighbour atom bond lengths on the modelled Au(19) + 1-fibrin, Au(38) + 1-fibrin, Au(55) + 1-fibrin, and Au(79) + 1-fibrin corona complexes respectively.

Comparing Au-H, Au-C, Au-N, and Au-O suggested bond lengths, the Au-H bond displays the lowest value in all modelled Au-nanosphere + 1-fibrin corona complexes (Table 4.4). Additionally, Table 4.4 also displays Au-H bonds of 2.37, 2.47, 2.57, and 2.35 Å respectively for Au(19) + 1-fibrin, Au(38) + 1-fibrin, Au(55) + 1-fibrin, and Au(79) + 1-fibrin coronas. These values are also in good agreement with the literature [375].

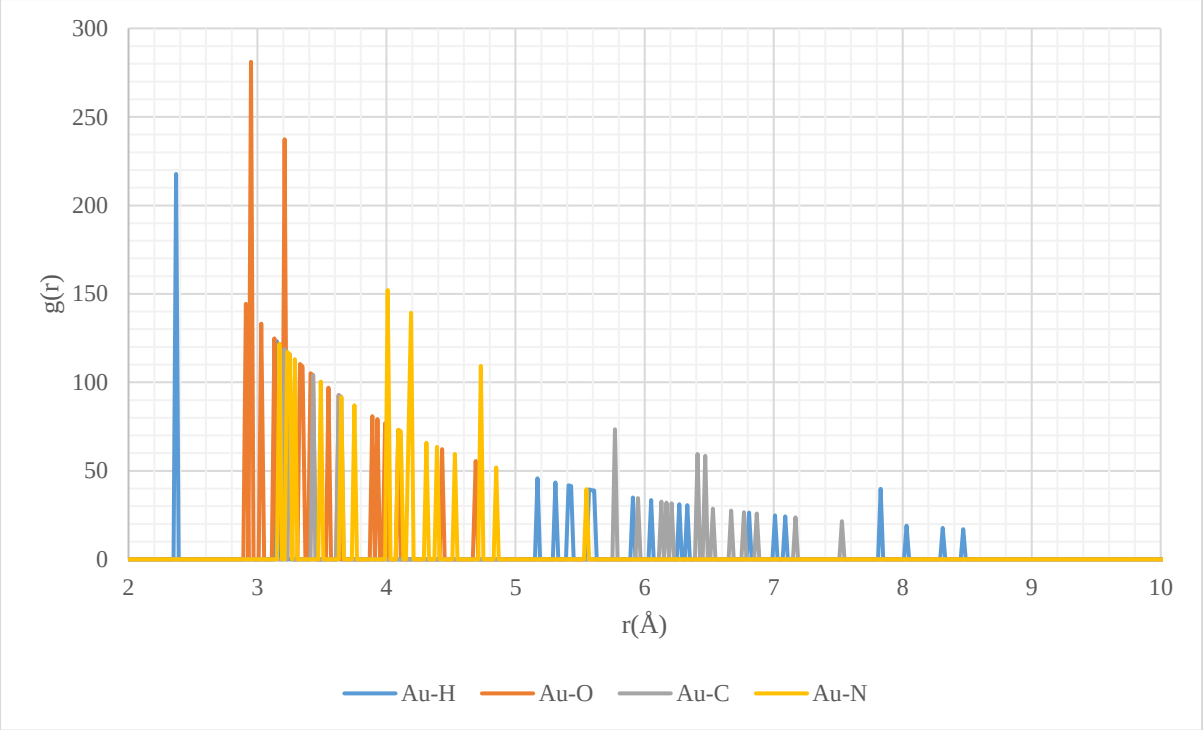

Figure 4.6: Radial distribution functions based on Au(19) +1-fibrin corona.

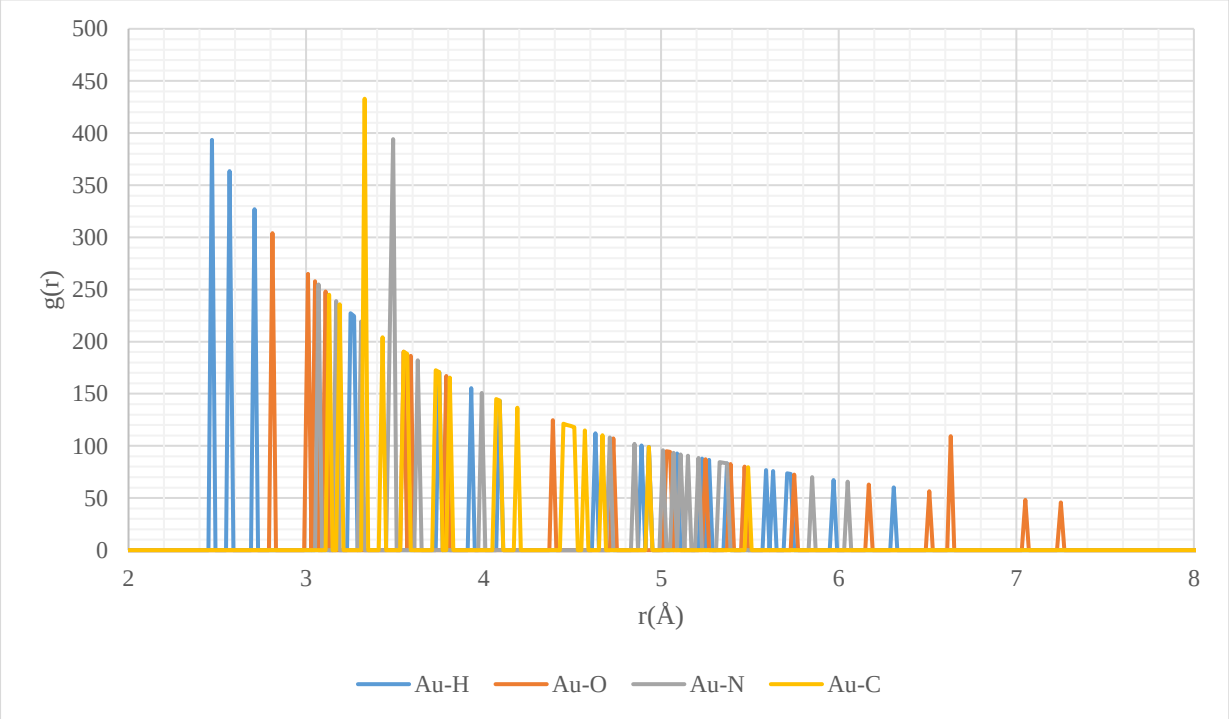

Figure 4.7: Radial distribution functions based on Au(38) + 1-fibrin corona.

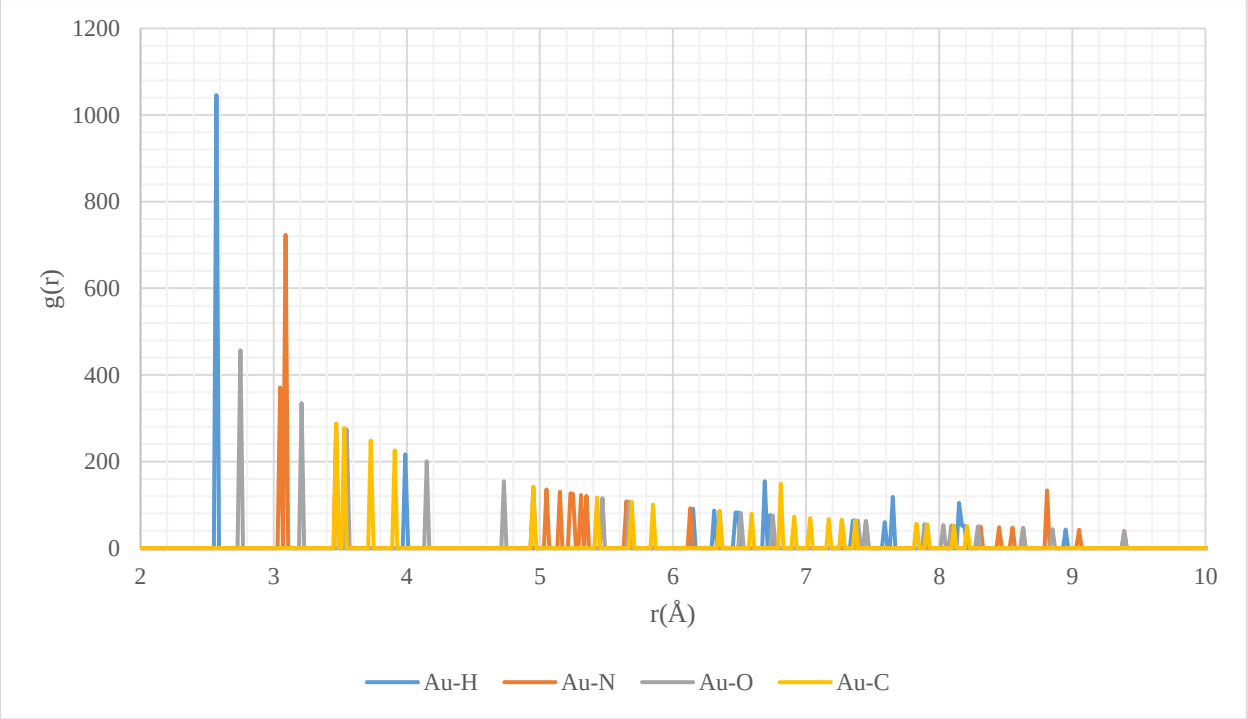

Figure 4.8: Radial distribution functions based on Au(55) + 1-fibrin corona.

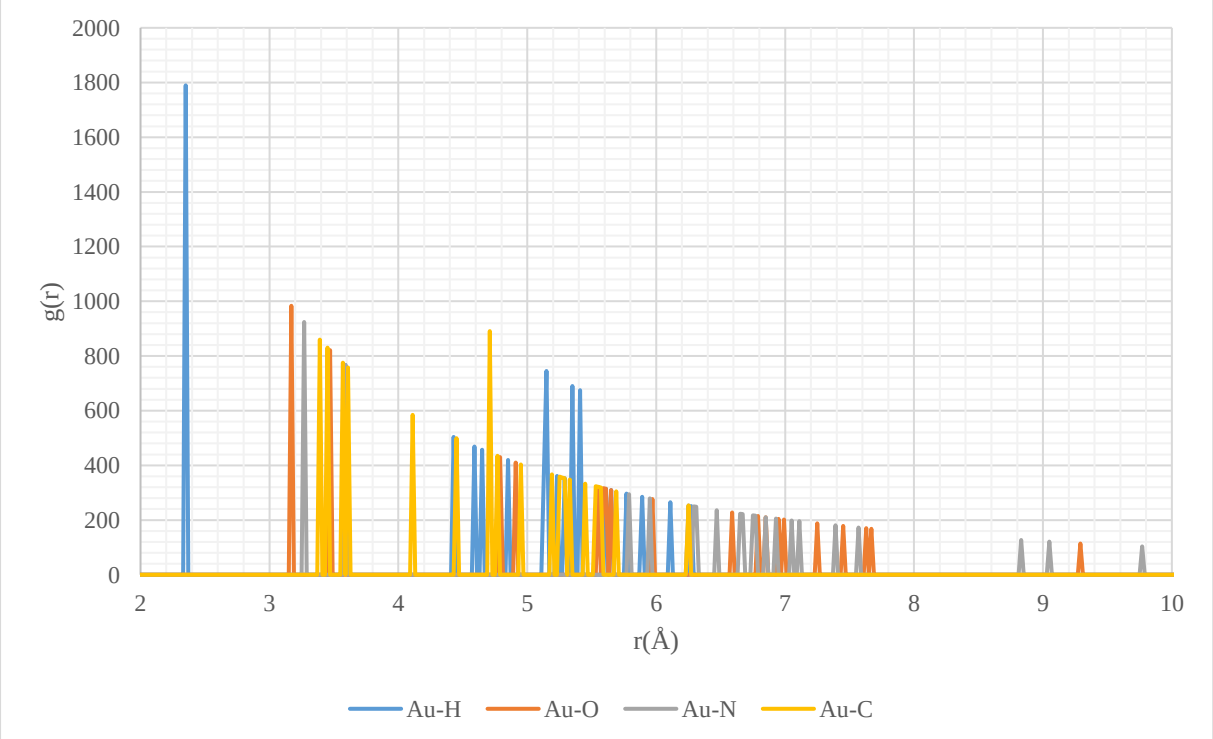

Figure 4.9: Radial distribution functions based on Au(79) + 1-fibrin corona.

Table 4.4: 1st (r_1) and 2nd (r_2) nearest neighbour atom distances as per RDFs on Au(19) + 1-fibrin, Au(38) + 1-fibrin, Au(55) + 1-fibrin, Au(79) + 1-fibrin corona complexes.

	Au(19) + 1-fibrin		Au(38) + 1-fibrin		Au(55) + 1-fibrin		Au(79) + 1-fibrin	
	r_1 (Å)	r_2(Å)	r_1(Å)	r_2 (Å)	r_1 (Å)	r_2(Å)	r_1(Å)	r_2 (Å)
Au-O	2.95	3.21	2.81	3.01	2.75	3.21	3.17	3.47
Au-C	3.21	3.25	3.33	3.13	3.47	3.53	3.39	4.71
Au-H	2.37	3.15	2.47	2.57	2.57	3.99	2.35	3.59
Au-N	4.01	4.19	3.49	3.07	3.09	3.47	3.27	3.59

4.3.3.2 Mean square displacement of Au(19) + 1-fibrin, Au(38) + 1-fibrin, Au(55) + 1-fibrin, and Au(79) + 1-fibrin corona complexes relative to Au, H, C, N and O atoms

Describing the behaviour of the system is of one of the key quantities in MD, hence the greatest valuable execution of molecular dynamics simulation is to compute the dynamic features of the molecules and atoms in their systems. So, the mean square displacement (MSD) is initiated to probe the variation of particle's mobility in a particular simulation system. Therefore, if $r_i(t)$ is the position of atom i at a particular time t, then the mean square displacement of atoms in a particular simulation can be enumerated by [314]:

$$\text{MSD} = R\ (t) = \langle |\ \mathrm{r}(t) - r\ (0)\ |^2 \rangle \qquad (4.2)$$

In this case, $\langle\rangle$ designates totalling across all the atoms, whilst $r(0)$ and $r(t)$ denotes relative distances at initial (0) and later time (t) [314]. Basically, atoms of a particular simulation system are known to be in continuous motion and their positions change

with changing moments. So, the variation of particle's mobility in simulation system can be attained by monitoring the change of mean square displacement curve slope.

To probe the possible mobility of the Au, H, C, N, and O atoms within a given corona complex, the mean square displacement (MSD) graphs relative to Au(19) + 1-fibrin, Au(38) + 1-fibrin, Au(55) + 1-fibrin, and Au(79) + 1-fibrin coronas were plotted, as elaborated in Figure 4.10. The mobility is investigated to observe the possible diffusion of the H, C, N, and O atoms into the Au-nanospheres matrices. Gao and Qu [376] reported that for possible diffusion of ions into solids, the MSDs increase linearly with time. Hence, the MSD in Figure 4.10 suggests that all the H, C, N, and O atoms may diffuse easily into the Au-nanospheres. The diffusion coefficient constants (*D*) were also calculated from the slopes of the MSD graphs and presented in Table 4.5. Still notable, the Au(55) + 1-fibrin corona matrix demonstrates the highest possible mobility of H, C, N, and O atoms as compared to other Au-nanospheres.

In relation to H, C, N, and O atoms in the Au-nanosphere + n-fibrin coronas, their diffusion coefficient constants are observed to be greater than that of Au atoms. As such, all H, C, N, and O atoms have a good probability of diffusing through the Au-nanospheres. Suggestion according to Figure 4.10; H, C, N, and O atoms may diffuse through the Au(19), Au(38), and Au(55) nanospheres after 10 ps. In the Au(79) nanosphere, the atoms may diffuse through the matrix immediately. Further on, such diffusion probabilities may signify the origin of non-toxicity of the Au-nanospheres.

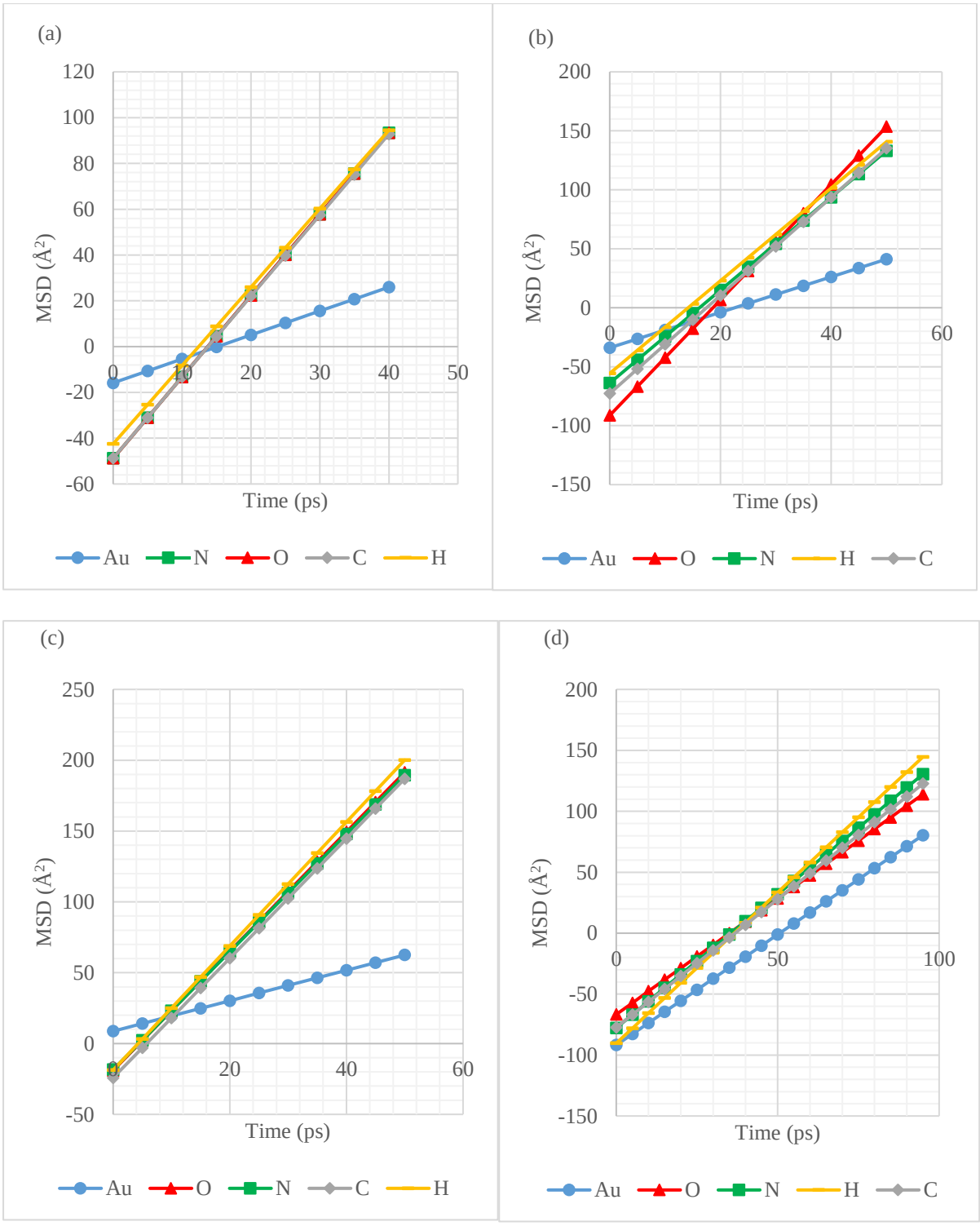

Figure 4.10: Mean Square Displacement (MSD) plots of (a) Au(19) + 1-fibrin, (b) Au(38) + 1-fibrin, (c) Au(55) + 1-fibrin, (d) Au(79) + 1-fibrin coronas relative to Au, H, C, N, and O atoms.

Table 4.5: Diffusion constants (*D*) for 1-fibrin molecule adsorbed onto Au(19), Au(38), Au(55), and Au(79) nanospheres.

		D of 1-fibrin +			
		Au(19) ($Å^2$/ps)	Au(38) ($Å^2$/ps)	Au(55) ($Å^2$/ps)	Au(79) ($Å^2$/ps)
Atoms	H	0.5707	0.6549	0.7295	0.4121
	C	0.5898	0.6929	0.7036	0.3509
	N	0.5598	0.6568	0.6929	0.3653
	O	0.5923	0.8162	0.7017	0.3169
	Au	0.1743	0.2505	0.1794	0.3021

4.3.4. Mulliken charges analysis on Au(55) + fibrin corona complex

Beside energetics and diffusivities, electronic structure of the bonding modes can also assist in understanding the interface interactions in nanosphere+fibrin corona complexes. The electronic structure at the bonding sites can provide insight on how charge transfer occurs between Au(55) and 1, 2, 3, and 4-fibrin molecules respectively, when a nanosphere+protein corona complex get formed. This can be achieved by comparing Mulliken charges of 1, 2, 3, and 4-fibrin before adsorption to Au(55) + 1-fibrin, Au(55) + 2-fibrin, Au(55) + 3-fibrin, and Au(55) + 4-fibrin coronas after adsorption processes. Mulliken charge population analysis will be applied and quantified through acquired atomic charge values. Au(55) + n-fibrin coronas relative to isolated 1, 2, 3, and 4-fibrins were identified for the intended Mülliken charges calculations and analysis. In particular, 1, 2, 3, and 4-fibrins will provide data values before and Au(55) + n-fibrin (n = 1, 2, 3, 4) coronas data values after adsorption processes. This was

motivated by the fact that the Au(55) had the most energetically stable configuration out of all studied Au-nanospheres.

Mülliken charge populations are useful when analysing the nature of atomic charge distributions in molecules through bonding of atomic orbitals in a neighborhood of atomic clusters [377]. For this reason, Mülliken charges were computed for carbon atoms in *n*-fibrin (*n* = 1, 2, 3, 4) molecules before and after adsorption as the carbon atoms outline the spine of these fibrin protein chains. Mülliken charge distribution of each carbon atom on a particular *n*-fibrin molecule with reference to Au-nanospheres are listed in Table 4.6 respectively.

Table 4.6 data suggest that negative charges of *n*-fibrin carbon atoms before adsorption acquire more negativity after adsorption once they materialise as Au(55) + *n*-fibrin coronas. Extra negativity can be assigned to their secondary attachment with acceptor atoms like H in $-CH_2$ or $-CH_3$ functional groups. In contrast, positively charged carbon atoms in *n*-fibrins reduce their positive values after adsorption as they now materialise as Au(55) + n-fibrin coronas. Such loss is associated with further bonding with donor atoms like O and N in -C=O and $-NH_2$ or $-NH_3$ functional groups.

During the adsorption reaction, some negative charges on the surface atoms of Au-nanospheres are transferred through the fibrin bonding atom and charge conservation to the first carbon (C1) of the fibrin molecule, enhancing the negativity value of the C1 atom. Considering the elementary Coulomb's law of charges, this leads to second (C2) and third (C3) carbon atoms of the fibrin also acquiring less positive and extra negative charges sequentially. The same behaviour of charge transfer through the carbon and sulphur atoms was observed in the findings of Carr *et al*. [309]. So, it can be concluded that extra electrons are gained through the Au-H bond, where H is associated with the

-CH_2 or -CH_3 functional groups as accumulated in Table 4.6. Conversely, some electrons get lost through the Au-O/Au-N bonding's, where O and N atoms belong to -C=O and -NH_2 or -NH_3 functional groups respectively.

Table 4.6: Carbon (C) atoms Mulliken charges (in Units of e) for 1, 2, 3, and 4-fibrin molecules before and after adsorption onto Au-nanosphere with 55 atoms.

1-fibrin			2-fibrin		3-fibrin		4-fibrin	
	Before	After	Before	After	Before	After	Before	After
C1	-0.173	-0.233	-0.171	-0.234	-0.169	-0.230	-0.166	-0.226
C2	0.401	0.385	0.428	0.426	0.426	0.416	0.406	0.383
C3	-0.153	-0.200	-0.160	-0.224	-0.170	-0.216	-0.156	-0.223

4.3.5 Radius of gyration for Au-nanospheres + fibrin protein corona complexes

Calculation of the radius of gyration (R_g) relative to some atomic clustering is a significant indicator used when predicting structural activities of macromolecules [378]. When a ligand compound or protein molecule gets attached to the nanoparticle surfaces, there exist a possible configurational change associated with the radius of gyration of the protein molecule [379]. After binding, protein molecules tend to not exhibit major changes in their secondary structure, instead undergo slight readjustment because of their interaction with the nanoparticles. Understanding the radius of gyration of these protein molecules or drug molecules relative to the

nanoparticles assist in forecasting the tightness and attachment criteria of drugs and protein molecules onto the nanoparticle's surfaces [380].

The stability and change in average molecular configuration of the fibrin molecules adsorbed onto Au-nanospheres or in every Au(m)-nanosphere + n-fibrin corona {(m = 19, 38, 55, and 79) and (n = 1, 2, 3, and 4)} complex can also be monitored by making use of the radius of gyration approach [381]. However, based on the fact that radius of gyration is indirectly related with how fibrin protein functional group atoms bond with nanoparticles surface atoms, only 1-fibrin adsorption onto Au-nanospheres corona complexes will be considered.

To analyse the distribution of the fibrin molecules around the Au-nanosphere surface, radius of gyrations were analysed for Au(19) + 1-fibrin, Au(38) + 1-fibrin, Au(55) + 1-fibrin and Au(79) + 1-fibrin corona complexes, whereby 1-fibrin molecule are adsorbed onto Au(19), Au(38), Au(55) and Au(79) as shown in Figure 4.11. In view of that, Au(19) +1-fibrin corona possesses the largest radius of gyration followed by Au(38) + 1-fibrin. Au(79) + 1-fibrin complex acquired the lowest radius of gyration of all the complexes analysed. Accordingly, a small radius of gyration for Au(79) + 1-fibrin complex may be attributed to its large spherical radius with 79 atoms. On the other side, the largest radius of gyration for Au(19) +1-fibrin corona may be attributed to its smallest spherical radius with 19 atoms.

Focusing on Au(19) + 1-fibrin, serious fluctuations of the radius of gyration about 0.125 Å can be seen as the time spans 0 - 100 ps. Au(38) + 1-fibrin and Au(55) + 1-fibrin have quite less fluctuations, but their radius of gyration are decreasing gradually from about 0.07 and 0.05 Å respectively towards about 0.06 and 0.04 Å, as the time spans

0 - 100 ps. To conclude, Au(79) + 1-fibrin corona produces an almost non-fluctuating radius of gyration about 0.033 Å throughout the time span 0 - 100 ps.

Studies by Kharazian *et al*. [382] suggest that a larger radius of gyration corresponds to less tight packing while a smaller radius of gyration suggests a tighter packing. With reference to Figure 4.11, a larger radius of gyration is observed for Au(19) + 1-fibrin corona complex while a smaller radius of gyration is observed for Au(79) + 1-fibrin corona complexes. Such behaviour suggest that chronologically, hard corona can be obtained on Au(79)+1-fibrin > Au(55) + 1-fibrin > Au(38) + 1-fibrin. Au(19) + 1-fibrin would signify a soft corona binding.

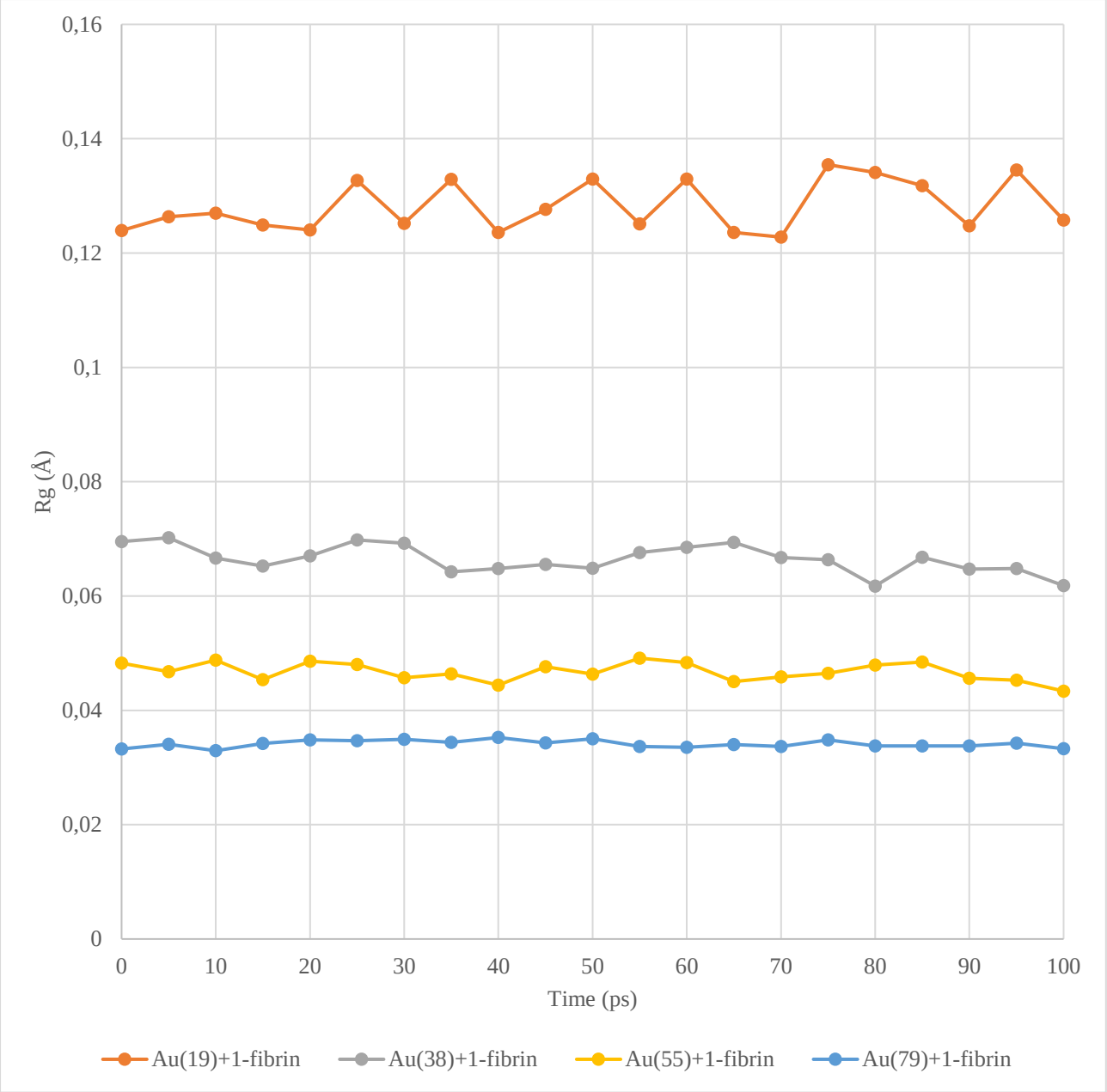

Figure 4.11: Radius of gyration (R_g) based on Au(19) + 1-fibrin, Au(38) + 1-fibrin, Au(55) + 1-fibrin, and Au(79) + 1-fibrin corona complexes.

4.4. Conclusion

All the 1, 2, 3 and 4-fibrin molecules interactions with Au-nanospheres modelled provide a possible formation of the Au-nanosphere + fibrin corona complex. This is additionally supported by the negative adsorption energies acquired for all the modelled configurations. Interface interactions of Au(55) + 1, 2, 3, and 4-fibrin coronas

have been found to be more energetically stable as compared to all other nanospheres. The concerning exception are the Au(19) + 3-fibrin and Au(19) + 4-fibrin coronas. Such anomaly was attributed to the compromised nanosphere size relative to the fibrin chain length.

To validate, mean square displacement graphs and corresponding diffusion coefficient constants suggests that upon adsorption, all the atoms of the fibrin molecules may diffuse easily into the Au-nanospheres. H, C, N, and O functional group atoms of fibrin tends to exhibit different diffusion coefficient constants into the different sizes of both Au-nanospheres. Explored possible bond lengths through the RDFs complement one another, hence, the Au-H bond appears to be the shortest for all the Au(m) + 1-fibrin coronas. This suggest that the fibrin molecules may prefer hydrogen bonding as their mode of Au-nanosphere + fibrin interface binding.

The enhanced negative and positive charges experienced through the Mülliken charge distributions before and after adsorption is attributed to the charge transfers which originate from the surface atoms of the Au-nanospheres onto the fibrin molecules. Such charge transfers may alter the original molecules functionality or be the source of immobilisation. The radius of gyration further suggest that a tighter packing is observed for the adsorption of fibrin molecules onto Au(38), Au(55), and Au(79) nanospheres with a sequence of Au(79) > Au(55) > Au(38). Less tight packing of Au(19) signifies soft Au(19) + 1-fibrin corona. Most probable Au-nanosphere sizes to transport fibrin species may be suggested from these outcomes.

CHAPTER 5

Interface interaction of Ag-nanoparticles with fibrin protein molecules

5.1 Introduction

As both gold (Au) and silver (Ag) belong in group IB precious metals, similar to Au-nanospheres interactions with fibrin protein species modelling procedures presented in the preceding chapter 4 could be expected in this chapter.

However, Ag nanomaterials present peculiar physical and chemical properties differing to those experienced by Au nanomaterials. Such unusual properties have attracted utilisation of silver in various medical based research processes [28, 383]. Ag-nanoparticles expose unique optical, electrical, thermal, conductive, and absorption properties [28, 383, 384]. In addition to this, some health and biological issues related to silver and its derivative compounds have been reported [385]. Drake and Hazelwood [386], have reported on how over-exposure of human tissues to silver and its related compounds may lead to suppressed blood pressure, diarrhoea, stomach irritation as well as respiratory problems.

Various types of Ag nanomaterials are known to be used in different biomedical applications such as biosensing and antimicrobial [387]. Such nanomaterials include but not limited to nanocubes, nanoplates, nanorods, nanodisks and nanospheres [387, 388]. Similar to gold (Au), silver (Ag), as a precious metal crystal also has a face-centred cubic (FCC) unit cell [389]. In this FCC symmetry, lattices of these metals are bound by low index crystal planes which have high atomic stacking in (100) and (111) faces [390]. In certainty, (111) plane possess highest atomic stacking in the Ag metal, which in turn leads to experiencing the lowest surface tension, yet being the most stable plane [390].

In this manner, silver has been identified as one of the precious metals that could be utilised for drug delivery process [391]. Interestingly, when silver nanoparticles are introduced into a biological environment, they simply induce the adsorption of various biological molecules such as proteins onto their surfaces leading to nanoparticle-protein corona [392]. Such mechanism can be imitated with the aid of computer-based simulation techniques. Sarker *et al*. [393] has conducted a multiscale simulation of protein corona formation on silver nanoparticles, which involves adsorption study of Ovispirin-1 Peptide onto the Ag nanoparticles, with the aid of mimicking the biological environment.

Correspondingly, according to Davey [389], at nanoscale the silver samples adopt the face-centred cubic (FCC) phase. In this FCC phase, thermodynamic properties of the nanomaterials can be studied well by variation of energy, temperature, and pressure. In this Chapter, a model interaction was also made between 19, 38, 55, and 79 atomic sizes of Ag-nanospheres and different chain lengths of fibrin protein molecules. In this regard, a combination of density functional theory (DFT), Monte Carlo (MC) methods, and classical molecular dynamics (MD) simulations has been used. Optimisation of several Ag-nanospheres – fibrin molecules complexes were carried out. Subsequently, the adsorption energies of Ag-nanospheres + fibrin molecules complexes were calculated. A focus was based on those models with the most stable Ag-nanospheres with fibrin molecules.

5.2 Modelling of Ag-nanospheres and fibrin.

5.2.1 Modelling of Ag-nanospheres

Making use of the similar procedure exercised in sub-section 4.2.1 in chapter 4, Ag-nanospheres were modelled making use of the Material Studio (MS) package. Each separately, Ag(19), Ag(38), Ag(55), and Ag(79) nanospheres were constructed into a spherical form and ultimately optimised to obtain the relaxed configurations. Figure 5.1 (a) presents the acquired Ag(19)-nanospheres before optimisation processes. Systematically, Figure 5.1 (b) also presents the acquired Ag(19)-nanosphere after optimisation processes. Changes in the immediate Ag - Ag bond lengths from the initial 2.889 (Figure 5.1 (a)) to 3.007 Å (Figure 5.1 (b)) was observed after optimisation. In this manner, in Figure 5.1 (b), the bulging of the atoms to form a more accurate nanosphere could be observed after geometrical optimisation. Same analogical procedure was followed when constructing the corresponding Ag(38), Ag(55), and Ag(79) nanospheres.

Consequently, as in chapter 4, sub-section 4.2.1 of Au-nanospheres, herein DMol^3 code as implemented in MS software, was also utilised to perform all calculations related to DFT-based geometry optimisations.

Modelling and optimisation procedures of the fibrin protein species have already been detailed in chapter 4, sub-section 4.2.2.

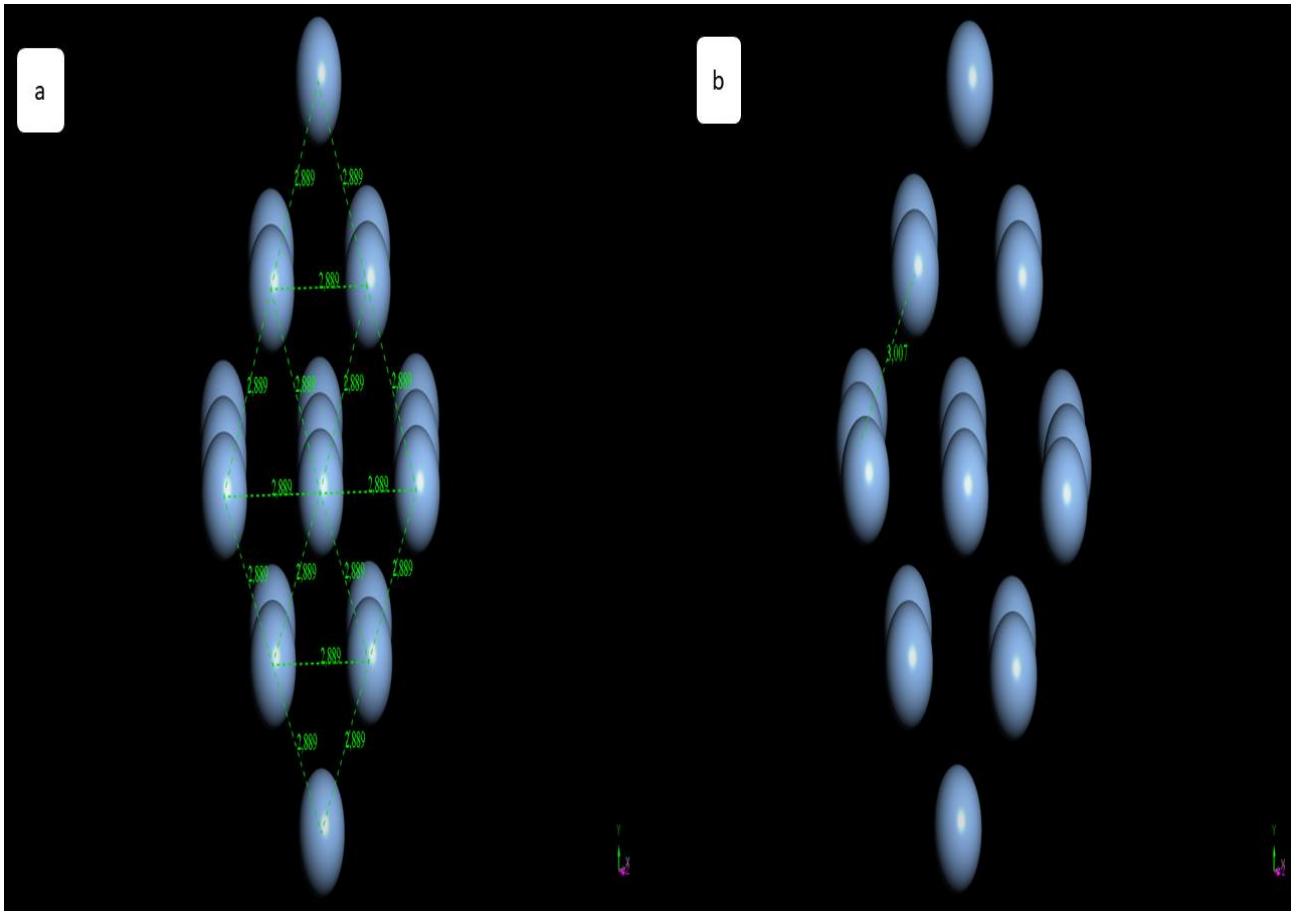

Figure 5.1: (a) The initial structure of Ag-nanosphere with 19 atoms with the triangle labelled as the FCC-structural character. (b) A typical geometrically optimised Ag(19)-nanosphere.

5.3 Results and Discussion

5.3.1. Ag-nanosphere + fibrin protein corona complexes

Procedures similar to those applied when modelling different Au-nanospheres and n-fibrin molecules have been considered as well in this section. As a result, Ag(19), Ag(38), Ag(55), and Ag(79) nanospheres as well as 1, 2, 3, and 4-fibrin molecules were generated and further optimised before modelling the ultimate Ag-nanospheres + n-fibrin corresponding corona complexes.

In the case of Ag-nanospheres, the following 16 model interactions with fibrin molecules were considered:

Ag(19) + 1-fibrin, Ag(19) + 2-fibrin, Ag(19) + 3-fibrin, and Ag(19) + 4-fibrin

Ag(38) + 1-fibrin, Ag(38) + 2-fibrin, Ag(38) + 3-fibrin, and Ag(38) + 4-fibrin

Ag(55) + 1-fibrin, Ag(55) + 2-fibrin, Ag(55) + 3-fibrin, and Ag(55) + 4-fibrin

Ag(79) + 1-fibrin, Ag(79) + 2-fibrin, Ag(79) + 3-fibrin, and Ag(79) + 4-fibrin

Figure 5.2 further demonstrates how the modelled adsorption of 1, 2, 3, and 4-fibrin chains onto Ag(55) nanosphere may occur. A similar procedure can be expected for the 1, 2, 3, and 4-fibrin chains adsorption onto other nanosphere geometries; Ag(19), Ag(38), and Ag(79).

For better comprehension of the interaction of Ag-nanoparticles with biological molecules, the study by Wasukan *et al.* [394] has illustrated the possible docking of enzymes onto Ag_3 cluster. In the study, the docking outcomes indicated that the Ag_3 cluster interconnected with crucial amino acids (building blocks of protein) of the CYP enzymes. Such amino acid residues of these CYP enzymes were found to have vigorously interacted with the Ag_3 cluster, giving further apprehension into the

mechanism of interaction between Ag_3 and CYP enzymes. The study also shows that the Ag_3 cluster interacted with the oxygen atom belonging to carbonyl group of some of the amino acid residues. Basically, silver nanoparticles can successfully interact with biological molecules or proteins through various chains of amino acids functional groups or atoms.

Advancing on, Figure 5.3 illustrates the total energies acquired when 1, 2, 3, and 4-fibrin molecules get adsorbed onto Ag(19), Ag(38), Ag(55), and Ag(79) nanospheres after geometrical optimisations. Accumulated results suggest that the total energy of the Ag-nanosphere + n-fibrin corona decreases as the number of fibrin (n-fibrin) molecules increases around the Ag-nanospheres. Similarly, some studies on the interaction energy of some silver nanoparticles with biological molecules such as serum albumin have also been explored in the literature [3]. The results concur that a negative value of the interaction energy corresponds to a stable non-toxic effect of Ag-nanoparticles interaction with human serum albumin protein. Also, similar to the Au related complexes, as the nanosphere sizes increase from Ag(19) to Ag(79), the total energies of the corresponding coronas are lowering in value, as Figure 5.3 demonstrates.

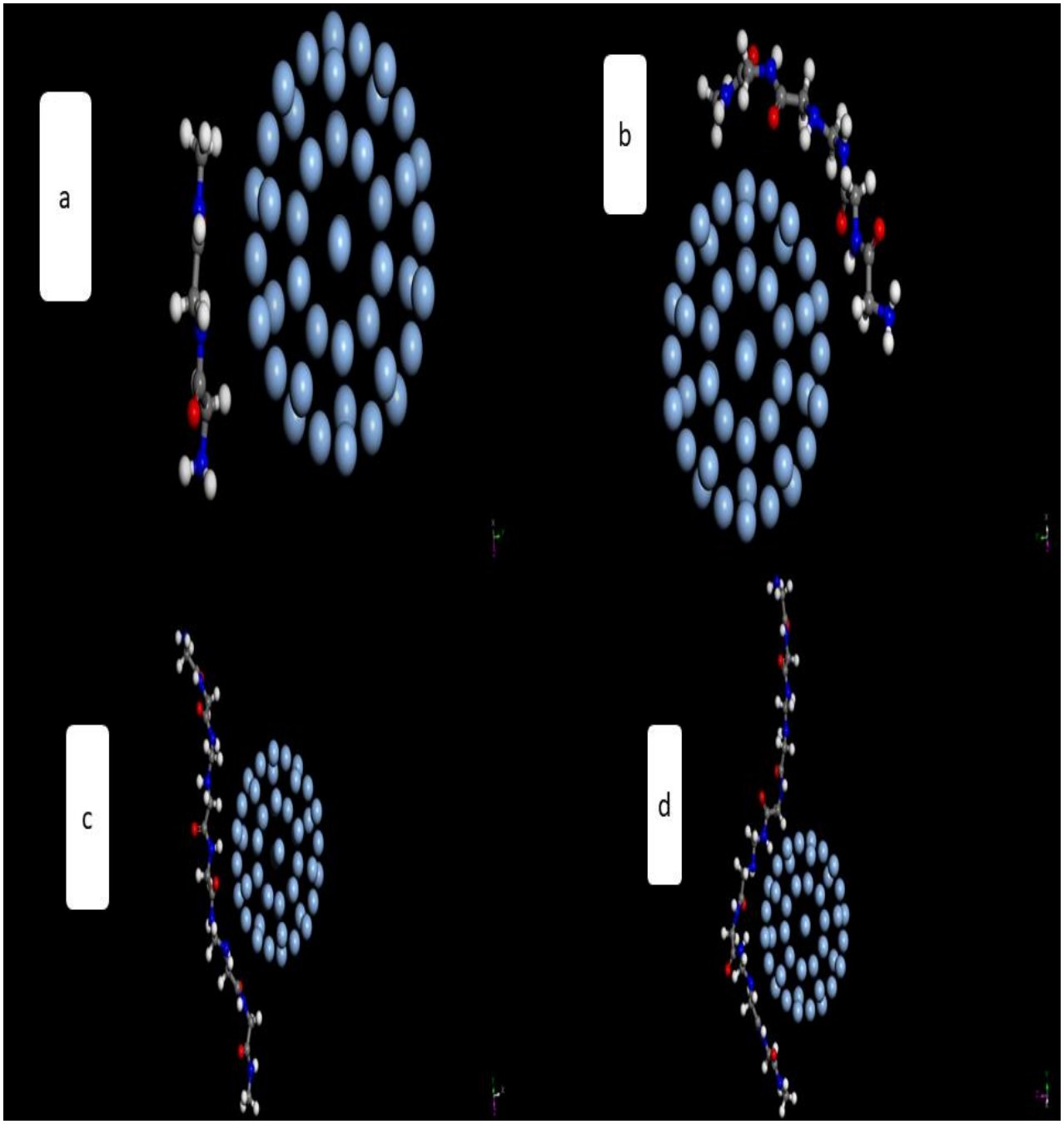

Figure 5.2: 1, 2, 3, and 4-fibrin molecule chains adsorption on the Ag(55) nanosphere. The purple balls represent the Ag atoms. The grey, blue, red, and white balls represent the C, N, O, and H atoms respectively in the 1, 2, 3, and 4-fibrin molecules.

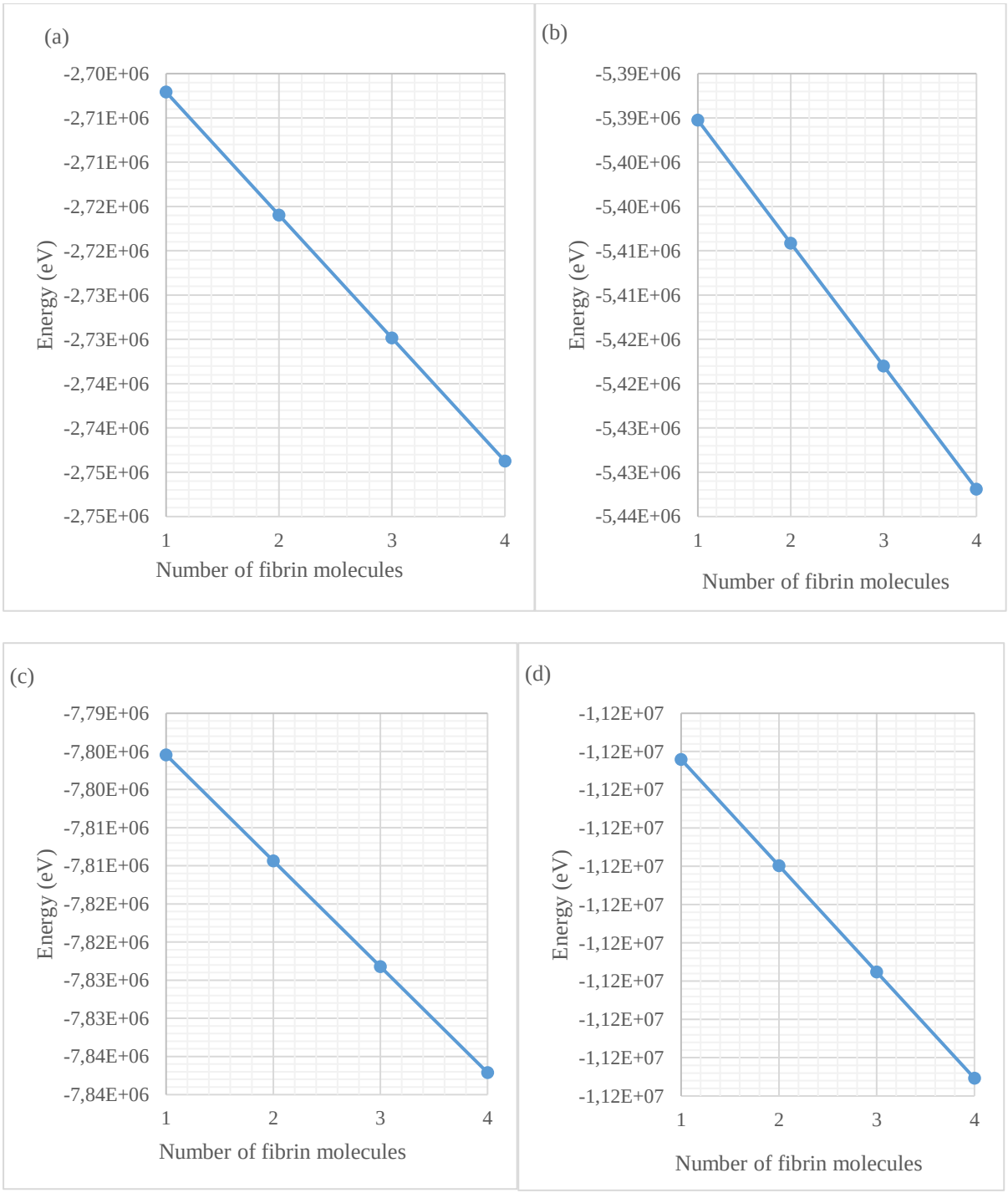

Figure 5.3: Ag-nanopshere + n-fibrin corona complex total energies versus n-fibrin molecules (n = 1, 2, 3, and 4). (a) Ag(19) + 1, 2, 3, and 4-fibrin total energy versus 1,2,3, and 4-fibrin, (b) Ag(38) + 1, 2, 3, and 4-fibrin total energy versus 1,2,3, and 4-fibrin, (c) Ag(55) + 1, 2, 3, and 4-fibrin total energy versus 1,2,3, and 4-fibrin, and (d) Ag(79)+ 1, 2, 3, and 4-fibrin total energy versus 1,2,3, and 4-fibrin.

5.3.2. Energetics and bond lengths of Ag-nanospheres + fibrin protein corona complexes

Making use of the adsorption energy equation 4.1 of chapter 4 subsection 4.3.2, the adsorption energies of n-fibrin molecules onto different Ag-nanospheres can be calculated. Acquired adsorption energy values will assist in predicting possible formation of Ag-nanospheres + n-fibrin corona complexes.

A similar equation (i.e. equation 4.1) was utilised by Chakroborty *et al.* [395] to examine the adsorption energy of the most favourable Ag_6+tyramine complex, whereby a negative adsorption energy signifies thermodynamic stability of the attained complex. In the process, recommending the empirical applications of tyramine-AgNPs biomolecular complexes in various fields such as bio-imaging, drug delivery, and bio-sensing. Wasukan *et al.* [394] have also considered the same equation (i.e. equation 4.1) when examining the adsorption of some enzymes onto Ag_3 clusters. In that study, enzymes were reported to have strong correlation with the Ag_3 clusters. In augmentation, acquired negative adsorption energies signify possible occurrence of Ag-nanosphere + fibrin corona systems.

Calculated adsorption energies of Ag(19), Ag(38), Ag(55), and Ag(79) possible permutations with 1, 2, 3, and 4-fibrin molecules are listed in Table 5.1. In a similar manner, Table 5.1 arrange negative adsorption energies which signify possible, stable formation of associated Ag(19), Ag(38), Ag(55), and Ag(79) with n-fibrin molecules. In particular, a trend similar to the one of the Au-nanospheres + 1, 2, 3, and 4-fibrins is observed. Also, a more energetically stable corona system still favours the Ag(55) interaction with 1, 2, 3, and 4-fibrin molecules. Zero adsorption energies recorded on Ag(19) + 3-fibrin and Ag(19) + 4-fibrin suggest improbable adsorption occurrence of

Ag(19) with 3 and 4-fibrin molecules, which is based on incompatible nanospherical size relative to the fibrin chain length. Similar behaviour was also noticed for Au(19) nanosphere in Chapter 4.

Further confirmation of possible Ag-nanosphere + n-fibrin corona formation, bond lengths of Ag-H, Ag-C, Ag-N, and Ag-O after n-fibrin docking onto Ag-nanospheres were extracted. Table 5.2 lay out all possible Ag-nanosphere + 1, 2, 3, and 4-fibrin bond length values extracted after docking. Smallest values will be the one in which fibrin will dock onto Ag-nanospheres using, while largest values would also suggest unlikely occurrence of the fibrin docking onto the Ag-nanospheres.

Table 5.1: Calculated adsorption energies (E_{Ad}) of 1, 2, 3, and 4-fibrin molecules onto Ag(19), Ag(38), Ag(55), and Ag(79) nanospheres.

E_{Ad} (eV)		1-fibrin	2-fibrin	3-fibrin	4-fibrin
	Ag(19) +	-0.27	-0.27	0.0	0.0
	Ag(38) +	-0.54	-0.28	-0.27	-0.28
	Ag(55) +	-2.99	-2.99	-2.72	-3.27
	Ag(79) +	-1.36	-1.37	-1.64	-1.10

Basically, with reference to Table 5.2, as the number of the fibrin molecule chains is increased from 1-fibrin to 4-fibrin, some of the bond lengths tend to decrease gradually for fibrin molecules adsorbed onto Ag(19), Ag(38), Ag(55), and Ag(79) nanospheres. In the similar manner, the bond lengths become shorter with the increasing nanosphere sizes.

Table 5.2: Predicted bond lengths in Angstroms (Å) between Ag-atoms and specified fibrin molecules atoms. All the nanospheres, Ag(19), Ag(38), Ag(55), and Ag(79) against 1, 2, 3, and 4-fibrin molecules have been considered.

		Ag(19) +				Ag(38) +				Ag(55) +				Ag(79) +			
		1-fibrin	2-fibrin	3-fibrin	4-fibrin	1-fibrin	2-fibrin	3-fibrin	4-fibrin	1-fibrin	2-fibrin	3-fibrin	4-fibrin	1-fibrin	2-fibrin	3-fibrin	4-fibrin
Bond lengths (Å)	Ag-H	3.171	2.966	3.070	2.996	3.187	3.479	2.775	2.817	3.217	3.024	2.713	2.736	3.262	2.885	2.877	2.920
	Ag-C	3.864	3.289	3.243	3.504	4.090	3.316	3.248	3.254	3.475	3.490	3.376	3.307	3.880	3.385	3.310	3.256
	Ag-N	3.753	2.898	3.897	2.785	3.816	3.884	3.619	3.582	3.479	3.387	2.798	2.467	3.717	2.484	2.538	2.821
	Ag-O	4.138	2.422	2.459	2.730	4.070	2.460	2.465	2.495	3.687	2.603	2.717	3.504	3.759	2.468	3.529	2.606

5.3.3. Molecular dynamics (MD) geometrically optimised Ag-nanospheres + fibrin protein corona complexes

Geometrically optimised structures of Ag(19)+1-fibrin, Ag(38)+1-fibrin, Ag(55)+1-fibrin, and Ag(79)+1-fibrin corona complexes were generated using the same procedure described in sub-section 4.3.3, for Au-nanosphere related corona complexes. Subsequently, all considered models are displayed sequentially in Figure 5.4.

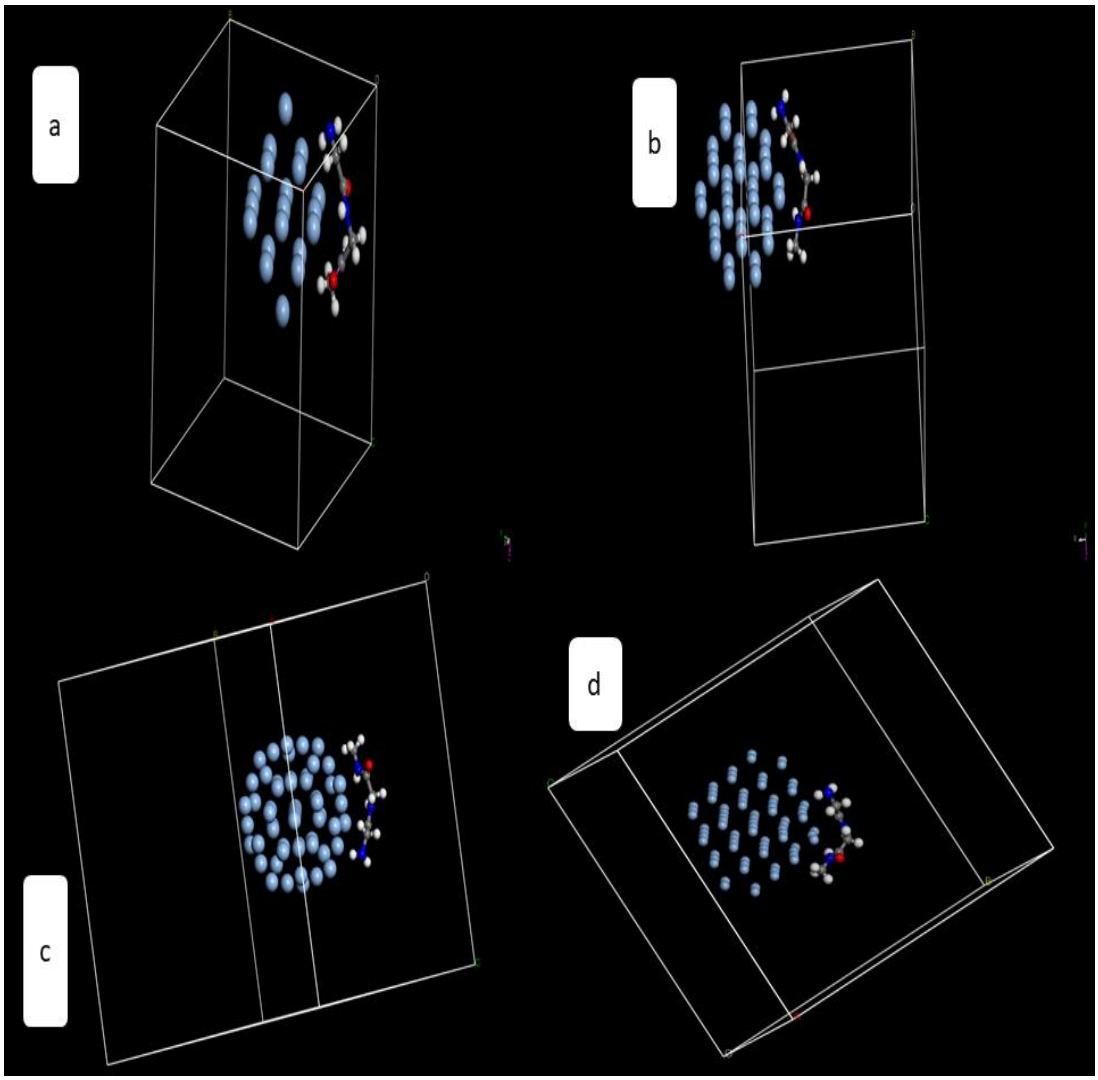

Figure 5.4: The MD simulated geometrically optimised structure of 1-fibrin molecule adsorbed onto Ag(19), Ag(38), Ag(55), and Ag(79) nanospheres.

5.3.3.1. Radial distribution functions of Ag(19) + 1-fibrin, Ag(38) + 1-fibrin, Ag(55) + 1-fibrin, and Ag(79) + 1-fibrin corona complexes

Plotted RDFs of Ag(19) + 1-fibrin, Ag(38) + 1-fibrin, Ag(55) + 1-fibrin, and Ag(79) + 1-fibrin coronas are shown in Figures 5.5 – 5.8. From the peak positions of the radial pair distribution functions, the most probable distances among the atoms can be accumulated. Such distances could be quantified into possible bond lengths between fibrin functional groups atoms and the Ag-nanospheres. Table 5.3 displays the 1st (r_1) and 2nd (r_2) nearest neighbour atom distances for Ag(19)+1-fibrin, Ag(38)+1-fibrin, Ag(55))+1-fibrin and Ag(79))+1-fibrin corona complexes.

With great contention, in all the Ag-H, Ag-C, Ag-N, and Ag-O possible bonding pairs, the Ag-H bonds are still having the shortest distances. The Ag-H predicted bond lengths with respect to Ag(19)+1-fibrin, Ag(38)+1-fibrin, Ag(55)+1-fibrin and Ag(79)+1-fibrin coronas are 2.11, 2.45, 2.57, and 2.47 Å respectively. These values are in good agreement with the literature-based values on the studies by Chakroborty *et al.* [395].

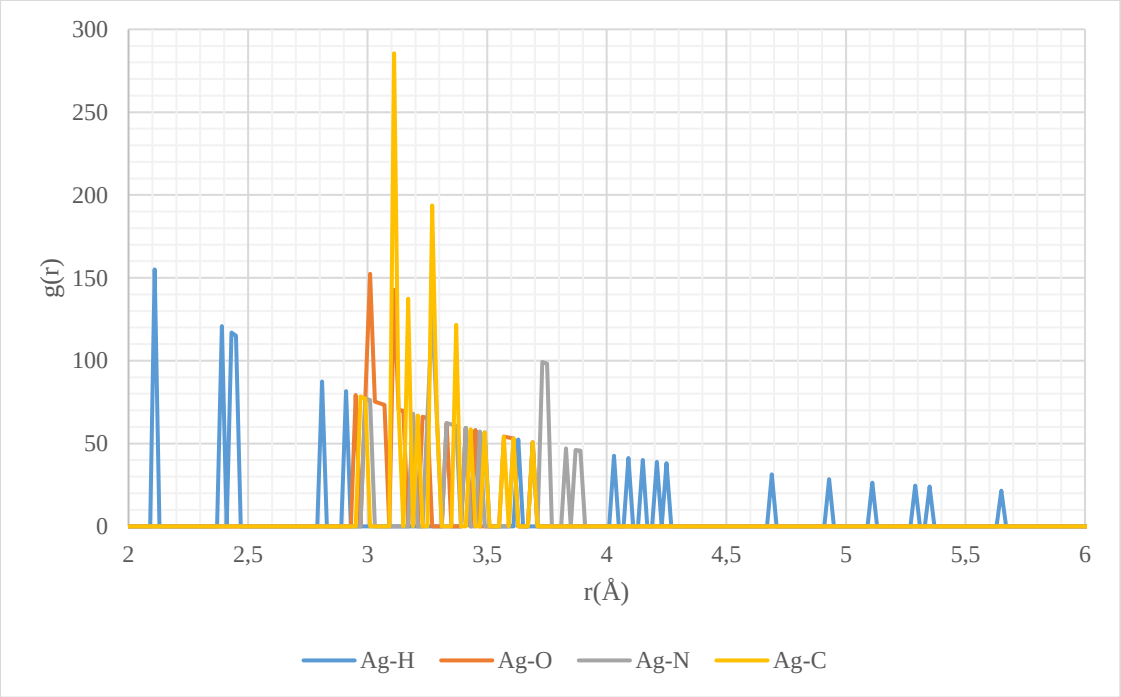

Figure 5.5: Radial distribution functions based on Ag(19) +1-fibrin corona.

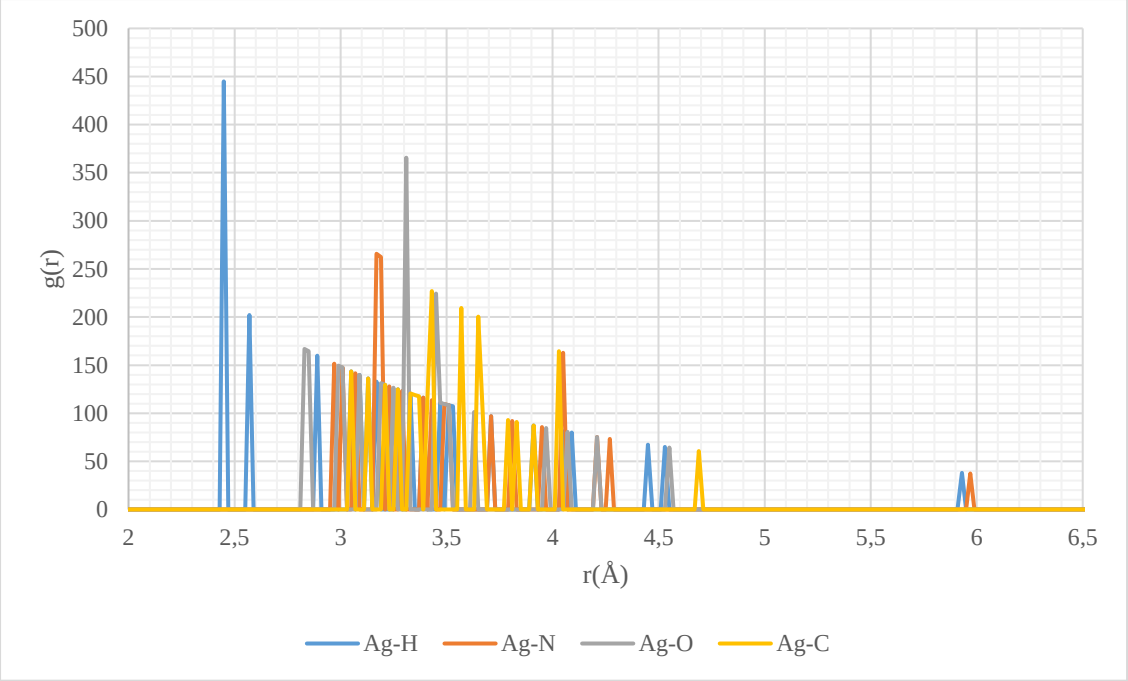

Figure 5.6: Radial distribution functions based on Ag(38) +1-fibrin corona.

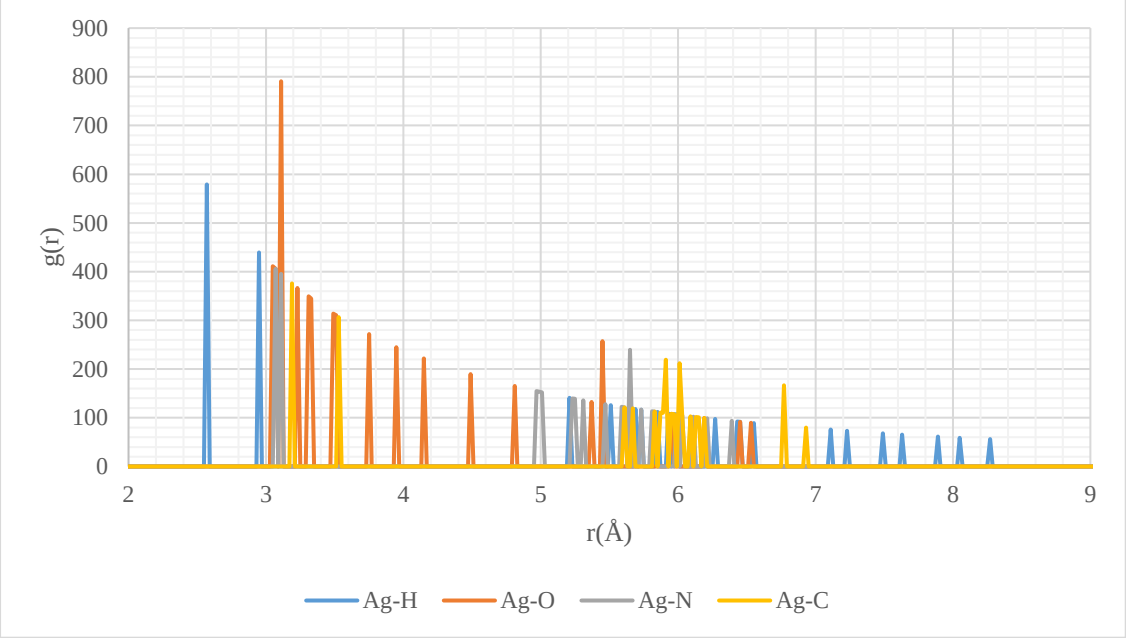

Figure 5.7: Radial distribution functions based on Ag(55) +1-fibrin corona.

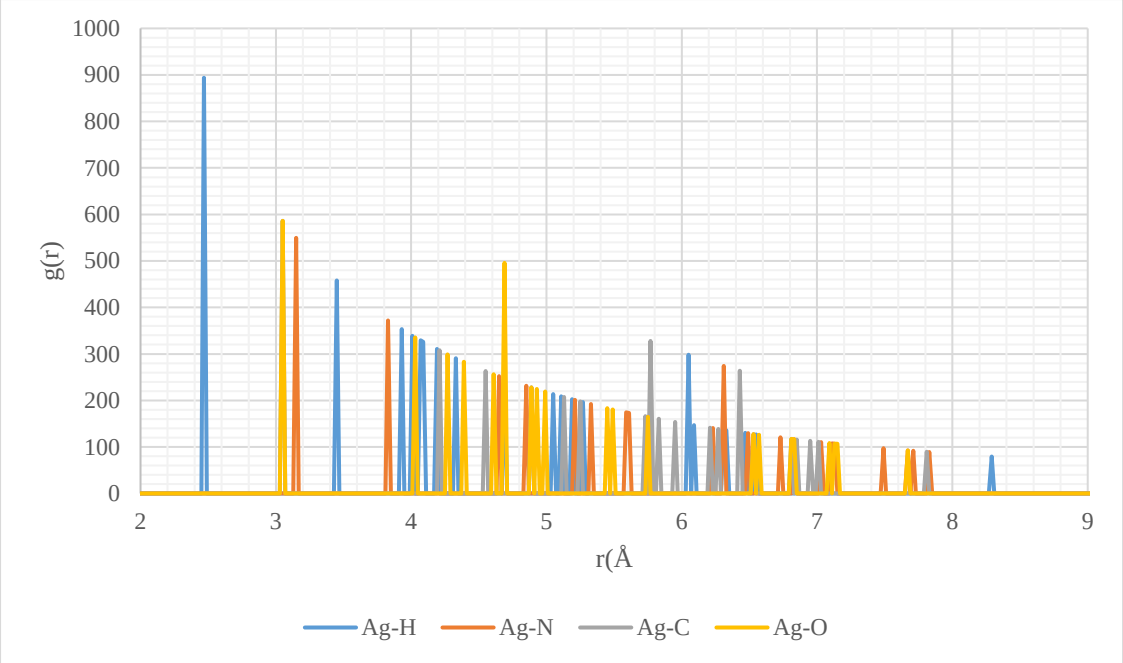

Figure 5.8: Radial distribution functions based on Ag(79) +1-fibrin corona.

Table 5.3: The 1st (r_1) and 2nd (r_2) nearest neighbour atom distances as per RDFs on Ag(19) + 1-fibrin, Ag(38) + 1-fibrin, Ag(55) + 1-fibrin, Ag(79) + 1-fibrin corona complexes.

	Ag(19) + 1-fibrin		Ag(38) + 1-fibrin		Ag(55) + 1-fibrin		Ag(79) + 1-fibrin	
	r_1 (Å)	r_2(Å)	r_1(Å)	r_2 (Å)	r_1 (Å)	r_2(Å)	r_1(Å)	r_2 (Å)
Ag-O	3.01	3.11	3.31	3.45	3.11	3.05	3.05	4.69
Ag-C	3.11	3.27	3.43	3.57	3.19	3.53	3.05	5.77
Ag-H	2.11	2.39	2.45	2.57	2.57	2.95	2.470	3.45
Ag-N	3.27	3.73	3.17	3.19	3.07	3.11	3.15	3.83

5.3.3.2. Mean square displacement of Ag(19) + 1-fibrin, Ag(38) + 1-fibrin, Ag(55) + 1-fibrin, and Ag(79) + 1-fibrin corona complexes relative to Ag, H, C, N and O atoms.

In a similar manner to the one subjected to the Au-nanospheres in chapter 4, possible mobility of the Ag, H, C, N, and O atoms in the Ag(19)+1-fibrin, Ag(38)+1-fibrin, Ag(55)+1-fibrin and Ag(79)+1-fibrin coronas was also modelled using the mean square displacement (MSD) graphs. Such acquired results are elaborated in Figure 5.9. The plots provide linear relation on the MSD against time. The calculated diffusion coefficient constants (*D*) are listed in Table 5.4. According to Figure 5.9, the diffusion of H, C, N, and O atoms in the Ag(19), Ag(38), Ag(55) and Ag(79) nanospheres is spontaneous as the diffusion constants of all these atoms are greater than that of Ag atoms within a given Ag-nanosphere. Specifically, the N atoms exhibits the highest mobility in the Ag(19)+1-fibrin with reference to other atoms. Also, for Ag(38)+1-fibrin, the H atoms exhibits the highest mobility. Moreover, in the case of Ag(55))+1-fibrin and Ag(79))+1-fibrin, the O atoms tend to exhibit highest mobility as compared to other atoms (i.e. H, C, and N).

Table 5.4: Diffusion constants (*D*) on 1-fibrin molecule adsorbed onto Ag(19), Ag(38), Ag(55), and Ag(79) nanospheres.

		D of 1-fibrin +			
		Ag(19) ($Å^2$/ps)	Ag(38) ($Å^2$/ps)	Ag(55) ($Å^2$/ps)	Ag(79) ($Å^2$/ps)
Atoms	H	0.0338	0.4139	0.3639	0.5968
	C	0.0249	0.3836	0.3716	0.6206
	N	0.0552	0.3893	0.3387	0.5669
	O	0.0352	0.3520	0.3798	0.7124
	Ag	0.0108	0.1061	0.2088	0.2789

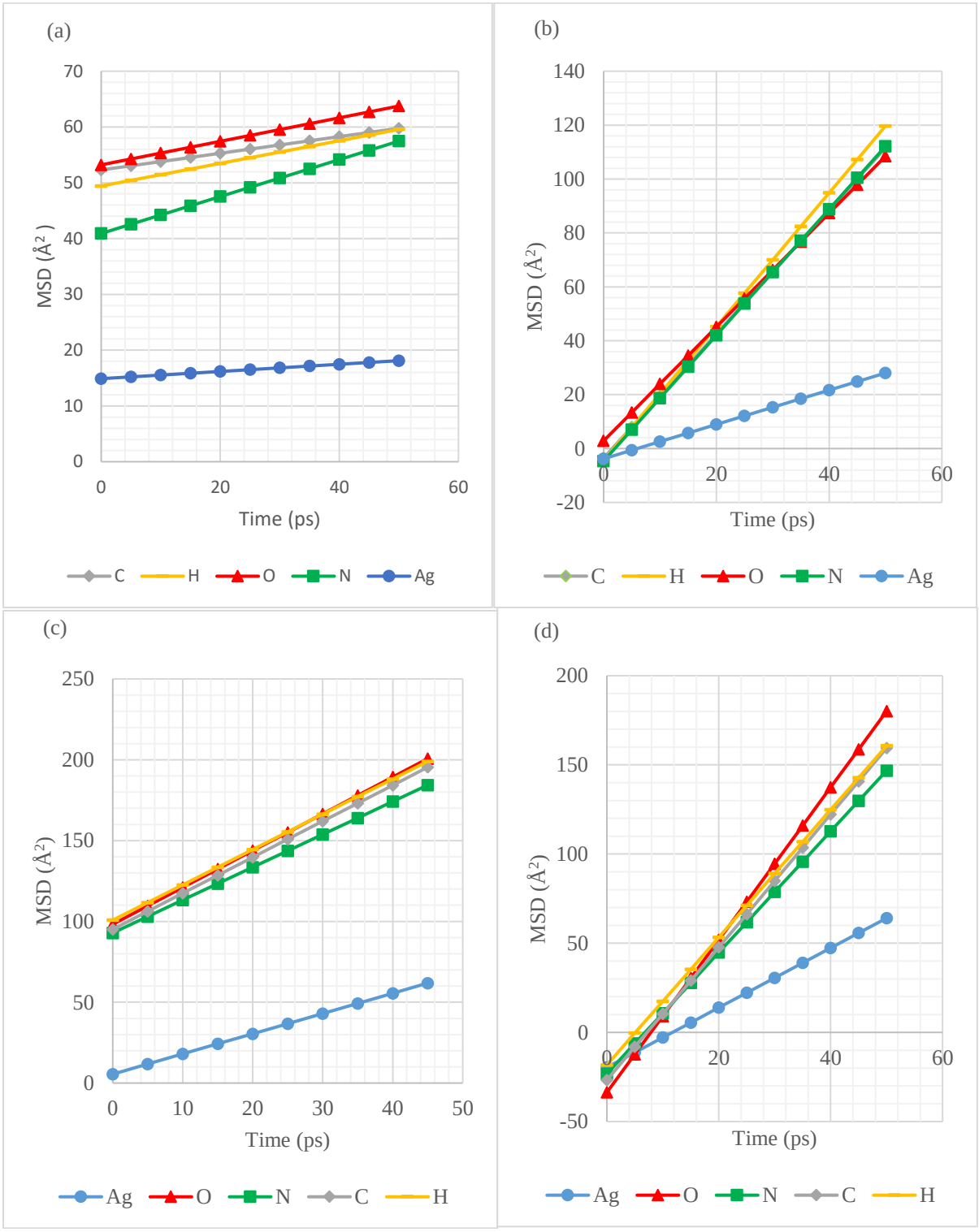

Figure 5.9: Mean Square Displacement (MSD) plots of (a) Ag(19) + 1-fibrin, (b) Ag(38) + 1-fibrin, (c) Ag(55) + 1-fibrin, (d) Ag(79) + 1-fibrin coronas relative to Ag, H, C, N, and O atoms.

5.3.4. Mulliken charges analysis on Ag(55)-nanosphere + fibrin protein corona complexes.

Mulliken charges with respect to carbon atoms of 1-, 2-, 3-, and 4-fibrin molecules before and those of Ag(55)+1-fibrin, Ag(55)+2-fibrin, Ag(55)+3-fibrin, and Ag(55)+4-fibrin coronas after adsorption/docking were also computed. All collected data is laid out in Table 5.5. A choice of Ag(55) relies on what was observed with the Au-nanospheres + n-fibrin in the preceding chapter. Detailed discussion on this choice of population analysis and how charge transfer is assumed can be found in sub-section 4.3.4 of the preceding chapter 4. The negative charge values of 1-, 2-, 3-, and 4-fibrin carbon atoms before adsorption enhances their negative values after adsorption due to their secondary interaction with acceptor atoms such as H in the CH_2 or CH_3 group. In a similar way, the positively charged values before adsorption uphold less positive values after adsorption due to their secondary bonding with donor atoms such as O and N in the C=O and NH_2 or NH_3 group, respectively.

For further validation with reference to Table 5.5 (focusing mainly on 1-fibrin since the same behaviour of charge is observed for all other 2, 3 and 4-fibrins), before adsorption a negative charge value of -0.173 (in Units of $\boldsymbol{e}$) for C1 atom was observed and upon adsorption an enhanced or increased negative value of -0.243 was noted. It can be articulated that in the adsorption process, the negative charge of Ag-nanospheres is transferred by the fibrin bonding atom and charge conservation to the first carbon (C1) of the fibrin molecule enhancing or increasing the negativity value of the C1 atom. As already stated in Chapter 4, considering the Coulomb's law of charges, this leads to second (C2) and third (C3) carbon atoms of the fibrin also acquiring less positive and extra negative charges sequentially as observed in Table 5.5. For clarification, still on Table 5.5, the positive charge of 0.401 (in Units of $\boldsymbol{e}$) was

observed for C2 atom before adsorption and later upon adsorption a less positive charge of 0.384 was observed. Onwards, a negative charge value of -0.153 (in Units of $\boldsymbol{e}$) was observed for C3 atom before adsorption and upon adsorption an increased or enhanced negative charge of -0.200 was visible.

Consequently, the same behaviour or distribution of charge before and after adsorption as in Table 5.5 for 1, 2, 3, and 4-fibrin molecules adsorption onto Ag-nanosphere with 55 atoms was observed for 1, 2, 3, and 4-fibrin molecules before and after adsorption onto Au-nanosphere with 55 atoms as in Table 4.6. This is not surprising as both gold (Au) and silver (Ag) belong to the same group IB precious metals.

Table 5.5: Carbon (C) atoms Mulliken charges (in Units of $\boldsymbol{e}$) for 1, 2, 3, and 4-fibrin molecules before and after adsorption onto Ag-nanosphere with 55 atoms.

1-fibrin			2-fibrin		3-fibrin		4-fibrin	
	Before	After	Before	After	Before	After	Before	After
C1	-0.173	-0.243	-0.171	-0.233	-0.169	-0.230	-0.166	-0.217
C2	0.401	0.384	0.428	0.417	0.426	0.422	0.406	0.384
C3	-0.153	-0.200	-0.160	-0.206	-0.170	-0.224	-0.156	-0.202

5.3.5 Radius of gyration analysis of Ag-nanospheres + fibrin protein corona complexes.

As in chapter 4, section 4.3.5, the stability and possible changes in average molecular configuration of the fibrin molecules adsorbed onto Ag-nanospheres were also monitored using the radius of gyration (R_g) approach [378-380].

Similarly, to investigate the distribution of the fibrin molecules around the Ag-nanospheres surface, the radius of gyration was also evaluated for Ag(19) + 1-fibrin, Ag(38) + 1-fibrin, Ag(55) + 1-fibrin and Ag(79) + 1-fibrin corona complexes as indicated in Figure 5.10. Built on sub-section 4.3.5 substantiation, only 1-fibrin strand onto Ag-nanospheres coronas have been investigated. The same behaviour of radius of gyration for Au-nanospheres+1-fibrin molecules complexes as in Chapter 4, section 4.3.5 was observed in this section whereby, Ag(19) +1-fibrin corona possesses the largest radius of gyration followed by Ag(38) + 1-fibrin. Meanwhile, Ag(79) + 1-fibrin complex acquired the lowest radius of gyration out of all the complexes analysed.

Correspondingly, with reference to Ag(19) +1-fibrin, major fluctuations of the radius of gyration about 0.126 Å can be observed as the time spans 0 - 100 ps. Advancing on, Ag(38) + 1-fibrin and Ag(55) + 1-fibrin possesses some less fluctuations with a less decrease in their radius of gyration about 0.0695 and 0.0493 Å respectively towards about 0.0690 and 0.0464 Å, as the time spans 0 - 100 ps. Lastly, Ag(79) + 1-fibrin corona exhibits an almost non-fluctuating radius of gyration at about 0.034 Å throughout the time span 0 - 100 ps.

Taking into account that a higher R_g corresponds to less tight packing while a lower R_g suggests a tighter packing [382]. In this moment, a tighter packing is observed for Ag(38) + 1-fibrin, Ag(55) + 1-fibrin and Ag(79) + 1-fibrin corona as compared to Ag(19)

+ 1-fibrin corona which shows a less tight packing with reference to Figure 5.10. Less tight packing of Ag(19) + 1-fibrin signifies soft corona. Meanwhile, a tighter packing signifies hard corona in the sequences of Ag(79) + 1-fibrin > Ag(55) + 1-fibrin > Ag(38) + 1-fibrin .

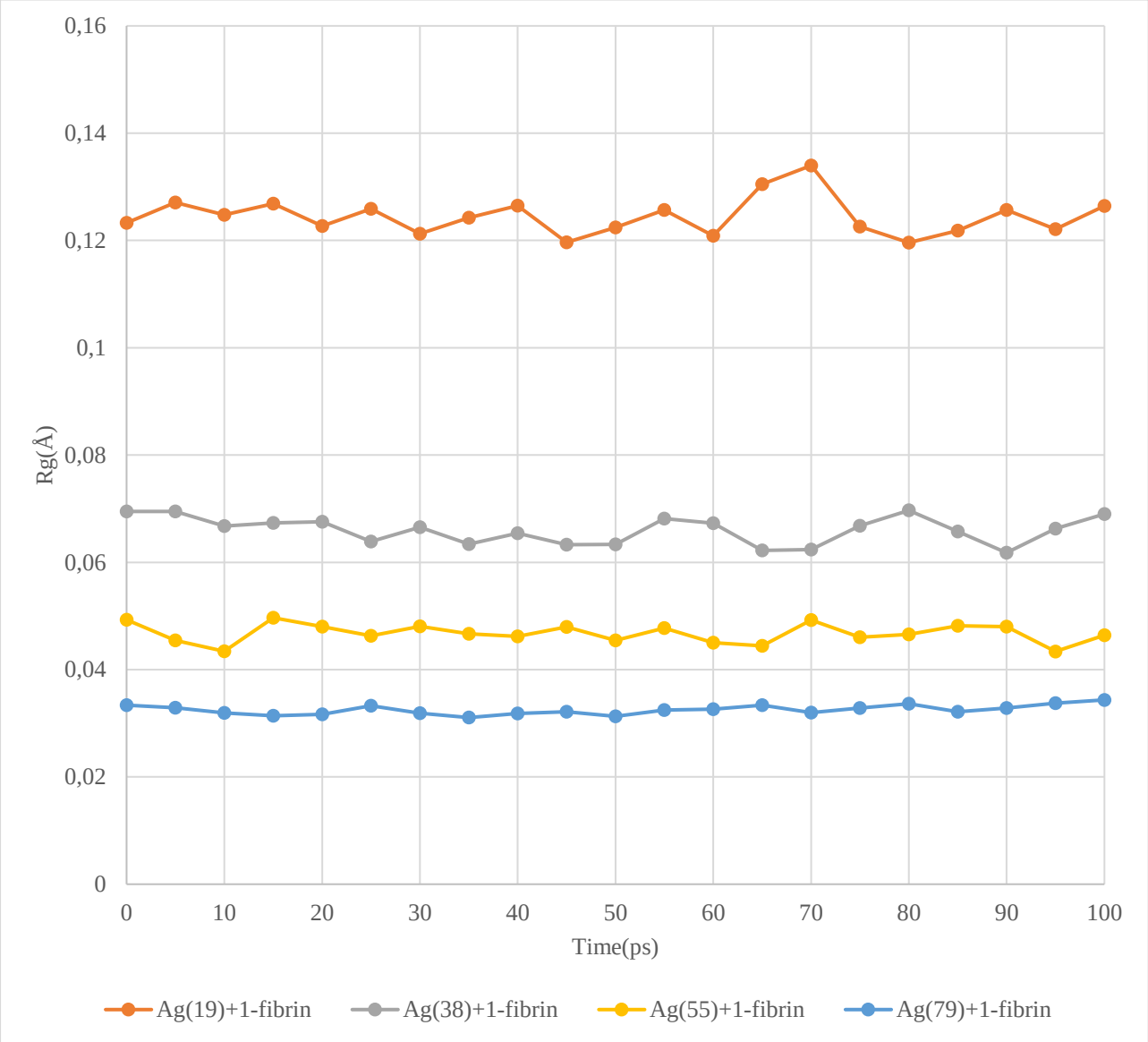

Figure 5.10: Radius of gyration (R_g) based on Ag(19) + 1-fibrin, Ag(38) + 1-fibrin, Ag(55) + 1-fibrin, and Ag(79) + 1-fibrin corona complexes.

5.4. Conclusion

Interestingly, with regard to nanoparticle-protein corona formation, all the 1, 2, 3 and 4-fibrin molecules interactions with Ag-nanospheres modelled provide a possible formation of the Ag-nanosphere – fibrin corona complex. This is additionally validated or verified by the negative adsorption energies acquired for all the modelled configurations. The complex interaction of Ag(55) nanospheres with fibrin molecules has been established to be more energetically stable as compared to all other nanospheres. The concerning exception are the Ag(19) nanospheres with 3 and 4-fibrin chains. Such anomaly was attributed to the compromised nanosphere size relative to the fibrin chain length. Further suggesting that various protein type and size may be associated with a prescribed nanosphere sizes.

The mean square displacement graphs and the calculated diffusion constants suggests that upon adsorption, all the atoms of the fibrin molecules will diffuse easily into the Ag-nanospheres. The H, C, N, and O atoms tends to exhibit different diffusion coefficient constants into the different sizes of Ag-nanospheres. The explored possible bond lengths and the RDFs complement one another, hence in both cases, the Ag-H bond appears to be the lowest or shortest for the structure of 1-fibrin molecule adsorbed onto all the Ag-nanospheres. So, this suggest that the fibrin molecules prefer hydrogen bonding onto the Ag-nanospheres.

Advancing on, the enhanced negative and positive charges experienced through the Mülliken charge distributions before and after adsorption is attributed to the charge transfers which originate from the Ag-nanospheres onto the fibrin molecules. Such charge transfers may alter the original molecules functionality or be the source of immobilisation. In anyway, the radius of gyration implies that a tighter packing

(signifying hard corona) is imminent for the adsorption of fibrin molecules onto Ag(38), Ag(55), and Ag(79) nanospheres with a sequence of Ag(79) > Ag(55) > Ag(38) as compared to Ag(19) which shows a less tight packing (signifying soft corona) due to its small nanosphere size. In all the cases, the overall results of this study also suggest Ag-nanospheres as potential transporters of fibrin protein species into cellular media.

CHAPTER 6

Adsorption studies of fibrin proteins onto Au- and Ag-nanoparticles

6.1. Introduction

When metal nanoparticles infiltrate the physiological fluids environment, some protein molecular species get adsorbed on the nanoparticle's surfaces. In due course, the 'nanoparticle+protein corona' complex gets formed [10, 11]. The successful phenomena is accompanied by the loss of the depletion energy of the nanoparticles [12, 13]. Upon the nanoparticle+protein corona formation, possible alteration of the original structure and properties of the nanoparticles may be encountered. In certain instances, when the nanoparticle+protein corona complex reaches the intended inter-cellular site, the nanoparticles and protein molecules detach. Now, depending on whether the original structure and properties of the nanoparticles have changed or not, the secondary nanoparticles may be beneficial or toxic at the target site. It is on this scenario that the actual mechanism of the interaction between the nanoparticles and protein molecules with emphasis on the interface functionality become crucial [14, 15].

Biological activity of various molecules on the associated nanoparticles is highly controlled by the stability of the nanoparticle+protein corona complex. Hence, the binding of protein molecules onto the nanoparticle surface may result in some configurational readjustment, consequently, leading to the alteration of the conformal structure and the functioning of the said protein molecules. Research studies by Galloway, Karlsson and Li *et al.* [17-19] indicate that majority of nanoparticles have the ability of altering the conformational structure of some biological molecular species. This leads to the changed purpose or disordered form of the expected protein

species function. Such a disordered effect on a given species outcome can be classified as nano-toxicity [17-19].

Zaved and Anupam's [3] article points out that important determinants playing a role to configurational alteration in the protein molecules includes size, kind of the nanomaterial, surface charge as well as the shape of the nanomaterial involved. As the functionality of different protein molecular species is based on their conformational structure, notable changes in this may lead to resistant on expected functional purpose which may as well be referred to as toxicity [3]. The fact that the functionality (activity) of protein molecules is associated with its conformational structure is adopted. Subsequently, interaction of nanoparticles with protein molecules may not alter the protein molecule's original conformational structure. Otherwise, the origins of toxicity on nanoparticle+protein corona complex remains unclarified. Recent studies by Zhang *et al*. [20] suggest oxidative stress as being the possible main source of nanoparticle's toxicity.

A limited understanding and astounding gap on the physio-chemical properties of metal nanoparticles in the physiological cell environment necessitates further related studies [25]. As such, clinical transferal and successfulness of nanoparticles might rely on essential interactions with protein molecules, and other biomolecules cells in the human or even other animal cells body. A study on the nanoparticle-protein interactions could assist in clarifying nanoparticle intercellular interactions, which in turn may lead to administering safe nanomedicines.

In this chapter, different spherical sizes of Au- and Ag-nanoparticles have been synthesised and thereafter incubated with fibrin protein species samples to investigate a possible mechanism of how the fibrin protein molecules get adsorbed onto these

nanoparticles. Ultraviolet Visible (UV-vis), Fourier Transmittance Infrared (FTIR), Transmission Electron Microscopy (TEM), and Zeta Potential (ZP) spectroscopies were utilised to characterise these Au/Ag-nanoparticles – fibrin protein-based adsorption arrangements.

6.2. Results and discussion

6.2.1. XRD of Au- and Ag-nanoparticles

XRD was used for the analysis of structural properties of Au- and Ag-nanoparticles. XRD plots of Au- and Ag-nanoparticles are shown in Figures 6.1 and 6.2 respectively. In both cases, XRD diffraction peaks exhibit face centred cubic (FCC) structured nanoparticles. Given that all studied Au-nanoparticles spherical diameter sizes were prepared using only the seeded growth method, only one XRD plot is considered here in Figure 6.1. The peak patterns correspond to the Bragg reflections which can only be indexed on the basis of FCC gold nanocrystals. Characterised samples possess diffraction peaks belonging to 2θ values of 38.184, 44.392, 64.576, and 77.547° which respectively correspond to (100), (200), (220), and (311) Bragg planes (JCPDS No. 36-1451). Similar studies by Rattan *et al*. [396] where gold nanoparticles were synthesised using wet chemical and green chemistry approach revealed similar results. The particle diameter of the characterised Au-nanoparticles samples can be calculated using the Debye-Scherrer equation [318, 397]. A value of ±18.14 nm of the particle diameter which corresponds to the TEM average diameter presented in Figure 6.4 was obtained. Such mode of analysis of results is relatable to the study conducted by Yang *et al.* [398] in which Au-nanoparticles were prepared through the utilisation of sodium citrate method or Turkevich method.

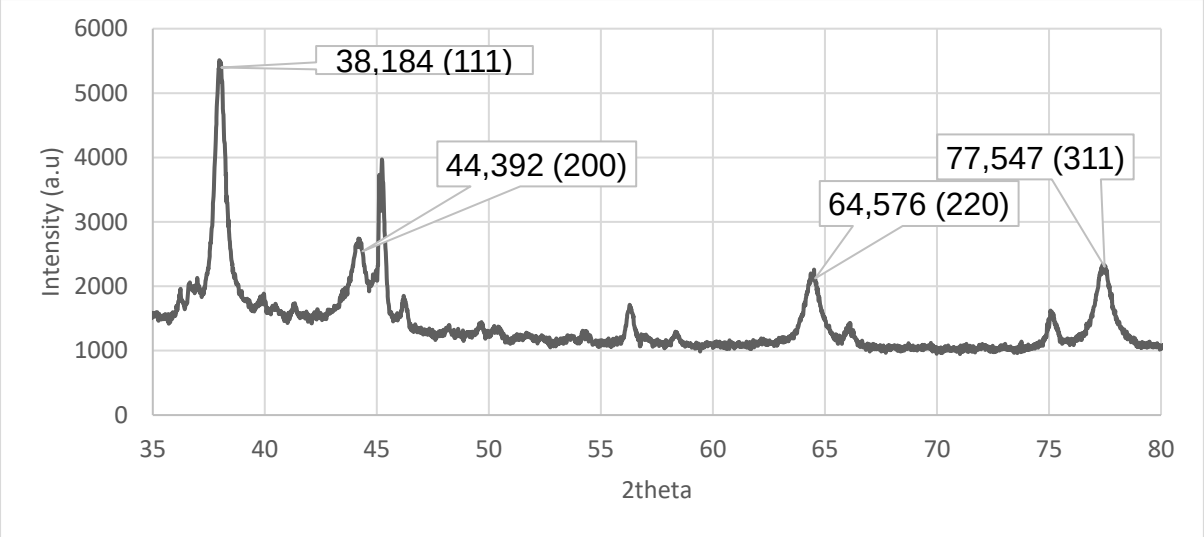

Figure 6.1: XRD spectral of Au-nanoparticles (AuNPs).

In the case of Ag-nanoparticles, the XRD peak patterns in Figure 6.2 correspond to Bragg reflections that may be indexed on the basis of the face-centred cubic structure of silver. It can be confirmed that acquired Ag-nanoparticles were in nanocrystals form, as evidenced by the peaks at 2θ values of 38. 116 °, 44.277 °, 64.426 °, and 77.472 ° corresponding to (111), (200), (220), and (311) Bragg's planes respectively. The results confirm that the synthesised Ag-nanoparticles are of FCC symmetry. Studies by Shameli *et al*. [397] where silver nanoparticles were synthesised through green biosynthesis using Curcuma longa tuber powder concurs with our results. Crystallite size calculation produced a nanoparticle diameter size of about ±24.34 nm. This value endorses average diameter size acquired in Figure 6.9, in accordance with the TEM micrographs. This mode of analysis of results is comparable with the mode of analysis of silver nanoparticles synthesised via Munro's approach as outlined by Tian *et al*. [399].

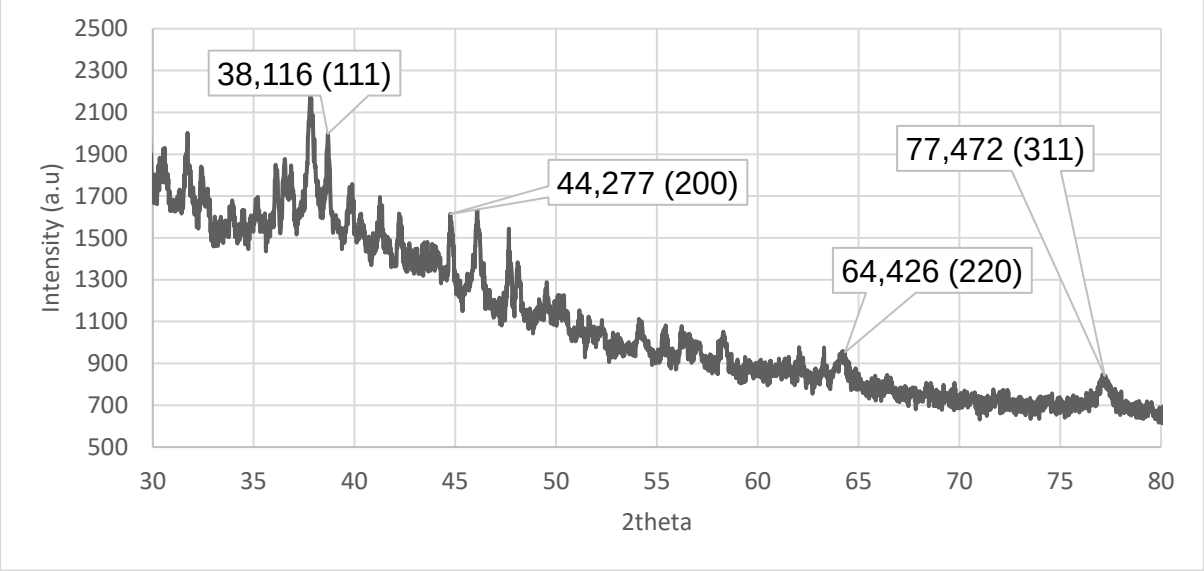

Figure 6.2: XRD spectral of Ag-nanoparticles (AgNPs).

6.2.2. TEM characterisation of Au- and Ag-nanoparticles

Subsequently, TEM was used to obtain images of Au- and Ag-nanoparticles so as to analyse and reflect on their sizes and morphology [336, 337]. In both Au- and Ag-nanoparticles, ultra-small nanoparticles with very little heterogeneous size distributions were recorded as displayed in Figures 6.3 – 6.9. In order to quantify accumulated Au- and Ag-nanoparticles samples micrographs, size distributions were also evaluated using the accompanying histogram plots approach. Different focal resolutions were also applied to further justify acquired sizes and morphology of the Au- and Ag-nanoparticles.

TEM morphology and characterisation of the Au-nanoparticles samples is exhibited in Figures 6.3 – 6.6. Each of the figures consist of two different TEM resolutions ((a) and (b)) together with a histogram plot (c). For instance, Figure 6.3(a) shows the Au-nanoparticles at a resolution of 100 nm while Figure 6.3(b) shows the same sample at a resolution of 20 nm. In both resolutions, crystalline, spherical samples of Au-nanoparticles can be observed in disorderly aggregates. Still on the Au-nanoparticles,

the corresponding TEM histogram data provides average spherical diameter sizes of 11, 18, 45 and 50 nm respectively, as shown in Figures 6.3(c) – 6.6(c). Bastús *et al*. [317] has further shown the growth and possibility of different sizes of AuNPs through TEM in which crystalline spherical samples of Au-nanoparticles can be observed. TEM micrographs along with their histogram graphs by Torres-Díaz *et al.* [352] confirm that Au-nanoparticles are expected from the sodium citrate reduction method with a possible wide range of nanoparticle distribution, which concurs with our results.

Similarly, average diameter sizes of 12, 14 and 26 nm of Ag-nanoparticles were obtained as displayed in Figures 6.7 (c) – 6.9 (c) respectively. The wide range distribution was observed for larger nanoparticles in some of the TEM images as shown in the histogram graphs. This is attributed to the increase in diameter of the nanoparticles with some few small nanoparticles in the background. Such a behaviour can be expected as the purpose of the capping agent (sodium citrate) is to congregate smaller nanoparticles into a consolidated larger sized nanoparticle. Intrinsically, the capping agent is necessary in synthesis process in order to promote enhanced nanoparticle sizes growth through aggregation. Ranoszek-Soliwoda *et al.* [400] further reported analogous TEM micrographs and histogram graphs which show that individual Ag-nanoparticles portray irregular scattered arrangement after seeded sodium citrate assisted synthesis.

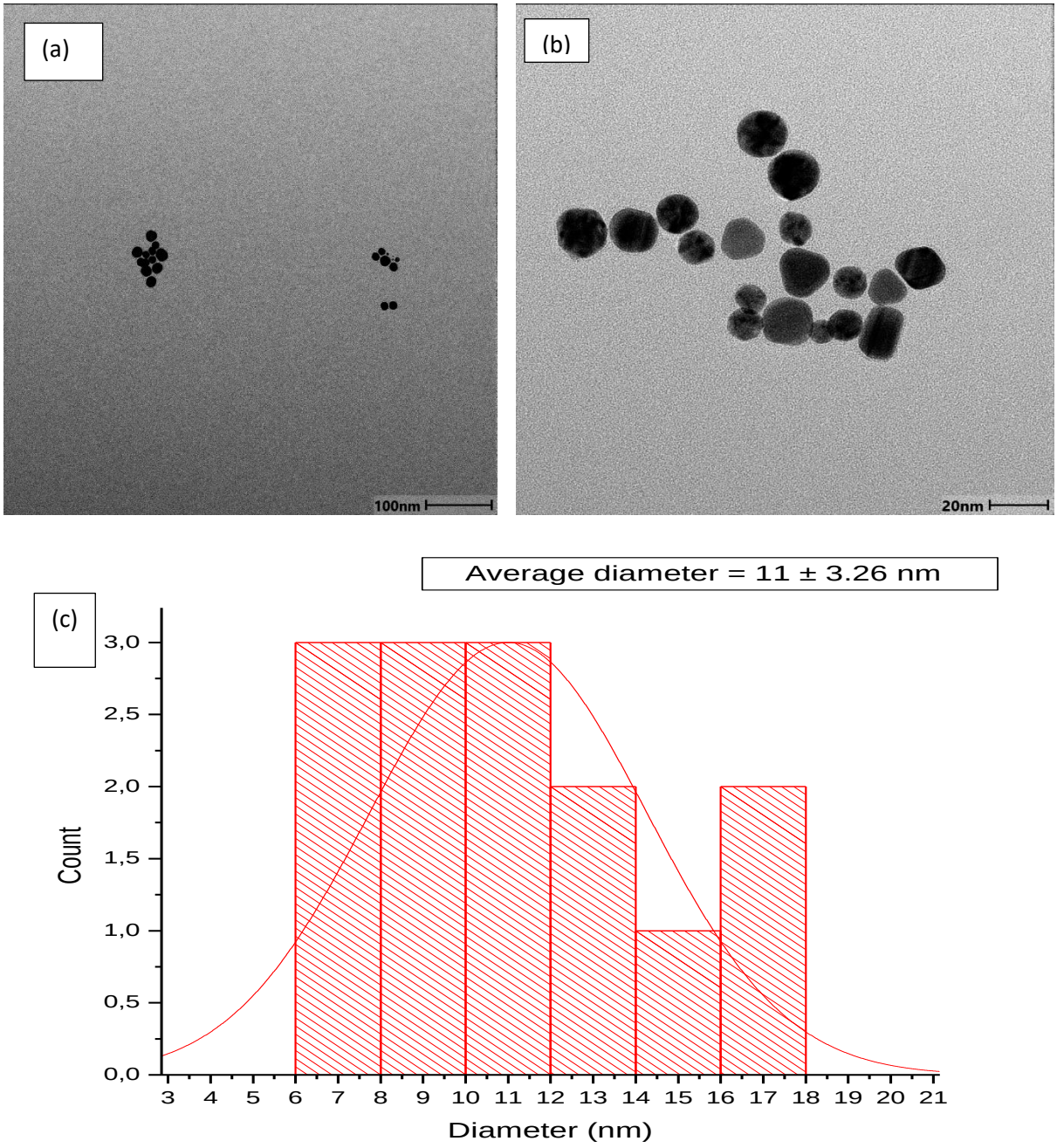

Figure 6.3: TEM profiles, (a) 100 nm and (b) 20 nm resolutions and (c) histogram graph of Au-nanoparticles (AuNPs) with an average diameter of 11 nm.

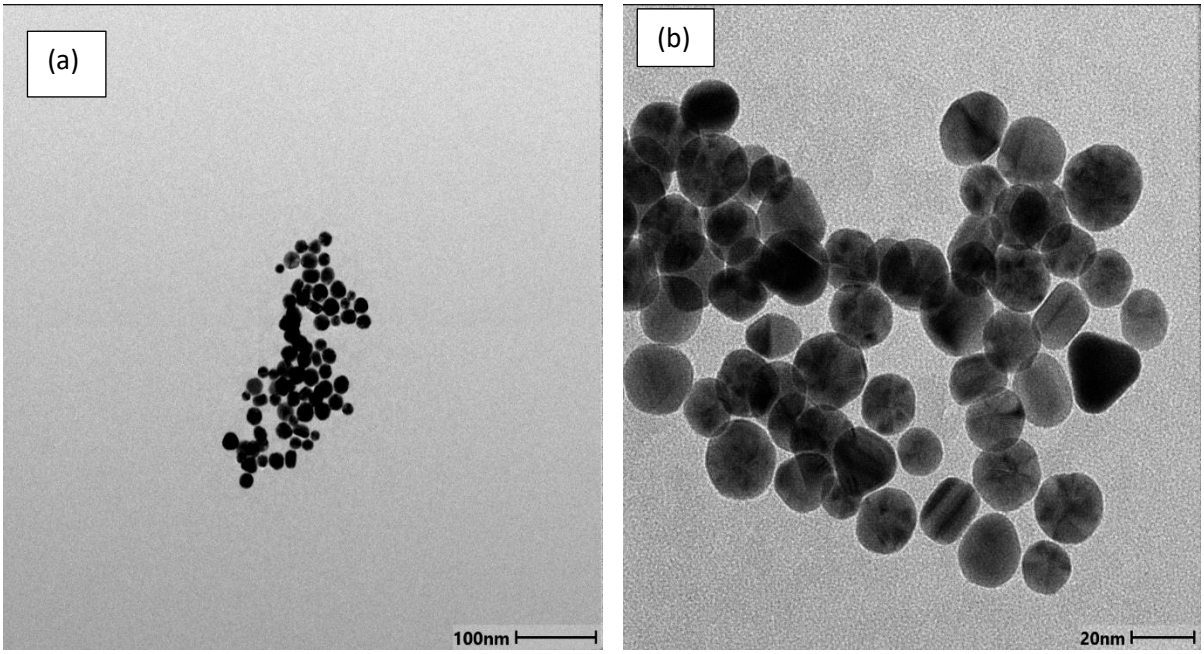

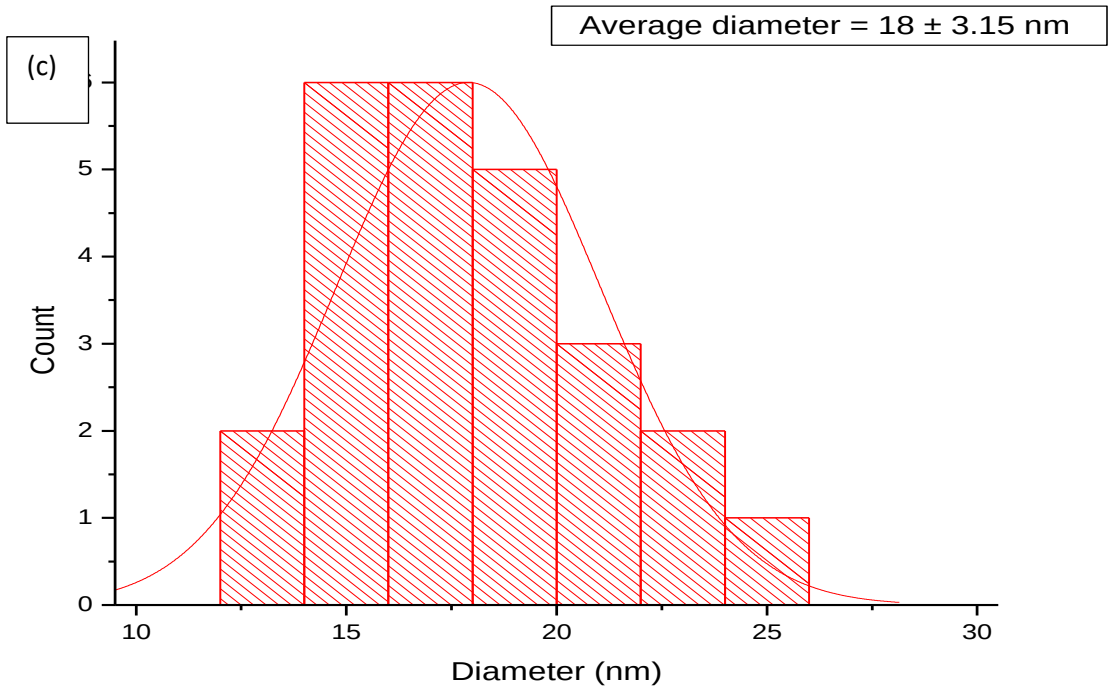

Figure 6.4: TEM profiles, (a) 100 nm and (b) 20 nm resolutions and (c) histogram graph of Au-nanoparticles (AuNPs) with an average diameter of 18 nm.

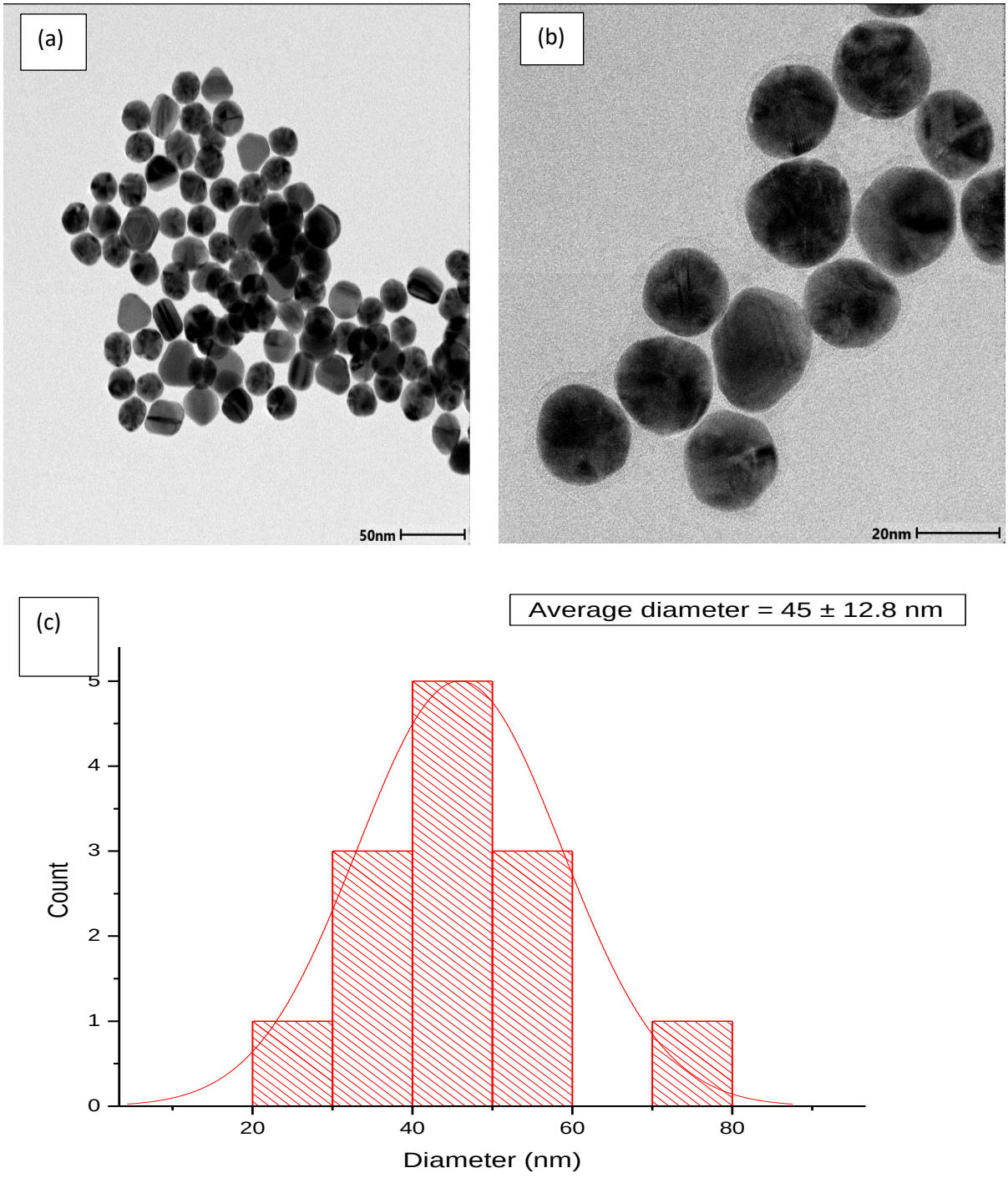

Figure 6.5: TEM profiles, (a) 50 nm and (b) 20 nm resolutions and (c) histogram graph of Au-nanoparticles (AuNPs) with an average diameter of 45 nm.

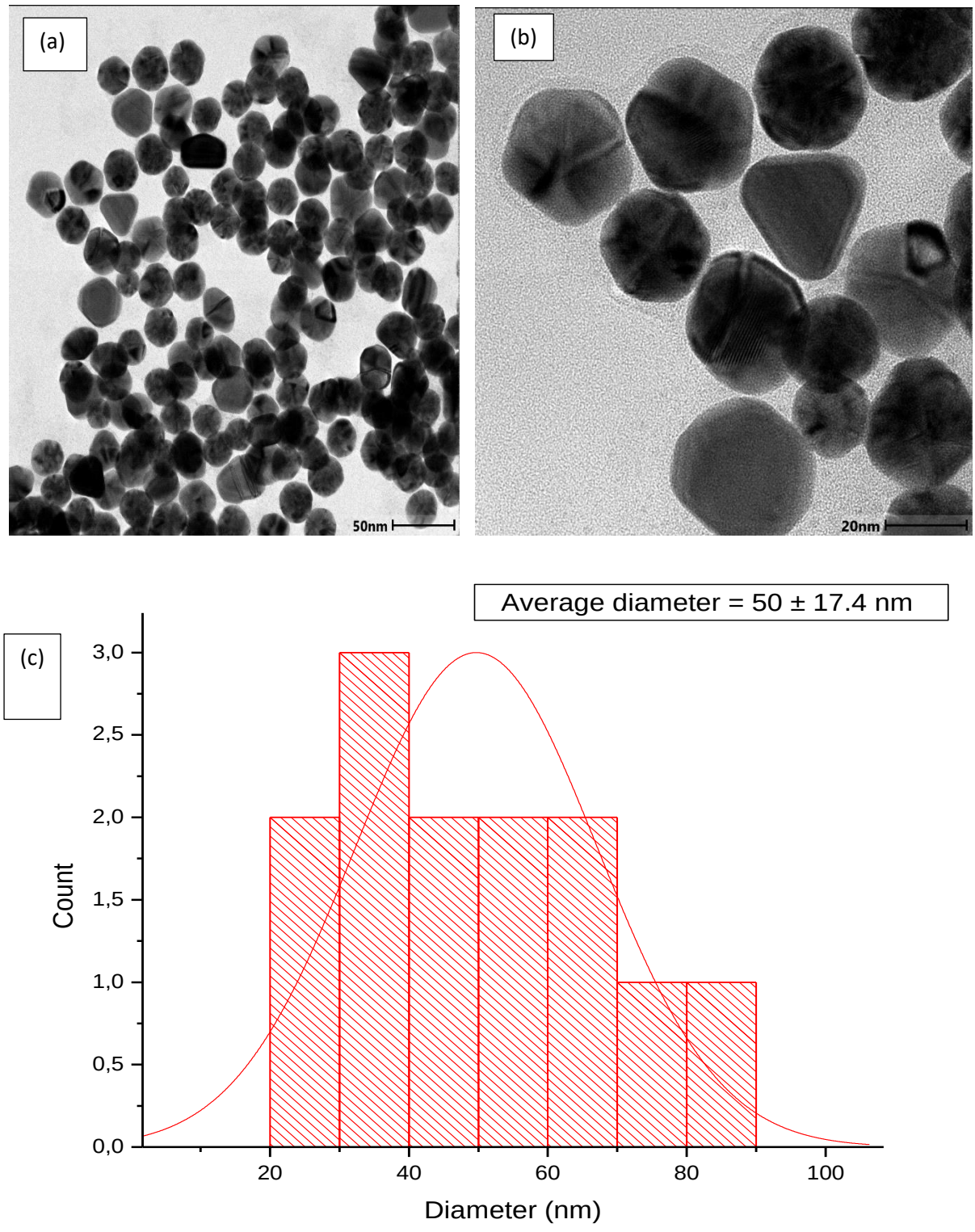

Figure 6.6: TEM profiles, (a) 50 nm and (b) 20 nm resolutions and (c) histogram graph of Au-nanoparticles (AuNPs) with an average diameter of 50 nm.

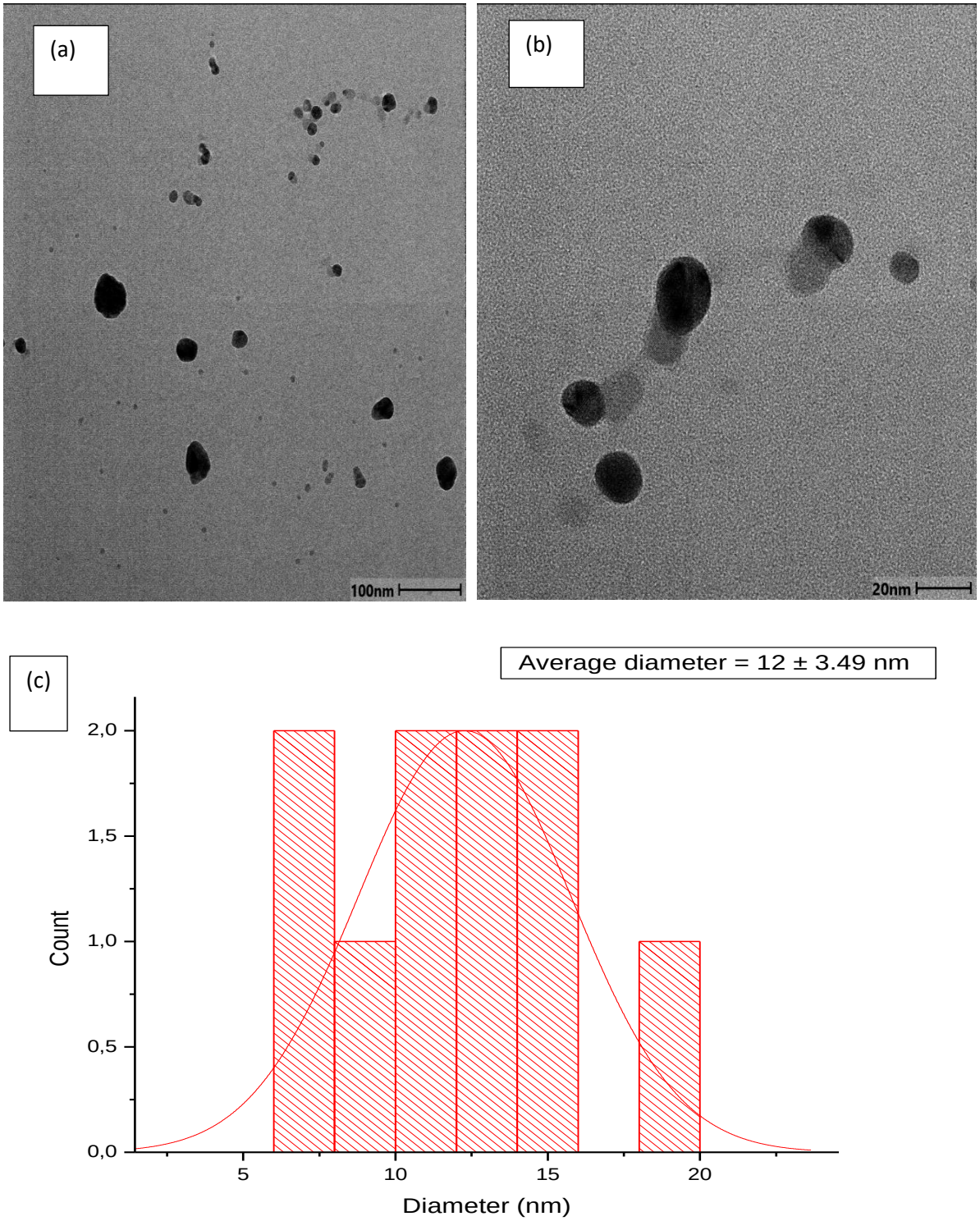

Figure 6.7: TEM profiles, (a) 100 nm and (b) 20 nm resolutions and (c) histogram graph of Ag-nanoparticles (AgNPs) with an average diameter of 12 nm.

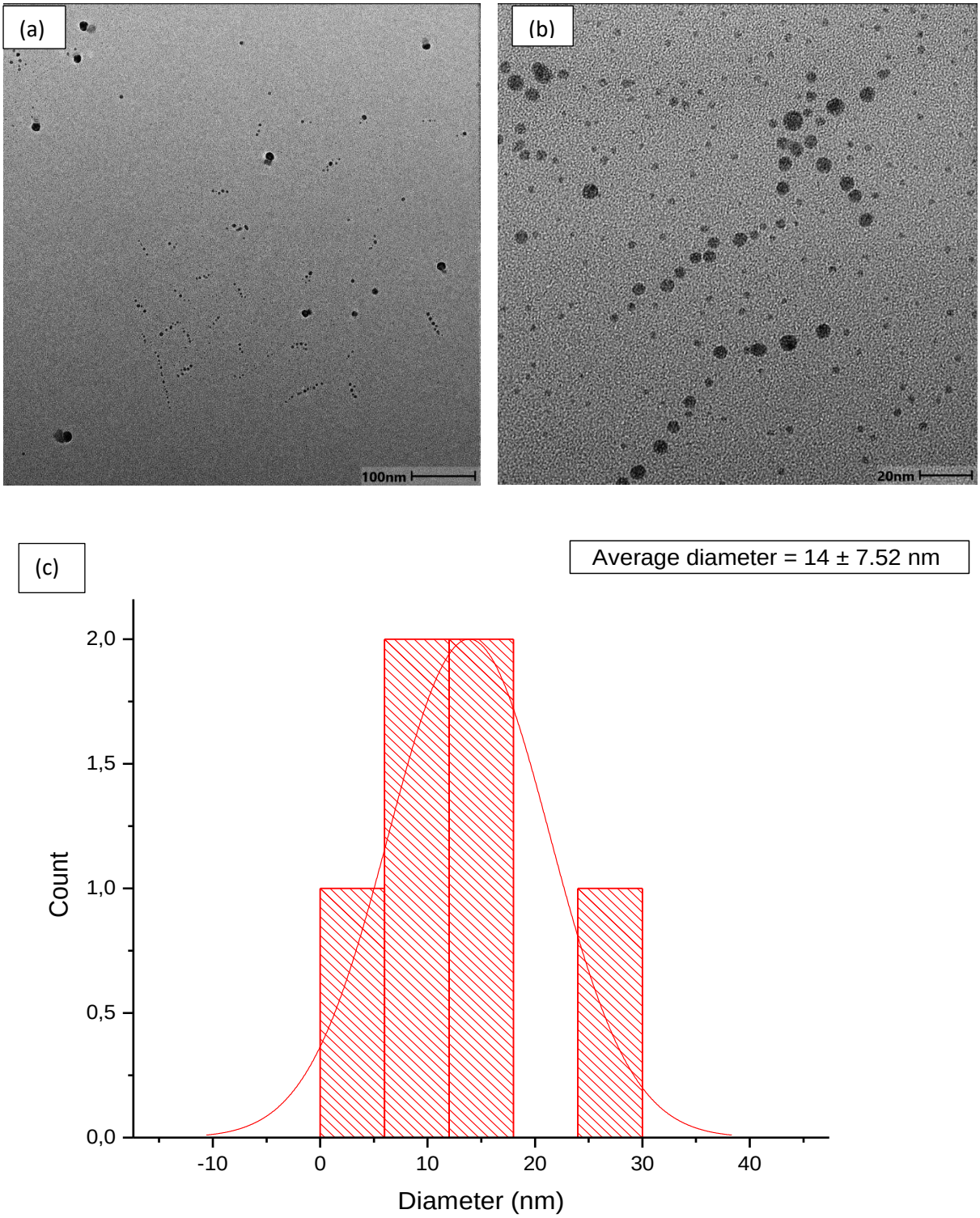

Figure 6.8: TEM profiles, (a) 100 nm and (b) 20 nm resolutions and (c) histogram graph of Ag-nanoparticles (AgNPs) with an average diameter of 14 nm.

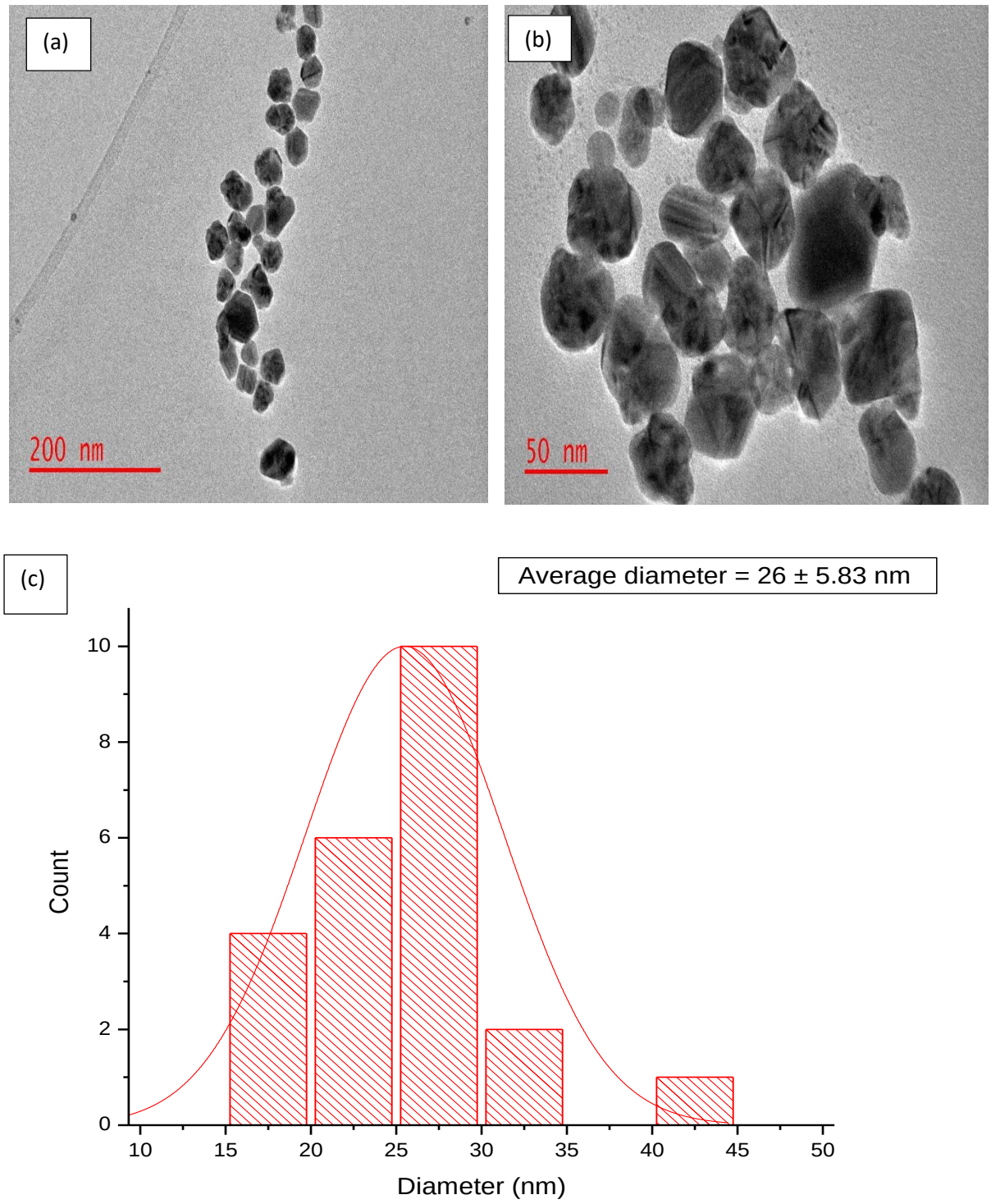

Figure 6.9: TEM profiles, (a) 200 nm and (b) 50 nm resolutions and (c) histogram graph of Ag-nanoparticles (AgNPs) with an average diameter of 26 nm.

6.2.3. UV-vis characterisation of Au- and Ag-nanoparticles

The UV-vis absorption spectroscopy was initiated to examine the optical properties of the Au- and Ag-nanoparticles [336, 337]. The surface plasmon resonance of the UV peak shifts to greater wavelengths as the particle sizes grow [401]. Such a behaviour is in line with the observation of Devi *et al*. [401], on cysteine capped gold nanoparticles, showing single prominent peak in the wavelength region 500 - 600 nm. Acquired UV-vis spectra confirmed that the synthesised Au-nanoparticles are indeed spherical, whilst the peaks shifts reveal the existence of different sizes of synthesised samples [336, 337, 401]. A good demonstration of how different sizes of Au-nanoparticles can be identified using UV-vis peak shifts appears in Figure 6.10(a).

In a similar manner, spherical Ag-nanoparticles are also associated with single peaks in the wavelength range 400 – 500 nm [397]. In accordance with this resonant wavelength range, different Ag-nanoparticle sizes were synthesised, and their related UV-vis peaks are displayed in Figure 6.10(b). Zong *et al*. [402] further certify that well-defined peaks which describe the expected different Ag-nanoparticle sizes can be observed.

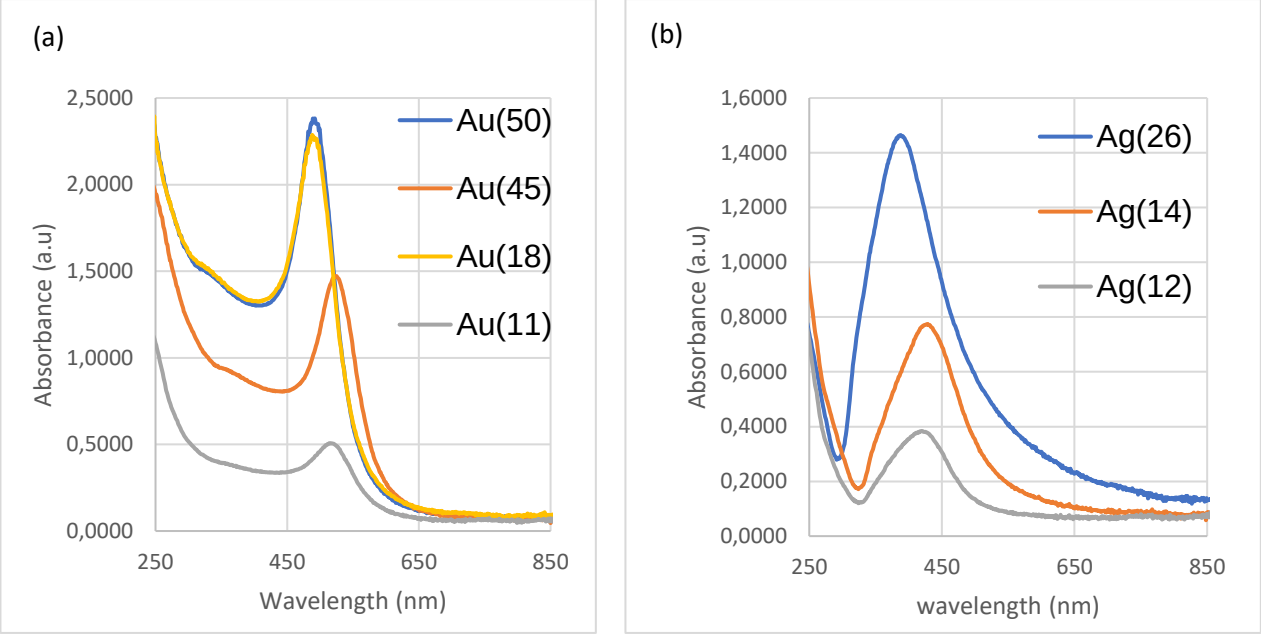

Figure 6.10: UV-vis spectroscopy of (a) Au-nanoparticles (AuNPs); Au(11), Au(18), Au(45), and Au(50) corresponding to spherical diameter sizes 11, 18, 45, and 50 nm and (b) Ag-nanoparticles (AgNPs); Ag(12), Ag(14), and Ag(26) corresponding to spherical diameter sizes 12, 14, and 26 nm.

6.2.4. FTIR of Au- and Ag-nanoparticles

FTIR was identified and utilised to probe functional groups available in the sodium citrate immersed with Au- and Ag-nanoparticles. Figure 6.11 illustrates the FTIR spectra of sodium citrate, Ag-nanoparticles, and Au-nanoparticles respectively. Analysis of this spectra suggest a traceable sodium citrate capping agent in the surface morphology of both Au and Ag-nanoparticles samples. It can then be concluded that Au- and Ag-nanoparticles crystallinity is compatible with the sodium citrate capping agent. The AuNPs spectra exhibits a broad peak in the stretch of 3240 cm^{-1}, which is aligned with the OH stretching. Other three peaks appear centred around 1033, 1370, and 1569 cm^{-1} which are associated with the stretching modes of carbonate (CO_3) complexes. According to Sylvestre *et al*. [403] and Mohan *et al*. [404] findings, controlled surface properties of Au-nanoparticles demonstrate similar FTIR peaks.

The FTIR peaks of AgNPs decorated with sodium citrate (Figure 3.4.1) shows vibrational bands features at 3284 cm^{-1} (aligned with H-OH stretching mode) and 2974 cm^{-1}, at 2845 cm^{-1} (corresponding to CH- asymmetric and symmetric stretching mode), 1571 cm^{-1} (aligned with COO- stretching mode) and 1384 cm^{-1} (corresponding to C-H bending). Segneanu *et al.* [405] reported similar vibrational peaks on Ag-nanoparticles synthesised using sodium citrate capping agent.

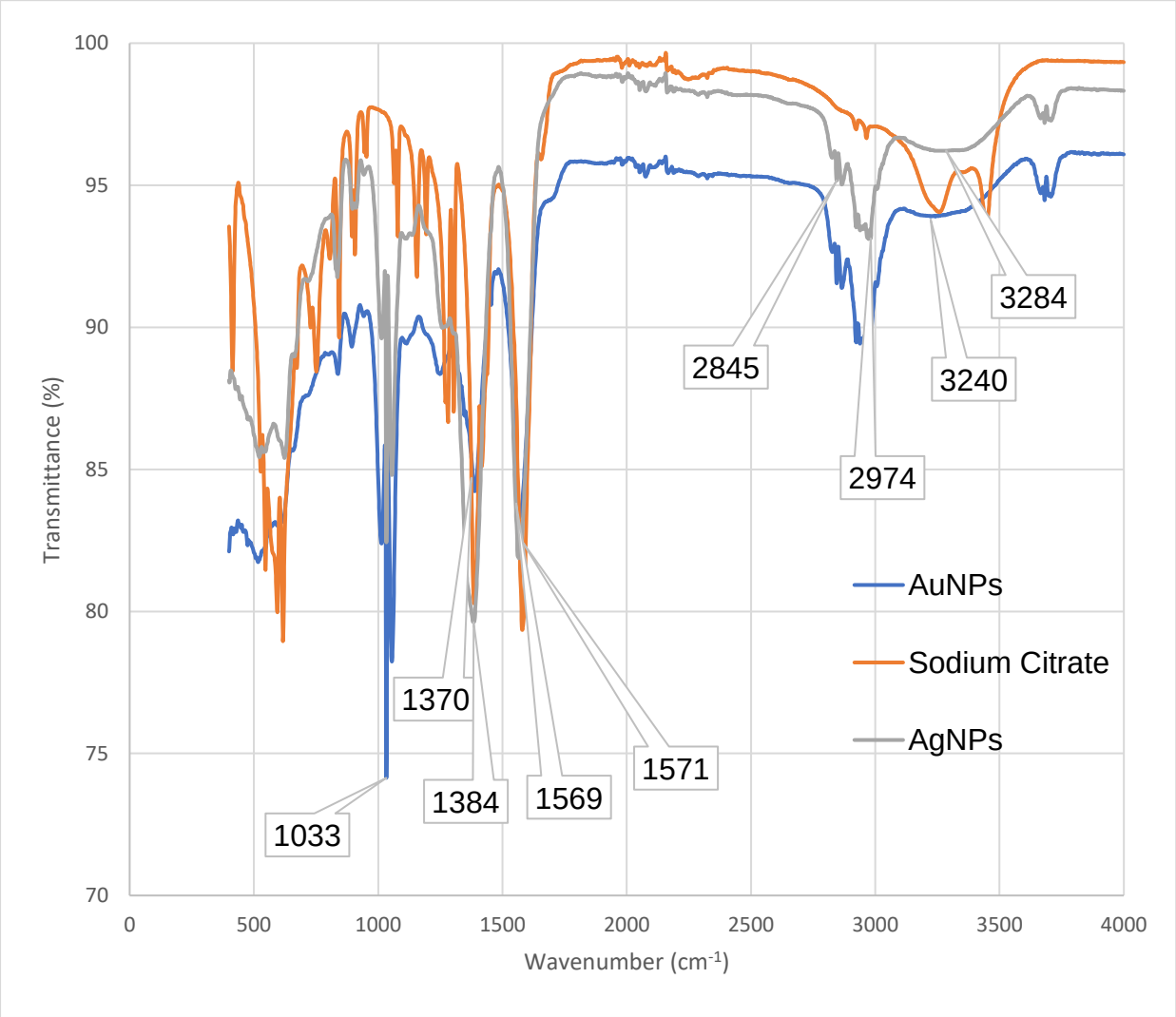

Figure 6.11: FTIR spectral of Sodium citrate, Au-nanoparticles (AuNPs) and Ag-nanoparticles (AgNPs).

6.3. Conjugation of the nanoparticles with fibrin proteins

6.3.1. Dissolution of fibrin protein in PBS

FTIR of powdered fibrin was conducted to investigate traces of existing functional groups in fibrin molecules. Acquired FTIR spectra of this powdered fibrin shown in Figure 6.12 is found to be in satisfactory concurrence with reported studies as indicated by Braga *et al.* [406] and Deepthi *et al.* [407]. Peaks appearing at 1238, 1514, and 1635 cm^{-1} are associated with the amide functional groups. Peak at 1238 cm^{-1} is aligned with the amide III bond, peak at 1514 cm^{-1} corresponds to the amide II bond, and lastly peak at 1635 cm^{-1} is associated with amide I bond. The amide functional group is given as $-CONH_2$. The amide I bond relates to the C=O stretching mode, amide II bond is due to the NH deformation, whilst the amide III bond, results from coupled C-N stretching and N-H bending motions [408]. Lastly, the peaks at 2855 and 2920 cm^{-1} are associated with the $-CH_2$ bonds.

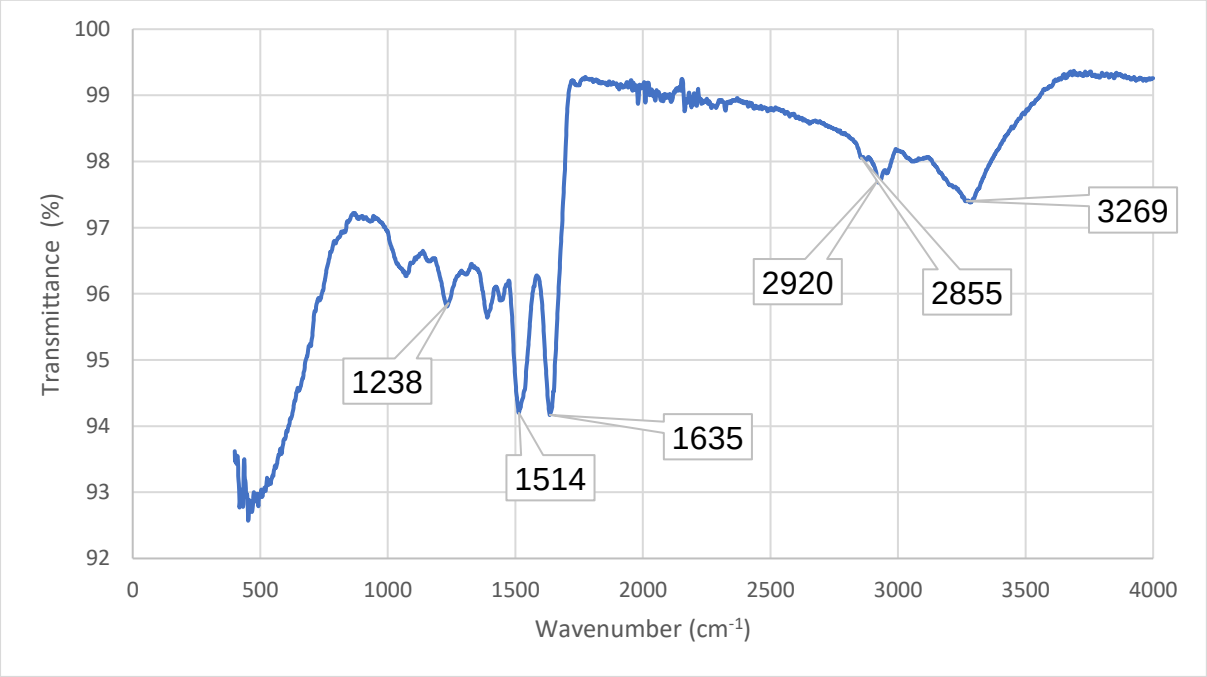

Figure 6.12: FTIR spectral of fibrin protein powders.

Onwards, a concentration of 0.193 mg/mL was prepared by dissolving 0.005 g of fibrin in a 25 mL of PBS with the pH of 7.4. The dissolution of fibrin in PBS took 48 hours at 37 °C. Upon preparation of fibrin concentration, the Au and Ag-nanoparticles were incubated with fibrin for 12 hours.

The UV-vis bands were also utilised to confirm the presence of the fibrin protein in PBS. UV-vis spectra of fibrin in PBS was attained as shown in Figure 6.13 and was found to be in good agreement with that of fibrinogen of which fibrin is extracted from [409]. Two peaks were found to be visible at 271 and 224 nm, which correspond to some functional groups' peaks of protein molecules [409].

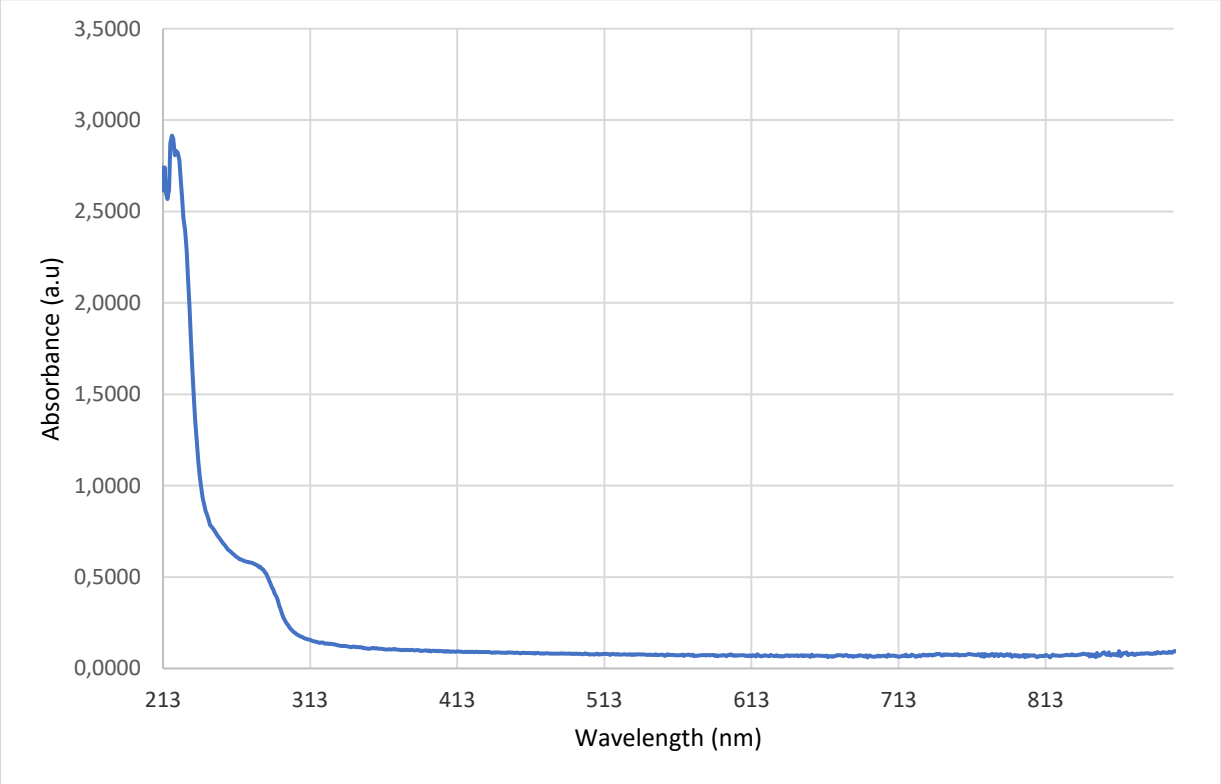

Figure 6.13: UV-vis spectroscopy of fibrin protein powders.

6.3.2. Adsorption studies of Au- and Ag-nanoparticles conjugation with fibrin proteins

The conjugation process was achieved at a ratio of 1:1 between fibrin protein samples and Au-/Ag-nanoparticles solutions. 1 mL each of the prepared concentration of fibrin solution was poured into two separate containers. Thereafter, 1 mL of Au-nanoparticles solution was introduced into one of the fibrin solution containers whilst 1 mL of Ag-nanoparticles solution was introduced into the other fibrin solution container. The entire process of combining Au-/Ag-nanoparticles and fibrin protein samples is regarded as conjugation.

UV-vis spectroscopy characterisation was later conducted in order to analyse possible shift on Au- and Ag-nanoparticles conjugated with fibrin proteins relative to the original Au- and Ag-nanoparticles samples before conjugation. Figures 6.14 (a - d) present Au-nanoparticles conjugated with fibrin protein samples (thereafter referred to as 'AuNPs+fibrin' relative to the Au-nanoparticles before conjugation (referred to as ‘AuNPs’) peaks at average spherical diameter sizes 11, 18, 45, and 50 nm in that order. Indeed, peak shifts of 'AuNPs+fibrin' relative to ‘AuNPs’ are observed, even though the absorbance is lower than that of the ‘AuNPs’. Such peak shifts signify possible adsorption of fibrin protein molecules onto Au-nanoparticles. Torres-Diaz *et al*. [352] made use of UV-vis peak shifts approach to encourage understanding of the surface functionalisation of peptides onto gold nanoparticles. In comprehension, similar peak shift behaviour are emphasised by Kaur *et al*. [410], Amini *et al*. [411], and Rutherford *et al*. [412], based on different protein molecular species interaction with gold nanoparticles.

Peak shifts were evident in all average spherical diameter sizes of the Au-nanoparticles (Figure 6.14 (a-d)), as well as Ag-nanoparticles (Figure 6.15 (a-c)). In

addition, peak shifts observed are towards longer wavelengths in all cases of both Au- and Ag-nanoparticles spectra. Prominent, distinct peak shifts in all average spherical diameter sizes studied, indicate good and robust adsorption of fibrin molecules onto Au/Ag-nanoparticles.

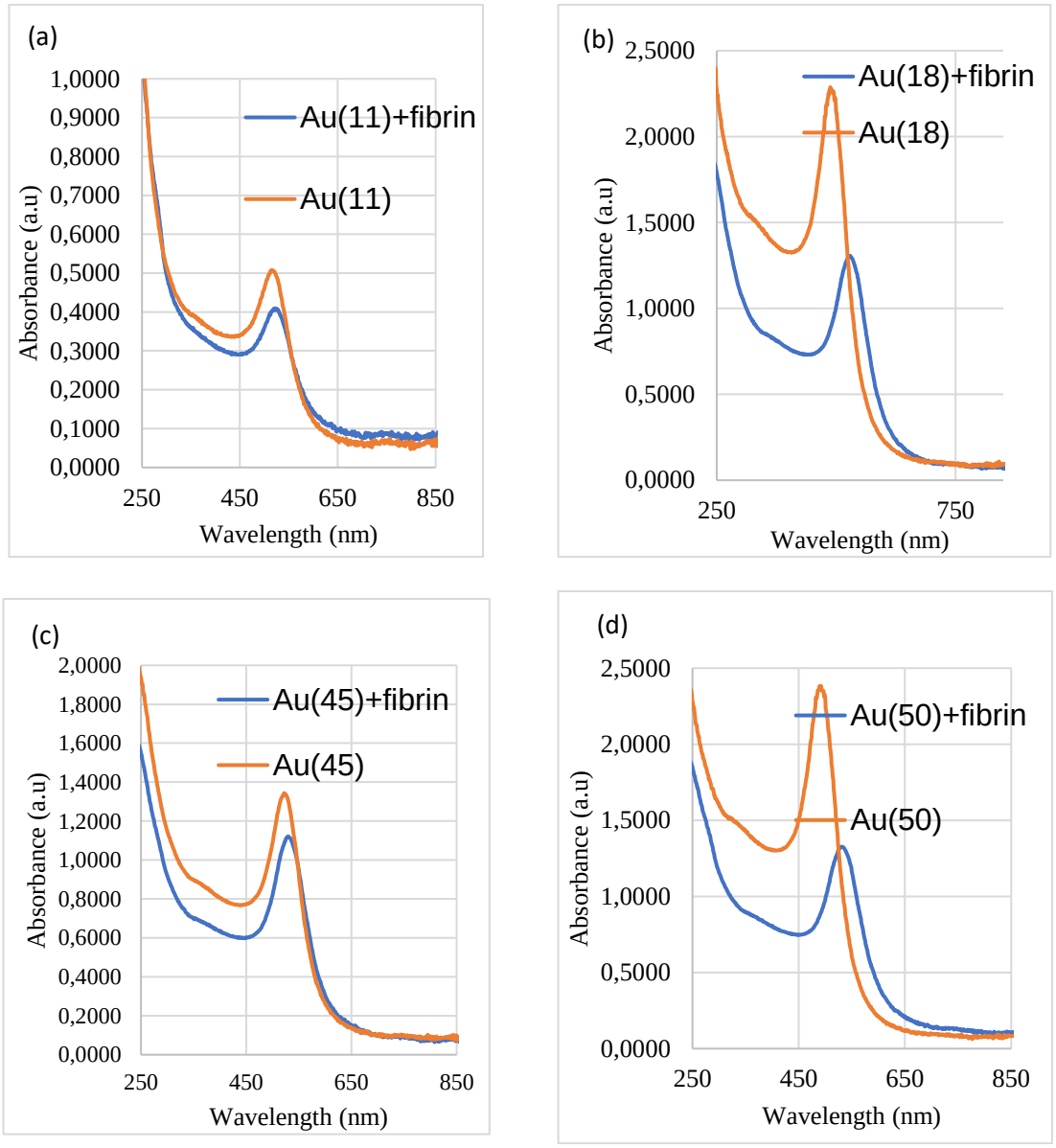

Figure 6.14: UV-vis spectroscopy of AuNPs+fibrin and AuNPs; (a) Au(11)+fibrin and Au(11), (b) Au(18)+fibrin and Au(18), (c) Au(45)+fibrin and Au(45), (d) Au(50)+fibrin and Au(50) which correspond to spherical diameters 11, 18, 45, and 50 nm after and before conjugation with fibrin proteins.

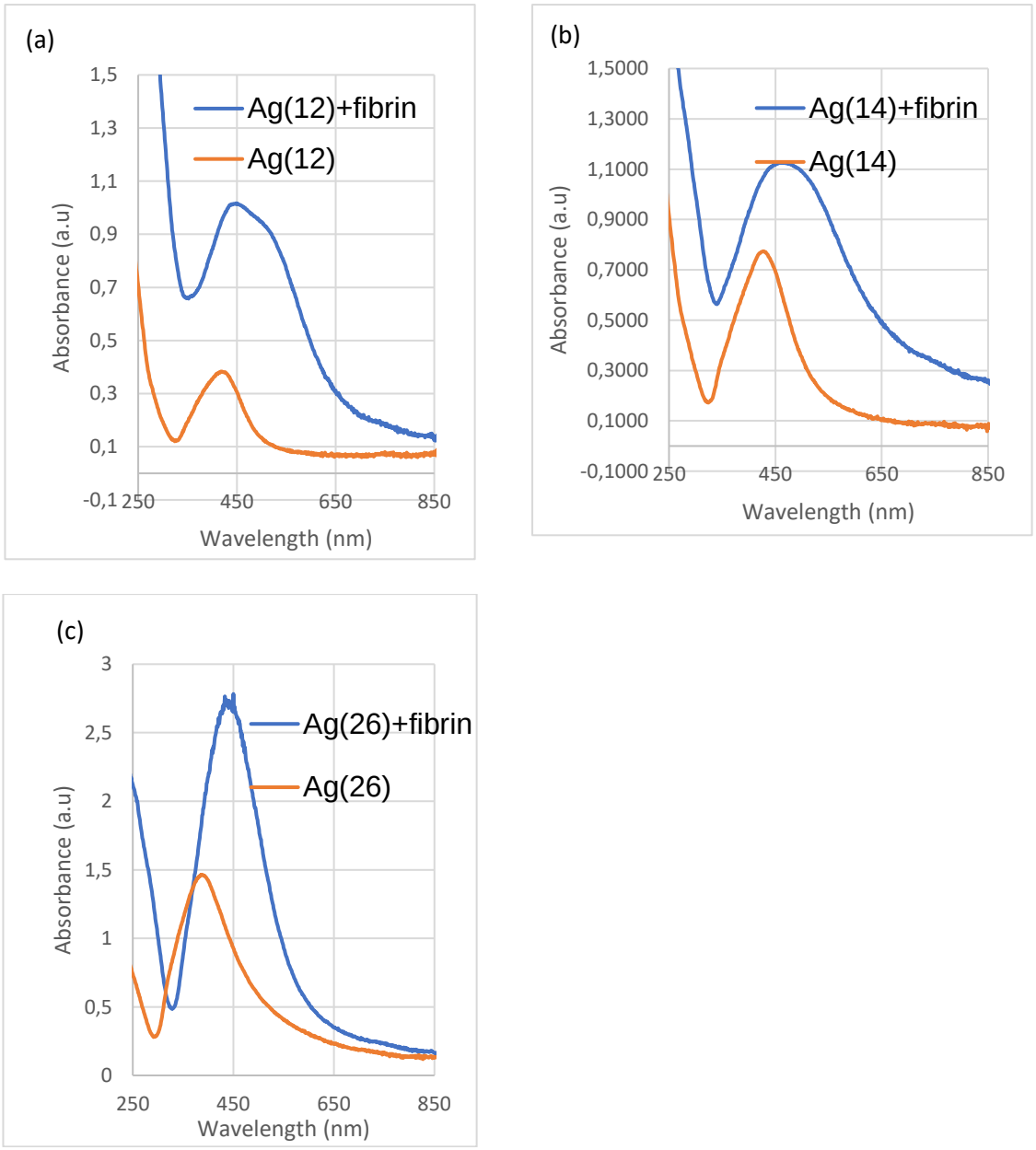

Figure 6.15: UV-vis spectroscopy of AgNPs+fibrin and AgNPs; (a) Ag(12)+fibrin and Ag(12), Ag(14)+fibrin and Ag(14), and Ag(26)+fibrin and Ag(26) which correspond to 12, 14, and 26 nm spherical diameter sizes after and before conjugation with fibrin proteins.

In a similar manner, FTIR spectra were also plotted and utilised to trace possible changes in the original fibrin protein samples FTIR functional groups peaks after fibrin protein was conjugated with Au- and Ag-nanoparticles. Forging ahead, FTIR spectra of fibrin protein before (referred to as 'fibrin' and after conjugation with AuNPs

(thereafter referred to as 'AuNPs+fibrin') in all average diameter sizes were mapped and displayed in Figures 6.16 (a - d). Generation of extra peaks, changes in the peak intensities, and peak shifts towards greater wavenumbers are evident with elevated transmittance % on the 'AuNPs+fibrin' related to average diameter sizes 11 and 18 nm. However, still observing new peaks generation and peak shifts to larger wavenumbers, transmittance spectra of ‘fibrin’ and 'AuNPs+fibrin' at 45 nm average spherical diameter size tend to overlap. At 50 nm average spherical diameter size, 'AuNPs+fibrin' spectral transmittance % is well below that of the original ‘fibrin’ molecules. The entire trend suggests that through conjugation, adsorption of fibrin protein onto AuNPs becomes spontaneous with 'AuNPs+fibrin' at 45 and 50 nm average spherical diameter sizes. At 11 and 18 nm average spherical diameter sizes, external factors such as temperature or pressure may be required for absolute adsorption of fibrin protein onto AuNPs. Researchers such as Xu *et al.* [413] have utilised FTIR profiles to show the difference in peak shifts of protein-encapsulated Au-nanoclusters and their associated free proteins (which include bovine serum albumin, Trypsin and Lysozyme) under denatured conditions whereby the shift, disappearance and emergence of new peaks can be observed after the Au-nanoparticles were conjugated with their respective protein molecular species.

Correspondingly, the FTIR spectra of ‘fibrin’ before and after conjugation ‘AgNPs+fibrin’ in all average spherical diameter sizes were also mapped and displayed in Figures 6.17 (a - c). The spectral trends of 12 and 14 nm average spherical diameter sizes follow those discussed above on ‘fibrin’ and ‘AgNPs+fibrin’. However, at 26 nm average spherical diameter size, 'AgNPs+fibrin' spectral transmittance % is well below that of the original isolated fibrin protein, while still observing new peaks generation and peak shifts to larger wavenumbers. The

corresponding observation suggest that through conjugation, adsorption of fibrin molecules onto AgNPs become spontaneous with 'AgNPs+fibrin' at all average spherical diameter sizes (i.e. 12, 14 and 26 nm AgNPs). Chakraborty *et al.* [414] used FTIR spectroscopy in demonstrating that mouse serum albumin ligands conjugate well onto AgNPs. The study differentiates between pure mouse serum albumin and mouse serum albumin-stabilised AgNPs using FTIR spectral analysis. Enhanced transmittance % and shift in peaks on the mouse serum albumin-stabilised AgNPs in which the continuous shift of the peaks to a greater wavenumber position suggests the successful binding of the serum albumin onto the AgNPs.

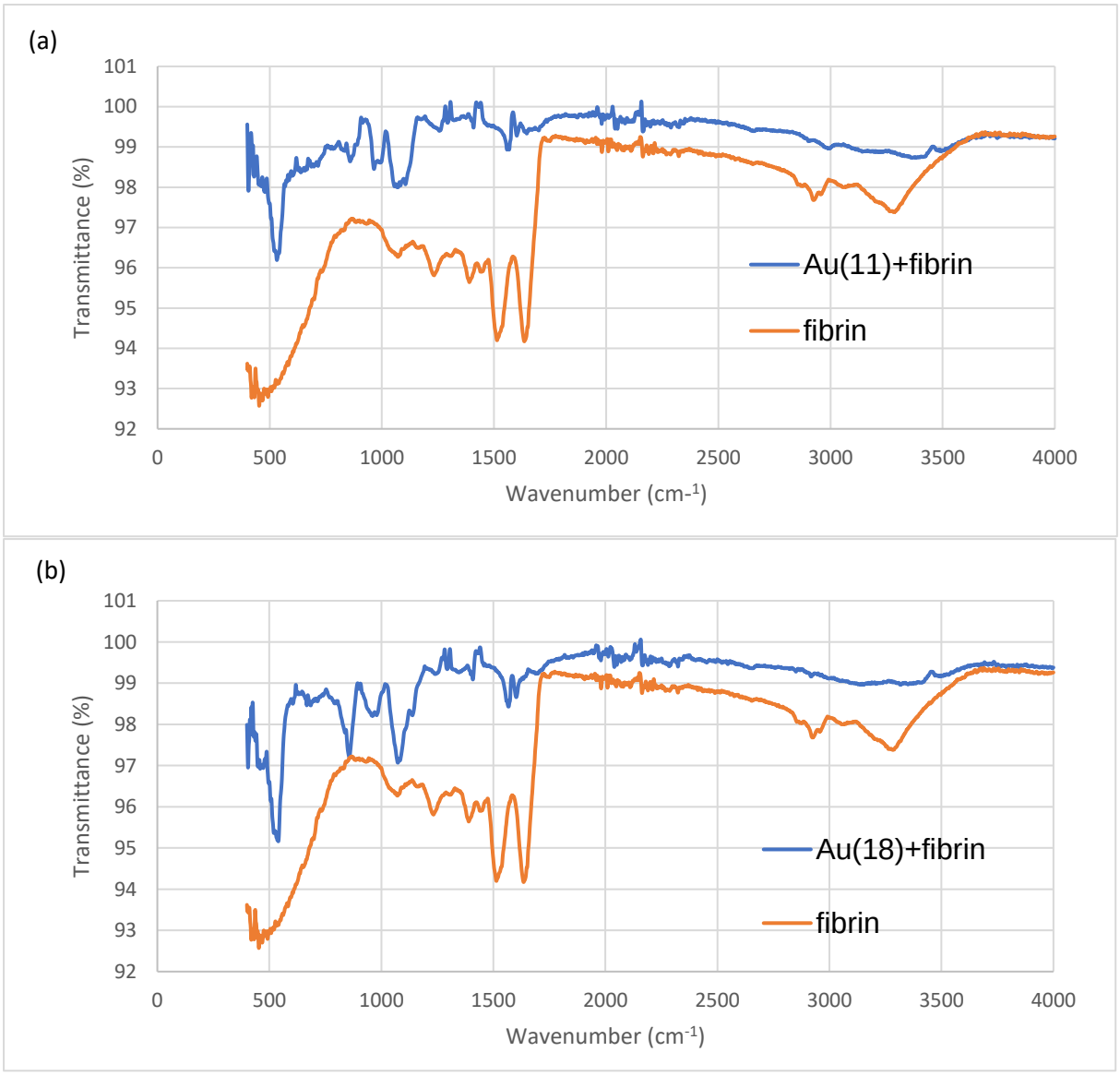

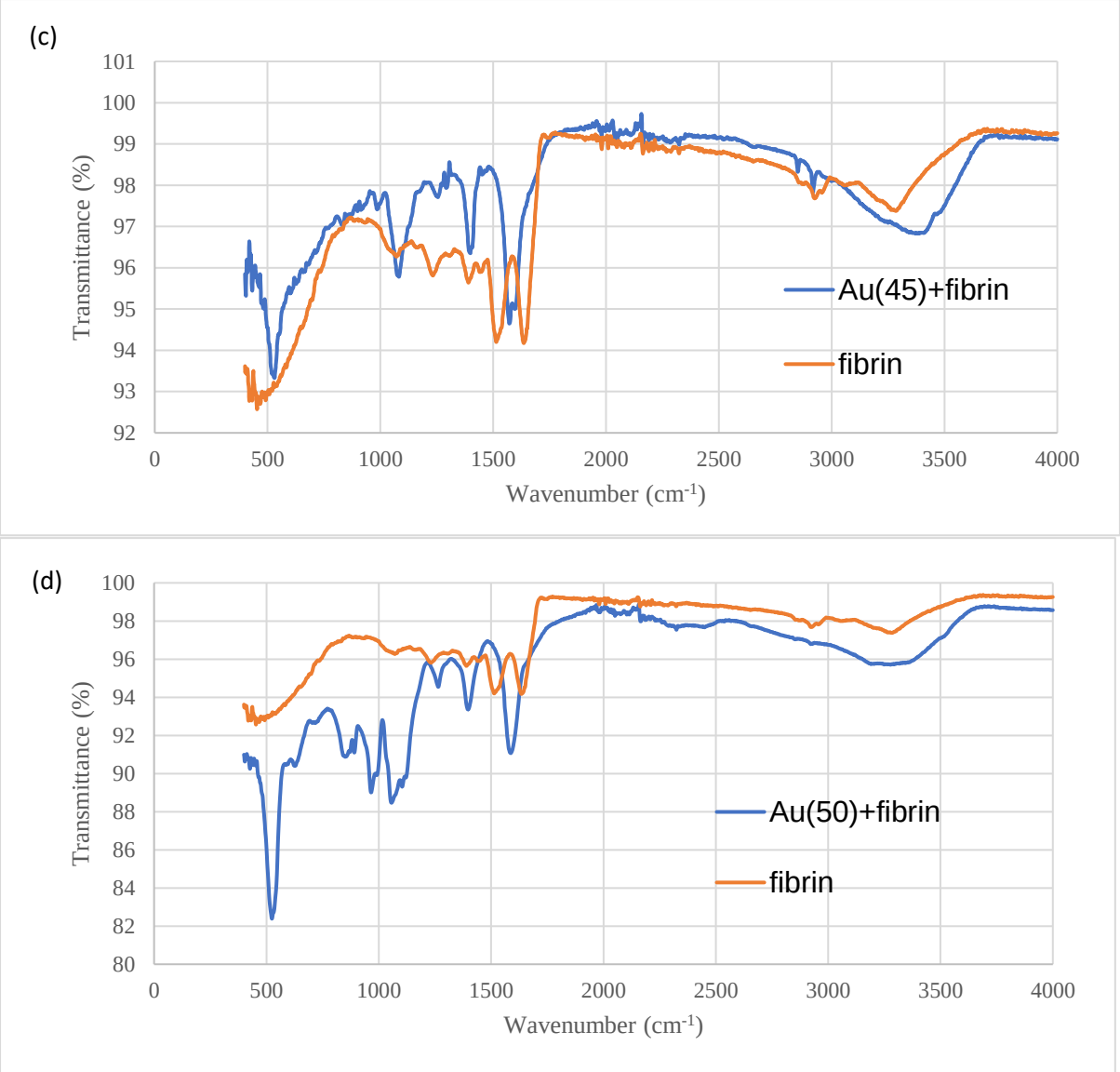

Figure 6.16: FTIR of fibrin protein after and before conjugation with Au-nanoparticles (AuNPs), (a) Au(11)+fibrin and fibrin, (b) Au(18)+fibrin and fibrin, (c) Au(45)+fibrin and fibrin, (d) Au(50)+fibrin and fibrin which correspond to 11, 18, 45, 50 nm spherical diameter sizes of AuNPs.

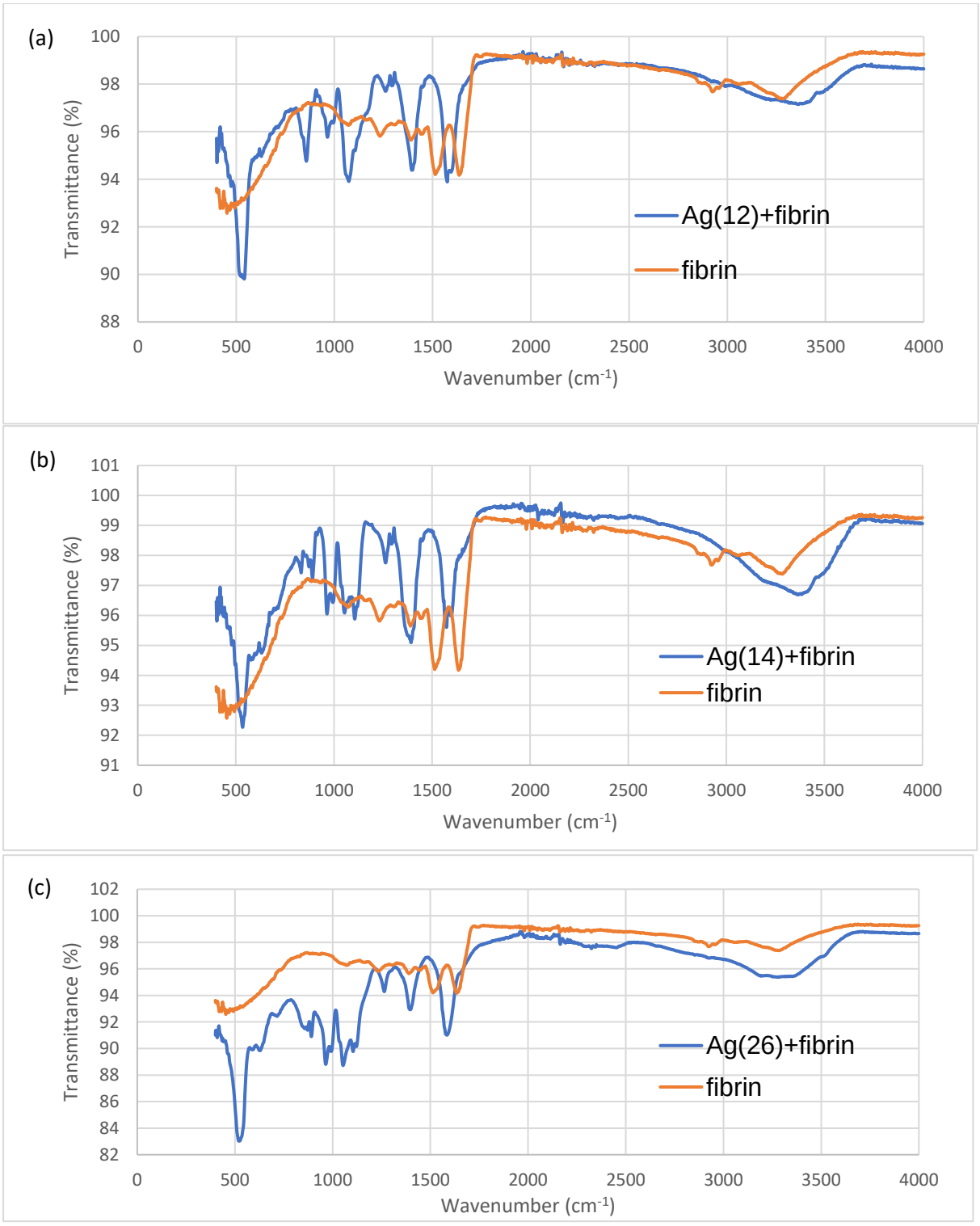

Figure 6.17: FTIR of fibrin protein after and before conjugation with Ag-nanoparticles (AgNPs); (a) Ag(12)+fibrin and fibrin, (b) Ag(14)+fibrin and fibrin, and (c) Ag(26)+fibrin and fibrin which correspond to 12, 14, and 26 nm spherical diameter sizes of AgNPs.

Zetal potential approach was also applied to assist in the verification of possible adsorption of fibrin protein molecules onto Au- and Ag-nanoparticles. In this approach, charge distribution of ‘AuNPs’ and ‘AgNPs’ before as well as ‘AuNPs+fibrin’ and ’AgNPs+fibrin’ after fibrin species conjugation with Au- and Ag-nanoparticles are compared based on their spherical average diameter sizes. Accumulated data on both ‘AuNPs’ and 'AuNPs + fibrin' samples are arranged in Table 4.2.1. Based on this data, negatively charged zeta potential values of ‘AuNPs’ are larger than those of 'AuNPs+fibrin' by an averaged 44% in the averaged diameter sizes 11 and 18 nm, which also lowers to an averaged 30% in the averaged diameter sizes 45 and 50 nm respectively. It must be noted that the zeta potential values listed in Table 6.1 are directly related to the charge distributions in a given spherical nanoparticle. Lowering of zeta potential values on ‘AuNPs’ with reference to the conjugated 'AuNPs+fibrin' signifies successful adsorption of fibrin molecules onto Au-nanoparticles. In the last column of Table 6.1, it can be seen that the difference in zeta potential of 'AuNPs+fibrin' relative to ‘AuNPs’ increases with average diameter sizes. Comparable charge distribution zeta potential values were noted by Parera *et al.* [415] on adsorption studies of peptides and certain protein species onto Au-nanoparticles.

In a similar manner, accumulated zeta potential data on both ‘AgNPs’ and 'AgNPs+fibrin' before and after conjugation samples respectively are listed in Table 6.2. Likewise, negatively charged zeta potential values which are associated with nanoparticle charge distributions of ‘AgNPs’ are greater than those of 'AgNPs+fibrin' in the averaged diameter sizes 12, 14 and 26 nm. A difference in zeta potential (ΔV) values listed in Table 6.2 fluctuates considerably with average diameter sizes. Yet, the lowering of zeta potential values of ‘AgNPs+fibrin’ relative to ‘AgNPs’ still highlights successful adsorption of fibrin molecules onto Ag-nanoparticles.

Polydispersity index (PDI) was also analysed to approximate the uniformity of the nanoparticles in the solution. Nanoparticle size distribution and aggregates play an important role when analysing polydispersity [416]. A given sample is considered monodispersed (a perfectly uniform sample with regard to the particle size) if its polydispersity index (PDI) is less than 0.1 [351, 352, 400]. A PDI value greater than 0.7 implies a sample with broad particle size distribution. Such a sample may not be suitable for analysis [352, 417]. In this instance, PDI distribution of ‘AuNPs’ and ‘AgNPs+fibrin’ are compared based on their spherical average diameter sizes. Accumulated data on both ‘AuNPs’ and 'AuNPs+fibrin' samples are arranged in Table 6.1. Values listed suggest PDIs which are moderately polydisperse (a non-uniform sample with regard to the particle size). PDI values decrease for average diameter sizes 11, 18, 50 nm after conjugation with fibrin, with the exception of 45 nm in which the PDI increases after conjugation. The overall attained PDI distribution points out the fact that both ‘AuNPs’ and 'AuNPs+fibrin' samples are moderately polydisperse. Accordingly, Danaei *et.al.* [417] further articulated that the reasonable PDI range of the nanoparticles considered by most researchers is 0.05-0.7.

Onwards, the accumulated data on both ‘AgNPs’ before and 'AgNPs+fibrin' after conjugation samples are arranged in Table 6.2. In a similar manner, PDI of all ‘AgNPs’ before and 'AgNPs+fibrin' after conjugation occur moderately polydispersed. To quantify, PDI values of 'AgNPs+fibrin' samples are lower in reference to individual ‘AgNPs’, which signifies better particle size distribution. Moreover, average spherical diameter size 26 nm display lowest PDI value which is associated with almost uniform particle size distribution.

Table 6.1: Zeta potential (ZP) in eV, poly-dispersity index (PDI) values of 'AuNPs' before and 'AuNPs+fibrin' after conjugation with fibrin proteins and zeta potential difference (ΔV) in eV at spherical average diameter sizes of 11, 18, 45 and 50 nm.

	AuNPs (isolated)		AuNPs (conjugated)		
Size (nm)	ZP (eV)	PDI	ZP (eV)	PDI	ΔV (eV)
11	-17.5	0.221	-7.68	0.200	9.82
18	-20.7	0.353	-9.23	0.203	11.47
45	-23.0	0.173	-7.17	0.341	15.83
50	-31.5	0.212	-8.85	0.198	22.65

Table 6.2: Zeta potential (ZP) in eV, poly-dispersity index (PDI) values of 'AgNPs' before and 'AgNPs+fibrin' after conjugation with fibrin proteins and zeta potential difference (ΔV) in eV at spherical average diameter sizes of 12, 14, and 26 nm.

	AgNPs		AgNPs+fibrin		
Size (nm)	ZP (eV)	PDI	ZP (eV)	PDI	ΔV (eV)
12	-20.7	0.447	-7.27	0.279	13.43
14	-26.0	0.445	-7.56	0.205	18.44
26	-23.7	0.245	-7.20	0.193	16.50

6.3.3. TEM of Au- and Ag-nanoparticles conjugation with fibrin proteins

After conjugation of Au- and Ag-nanoparticles with fibrin protein powders, further TEM micrographs were collected and compared with those of nanoparticles before conjugation processes. This procedure was followed to further verify possible fibrin protein molecules adsorption onto AuNPs and AgNPs. Figures 6.18 - 6.21 present 'AuNPs' before and 'AuNPs + fibrin' after fibrin conjugation onto AuNPs at different spherical diameter sizes on TEM resolutions of 100 and 50 nm. Also, Figures 6.22 -

6.24 present ‘AgNPs’ before and ‘AgNPs + fibrin’ after fibrin conjugation at different spherical diameter sizes on TEM resolutions of 100 and 200 nm.

Before conjugation process, AuNPs materialise as agglomerates of nano-clusters. Figures 6.18 (a), 6.19 (a), and 6.20 (a), and 6.21 (a) present such seeded grown average diameter sizes 11, 18, 45, and 50 nm of AuNPs nano-clusters at 100 and 50 nm TEM resolutions. Conjugation of fibrin protein samples into these nano-clusters stimulate dispersion of nanoparticles as such ‘AuNPs + fibrin’ suspension projects isolated random AuNPs on the fibrin protein fluid. Figures 6.18 (b), 6.19 (b), 6.20 (b), and 6.21 (b) proceed to display such a dispersion relation. Such a behaviour may be expected as nanoparticles dunked into a biological environment fluid spontaneously induces adsorption of immediate protein molecules onto their surfaces. In this case, adsorbed fibrin molecules onto AuNPs induces repulsive force among individual AuNPs which leads to AuNPs being randomly dispersed. Devi *et al*. [401] reported a similar situation on cysteine-capped gold nanoparticles. Their results argue that gold nanoparticles conjugated with cysteine appear as individual nanoparticles diffused in cysteine fluid. However, D’souza *et al*. [418] are of the view that aggregates of ascorbic acid capped gold nanoparticles may be due to hydrogen bonding with dichlorvos. Therefore, in the absence of hydrogen bonding between AuNPs and fibrin molecules - sodium citrate capping, AuNPs aggregates disintegrate into individual species within the fibrin-sodium citrate medium.

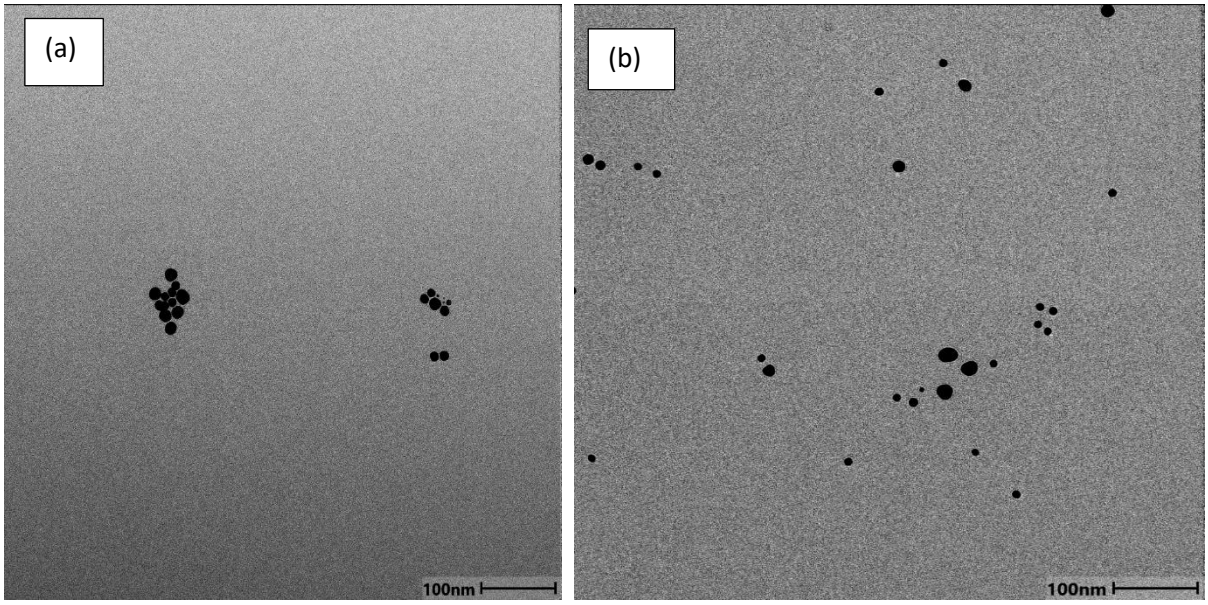

Figure 6.18: TEM 100 nm resolution profiles on 11 nm average diameter sizes of Au-nanoparticles (AuNPs). (a) isolated AuNPs and (b) fibrin conjugated AuNPs.

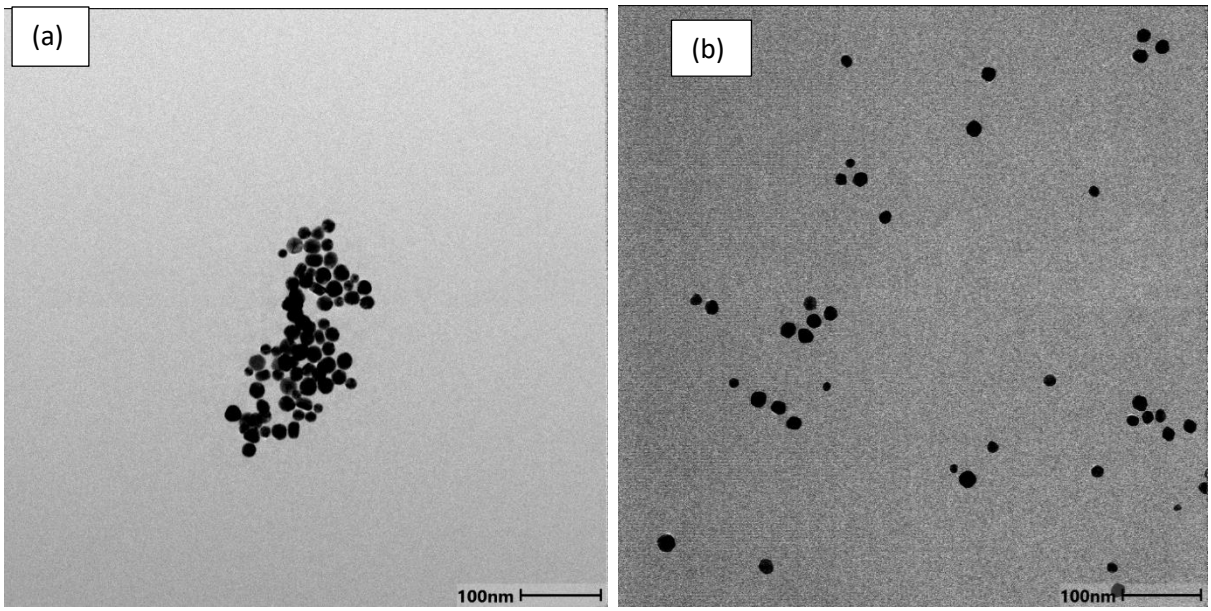

Figure 6.19: TEM 100 nm resolution profiles on 18 nm average diameter sizes of Au-nanoparticles (AuNPs). (a) isolated AuNPs and (b) fibrin conjugated AuNPs.

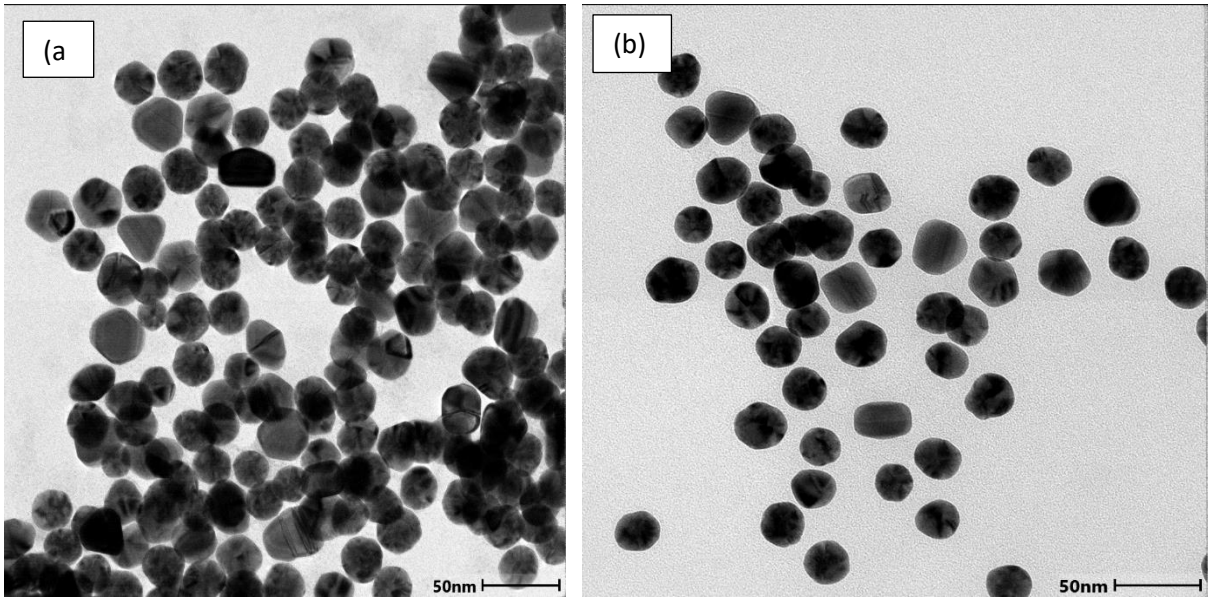

Figure 6.20: TEM 50 nm resolution profiles on 45 nm average diameter sizes of Au-nanoparticles (AuNPs). (a) isolated AuNPs and (b) fibrin conjugated AuNPs.

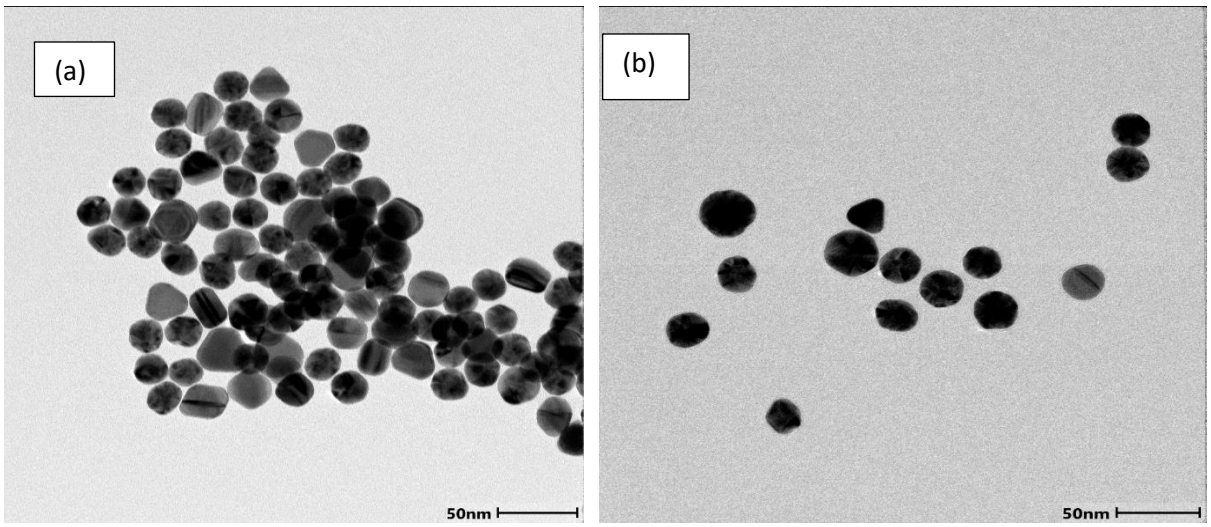

Figure 6.21: TEM 50 nm resolution profiles on 50 nm average diameter sizes of Au-nanoparticles (AuNPs). (a) isolated AuNPs and (b) fibrin conjugated AuNPs.

Looking at Ag-nanoparticles interaction with fibrin proteins, Figures 6.22 (b) and 6.23 (b) demonstrate appreciable agglomerations on 'AgNPs + fibrin' conjugation at 12 and 14 nm average diameter sizes. In addition, a dark film can be observed, encompassing the nano-clusters. It is noteworthy that nano-clustered 'AgNPs + fibrin' are having smaller average diameter sizes when compared to disorderly spaced AgNPs before conjugation process (Figures 6.22 (a) and 6.23 (a)). Moreover, Figures 6.22 (a) and

6.23 (a) demonstrate dispersed, isolated AgNPs at average spherical diameter sizes of 12 and 14 nm respectively. This scenario is exactly opposite that which is observed with the AuNPs before and after conjugation with fibrin 'AuNPs + fibrin'. Similar observation was noted by Halamoda-Kenzaoui *et al*. [419] in which 30 and 80 nm size distribution of Rubipy-SiO_2 nanoparticles in CaCo-2 solution indicated agglomeration and precipitation. Evidence of small and large nanoparticles agglomerations were also reported by Murugadoss *et al*. [420], whereby TiO_2 nanoparticles are stabilised with bovine serum albumin (BSA). TEM 200 nm resolution of 26 nm diameter sizes displayed in Figure 6.24 (a) and (b) provide a good demonstration of how before conjugation, scattered, individual AgNPs are having enlarged diameter sizes in comparison with fibrin conjugated 'AgNPs + fibrin' random aggregates. Diameter size reduction in aggregates may be associated with summed attractive forces which reduces individual nanoparticle sizes.

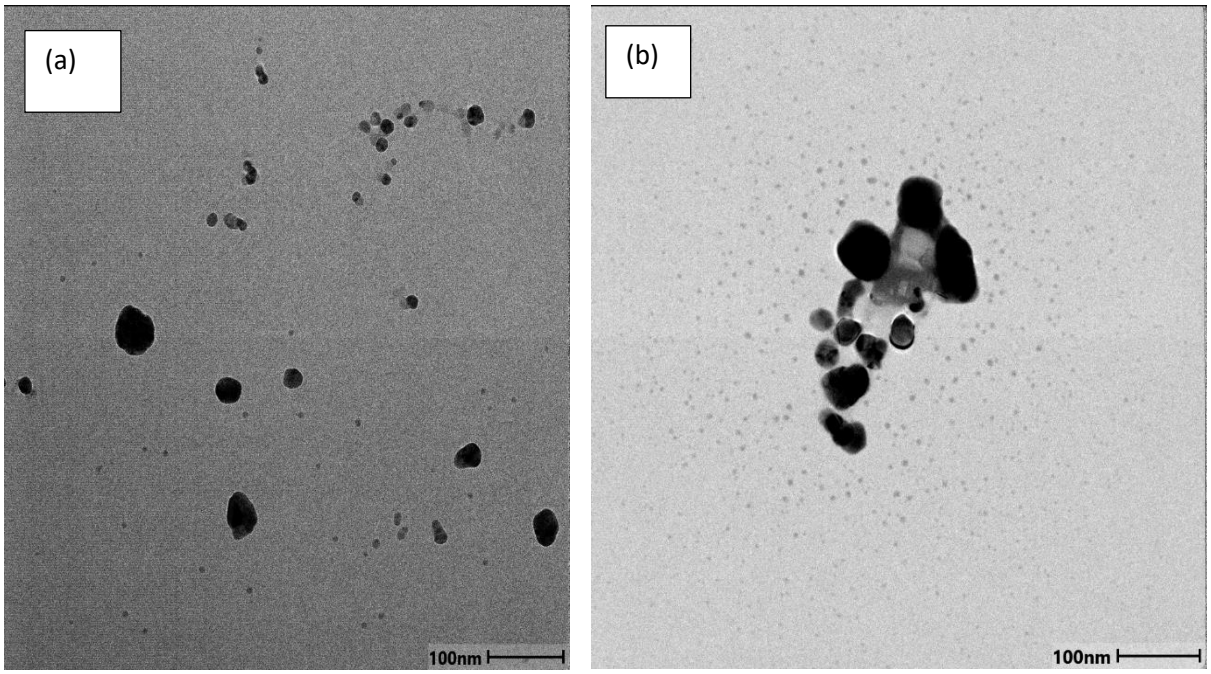

Figure 6.22: TEM 100 nm resolution profiles on 12 nm average diameter sizes of Ag-nanoparticles (AgNPs). (a) isolated AgNPs and (b) fibrin conjugated AgNPs.

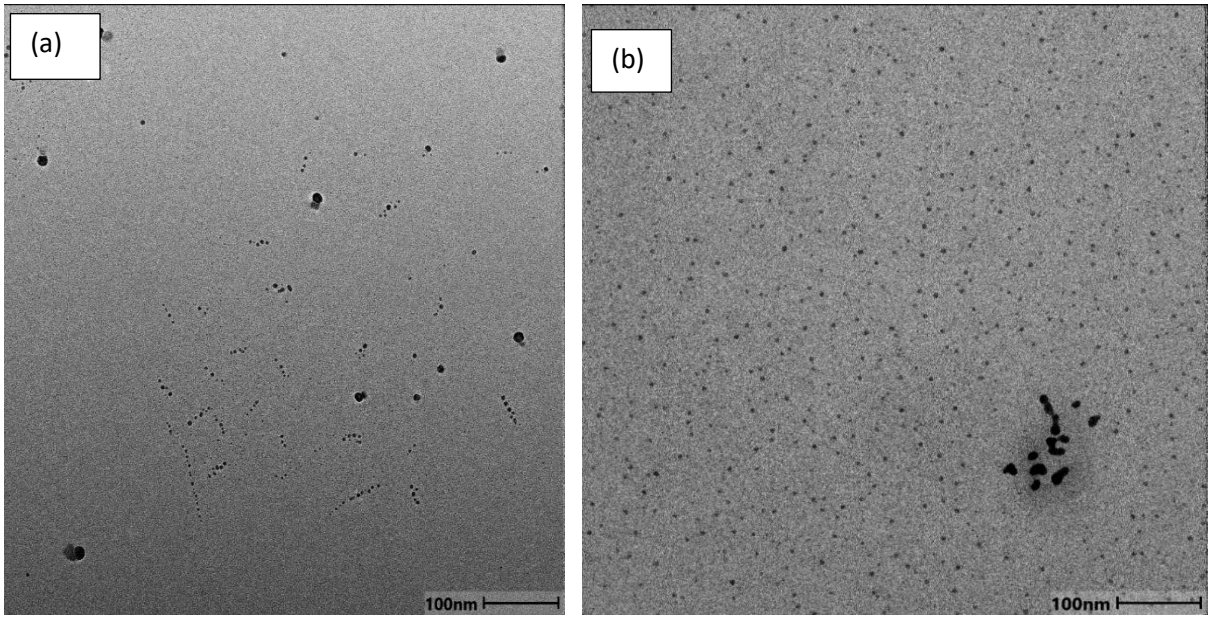

Figure 6.23: TEM 100 nm resolution profiles on 14 nm average diameter sizes of Ag-nanoparticles (AgNPs). (a) isolated AgNPs and (b) fibrin conjugated AgNPs.

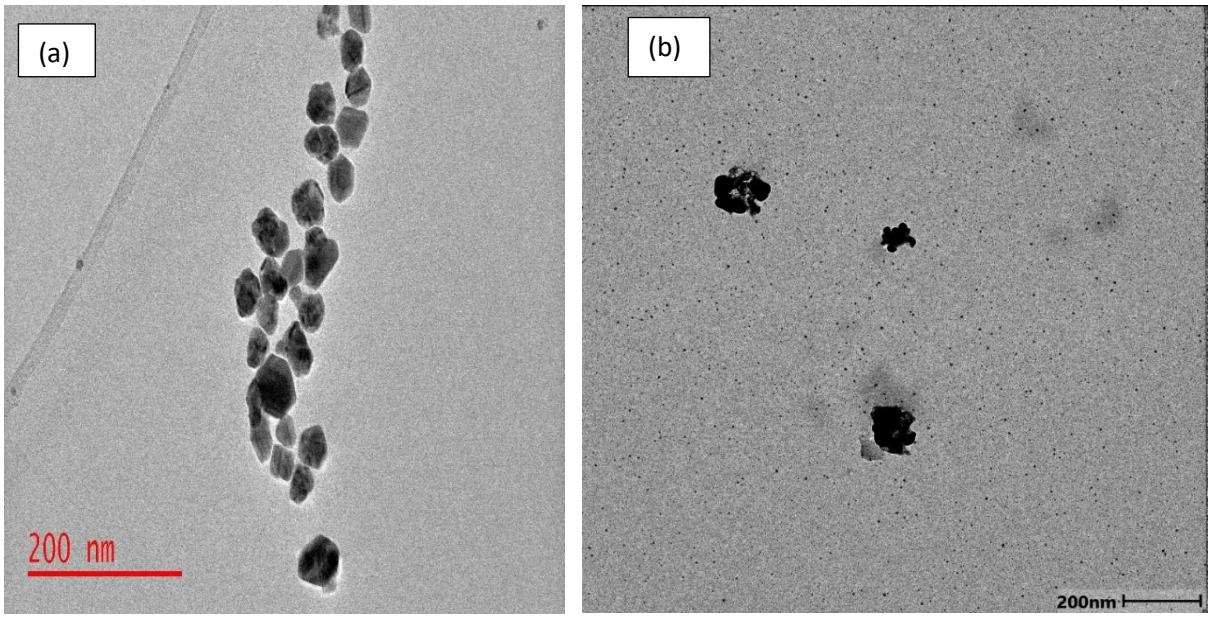

Figure 6.24: TEM 200 nm resolution profiles on 26 nm average diameter sizes of Ag-nanoparticles (AgNPs). (a) isolated AgNPs and (b) fibrin conjugated AgNPs.

6.4. Conclusion

The XRD plots confirms that the synthesised Au- and Ag-nanoparticles under sodium citrate method exhibit face centred cubic symmetry. UV-vis peak shifts of AuNPs and AgNPs relative to conjugated 'AuNPs+fibrin' and 'AgNPs+fibrin' respectively towards longer wavelengths suggest successful adsorption of fibrin molecules onto Au- and Ag-nanoparticles. On the other hand, 'fibrin' before as well as 'AuNPs+fibrin' and AgNPs+fibrin' after conjugation FTIR spectra peaks remain similar but shifted towards shorter wavenumbers, which suggest successful adsorption with no change in the conformational structure of the fibrin protein molecules. The difference in zeta potential further validates charge re-distribution from 'AuNPs' and AgNPs' before towards 'AuNPs+fibrin' and AgNPs+fibrin' after conjugation, with the PDI data suggesting moderate to uniform particle size distributions. TEM micrographs present aggregates of AuNPs, which disperse into individual AuNPs upon conjugating with fibrin protein powders. In the case of Ag-nanoparticles the situation is exactly opposite. Individually scattered AgNPs conglomerate into nano-clusters upon conjugation with fibrin protein samples. At cellular environment, irregularly dispersed ‘AuNPs+fibrin’ may be linked to non-toxicity whilst the aggregated ‘AgNPs+fibrin’ may be the source of toxicity.

CHAPTER 7

Conclusion

Computational and experimental adsorption interface interactions between biological protein based molecules and precious gold and silver nanoparticles were successfully studied. In the study, the ultimate formation of Au/Ag-nanoparticle+protein corona complexes were incorporated. Computational techniques that include MD, DFT, and MC collective simulations suggest both Au-nanosphere+protein and Ag-nanosphere+protein coronas as energetically, bonding, and charge density possible. In particular, fibrin protein molecules were successfully adsorbed onto the surfaces of both Au- and Ag-nanospheres resulting in the Au/Ag-nanosphere+fibrin protein coronas. In this regard, all the 1, 2, 3 and 4-fibrin molecules chain interactions with Au- and Ag-nanospheres modelled provide a possible formation of the Au-/Ag-nanosphere+fibrin corona complexes. This is additionally supported by the negative adsorption energies acquired for all the modelled configurations. Au(55) + 1, 2, 3, and 4-fibrin and Ag(55) + 1, 2, 3, and 4-firbin nanospheres produced more energetically stable coronas as compared to all other nanosphere corona complexes. Exceptional Au(19) + 3 and 4-fibrin and Ag(19) + 3 and 4-fibrin coronas obtained zero energies. Such behavior was attributed to the compromised nanosphere size relative to the fibrin chain length. Further validating the fact that various protein types and sizes may be associated with prescribed nanosphere sizes. Binding distances between the terminal functional group atoms of the fibrin protein molecules and either Au- or Ag-nanospheres were also successfully investigated. Bond lengths estimations suggest that fibrin molecules binding onto Au- and Ag-nanospheres prefer hydrogen bonds. Mean square displacements and diffusion coefficient constants suggest that the functional group atoms H, C, N, and O atoms may diffuse readily onto Au-/Ag-

nanospheres. Mülliken charge distributions suggest that interface exchange of electrons through Au-H and Ag-H lead to negatively charged Au-nanosphere+fibrin and Ag-nanosphere+fibrin coronas. Otherwise, Au-O/Au-N and Ag-O/Ag-N electron interface reduction may result in positively charged Au-nanosphere+fibrin and Ag-nanosphere+fibrin coronas.

The radius of gyration further suggests that a tighter packing (which signifies hard corona type) is observed for the adsorption of fibrin molecules onto Au(38)/Ag(38), Au(55)/Ag(55), and Au(79)/Ag(79) nanospheres with a preferred sequence of Au(79)/Ag(79) > Au(55)/Ag(55) > Au(38)/Ag(38). Hence, less tight packing of Au(19)/Ag(19) signifies soft Au(19)/Ag(19) + n-fibrin corona. The less tight packing was attributed to the small nanosphere size.

To compliment computational studies, experimental characterization using UV-vis, FTIR and TEM spectroscopties together with Zeta potential analysis further confirm the possible formation of the Au- and Ag-nanoparticles+fibrin corona. Experimentally, both Au- and Ag-nanoparticles were synthesised and incubated with the fibrin protein powders. Firstly, UV-vis peak shifts of AuNPs and AgNPs with reference to the conjugated 'AuNPs+fibrin' and 'AgNPs+fibrin' confirmed the adsorption and formation of Au- and Ag-nanoparticle+fibrin coronas. FTIR peak shifts of conjugated 'AuNPs+fibrin' and AgNPs+fibrin' relative to the unconjugated fibrin solutions further validates and confirm the adsorption and ultimate formation of Au- and Ag-nanoparticle+fibrin coronas. The attained difference in zeta potential between fibrin and fibrin conjugated 'AuNPs+fibrin' and AgNPs+fibrin' coronas also confirm the adsorption and formation of Au- and Ag-nanoparticle+fibrin corona as well as the distribution of charges in the Au- and Ag-nanoparticle+fibrin coronas. TEM

micrographs display aggregates of AuNPs, which disperse into individual AuNPs upon conjugating with fibrin proteins in the assumed Au-nanoparticle+fibrin coronas. However, individually scattered AgNPs conglomerate into nano-clusters upon conjugation with fibrin protein samples towards the assumed Ag-nanoparticle+fibrin coronas.

In any case, since it was found that the fibrin molecules prefer hydrogen bonding onto either the Au or Ag-nanospheres. Such hydrogen bonding could lead to attraction or repulsion of Au/Ag-nanoparticles. This was observed through the experimental findings, in which the adsorbed fibrin molecules onto AuNPs induces repulsive force through hydrogen bonding among individual AuNPs which leads to AuNPs being randomly dispersed, whereas adsorbed fibrin molecules onto AgNPs induces attractive force through hydrogen bonding resulting in Ag-nanoparticle agglomerates. Accordingly, both Au- and Ag-nanoparticles behave differently in the presence of fibrin protein. Through Mulliken charges and zeta potential, it was noted that, the polar nature of fibrin molecules functional group atoms bonding on CH_3, CH_2, CO, NH_2 encourage further covalency sharing of electrons with the Au/Ag-nanosphere's surface electron density. With reference to radius of gyration, a tighter packing may be associated with Au/Ag-nanosphere-fibrin hard corona while a lower tight packing may be associated with Au/Ag-nanosphere-fibrin soft corona. On the other hand, with reference to the UV spectra, prominent, distinct peak shifts in all average diameter sizes studied, indicate good and robust adsorption of fibrin molecules onto Au/Ag-nanoparticles. In this instance, greater shift towards longer wavelengths may be associated with Au-/Ag-nanoparticles-fibrin hard corona meanwhile a lower shift may be associated with Au-/Ag-nanoparticles-fibrin soft corona. Computationally, stable exothermic interactions signify feasible transportation of fibrin protein molecules

through Au-/Ag-nanoparticle+protein complexes into cellular environment. Meanwhile experimentally, concerning cellular environment, irregularly dispersed ‘AuNPs+fibrin’ may be associated with non-toxicity whilst the aggregated ‘AgNPs+fibrin’ may be associated with toxicity.

References

[1] H. Farah, “Nanocarriers as delivery systems for therapeutics agents,” *Int. J. Pharm. Sci. Res.*, 10 (2019) 3487-3507.

[2] X. Zhu, C. Vo, M. Taylor, B. R. Smith, “Non-spherical micro- and nanoparticles in nanomedicine,” *Mater. Horiz.*, 6 (2019) 1094-1121.

[3] Z. Hazarika, A.N. Jha, Computational Analysis of the Silver Nanoparticle−Human Serum Albumin Complex, *ACS Omega* 5 (2020) 170-178.

[4] A.Z. Wilczewska, K. Niemirowicz, K.H. Markiewicz, H. Car, Nanoparticles as drug delivery systems, *Pharmacol. Rep.*, 64 (2012) 1020-1037.

[5] Committee on use of Laboratory Animals in Biomedical and Behavioural Research, National Research Council and Institute of Medicine. Use of Laboratory Animals in Biomedical and Behavioural Research. Washington, D.C.: National Academy Press, (1988).

[6] T.I. Moy, A.R. Ball, Z. Anklesaria, G. Casadei, K. Lewis, F.M. Ausubel, Identification of novel antimicrobials using a live-animal infection model. *Proc. Natl Acad. Sci.* 103 (2006) 10414- 10419.

[7] D.R. Spring, Chemical genetics to chemical genomics: small molecules offer big insights. *Chem. Soc. Rev*. 34 (2005) 472-482.

[8] J. Giacomotto, L. Segalat, High-throughput screening and small animal models, where are we? *Br. J. Pharmacol.,* 160 (2010) 204-216.

[9] U. Lendahl, S. Orrenius, [Sydney Brenner, Robert Horvitz and John Sulston]. Winners of the 2002 Nobel Prize in medicine or physiology. Genetic regulation of organ development and programmed cell death], *Lakartidningen*.99 (2002) 4026-4032.

[10] A.E Nel, L. Madler, D. Velegol, T. Xia, E.M.V. Hoek, P. Somasundaran, F. Klaessig, V. Castranova, M. Thompson, Understanding biophysicochemical interactions at the nano-bio interface, *Nat. Mater*.8 (2009) 543-557.

[11] M.P. Monopoli, C. Aberg, A. Salvati, K.A. Dawson, Biomolecular coronas provide the biological identity of nanosized materials, *Nat. Nanotechnol*.7 (2012) 779-786.

[12] C.D. Walkey, J.B. Olsen, H. Guo, A. Emili, W.C.W. Chan, Nanoparticle Size and Surface Chemistry Determine Serum Protein Adsorption and Macrophage Uptake, *J. Am. Chem. Soc*. 134 (2011) 2139-2147.

[13] S. Laera, G. Ceccone, F. Rossi, D. Gilliland, R. Hussain, G. Siligardi, L. Calzolai, Measuring Protein Structure and Stability of Protein-Nanoparticle Systems with Synchrotron Radiation Circular Dichroism, *Nano Lett*.11 (2011) 4480-4484.

[14] X. Lu, P. Xu, H.M. Ding, Y.S. Yu, D. Huo, Y.Q. Ma, Tailoring the component of protein corona via simple chemistry, *Nat. Commun*.10 (2019) 4520.

[15] S. Ritz, S. Schöttler, N. Kotman, G. Baier, A. Musyanovych, J. Kuharev, K. Landfester, H. Schild, O. Jahn, S. Tenzer, V. Mailänder, Protein corona of nanoparticles: distinct proteins regulate the cellular uptake, *Biomacromolecules.*16 (2015) 1311-1321.

[16] S.R. Saptarshi, A. Duschl, A.L. Lopata, Interaction of nanoparticles with proteins: relation to bio-reactivity of the nanoparticle. *J Nanobiotechnology*. 11 (2013) 26.

[17] T. Galloway, C. Lewis, I. Dolciotti, B.D. Johnston, J. Moger, F. Regoli. Sublethal toxicity of nano-titanium dioxide and carbon nanotubes in a sediment dwelling marine polychaete. *Environ. Pollut.* 158 (2010) 1748-1755.

[18] H.L Karlsson, J. Gustafsson, P. Cronholm, L. Möller, Size-dependent toxicity of metal oxide particles - a comparison between nano- and micrometer size. *Toxicol. Lett.* 188 (2009) 112-118.

[19] Z. Li, K. Greden, P.J.J Alvarez, K.B. Gregory, G.V. Lowry, Adsorbed polymer and nom limits adhesion and toxicity of nano scale zerovalent iron to coli, *E. Environ. Sci. Technol.* 44 (2010) 3462-3467.

[20] N. Zhang, G. Xiong, Z. Liu, Toxicity of metal-based nanoparticles: Challenges in the nano era, *Front. Bioeng. Biotechnol.,* 10 (2022) 1001572.

[21] C.W. Yong, Study of interactions between polymer nanoparticles and cell membranes at atomistic levels. *Phil. Trans. R. Soc. B* 370 (2015) 20140036.

[22] J. Tian, Z. Shi, G. Wang, Thermodynamic and Kinetic Binding Behaviors of Human Serum Albumin to Silver Nanoparticles, *Materials,* 15 (2022) 4957.

[23] M. Suvarna, S. Dyawanapelly, B. Kansara, P. Dandekar, R.D. Jain, Understanding the stability of nanoparticle-protein interactions: effect of particle size on adsorption, conformation and thermodynamic properties of serum albumin proteins. *ACS Appl. Nano Mater.* 1 (2018) 5524-5535.

[24] F. Tavanti, M.C. Menziani, Computational Insight on the Interaction of Common Blood Proteins with Gold Nanoparticles, *Int. J. Mol. Sci*. 22 (2021) 8722.

[25] W.E. Doering, S. Nie, Single-molecule and single-nanoparticle SERS: Examining the roles of surface-active sites and chemical enhancement. *J. Phys. Chem. B* 106 (2002) 311-317.

[26] N. Elahi, M. Kamali, M.H. Baghersad, Recent biomedical applications of gold nanoparticles: A review. Talanta., 184 (2018) 537-556.

[27] D. Hense, A. Büngeler, F. Kollmann, M. Hanke, A. Orive, A. Keller, G. Grundmeier, K. Huber, O.I. Strube, Self-Assembled Fibrinogen Hydro- and Aerogels with Fibrin-like 3D Structures, *Biomacromolecules*, 22 (2021) 4084−4094.

[28] S. Gurunathan, J.H. Park, J.W. Han, J.H. Kim. Comparative assessment of the apoptotic potential of silver nanoparticles synthesized by Bacillus tequilensis and Calocybe indica in MDA-MB-231 human breast cancer cells: Targeting p53 for anticancer therapy. *Int. J. Nanomed*. 10 (2015) 4203-4222.

[29] M. Rai, K. Kon, A. Ingle, N. Durán, S. Galdiero, M. Galdiero, Broad-spectrum bioactivities of silver nanoparticles: the emerging trends and future prospects. *Appl Microbiol Biotechnol.* 98 (2014) 1951-1961.

[30] X.F. Zhang, Z.G. Liu, W. Shen, S. Gurunathan, Silver Nanoparticles: Synthesis, Characterization, Properties, Applications, and Therapeutic Approaches. *Int J Mol Sci*. 17 (2016) 1534.

[31] X. Kang, S. Jadhav, M. Annaji, C.H. Huang, R. Amin, J. Shen, C.R. Ashby, A.K. Jr.; A.K. Tiwari, R.J. Babu, P. Chen, Advancing Cancer Therapy with Copper/Disulfiram Nanomedicines and Drug Delivery Systems. *Pharmaceutics* 15 (2023**)** 1567.

[32] G.Y. Karaca, F. Kuralay, E. Uygun, K. Ozaltin, S.E. Demirbuken, B. Garipcan, A.U. Oksuz, Gold–Nickel Nanowires as Nanomotors for Cancer Marker Biodetection and Chemotherapeutic Drug Delivery. *ACS Appl. Nano Mater.,* 4 (2021) 3377-3388.

[33] R.J. Browning, P.J.T Reardon, M. Parhizkar, R.B. Pedley, M. Edirisinghe, J.C. Knowles, E. Stride, Drug Delivery Strategies for Platinum-Based Chemotherapy. *ACS Nano,* 11 (2017) 8560-8578.

[34] R. Safdar Ali, H. Meng, Z. Li, Zinc-Based Metal-Organic Frameworks in Drug Delivery, Cell Imaging, and Sensing. *Molecules*. 27(2022) 100.

[35] J.A. Webb, R. Bardhan, Emerging advances in nanomedicine with engineered gold nanostructures, *Nanoscale*, 6 (2014) 2502-2530.

[36] Y. Xia, Y. Xiong, B. Lim, S.E. Skrabalak, Shape-controlled synthesis of metal nanocrystals: simple chemistry meets complex physics? Angew. *Chem. Int. Ed. Engl.* 48 (2009) 60-103.

[37] M. Faraday, The bakerian lecture: Experimental relations of gold (and other metals) to light. *Philos. Trans. R. Soc. Lond*. 147 (1857) 145-181.

[38] I.K. Suh, H. Ohta, Y. Waseda, High-temperature thermal expansion of six metallic elements measured by dilatation method and X-ray diffraction. *J. Mater. Sci*., 23 (1988), 757−760.

[39] S. Link, M. A. El-Sayed, “Size and temperature dependence of the plasmon absorption of colloidal gold nanoparticles,” *J. Phys. Chem. B*, 103 (1999) 4212-4217.

[40] J.F. Hillyer, R.M. Albrecht, “Gastrointestinal persorption and tissue distribution of differently sized colloidal gold nanoparticles,” *J. Pharm. Sci.*, 90 (2001) 1927-1936.

[41] J. Zhang, M. Ahmadi, G. Fargas, N. Perinka, J. Reguera, S. Lanceros-Méndez, L. Llanes, E. Jiménez-Piqué, Silver Nanoparticles for Conductive Inks: From Synthesis and Ink Formulation to Their Use in Printing Technologies. *Metals,* 12 (2022) 234.

[42] H. Feng, Y. Yang, Y. You, G. Li, J. Guo, T. Yu, B. Xing, “Simple and rapid synthesis of ultrathin gold nanowires, their self-assembly and application in surface-enhanced Raman scattering,” *Chem. Comm*, 15 (2009) 1984–1986.

[43] Y. Sun, Y. Xia, “Increased sensitivity of surface plasmon resonance of gold nanoshells compared to that of gold solid colloids in response to environmental changes,” *Anal. Chem.*, 74 (2002) 5297-5305.

[44] Y. Sun, Y. Xia, “Mechanistic study on the replacement reaction between silver nanostructures and chloroauric acid in aqueous medium,” *J. Am. Chem. Soc.*, 126 (2004) 3892-3901.

[45] L. Lu, K. Ai, Y. Ozaki, “Environmentally friendly synthesis of highly monodisperse biocompatible gold nanoparticles with urchin-like shape,” *Langmuir,* 24 (2008) 1058-1063.

[46] Z. Yang, Z. Li, X. Lu, “Controllable biosynthesis and properties of gold nanoplates using yeast extract,” *Nano-Micro Letters*, 9 (2017) 5.

[47] V. M. Cepak, C. R. Martin, “Preparation and stability of template-synthesized metal nanorod sols in organic solvents,” *J. Phys. Chem. B*, 102 (1998) 9985–9990.

[48] I.K. Suh, H. Ohta, Y. Waseda, High-temperature thermal expansion of six metallic elements measured by dilatation method and X-ray diffraction. *J. Mater. Sci*., 23 (1988), 757-760.

[49] M. Diantoro, R. Fitrianingsih, N. Mufti, A. Fuad, Synthesis of silver nanoparticles by chemical reduction at various fraction of MSA and their structure characterization, American Institute of Physics, In *AIP Conference Proceedings*, 1589 (2014) 257-261.

[50] A. Tomak, B. Yilancioglu, D. Winkler, C.O. Karakus, Protein corona formation on silver nanoparticles under different conditions, *Colloids Surf. A*: *Physicochemical and Engineering Aspects* 651 (2022) 129666

[51] R.L. Pinals, D. Yang, D.J. Rosenberg, T. Chaudhary, A.R. Crothers, A.T. Iavarone, M. Hammel, M.P. Landry, Protein corona composition and dynamics on carbon nanotubes in blood plasma and cerebrospinal fluid, *bio-Rxiv.*1 (2020) 13.

[52] F. Bertoli, G.L. Davies, M.P. Monopoli, M. Moloney, Y.K. Gun'ko, A. Salvati, K.A. Dawson, Magnetic nanoparticles to recover cellular organelles and study the time resolved nanoparticle-cell interactome throughout uptake, *Small*, 10 (2014) 3307-3315.

[53] A.A. Vodyashkin, P. Kezimana, F.Y. Prokonov, I.A. Vasilenko, Y.M. Stanishevskiy, Current methods for synthesis and potential applications of cobalt nanoparticles: A review. *Crystals*, 12 (2022) 272.

[54] X. Huang, H. Li, S. Li, S. Wu, F. Boey, J. Ma, H. Zhang, Synthesis of gold square-like plates from ultrathin gold square sheets: the evolution of structure phase and shape. Angew *Chem. Int. Ed.* 50 (2011) 12245-12248.

[55] X.F. Zhang, Z.G. Liu, W. Shen, S. Gurunathan, Silver Nanoparticles: Synthesis, Characterization, Properties, Applications, and Therapeutic Approaches. *Int J Mol Sci*. 17 (2016) 1534.

[56] G.A. Vinnacombe-Willson, N. Chiang, P.S. Weiss, S.H. Tolbert, L. Scarabelli, Seeded-Growth Experiment Demonstrating Size- and Shape-Dependence on Gold Nanoparticle-Light Interactions. *J Chem Educ.*, 98 (2021) 546-552.

[57] N.R. Jana, L. Gearheart, C.J. Murphy, Seeding growth for size control of 5 - 40 nm diameter gold nanoparticles. *Langmuir* 17 (2001) 6782-6786.

[58] B. Nikoobakht, M.A. El-Sayed, Preparation and growth mechanism of gold nanorods (NRs) using seed-mediated growth method. *Chem. Mater.* 15 (2003) 1957-1962.

[59] N.R. Jana, L. Gearheart, C.J. Murphy, Wet chemical synthesis of high aspect ratio cylindrical gold nanorods. *J. Phys. Chem. B* 105 (2001) 4065-4067.

[60] H. Masuda, K. Fukuda, Ordered metal nanohole arrays made by a two-step replication of honeycomb structures of anodic alumina. *Science* 268 (1995) 1466-1468.

[61] J. Kyler Carroll, J. Ulises Reveles, D. Michael Shultz, N. Shiv Khanna, E. Everett Carpenter, Preparation of Elemental Cu and Ni Nanoparticles by the Polyol Method: An Experimental and Theoretical Approach, *J. Phys. Chem. C* 2011 *115* (6), 2656-2664.

[62] W.J. Liu, T.T. Qian, H. Jiang, Bimetallic Fe nanoparticles: Recent advances in synthesis and application in catalytic elimination of environmental pollutants. *Chem. Eng. J.,* 236 (2014) 448-463.

[63] A. Kumar, A.S. Mukasyan, E.E. Wolf, Combustion synthesis of Ni, Fe and Cu multi-component catalysts for hydrogen production from ethanol reforming. *Appl. Catal. A: General,* 401 (2011) 20-28.

[64] R. Raliya, J.C. Tarafdar, Biosynthesis and characterization of zinc, magnesium and titanium nanoparticles: an eco-friendly approach. *Int Nano Lett* 4 93 (2014) 93.

[65] G. Sainath, B.K. Choudhary, T. Jayakumar, Molecular dynamics simulation studies on the size dependent tensile deformation and fracture behaviour of body centred cubic iron nanowires. *Comput. Mater. Sci.*, 104 (2015) 76-83.

[66] W.S. Lin, H.M. Lin, H.H. Chen, Y.K. Hwu, Y.J. Chiou, Shape effects of iron nanowires on hyperthermia treatment. *J. Nanomater.*, *2013* (2013) 237439.

[67] W.S. Lin, Z.J. Jian, H.M. Lin, L.C. Lai, W.A. Chiou, Y.K. Hwu, S.H. Wu, W.C. Chen, Y.D. Yao, Synthesis and characterization of iron nanowires. *Journal of the Chinese Chemical Society*, 60 (2013) 85-91.

[68] S. Xu, Y. Su, D. Chen, L. Li, An atomistic study of the deformation behavior of tungsten nanowires. *Appl. Phys. A*, 123 (2017) 788.

[69] S. Vaddiraju, H. Chandrasekaran, M.K. Sunkara, (2003). *Vapor Phase Synthesis of Tungsten Nanowires. J. Am. Chem. Soc.,* 125 (2003), 10792-10793.

[70] M.Z. Alyami, Y. Li, N. Patel, W. Baslyman, O. Alahmed, N.A. Alsharif, J. Sleiman, J. Kosel, J.S. Merzaban, N.M. Khashab, Iron Nanowires Coated with Metal–Organic Frameworks for Cell-Type-Specific Multimodal Therapy. *ACS Appl. Nano Mater.,* 5 (2022) 13903-13911.

[71] V.C.A. de la Pen~ a O'Shea, I.D.P. Moreira, A. Rolda´ n, F. Illas, Electronic and magnetic structure of bulk cobalt: The and-phases from density functional theory calculations, *J. Chem. Phys.*, 133 (2010) 024701.

[72] B. Farkaš, D. Santos-Carballal, A. Cadi-Essadek, N.H. de Leeuw, A DFT+U study of the oxidation of cobalt nanoparticles: Implications for biomedical applications. *Materialia,* (2019) 100381.

[73] C.P. Gräf, R. Birringer, A. Michels, *Synthesis and magnetic properties of cobalt nanocubes. Phys. Rev. B,* 73 (2006) 212401.

[74] Y.J. Chen, B. Chi, H.Z. Zhang, H. Chen, Y. Chen, Controlled growth of zinc nanowires. *Mater. Lett.,* 61 (2007), 144-147.

[75] Y. Yan, P. Liu, M.J. Romero, M.M. Al-Jassim, Formation of metallic zinc nanowires. *J. Appl. Phys.,* 93 (2003), 4807-4809.

[76] H. Hong, J. Shi, Y. Yang, Y. Zhang, J.W. Engle, R.J. Nickles, W. Cai, Cancer-Targeted Optical Imaging with Fluorescent Zinc Oxide Nanowires. *Nano Letters*, 11 (2011), 3744-3750.

[77] E. Rauwel, S. Al-Arag, H. Salehi, C.O. Amorim, F. Cuisinier, M. Guha, P. Rauwel, Assessing Cobalt Metal Nanoparticles Uptake by Cancer Cells Using Live Raman Spectroscopy. *Inter. J. Nanomedicine*, 15 (2020) 7051-7062.

[78] D. Holec, P. Dumitraschkewitz, D. Vollath, F.D. Fischer, Surface Energy of Au Nanoparticles Depending on Their Size and Shape, *Nanomaterials* 10 (2020) 484.

[79] C.J. Huang, P.H. Chiu, Y.H. Wang, W.R. Chen, T.H. Meen, Synthesis of the Gold Nanocubes by Electrochemical Technique. *J. Electrochem. Soc.,* 153 (2006) D129.

[80] Y. Inoue, Y. Tsutamoto, D. Muko, K. Nanamura, T. Sawada, Y. Niidome, Stepwise Preparation of Spherical Gold Nanoparticles Passivated with Cationic Amphiphiles. *Anal. Sci.,* 32 (2016) 875-880.

[81] H. Ding, D. Yang, C. Zhao, Z. Song, P. Liu, Y. Wang, J. Shen, Protein–Gold Hybrid Nanocubes for Cell Imaging and Drug Delivery. *ACS Appl Mater Interfaces,* 7 (2015) 4713-4719.

[82] X. Huang, W. Qian, I.H. El-Sayed, M.A. El-Sayed, The potential use of the enhanced nonlinear properties of gold nanospheres in photothermal cancer therapy. *Lasers. Surg. Med.,* 39 (2007) 747-753.

[83] R.S. Molla, A study on Manufacturing of Deformed Bar (G 60-400W) at Elite Iron and Steel Industries. (2018) 123.

[84] W. Betteridge, The properties of metallic cobalt, *Prog. Mater. Sci*., 24 (1980) 51-142.

[85] A. Rahman, A.K. Rahman, W. Ghann, H. Kang, J. Uddin, Terahertz multispectral imaging for the analysis of gold nanoparticles' size and the number of unit cells in comparison with other techniques, *Int. J. Biosen. Bioelectron.*, 4 (2018) 169.

[86] https://www.webelements.com/crystal_structure.html

[87] L. Chen, Q. Wang, L. Xiong, Molecular dynamics study on structure stability, lattice variation, and melting behavior of silver nanoparticles. *J. Nanoparticle Research,* 19 (2017) 1-11.

[88] X. Liu, K. Xu, H. Zhai, Pressure dependence of structural and mechanical properties of single-crystal tungsten: A molecular dynamics study. *Metals*, 11 (2021) 1898.

[89] J.A.M. Aquino, Magnetic and electronic properties of the compound Y (Co, Fe) 5 calculated by the augmented spherical wave method (2011).

[90] R.W. Lynch, H.G. Drickamer, The effect of pressure on the resistance and lattice parameters of cadmium and zinc. *J. Phys. Chem. Sol.,* 26 (1965) 63-68.

[91] H. Chen, Y. Gao, H. Yu, H. Zhang, L. Liu, Y. Shi, J. Li, Structural properties of silver nanorods with fivefold symmetry, *Micron,* 35 (2004), 469-474.

[92] A.S. Lanje, S.J. Sharma, R.B. Pode, Synthesis of silver nanoparticles: a safer alternative to conventional antimicrobial and antibacterial agents. *J. Chem. Pharm. Res*, 2 (2010) 478-483.

[93] D. Lomelí-Marroquín, D. Medina Cruz, A. Nieto-Argüello, A. Vernet Crua, J. Chen, A. Torres-Castro, T.J. Webster, J.L. Cholula-Díaz, Starch-mediated synthesis of mono-and bimetallic silver/gold nanoparticles as antimicrobial and anticancer agents. *Int. J. nanomedicine*, 14 (2019) 2171-2190.

[94] A.E. Shumskaya, E.Y. Kaniukov, A.L. Kozlovskiy, M.V. Zdorovets, V.S. Rusakov, K.K. Kadyrzhanov, Structure and physical properties of iron nanotubes obtained by template synthesis. *Phys. Solid State*, 59 (2017) 784-790.

[95] H. Cao, L. Wang, Y. Qiu, Q. Wu, G. Wang, L. Zhang, X. Liu, Generation and Growth Mechanism of Metal (Fe, Co, Ni) Nanotube Arrays. *Chem. Phys. Chem*, 7 (2006) 1500-1504.

[96] O Milkovič, J. Gamcová, M. Sopko, I. Škorvánek, Structure and magnetic properties of iron/iron-oxide nanoparticles prepared by precipitation from solid state solution. *Acta Physica Polonica A.* 131 (2017) 747-9.

[97] T.N. Narayanan, M.M. Shaijumon, P.M. Ajayan, M.R. Anantharaman, Synthesis of High Coercivity Cobalt Nanotubes with Acetate Precursors and Elucidation of the Mechanism of Growth*. J. Phys. Chem. C,* 112 (2008), 14281–14285.

[98] J. Hu, Q. Li, X.M. Meng, C.S. Lee, S.T. Lee, Thermal reduction route to the fabrication of coaxial Zn/ZnO nanocables and ZnO nanotubes. *Chem. Mater.*, 15 (2003) 305-308.

[99] S. Roy, A.K. Dasgupta, Controllable self-assembly from fibrinogen-gold (fibrinogen-Au) and thrombin-silver (thrombin-Ag) nanoparticle interaction*. FEBS Letters,* 581 (2007), 5533-5542.

[100] S. Rai, H. Singh, Electronic structure theory based study of proline interacting with gold nano clusters. *J Mol Model* 19 (2013) 4099-4109.

[101] S. Karmakar, N. Sarkar, L.M. Pandey, (2019). Proline functionalized gold nanoparticles modulates lysozyme fibrillation. *Colloids Surf. B: Biointerfaces,* 174 (2019) 401-408.

[102] S. Adnan, N.H. Kalwar, M.W. Abbas, Enzyme-free colorimetric sensing of glucose using l-cysteine functionalized silver nanoparticles. *SN Appl. Sci.* 1 (2019) 144.

[103] https://pubchem.ncbi.nlm.nih.gov/compound/Proline

[104] https://pubchem.ncbi.nlm.nih.gov/compound/Cysteine

[105] A. Pawlukojć, J. Leciejewicz, A.J. Ramirez-Cuesta, J. Nowicka-Scheibe, l-Cysteine: Neutron spectroscopy, Raman, IR and ab initio study. *Spectrochim Acta A Mol Biomol Spectrosc*. 61 (2005) 2474-81.

[106] M.M. Borah, Structural and spectroscopic analysis of L-Proline monomer and dimer by DFT approach. *Vietnam J. Chem.*, 60 (2022) 718-737.

[107] P. Vu Nhat, N.T. Si, N.T. Tien, M.T. Nguyen, Theoretical Study of the Binding of the Thiol-Containing Cysteine Amino Acid to the Silver Surface Using a Cluster Model. *J. Phys. Chem. A.* 125 (2021) 3244-3256.

[108] R.I. Litvinov, J.W. Weisel, Fibrin mechanical properties and their structural origins, *Matrix Biol*. 60-61 (2017) 110-123.

[109] A.S. Wolberg, R.A. Campbell, Thrombin generation, fibrin clot formation and hemostasis. *Transfus. Apher. Sci.*, 38 (2008) 15-23.

[110] J.W. Weisel, R. I. Litvinov, Fibrin Formation, Structure and Properties. *Subcell. Biochem*. 82 (2017) 405-456.

[111] J. W. Weisel, Fibrinogen and fibrin. *Adv Protein Chem.* 70 (2005) 247-299.

[112] https://pubchem.ncbi.nlm.nih.gov/compound/Fibrin

[113] K. Tomii, Protein Properties. Reference Module in Life Sciences (2018). doi:10.1016/b978-0-12-809633-8.20266-5

[114] T. Wang, H. Tang, The physical characteristics of human proteins in different biological functions. *PLoS One*. 12 (2017) 0176234.

[115] W.S. Vedakumari, P. Prabu, S.C. Babu, T.P. Sastry, Fibrin nanoparticles as Possible vehicles for drug delivery, *Biochimica et Biophysica Acta (BBA)* 1830 (2013) 4244-4253.

[116] O. Vilanova, J.J. Mittag, P.M. Kelly, S. Milani, K.A. Dawson, J.O. Radler, G. Franzese, Understanding the Kinetics of Protein-Nanoparticle Corona Formation, *ACS Nano* 10 (2016) 10842–10850.

[117] S. Zanganeh, R. Spitler, M. Erfanzadeh, A.M. Alkilany, M. Mahmoudi, Protein corona, Opportunities and challenges, *Int. J. Biochem. Cell Biol.* 75 (2016) 143–147.

[118] P. Foroozandeh, A.A. Aziz, Merging worlds of nanomaterials and biological environment: factors governing protein corona formation on nanoparticles and its biological consequences, *Nanoscale Res. Lett.* 10 (2015) 221.

[119] T. Zhang, L. Wang, Q. Chen, C. Chen, Cytotoxic potential of silver nanoparticles, *Yonsei Med. J.* 55 (2014) 283-291.

[120] P.V. AshaRani, G. Low Kah Mun, M.P. Hande, S. Valiyaveettil, Cytotoxicity and genotoxicity of silver nanoparticles in human cells. *ACS Nano* 3 (2009) 279-290

[121] P.V. AshaRani, M.P. Hande, S. Valiyaveettil, Anti-proliferative activity of silver nanoparticles. *BMC Cell. Biol.* 10 (2009) 65

[122] Y.C. Yeh, B. Creran, V.M. Rotello, Gold nanoparticles: preparation, properties, and applications in bionanotechnology, *Nanoscale*, 4 (2012) 1871-1880.

[123] L. Venditti, G. Testa, F. Sciubba, L. Carlini, F. Porcaro, C. Meneghini, S. Mobilio, C. Battocchio, I. Fratoddi, Hydrophilic metal nanoparticles functionalized by 2-diethylaminoethane thiol: a close look on the metal-ligand interaction and interface chemical structure, *J. Phys. Chem. C,* 121 (2017) 8002-8013.

[124] L. Rodzik-Czałka, J. Lewandowska-Łańcucka, V. Gatta, I. Venditti, I. Fratoddi, M. Szuwarzyński, M. Romek, M. Nowakowska, Nucleobases functionalized quantum dots and gold nanoparticles bioconjugates as a FRET system: synthesis, characterization and potential applications *J. Colloid Interf. Sci.,* 514 (2018) 479-490.

[125] I. Fratoddi, A. Cartoni, I. Venditti, D. Catone, P. O'Keeffe, A. Paladini, F. Toschi, S. Turchini, F. Sciubba, G. Testa, C. Battocchio, L. Carlini, R. Proietti-Zaccaria, E. Magnano, I. Pis, L. Avaldi, Gold nanoparticles functionalized by rhodamine B isothiocyanate to tune plasmonic effects *J. Colloid Interf. Sci.,* 513 (2018) 10-19.

[126] S. Kim, J.E. Choi, J. Choi, K.H. Chung, K. Park, J. Yi, D.Y. Ryu, Oxidative stress-dependent toxicity of silver nanoparticles in human hepatoma cells. *Toxicol. In Vitro,* 23 (2009) 1076-1084

[127] J.E. Gagner, M.D. Lopez, J.S. Dordick, R.W. Siegel, Effect of gold nanoparticle morphology on adsorbed protein structure and function, *Biomaterials*, 32 (2011) 7241-7252.

[128] R. Chen, J.E. Riviere, Biological and environmental surface interactions of nanomaterials: characterization, modeling, and prediction. *WIREs Nanomed. Nanobi.,* 9 (2017) 1440-1470.

[129] A.M. Pudlarz, K. Ranoszek-Soliwoda, E. Czechowska, E. Tomaszewska, G. Celichowski, J. Grobelny, J. Szemraj, A study of the activity of recombinant Mn-

Superoxide dismutase in the presence of gold and silver nanoparticles, *Appl. Biochem. Biotechnol.,* 187 (2019) 1551-1568.

[130] E. Czechowska, K. Ranoszek-Soliwoda, E. Tomaszewska, A. Pudlarz, G. Celichowski, D. Gralak-Zwolenik, J. Szemraj, J. Grobelny, Comparison of the antioxidant activity of catalase immobilized on gold nanoparticles via specific and non-specific adsorption, *Colloids Surf. B Biointerfaces*, 171 (2018) 707-714.

[131] A.M. Pudlarz, E. Czechowska, K. Ranoszek-Soliwoda, E. Tomaszewska, G. Celichowski, J. Grobelny, J. Szemraj, Immobilization of recombinant human catalase on gold and silver nanoparticles, *Appl. Biochem. Biotechnol*., 185 (2018) 717-735.

[132] Y. Tauran, A. Brioude, A.W. Coleman, M. Rhimi, B. Kim, Molecular recognition by gold, silver and copper nanoparticles. *World J Biol Chem.* 4 (2013) 35-63.

[133] K. Ranoszek-Soliwoda, E. Czechowska, E. Tomaszewska, A. Pudlarz, J. Szemraj, G. Celichowski, J. Grobelny, Differences in corona formation of catalase immobilised on gold and silver nanoparticles. *Colloids and Surfaces A: Physicochemical and Engineering Aspects, J. Col. Surfa*. (2020)125003.

[134] F. Rusmini, Z. Zhong, J. Feijen, Protein immobilization strategies for protein biochips, *Biomacromolecules*, 8 (2007) 1775-1789.

[135] C. Gr¨afe, A. Weidner, M. vd Lühe, C. Bergemann, F.H. Schacher, J.H. Clement, S. Dutz, Intentional formation of a protein corona on nanoparticles: serum concentration affects protein corona mass, surface charge, and nanoparticle–cell interaction, *Int. J. Biochem. Cell Biol.* 75 (2016) 196-202.

[136] A.N. Kharlamov, J.L. Gabinsky, Plasmonic photothermic and stem cell therapy of atherosclerotic plaque as a novel nanotool for angioplasty and artery remodelling. *Rejuvenation Res.* 15 (2012) 222-230.

[137] F. Farjadian, A. Ghasemi, O. Gohari, A. Roointan, M. Karimi, M.R. Hamblin, Nanopharmaceuticals and nanomedicines currently on the market: challenges and opportunities. *Nanomedicine (Lond.)* 14 (2019) 93-126.

[138] S. Xiaoting, G. Xiang, L. Jie, W. Jingyuan, L. Yaping, Z. Zhiwen, Current approaches of nanomedicines in the market and various stage of clinical translation. *Acta Pharma. Sin. B,* 12 (2022) 3028-3048.

[139] A.N. Kharlamov, J.A. Feinstein, J.A. Cramer, J.A. Boothroyd, E.V. Shishkina, V. Shur, Plasmonic photothermal therapy of atherosclerosis with nanoparticles: long-term outcomes and safety in NANOM-FIM trial. *Future Cardiol*. 13 (2017) 345-363.

[140] P. Kumthekar, C.H. Ko, T. Paunesku, K. Dixit, A.M. Sonabend, O. Bloch, M. Tate, A first-in-human phase 0 clinical study of RNA interference-based spherical nucleic acids in patients with recurrent glioblastoma. *Sci Transl Med.* 13 (2021) 3945

[141] A. Sharma, R. Kumar, P. Varadwaj, Smelling the Disease: Diagnostic Potential of Breath Analysis. *Mol Diagn Ther.* 27 (2023) 321-347.

[142] W. Wang, Z. Huang, Y. Li, W. Wang, J. Shi, F. Fu, C. Wu, Impact of particle size and pH on protein corona formation of solid lipid nanoparticles: A proof-of-concept study, *Acta. Pharm. Sin. B,* 11 (2021) 1030-1046.

[143] N. Khlebtsov, L. Dykman, Biodistribution and toxicity of engineered gold nanoparticles: a review of in vitro and in vivo studies, *Chem. Soc. Rev*., 40 (2011) 1647-1671.

[144] Y.C. Yeh, B. Creran, V.M. Rotello, Gold nanoparticles: preparation, properties, and applications in bio-nanotechnology, *Nanoscale*, 4 (2012) 1871-1880.

[145] Z. Ferdous, A. Nemmar, Health Impact of Silver Nanoparticles: A Review of the Biodistribution and Toxicity Following Various Routes of Exposure. *Int J Mol Sci*. 21 (2020) 2375.

[146] V. De Matteis, Exposure to Inorganic Nanoparticles: Routes of Entry, Immune Response, Biodistribution and In Vitro/In Vivo Toxicity Evaluation. *Toxics*. 5 (2017) 29.

[147] F.N. Spagnoletti, F. Kronberg, C. Spedalieri, E. Munarriz, R. Giacometti, Protein corona on biogenic silver nanoparticles provides higher stability and protects cells from toxicity in comparison to chemical nanoparticles. *J Environ Manage*. 297 (2021) 113434.

[148] M. Del Pilar Chantada-Vázquez, A.C. López, S.B. Bravo, S. Vázquez-Estévez, B. Acea-Nebril, C. Núñez. Proteomic analysis of the bio-corona formed on the surface of (Au, Ag, Pt)-nanoparticles in human serum. *Colloids Surf B Biointerfaces*. 177 (2019) 141-148.

[149] W. Bal, M. Sokołowska, E. Kurowska, P. Faller, Binding of transition metal ions to albumin: Sites, affinities and rates. *Biochimica et Biophysica Acta (BBA) - General Subjects,* 1830 (2013) 5444-5455.

[150] P.P. Jing, Y.X. Li, Y.H. Su, W.L. Liang, Y.X. Leng, The role of metal ions in the behavior of bovine serum albumin molecules under physiological environment. *Spectrochimica Acta Part A Mol. Biomol. Spectrosc.*, *267* (2022) 120604.

[151] C. Weber, J. Simon, V. Mailänder, S. Morsbach, K. Landfester, Preservation of the soft protein corona in distinct flow allows identification of weakly bound proteins, *Acta biomater.*, 76 (2018) 217-224.

[152] D. Walczyk, F.B. Bombelli, M.P. Monopoli, I. Lynch, K.A. Dawson, What the cell "sees" in bionanoscience, *J. Am. Chemical Soc*. 132 (2010) 5761–5768.

[153] A. Bhargava, A. Dev, S.J. Mohanbhai, V. Pareek, N. Jain, S.R. Choudhury, S. Karmakar, Pre-coating of protein modulate patterns of corona formation, physiological stability and cytotoxicity of silver nanoparticles. *Sci. Total Environ., 772,* (2021) 144797.

[154] A. Tsuda, N.K. Venkata, The role of natural processes and surface energy of inhaled engineered nanoparticles on aggregation and corona formation, *NanoImpact*. 2 (2016) 38-44.

[155] A. Sasidharan, J.E. Riviere, N.A. Monteiro-Riviere, Gold and silver nanoparticle interactions with human proteins: impact and implications in biocorona formation. *J. Mater. Chem. B,* 3 (2015) 2075-2082.

[156] E. Casals, T. Pfaller, A. Duschl, G.J. Oostingh, V. Puntes, Time Evolution of the Nanoparticle Protein Corona. *ACS Nano*, 4 (2010) 3623-3632.

[157] G.S. Maiorano, S. Sabella, B. Sorce, V. Brunetti, M.A. Malvindi, R. Cingolani, P.P. Pompa, Effects of cell culture media on the dynamic formation of protein−nanoparticle complexes and influence on the cellular response. *ACS nano*, *4* (2010) 7481-7491.

[158] A.A. Vertegel, R.W. Siegel, J.S. Dordick, Silica Nanoparticle Size Influences the

Structure and Enzymatic Activity of Adsorbed Lysozyme, *Langmuir* 20 (2004) 6800-6807.

[159] T. Cedervall, I. Lynch, S. Lindman, T. Berggard, E. Thulin, H. Nilsson, K.A. Dawson, S. Linse, Understanding the nanoparticle–protein corona using methods to quantify exchange rates and affinities of proteins for nanoparticles, *Proc. Natl. Acad. Sci.* 104 (2007) 2050-2055.

[160] J. Klein, Probing the interactions of proteins and nanoparticles, *Proc. Natl. Acad. Sci.* 104 (2007) 2029-2030.

[161] S. Tenzer, D. Docter, J. Kuharev, A. Musyanovych, V. Fetz, R. Hecht, F. Schlenk, D.Fischer, K. Kiouptsi, C. Reinhardt, K. Landfester, H. Schild, M. Maskos, S.K. Knauer, R.H. Stauber, Rapid formation of plasma protein corona critically affects nanoparticle pathophysiology, *Nat. Nanotechnol*. 8 (2013) 772-781.

[162] M.S. Ehrenberg, A.E. Friedman, J.N. Finkelstein, G. Oberdörster, J.L. McGrath, The influence of protein adsorption on nanoparticle association with cultured endothelial cells, *Biomaterials* 30 (2009) 603-610.

[163] V.H. Nguyen, B.J. Lee, Protein corona: a new approach for nanomedicine design, *Int. J. Nanomed.* 12 (2017) 3137-3151.

[164] A. Kondo, S. Oku, F. Murakami, K.O. Higashitani, Conformational changes in protein molecules upon adsorption on ultrafine particles, *Colloids Surf. B* 1 (1993) 197-201.

[165] R. García-Álvarez, M. Hadjidemetriou, A. Sánchez-Iglesias, L.M. Liz-Marzán, K. Kostarelos, In vivo formation of protein corona on gold nanoparticles. The effect of their size and shape, *Nanoscale* 10 (2018) 1256-1264.

[166] L. Ding, C. Yao, X. Yin, C. Li, Y. Huang, M. Wu, B. Wang, X. Guo, Y. Wang, M. Wu, Size, Shape, and Protein Corona Determine Cellular Uptake and Removal Mechanisms of Gold Nanoparticles, *Small* 14 *(*2018) 1801451.

[167] P. Wang, X. Wang, L. Wang, X. Hou, W. Liu, C. Chen, Interaction of gold nanoparticles with proteins and cells, *Sci. Technol. Adv. Mater*. 16 (2015) 034610.

[168] A.A. Ashkarran, M. Ghavami, H. Aghaverdi, P. Stroeve, M. Mahmoudi, Bacterial effects and protein corona evaluations: crucial ignored factors in the prediction of bio-

efficacy of various forms of silver nanoparticles. *Chem. Res. Toxicol*. 25 (2012) 1231-1242

[169] M. Schäffler, M. Semmler-Behnke, H. Sarioglu, S. Takenaka, A. Wenk, C. Schleh, S.M. Hauck, B.D. Johnston, W.G. Kreyling, Serum protein identification and quantification of the corona of 5, 15 and 80 nm gold nanoparticles, *Nanotechnology*, 24 (2013) 265103.

[170] S.H. Lacerda, J.J. Park, C. Meuse, D. Pristinski, M.L. Becker, A. Karim, J.F. Douglas, Interaction of gold nanoparticles with common human blood proteins, *ACS Nano* 4 (2010) 365-379.

[171] Z.J. Deng, M. Liang, I. Toth, M.J. Monteiro, R.F. Minchin, Molecular interaction of poly(acrylic acid) gold nanoparticles with human fibrinogen. *ACS Nano* 6 (2012) 8962-8969.

[172] D. Glancy, Y. Zhang, J.L.Y. Wu, B. Ouyang, S. Ohta, W.C.W. Chan, Characterizing the protein corona of sub-10 nm nanoparticles, *J. Control. Release,* 304 (2019) 102-110.

[173] I. Fratoddi, Hydrophobic and Hydrophilic Au and Ag Nanoparticles. Breakthroughs and Perspectives. *Nanomaterials (Basel).* 8 (2017) 11.

[174] S. Lindman, I. Lynch, E. Thulin, H. Nilsson, K.A. Dawson, S. Linse, Systematic investigation of the thermodynamics of HSA adsorption to N-iso-propylacrylamide/N-tert-butylacrylamide copolymer nanoparticles. Effects of particle size and hydrophobicity. *Nano Lett.* 7 (2007) 914-920.

[175] Q. Yu, L. Zhao, C. Guo, B. Yan, G. Su, Regulating Protein Corona Formation and Dynamic Protein Exchange by Controlling Nanoparticle Hydrophobicity, *Front. Bioeng. Biotechnol*, 8 (2020) 210.

[176] J. Ashby, S. Pan, S, W. Zhong, Size and surface functionalization of iron oxide nanoparticles influence the composition and dynamic nature of their protein corona. *ACS Appl. Mater. Interfaces* 6 (2014) 15412-15419.

[177] C.M. Goodman, C.D. McCusker, T. Yilmaz, V.M. Rotello, Toxicity of gold nanoparticles functionalized with cationic and anionic side chains, *Bioconjug. Chem*. 15 (2004) 897-900.

[178] S. Hirn, M. Semmler-Behnke, C. Schleh, Particle size-dependent and surface charge-dependent biodistribution of gold nanoparticles after intravenous administration, *Eur. J. Pharm. Biopharm*. 77 (2011) 407-416.

[179] C. Schleh, S. Semmler-Behnke, J. Lipka, Size and surface charge of gold nanoparticles determine absorption across intestinal barriers and accumulation in secondary target organs after oral administration, *Nanotoxicology* 6 (2012) 36-46.

[180] C.W. Kuo, J.J.L. Lai, P. Chen, Cytotoxicity of the Functionalized Gold and Silver Nanorods*. MRS Proceedings,* 951 (2006) 0951-E12*.*

[181] Z.J Deng, M. Liang, I. Toth, M. Monteiro, R.F. Minchin, Plasma protein binding of positively and negatively charged polymer-coated gold nanoparticles elicits different biological responses. *Nanotoxicology* 7 (2013) 314–322.

[182] S. Fertsch-Gapp, M. Semmler-Behnke, A. Wenk, W.G. Kreyling, Binding of polystyrene and carbon black nanoparticles to blood serum proteins. *Inhal Toxicol*., 23 (2011) 468-475.

[183]W. Shang, J.H. Nuffer, V.A. MuñizPapandrea, W. Colón, R.W. Siegel, J.S. Dord ick, Cytochrome c on silica nanoparticles: influence of nanoparticle size on protein structure, stability, and activity, *Small*, 5 (2009) 470-476.

[184] Z.J. Deng, M. Liang, M. Monteiro, I. Toth, R.F. Minchin, Nanoparticle-induced unfolding of fibrinogen promotes Mac-1 receptor activation and inflammation. *Nat. Nanotechnol*. 6 (2011) 39-44.

[185] R. Eigenheer, E.R. Castellanos, M.Y. Nakamoto, K.T. Gerner, A.M. Lampeb, K.E. Wheeler, Silver nanoparticle protein corona composition compared across engineered particle properties and environmentally relevant reaction conditions. *Environ. Sci. Nano.* 1 (2014) 238-247.

[186] R. García-Álvarez and M. Vallet-Regí, Hard and Soft Protein Corona of Nanomaterials: Analysis and Relevance, *Nanomaterials*, 11 (2021) 888.

[187] L. Vroman, A.L. Adams, G.C. Fischer, P.C. Munoz, Interaction of high molecular weight kininogen, factor XII, and fibrinogen in plasma at interfaces, *Blood* 55 (1980) 156-159.

[188] L. Treuel, S. Brandholt, P. Maffre, S. Wiegele, L. Shang, G.U. Nienhaus, Impact of protein modification on the protein corona on nanoparticles and nanoparticle-cell interactions. *ACS Nano* 8 (2014) 503-513.

[189] L.M. Wang, J.Y. Li, J. Pan, X.M. Jiang, Y.L. Ji, Y.F. Li, Y. Qu, Y.L. Zhao, X.C. Wu, C.Y. Chen, Revealing the binding structure of the protein corona on gold nanorods using synchrotron radiation-based techniques: understanding the reduced damage in cell membranes. *J. Am. Chem. Soc*. 135 (2013) 17359-17368.

[190] H.K. Baca, E. Carnes, S. Singh, C. Ashley, D. Lopez, C.J. Brinker, Cell-Directed Assembly of Bio/Nano Interfaces - A New Scheme for Cell Immobilization, *Acc. Chem. Res*. 40 (2007) 836-845.

[191] H. Grönbeck, A. Curioni, W. Andreoni, Thiols and Disulfides on the Au(111) Surface: The Headgroup−Gold Interaction, *J. Am. Chem. Soc.* 122 (2000) 3839-3842.

[192] L.E. Valenti, C.E. Giacomelli, Unaffected features of BSA stabilized Ag nanoparticles after storage and reconstitution in biological relevant media. *Colloids and Surfaces B: Biointerfaces,* 132 (2015) 71-77.

[193] J.E. Diederichs, Plasma protein adsorption patterns on liposomes: establishment of analytical procedure. *Electrophoresis*. 17 (1996) 607-611

[194] M. Lück, B.R. Paulke, W. Schröder, T. Blunk, R. Müller, Analysis of plasma protein adsorption on polymeric nanoparticles with different surface characteristics. *J. Biomed. Mater. Res.* 39 *(*1998) 478-485.

[195] A. Gessner, R. Waicz, A. Lieske, B.R. Paulke, K. Mäder, R. Müller, Nanoparticles with decreasing surface hydrophobicities: influence on plasma protein adsorption. *Int. J. Pharm.* 196 (2000) 245-249.

[196] T. Cedervall, I. Lynch, S. Lindman, Understanding the nanoparticle–protein corona using methods to quantify exchange rates and affinities of proteins for nanoparticles. *Proc. Natl Acad. Sci. USA*. 104 (2007) 2050-2055.

[197] A. Patra, T. Ding, G. Engudar, Y. Wang, M.M. Dykas, B. Liedberg, J.C.Y. Kah, T. Venkatesan, C.L. Drum, Component-specific analysis of plasma protein corona

formation on gold nanoparticles using multiplexed surface plasmon resonance, *Small*, 12 (2016) 1174-1182.

[198] A. Chaudhary, S. Khan, A. Gupta, C.K. Nandi, Effect of surface chemistry and morphology of gold nanoparticle on the structure and activity of common blood proteins *New J. Chem.,* 40 (2016) 4879-4883.

[199] N. Durán, C.P. Silveira, M. Durán, D.S.T. Martinez, Silver nanoparticle protein corona and toxicity: *a mini-review. J. Nanobiotechnology,* 13 (2015).

[200] M. Taha, M.J. Lee, Influence of the alanine side-chain methyl group on the peptide-gold nanoparticles interactions*. J. Mol. Liq*. 302 (2020) 112528.

[201] G. Brancolini, D.B. Kokh, L. Calzolai, R.C. Wade, S. Corni, Docking of Ubiquitin to Gold Nanoparticles, *ACS Nano* 6 (2012) 9863-9878.

[202] A.A. Buglak, R.R. Ramazanov, A.I. Kononov, Silver cluster-amino acid interactions: a quantum-chemical study. *Amino Acids*. 51 (2019) 855-864.

[203] M. Di Foggia, P. Taddei, A. Torreggiani, Self-assembling peptides for biomedical applications: IR and Raman spectroscopies for the study of secondary structure, *Proteomics Res J.*, 2 (2012) 231-272.

[204] L. Fei, S. Perrett, Effect of Nanoparticles on Protein Folding and Fibrillogenesis, *Int. J. Mol. Sci.* 10 (2009) 646-655.

[205] L. Shang, Y. Wang, J. Jiang, S. Dong., pH-Dependent protein conformational changes in albumin: Gold nanoparticle bioconjugates: A spectroscopic study. *Langmuir.* 23 (2007) 2714-2721.

[206] A. Ravindran, A. Singh, A.M. Raichur, N. Chandrasekaran, A. Mukherjee, Studies on interaction of colloidal Ag nanoparticles with Bovine Serum Albumin (BSA). *Colloids Surf B Biointerfaces*.76 (2010) 32-37.

[207] A.H. Pakiari and Z. Jamshidi, Interaction of Amino Acids with Gold and Silver Clusters, *J. Phys. Chem. A*, 111 (2007) 4391-4396.

[208] R. Li, R. Chen, P. Chen, Y. Wen, P.C. Ke, S.S. Cho, Computational and experimental characterizations of silver nanoparticle-apolipoprotein biocorona. *J Phys Chem B*. 117 (2013) 13451-6.

[209] D. Power, I. Rouse, S. Poggio, E. Brandt, H. Lopez, A. Lyubartsev, V.A. Lobaskin, Multiscale model of protein adsorption on a nanoparticle surface. *Model. Simul. Mater. Sci. Eng.* 27 (2019) 084003.

[210] S.K. Sohaebuddin, P.T. Thevenot, D. Baker, J.W. Eaton, L.P. Tang, Nanomaterial cytotoxicity is composition, size, and cell type dependent. *Part. Fibre. Toxicol.* 7 (2010) 22.

[211] A. Gojova, B. Guo, R.S. Kota, J.C. Rutledge, I.M. Kennedy, A.I. Barakat, Induction of inflammation in vascular endothelial cells by metal oxide nanoparticles: Effect of particle composition. *Environ Health Perspect* 115 (2007) 403-409.

[212] F. Turci, E. Ghibaudi, M. Colonna, B. Boscolo, I. Fenoglio, B. Fubini., An Integrated Approach to the Study of the Interaction between Proteins and Nanoparticles. *Langmuir* 26 (2010) 8336-8346.

[213] T. Kopac, K. Bozgeyik, J. Yener., Effect of pH and temperature on the adsorption of bovine serum albumin onto titanium dioxide. *Colloids Surf, A Physicochem Eng Asp* 322 (2008) 19-28.

[214] E.C Cho, Q. Zhang, Y. Xia., The effect of sedimentation and diffusion on cellular uptake of gold nanoparticles. *Nat Nano* 6 (2011) 385-391.

[215] J. Piella, N.G. Bastus, V. Puntes, Size-dependent protein-nanoparticle interactions in citrate-stabilized gold nanoparticles: the emergence of the protein corona, *Bioconjug. Chem*., 28 (2017) 88-97.

[216] J.H. Shannahan, R. Podila, A.A. Aldossari, H. Emerson, B.A. Powell, P.C. Ke, A.M. Rao, J.M. Brown, Formation of a protein corona on silver nano particles mediates cellular toxicity via scavenger receptors. *Toxicol. Sci.* 143 (2015) 136-146.

[217] M. Mahmoudi, I. Lynch, M.R. Ejtehadi, M.P. Monopoli, F.B. Bombelli, S. Laurent, Protein nanoparticle interactions: opportunities and challenges, *Chem. Rev.* 111 (2011) 5610-5637.

[218] M. Rabe, D. Verdes, S. Seeger, Understanding protein adsorption phenomena at solid surfaces, *Adv. Colloid Interf. Sci.* 162 (2011) 87-106.

[219] Q. Wei, T. Becherer, S. Angioletti-Uberti, J. Dzubiella, C. Wischke, A.T. Neffe, A. Lendlein, M. Ballauff, R. Haag, Protein interactions with polymer coatings and biomaterials, Angew. *Chem. Int. Ed*. 53 (2014) 8004-8031.

[220] C. Carrillo-Carrion, M. Carril, W.J. Parak, Techniques for the experimental investigation of the protein corona, *Curr. Opin. Biotechnol*. 46 (2017) 106–11.

[221] C. Gruian, E. Vanea, S. Simon, V. Simon, FTIR and XPS studies of protein adsorption onto functionalized bioactive glass, *Biochim. Biophys. Acta* 1824 (2012) 873-881.

[222] E. Vanea, V. Simon, XPS and Raman study of zinc containing silica microparticles loaded with insulin, *Appl. Surf. Sci.* 280 (2013) 144-150.

[223] G.L. Bovenkamp, U. Zanzen, K.S. Krishna, J. Hormes, A. Prange, X-ray absorption near-edge structure (XANES) spectroscopy study of the interaction of silver ions with Staphylococcus aureus, Listeria monocytogenes, and Escherichia coli. *Appl Environ Microbiol.* 79 (2013) 6385-6390.

[224] M. Kahraman, B.N. Balz, S. Wachsmann-Hogiu, Hydrophobicity-driven self-assembly of protein and silver nanoparticles for protein detection using surface-enhanced Raman scattering. *The Analyst,* 138 (2013) 2906.

[225] A. El-Ghannam, P. Ducheyne, I.M. Shapiro, Effect of serum proteins on osteoblast adhesion to surface-modified bioactive glass and hydroxyapatite, *J. Orthop. Res.* 17 (1999) 340-345.

[226] A. Vulpoi, C. Gruian, E. Vanea, L. Baia, S. Simon, H.J. Steinhoff, G. Göller, V. Simon, Bioactivity and protein attachment onto bioactive glasses containing silver nanoparticles, *J. Biomed. Mater. Res. A* 100 (2012) 1179-1186.

[227] G.K. Wang, C.L. Yan, S.Y. Gao, Y.F. Liu, Surface chemistry of gold nanoparticles determines interactions with bovine serum albumin, *Sci. Mater. Eng. C* 103 (2019) 109856.

[228] H. Zhang, J. Cao, S. Wu, Y. Wang, Mechanism of gold nanoparticles-induced trypsin inhibition: a multi-technique approach, *Mol. Biol. Rep*. 41 (2014) 4911-4918.

[229] H. Liu, N. Pierre-Pierre, Q. Huo, Dynamic light scattering for gold nanorod size

characterization and study of nanorod–protein interactions, *Gold Bull.* 45 (2012) 187-195.

[230] H. Jans, X. Liu, L. Austin, G. Maes, Q. Huo, Dynamic light scattering as a powerful tool for gold nanoparticle bioconjugation and biomolecular binding studies, *Anal. Chem.* 81 (2009) 9425-9432.

[231] L. Austin, X. Liu, Q. Huo, An immunoassay for monoclonal antibody isotyping and quality analysis using gold nanoparticle probes and dynamic light scattering, *Am. Biotech. Lab.* 28 (2010) 10-12.

[232] G.K. Wang, Y.F. Lu, H.M. Hou, Y.F. Liu, Probing the binding behavior and kinetics of silver nanoparticles with bovine serum albumin, *RSC Adv.* 7 (2017) 9393-9401.

[233] D.H. Tsai, F.W. DelRio, A.M. Keene, K.M. Tyner, R.I. MacCuspie, T.J. Cho, M.R. Zachariah, V.A. Hackley, Adsorption and conformation of serum albumin protein on gold nanoparticles investigated using dimensional measurements and in situ spectroscopic methods, *Langmuir* 27 (2011) 2464–2477.

[234] L. Calzolai, F. Franchini, D. Gilliland, F. Rossi, Protein–nanoparticle interaction: identification of the ubiquitin−gold nanoparticle interaction site, *Nano Lett.* 10 (2010) 3101-3105.

[235] G. Brancolini, D.B. Kokh, L. Calzolai, R.C. Wade, S. Corni, Docking of ubiquitin to gold nanoparticles, *ACS Nano* 6 (2012) 9863-9878.

[236] F. Charbgoo, M. Nejabat, K. Abnous, F. Soltani, S.M. Taghdisi, M. Alibolandi, W.T. Shier, T.W.J. Steele, M. Ramezani, Gold nanoparticle should understand protein corona for being a clinical nanomaterial, *J. Control. Release* 272 (2018) 39-53,

[237] K.P. Fears, T.D. Clark, D.Y. Petrovykh, Residue-dependent adsorption of model oligopeptides on gold, *J. Am. Chem. Soc.,* 135 (2013) 15040-15052.

[238] N.A. Belsey, A.G. Shard, C. Minelli, Analysis of protein coatings on gold nanoparticles by XPS and liquid-based particle sizing techniques, *Biointerphases*, 10 (2015) 019012.

[239] N.V. Konduru, R.M. Molina, A. Swami, F. Damiani, G. Pyrgiotakis, P. Lin, P. Andreozzi, T.C. Donaghey, P. Demokritou, S. Krol, Protein corona: Implications for nanoparticle interactions with pulmonary cells. *Part. Fibre Toxicol*. 14 (2017) 42.

[240] M. Cui, R. Liu, Z. Deng, G. Ge, Y. Liu, L. Xie, Quantitative study of protein coronas on gold nanoparticles with different surface modifications. *Nano Res.* 7 (2014) 345-352.

[241] R.P. Carney, J.Y. Kim, H. Qian, R. Jin, H. Mehenni, F. Stellacci, O.M. Bakr, Determination of nanoparticle size distribution together with density or molecular weight by 2D analytical ultracentrifugation, *Nat. Commun*., 2 (2011) 335.

[242] Ž. Krpetić, A.M. Davidson, M. Volk, R. Lévy, M. Brust, D.L. Cooper, High-resolution sizing of monolayer-protected gold clusters by differential centrifugal sedimentation ACS Nano, 7 (2013) 8881-8890.

[243] R. Capomaccio, I.O. Jimenez, P. Colpo, D. Gilliland, G. Ceccone, F. Rossi, L. Calzolai, Determination of the structure and morphology of gold nanoparticle–HSA protein complexes, *Nano*, 7 (2015) 17653-17657.

[244] L. Calzolai, D. Gilliland, C.P. Garcìa, F. Rossi, Separation and characterization of gold nanoparticle mixtures by flow-field-flow fractionation *J. Chromatogr. A,* 1218 (2011) 4234-4239.

[245] J.C. Giddings, Field-flow fractionation: analysis of macromolecular, colloidal, and particulate materials, *Science*, 260 (1993) 1456-1465.

[246] L. Treuel, M. Malissek, S. Grass, Quantifying the influence of polymer coatings on the serum albumin corona formation around silver and gold nanoparticles. *J Nanopart Res.,* 14 (2012) 1102.

[247] C. Palocci, L. Chronopoulou, I. Venditti, E. Cernia, M. Diociaiuti, I. Fratoddi, M.V. Russo. Lipolytic Enzymes with Improved Activity and Selectivity upon Adsorption on Polymeric Nanoparticles, *Biomacromolecules*, 8 (2007) 3047-3053.

[248] P. Asuri, S.S. Karajanagi, A.A. Vertegel, J.S. Dordick, R.S. Kane. Enhanced stability of enzymes adsorbed onto nanoparticles, *J Nanosci Nanotechnol.* 7 (2007) 1675-1678.

[249] G. Brancolini, V. Tozzini, Building Minimalist Models for Functionalized Metal Nanoparticles, *Front Mol Biosci*. 6 **(**2019) 50.

[250] A.S. Joshi, P. Singh, I. Mijakovic, Interactions of Gold and Silver Nanoparticles with Bacterial Biofilms: Molecular Interactions behind Inhibition and Resistance. *Int. J. Mol. Sci.* 21 (2020**)** 7658.

[251] P.A. Webb, Introduction to chemical adsorption analytical techniques and their applications to catalysis. *MIC Tech. Publ*, 13 (2003) 1-4.

[252] X.M. Jiang, L.M. Wang, C.Y. Chen, Cellular Uptake, Intracellular Trafficking and Biological Responses of Gold Nanoparticles, *J. Chin. Chem. Soc*. 58 (2011) 273-278.

[253] M. Ozboyaci, D. B. Kokh, R. C. Wade, Three steps to gold: mechanism of protein adsorption revealed by Brownian and molecular dynamics simulations, *Phys. Chem. Chem. Phys.*, 18 (2016) 10191-10200.

[254] D.B. Kokh, S. Corni, P.J. Winn, M. Hoefling, K.E. Gottschalk, R.C. Wade. ProMetCS: An Atomistic Force Field for Modelling Protein-Metal Surface Interactions in a Continuum Aqueous Solvent, *J. Chem. Theory Comput*., 6 (2010) 1753-1768.

[255] S. Dutta, M. Gagliardi, L. Bellucci, M. Agostini, S. Corni, M. Cecchini, G. Brancolini, Tuning gold-based surface functionalization for streptavidin detection: A combined simulative and experimental study. *Front Mol Biosci*. 9 (2022) 1006525.

[256] L. Abarca-Cabrera, P. Fraga-García, S. Berensmeier. Bio-nano interactions: binding proteins, polysaccharides, lipids and nucleic acids onto magnetic nanoparticles. *Biomater Res*. 25 (2021) 12.

[257] S.L. Hirsh, D.R. McKenzie, N.J. Nosworthy, J.A. Denman, O.U. Sezerman, M.M. Bilek, The Vroman effect: Competitive protein exchange with dynamic multilayer protein aggregates, *Colloids Surf. B: Biointerfaces* 103 (2013) 395-404.

[258] N.H. Noh, E.A. Vogler, Volumetric interpretation of protein adsorption: competition from mixtures and the Vroman effect. *Biomaterials*. 28 (2007) 405-22.

[259] N. Sandhyarani, Surface modification methods for electrochemical biosensor. *Electrochemical Biosensors,* (2019) 45-75.

[260] R. Podila, R. Chen, P. C. Ke, A.M. Rao, Effects of surface functional groups on the formation of nanoparticle-protein'corona. *Appl. Phys. Lett.* 101, (2012) 263701.

[261] S.J. Park, Protein–Nanoparticle Interaction: Corona Formation and Conformational Changes in Proteins on Nanoparticle, *Int. J. Nanomedicine* 15 (2020) 5783-5802.

[262] A. Wang, K. Vangala, T. Vo, D. Zhang, N.C. Fitzkee, A Three-Step Model for Protein–Gold Nanoparticle Adsorption. *J. Phys. Chem. C*, 118 (2014) 8134-8142.

[263] J.S. Al-Otaibi, Y.S. Mary, Adsorption behaviour on silver nanocolloids at various concentrations of a bioactive therapeutic derivative of methylhydrazine: Experimental, DFT and molecular docking investigations, *J. Mol. Liq.,* 385 (2023) 122312.

[264] D. Frenkel, B. Smit, Understanding Molecular Simulation, 2nd ed., Academic, San Diego, 2002.

[265] S.A. Hollingsworth, R.O. Dror, Molecular Dynamics Simulation for All. *Neuron*. 99 (2018) 1129-1143.

[266] W. Smith, T.R. Forester, I.T. Todorov, The DL_POLY 2 User Manual, STFC Daresbury Laboratory, Daresbury, Warrington WA4 4AD Cheshire, UK (2009).

[267] Q. Mao, M. Feng, X.Z. Jiang, Y. Ren, K.H. Luo, A.C van Duin, Classical and reactive molecular dynamics: Principles and applications in combustion and energy systems. *Progress in Energy and Combustion Science*, 97 (2023)101084.

[268] B.J. Alder, T.E. Wainwright, Phase transition for a hard sphere system, *J. Chem. Phys.* 27 (1957) 1208.

[269] B.J. Alder, T.E. Wainwright, Studies in Molecular Dynamics. I. General Method. *J. Chem. Phys*., 31 (1959) 459-466.

[270] P. Steneteg, Development of Molecular Dynamics Methodology for Simulations of Hard Materials, (2012).

[271] S. Pramanick, Simulation Scenarios in One-Dimensional Self-Gravitating System, Computational Physics (2021).

[272] K.B. Keilen, Polymer failure modelled by Molecular Dynamics, *Mat. Sci. Eng.* (2014).

[273] I.T. Todorov, W. Smith, K. Trachenko, M. T Dove, DL_POLY_3: new dimensions in molecular dynamics simulations via massive parallelism, *J. Mater. Chem.* 16 (2006) 1911.

[274] V. Antohe, I. Gladwell, Performance of variable step size methods for solving model separable Hamiltonian systems, *Comput. Math. Appl.,* 40 (2004) 1245-1262.

[275] M.A. López-Marcos, J.M. Sanz-Serna, R.D. Skeel, Explicit symplectic integrators using Hessian-vector products, SIAM, *J. Sci. Comput*. 18 (1997) 223-238.

[276] D.C. Rapaport, The Art of Molecular Dynamics Simulation, Cambridge Univ. Press, Cambridge, UK, (1995).

[277] W.C. Swope, H.C. Andersen, P.H. Berens, K.R. Wilson, A Computer simulation method for the calculation of equilibrium constants for the formation of physical clusters of molecules: application to small water clusters, *J. Chem. Phys. 76* (1982) 637-649.

[278] A. P. Sutton, J. Chen, The Sutton-Chen Potential, *Phil. Mag. Lett*. 61 (1990) 139-146.

[279] H. Arslan, M.H. Güven, Melting dynamics and isomer distributions of small metal clusters, *New J. Phys*, 7 (2005) 60.

[280] S.K. Nayak, S.N. Khanna, B.K. Rao, P. Jena, Thermodynamics of small nickel clusters. Journal of Physics: Condensed Matter, 10 (1998) 10853-10862.

[281] B.D. Todd, R.M. Lynden-Bell, Surface and Bulk Properties of Metals Modelled with Sutton-Chen Potentials. *Surface Science*, 281 (1993) 191-206.

[282] J.P.K. Doye, D.J. Wales, Global minima for transition metal clusters described by Sutton-Chen potentials, *New. J. Chem*. 22 (1998) 733-744.

[283] Y. Kimura, Y. Qi, T. Cagin, W. A. Goddard III. The Quantum Sutton-Chen Many-Body Potential for Properties of fcc Metals, Caltech ASCI Technical Report, 003, (1998).

[284] Y. Qi, T. Cagin, Y. Kimura, W. A. Goddard III. Viscosities of liquid metal alloys from nonequilibrium molecular dynamics, *J. Comput. Aided Mater. Des*., 8 (2001) 233-243.

[285] D.S. Biovia, Material Studio Modelling, Dassault Systemes, San Diego, (2016).

[286] W. Kohn, Density functional theory for systems of very many atoms, *Int. J. Quant. Chem.* 56 (1994) 229-232.

[287] B. Delley, From molecules to solids with the DMol^3 approach, *J. Chem. Phys*. 113 (2000) 7756-7764.

[288] B. Delley, An all-electron numerical method for solving the local density functional for polyatomic molecules, *J. Chem. Phys*. 92 (1990) 508-517.

[289] Materials Studio 8.0 • DMol^3 Guide, Bovia.

[290] T.L. Gilbert, Hohenberg-Kohn theorem for nonlocal external potentials. *Physical Review B.* 12 (1957) 2111.

[291] M. Aamir Iqbal, N. Ashraf, W. Shahid, Fundamentals of Density Functional Theory: Recent Developments, Challenges and Future Horizons. Density Functional Theory - Recent Advances, New Perspectives and Applications. IntechOpen, (2022).

[292] M. Freyss, Density functional theory, CEA, DEN, DEC, Centre de Cadarache, France, NEA/NSC/R, 5 (2015).

[293] J.P. Perdew, K. Burke, M. Ernzerho, Generalized Gradient Approximation Made Simple, *Phys. Rev. Lett*.77 (1996) 3865.

[294] J.P. Perdew, Y. Wang, Accurate and simple analytic representation of the electron-gas correlation energy. *Phys Rev B Condens Matter.* 45(1992) 13244-13249.

[295] M. Arrigoni, G.K.H. Madsen, Comparing the performance of LDA and GGA functionals in predicting the lattice thermal conductivity of III-V semiconductor materials in the zincblende structure: The cases of AlAs and BAs. *Comput. Mater. Sci*., 156 (2019) 354-360.

[296] P. Ziesche, S. Kurth, J.P. Perdew, Density functionals from LDA to GGA. *Comput. Mater. Sci*, 11(1998) 122-127.

[297] S. Kurth, M.A.L. Marques, E.K.U. Gross, Density-Functional Theory. *Condens. Matter. Phys*., (2005) 395-402.

[298] W. Kohn, L.J. Sham, Self-consistent equations including exchange and correlation effects. *Phys. rev*., 140(1965) 1133.

[299] L. Goerigk, S. Grimme, Double hybrid density functionals. Wiley Interdisciplinary Reviews: *Comput. Mol. Sci.*, 4 (2014) 576-600.

[300] S. J. Mason, R. R. Hill, L. Mönch, O. Rose, T. Jefferson, J. W. Fowler eds. Introduction to Monte Carlo simulation, Proceedings of the Winter Simulation Conference (2008).

[301] R.L. Harrison, Introduction to Monte Carlo Simulation. *AIP Conf Proc*. 1204 (2010) 17-21.

[302] G.S. Fishman, Monte Carlo: Concepts, algorithms, and applications. N.Y., USA: Springer-Verlag (1995).

[303] P.L. Bonate, A Brief Introduction to Monte Carlo Simulation. *Clin Pharmacokinet,* 40 (2001) 15-22.

[304] M. Ozboyaci, D.B. Kokh, S. Corni, R.C. Wade, Modeling and simulation of protein–surface interactions: achievements and challenges. *Quarterly reviews of biophysics*, 49 (2016) 4.

[305] V.P. Zhdanov, Formation of a protein corona around nanoparticles. *Curr. Opin. colloid interface sci.*, 41 (2019) 95-103.

[306] L. Jaillet, S. Artemova, S. Redon, IM-UFF: Extending the universal force field for interactive molecular modeling. *J. Mol. Graph. Model*. 77 (2017) 350-362.

[307] A.K. Rappe, K.S. Colwell, C.J. Casewit, Application of a universal force field to metal complexes, *Inorg. Chem*. 32 (1993) 3438.

[308] M.A. Addicoat, N. Vankova, I.F. Akter, T. Heine, Extension of the universal force field to metal-organic frameworks, *J. Chem. Theory Comput*. 10 (2014) 880.

[309] J.A. Carr, H. Wang, A. Abraham, T. Gullion, J.P. Lewis, L-Cysteine Interaction with Au_{55} Nanoparticle, *J. Phys. Chem. C,* 116 (2012) 25816-25823.

[310] A.K. Rappé, C.J. Casewit, K.S. Colwell, W.A. Goddard III, W.M. Skiff, P. Rapp, UFF, a Full Periodic Table Force Field for Molecular Mechanics and Molecular Dynamics Simulations, *J. Am. Chem*. Soc. 114 (1992) 10024-10039.

[311] H. Sun, COMPASS: an ab initio force-field optimized for condensed-phase applications overview with details on alkane and benzene compounds, *J. Phys. Chem. B* 102 (1998) 7338.

[312] D. Rigby, Fluid density predictions using the COMPASS force field, Fluid Phase Equilibria 217 (2004) 77-87.

[313] Biovia Materials Studio Forcite datasheet.

[314] Y. Zhao, D. Liu, H. Tang, J. Lu, F. Cui, A MD Simulation and Analysis for Aggregation Behaviors of Nanoscale Zero-Valent Iron Particles in Water via MS. *Sci. World J.,* 2014 (2014) 768780.

[315] W. Wu, A. Al-Ostaz, A.H.D. Cheng, C.R. Song, Computation of Elastic Properties of Portland Cement Using Molecular Dynamics. *J. Nanomech. Micromech*, 1 (2011) 84-90.

[316] R. Nicoară, M. Ilies, A. Uifălean, C.A. Iuga, F. Loghin, Quantification of the PEGylated Gold Nanoparticles Protein Corona. Influence on Nanoparticle Size and Surface Chemistry, *Appl. Sci.* 9 (2019) 4789.

[317] N.G. Bastús, J. Comenge, V. Puntes, Kinetically Controlled Seeded Growth Synthesis of Citrate-Stabilized Gold Nanoparticles of up to 200 nm: Size Focusing versus Ostwald Ripening. *Langmuir,* 27 (2011) 11098-11105.

[318] P. Prema, Chemical Mediated Synthesis of Silver Nanoparticles and its Potential Antibacterial Application. Progress in Molecular and Environmental Bioengineering - From Analysis and Modelling to Technology Applications. InTech. (2011).

[319] J. Epp, X-ray diffraction (XRD) techniques for materials characterization. Materials Characterization Using Non-destructive Evaluation (NDE) Methods, (2016) 81-124.

[320] M. Ermrich, D. Opper, XRD for the analyst. Getting acquainted with the principles. *Second. Panalytical*. (2013).

[321] H.E. Fischer, A.C. Barnes, P.S. Salmon, Neutron and X-ray diffraction studies of liquids and glasses, *Rep. Prog. Phys.* 69 (2006) 233-299.

[322] H. Khan, A.S. Yerramilli, A. D'Oliveira, T.L. Alford, D. C. Boffito, G.S. Patience, Experimental methods in chemical engineering: X-ray diffraction spectroscopy-XRD. *Can. J. Chem. Eng.* 98 (2020) 1255-1266.

[323] R.F. Egerton, Electron energy-loss spectroscopy in the TEM. Reports on Progress in Physics, 72 (2008) 016502.

[324] P.W. Hawkes, Advances in Imaging and Electron Physics, *Elsevier*, 153 (2008).

[325] C. Angeles-Chavez, HRTEM study of crystal defects in gold nanoparticles, *MRS Advances* 6 (2021) 834-838.

[326] H. Chen, Y. Gao, H. Zhang, L. Liu, H. Yu, H. Tian, J. Li, Transmission-Electron-Microscopy Study on Fivefold Twinned Silver Nanorods. *J. Phys. Chem. B*, 108 (2004), 12038-12043.

[327] Kabita Sharma, Transmission Electron Microscope (TEM): Principle, Instrumentation, Uses (2023).

[328] M.M Freundlich. Origin of the electron microscope. *Science*, 142 (1963) 185-188.

[329] G. McMahon, Analytical instrumentation: A guide to laboratory, portable and miniaturized instruments (1st ed. pp. 296). Chichester: Wiley, (2007).

[330] J.K. Goldstein, H. Yakowitz. Practical scanning electron microscopy: Electron and ion microprobe analysis (p. 582). New York: Plenum Press (1975).

[331] D.B. Williams, C.B. Carter, Transmission Electron Microscopy (TEM). Humphreys and Beanland, 3rd Edition. The University of Liverpool, L69 3GH, U.K. (2000).

[332] J.I Goldstein, D.E. Newbury, D.C. Joy, C.E. Lyman, P. Echlin, E. Lifshin, L. Sawyer, J.R. Michael, Scanning Electron Microscopy and X-Ray Microanalysis: Third Edition Springer (2007).

[333] J.C. Hower, D. Berti, M.F. Hochella, S.M. Rimmer, D.N. Taulbee, Submicron-scale mineralogy of lithotypes and the implications for trace element associations: Blue Gem coal, Knox County, Kentucky, *Int. J. Coal Geol.,* 192 (2018) 73-82.

[334] K. Jurkiewicz, M. Pawlyta, A. Burian, Structure of carbon materials explored by local transmission electron microscopy and global power diffraction probes, *J. Carbon Res*., 4 (2018) 68.

[335] R. Ward, Analysis, origin and significance of mineral matter in coal: An updated review, *Int. J. Coal Geol*., 165 (2016) 1-27.

[336] J. Dong, P.L. Carpinone, G. Pyrgiotakis, P. Demokritou, B.M. Moudgil, Synthesis of Precision Gold Nanoparticles Using Turkevich Method, *Kona*, *Powder and Part. J*, 37 (2020) 224-232.

[337] D. Paramelle, A. Sadovoy, S. Gorelik, P. Free, J. Hobley, D.G. Fernig, A rapid method to estimate the concentration of citrate capped silver nanoparticles from UV-visible light spectra. *The Analyst*, 139 (2014) 4855-4861.

[338] M.V. Pavan Raja, R. Andrew Barron, Spectroscopic Characterization of Nanoparticles, Rice University Physical Methods in Chemistry and Nano Science, (2022).

[339] M. Picollo, M. Aceto, T. Vitorino, UV-Vis spectroscopy. *Phys. Sci. Rev.* 4 (2019) 20180008.

[340] H.H. Perkampus, UV-VIS Spectroscopy and its Applications. Springer Science and Business Media (2013).

[341] F.S. Rocha, A.J. Gomes, C.N. Lunardi, S. Kaliaguine, G.S. Patience, Experimental Methods in Chemical Engineering: Ultraviolet Visible Spectroscopy/UV-Vis. *Canadian J. Chem. Eng. (CJCE),* 96 (2018) 2512-2517.

[342] Justin Tom, PhD, UV-Vis Spectroscopy: Principle, Strengths and Limitations and Applications, (2021).

[343] B. Faramarzi, M. Moggio, N. Diano, M. Portaccio, M. Lepore, A Brief Review of FT-IR Spectroscopy Studies of Sphingolipids in Human Cells, *Biophysica*, 3 (2023) 158-180.

[344] W.D. Perkins, "Fourier Transform-Infrared Spectroscopy". Part 1. Instrumentation. Topics in Chemical Instrumentation. Ed. Frank A. Settle, Jr. *J. Chem. Educ.*, 63 (1986) 5-10.

[345] C. Berthomieu, R. Hienerwadel, Fourier transform infrared (FTIR) spectroscopy. *Photosynth Res*, 101 (2009) 157-170.

[346] S.A. Agrawal, T.N. Shaikh, Qualitative and Quantitative characterization of textile material by Fourier transform infra-red, International *J. Innov. Res. Sci. Eng. Technol.*, 3 (2014) 8496-8502

[347] A. Abo-Riziq, J.E. Bushnell, B. Crews B, M. Callahan, L. Grace, M.S. de Vries, Gas phase spectroscopy of the pentapetide FDAVS. *Chem. Phys. Lett*. 431 (2006) 227-230.

[348] J.O Leppinen, 22 Fourier-transform infrared spectroscopy. Surface Characterization: A User's Sourcebook, (1997) 369.

[349] F. Carrillo, X. Colorn, J.J. Sunol, J. Saurina, Structural FTIR analysis and thermal characterization of lyocell and viscose-type fibers, *Polymer Journal*, 40 (2004) 2229-2234

[350] Y.R. Perera, J.X. Xu, D.L. Amarasekara, A.C. Hughes, I. Abbood, N.C. Fitzkee, Understanding the Adsorption of Peptides and Proteins onto PEGylated Gold Nanoparticles, *Molecules,* 26 (2021) 5788.

[351] S. Bhattacharjee, DLS and zeta potential – What they are and what they are not? *J. Controlled Release,* 235 (2016) 337-351.

[352] M. Torres-Díaz, C. Abreu-Takemura, L.M. Díaz-Vázquez, Microalgae Peptide-Stabilized Gold Nanoparticles as a Versatile Material for Biomedical Applications, *Life,* 12 (2022) 831.

[353] M. Kaszuba, J. Corbett, F.M. Watson, A. Jones, High-concentration zeta potential measurements using light-scattering techniques, *Philos. Transact. A Math. Phys. Eng. Sci.* 368 (2010) 4439-4451.

[354] F.J. Montes Ruiz-Cabello, G. Trefalt, P. Maroni, M. Borkovec, Electric double-layer potentials and surface regulation properties measured by colloidal-probe atomic force microscopy, *Phys. Rev. E* 90 (2014) 012301.

[355] Z. Chen, Z. Wei, Y. Chen, C. Dames, Anisotropic Debye model for the thermal boundary conductance, *Phys. Rev. B* 87 (2013) 125426.

[356] F.Y. Kong, J.W. Zhang, R.F. Li, Z.X. Wang, W.J. Wang, W. Wang, Unique Roles of Gold Nanoparticles in Drug Delivery, Targeting and Imaging Applications. *Molecules*, 22 (2017) 1445.

[357] A.B.G. Lansdown, GOLD: human exposure and update on toxic risks, *Crit. Rev. Toxic*ol., 48 (2018) 596-614.

[358] M. Taha, H.R.A. El-Mageed, M.J. Lee, DFT Study of cyclic glycine-alanine dipeptide binding to gold nanoclusters. *J. Mol. Graph. Model*., 103 (2021) 107823.

[359] M.S. Jahan Sajib, P. Sarker, Y. Wei, X. Tao, T. Wei, Protein Corona on Gold Nanoparticles Studied with Coarse-Grained Simulations. *Langmuir*, 36 (2020) 13356-13363.

[360] A.A. Buglak, A.I. Kononov, Comparative study of gold and silver interactions with amino acids and nucleobases. *RSC Adv.,* 10 (2020), 34149-34160.

[361] S. Rai, N. V. Suresh Kumar, H. Singh, A theoretical study on interaction of proline with gold cluster, *Bull. Mater. Sci.* 35 (2012) 291-295.

[362] G. Hu, R. Jin, D. Jiang, Beyond the staple motif: a new order at the thiolate–gold interface. *Nanoscale*, 8 (2016) 20103-20110.

[363] S. K. Jalal, S. A. mawlood, Size dependent thermodynamic properties of nanoparticles, *int. J. Thermodyn,* 23 (2020) 245-250.

[364] Charles P. Poole Jr, Frank J. Owens, Introduction to Nanotechnology, john wiley & sons (2003).

[365] Y. Zhang, W. Chu, A.D. Foroushani, H. Wang, D. Li, J. Liu, C.J. Barrow, X. Wang, W. Yang, New gold nanostructures for sensor applications: A review. *Materials*, 7 (2014) 5169-5201.

[366] G.W. Buchanan, A.B. Driega, A. Moghimi, C. Bensimon, R.A. Kirby, T.D. Bouman. Benzo-9-crown-3 ether: X-ray crystal structure, NMR studies in solution and the solid phase, and ab initio calculations of isotropic 13C chemical shifts using LORG with a D95V basis set. *Can. J. Chem.,* 71 (1993) 1983-1989.

[367] E.D. Raczyńska, M. Hallman, K. Kolczyńska, T.M. Stępniewski, On the Harmonic Oscillator Model of Electron Delocalization (HOMED) Index and its Application to Heteroatomic π-Electron Systems. *Symmetry*, 2 (2010), 1485-1509.

[368] P.F. Yuan, F. Wang, Q. Sun, Y. Jia, Z.X. Guo, Dehydrogenation mechanisms of $Ca(NH_2BH_3)_2$: The less the charge transfer, the lower the barrier. *Int. J. Hydrogen Energy*, 38 (2013) 11313-11320.

[369] S. Grimme, Accurate description of van der Waals complexes by density functional theory including empirical corrections, *J. Comput. Chem*. 25 (2004) 1463-1473.

[370] S. Grimme, Semiempirical GGA-type density functional constructed with a long-range dispersion correction, *J. Comput. Chem*. 27 (2006) 1787-1799.

[371] B.T. Murti, A.D. Putri, S. Kanchi, M.I. Sabela, K. Bisetty, A.M. Asiri, Light induced DNA-functionalized TiO_2 nanocrystalline interface:Theoretical and experimental insights towards DNA damage detection, *J. Photochem. & Photobiol, B*: Biology 188 (2018) 159-176.

[372] A.E. Ledesma, D.M. Chemes, M. Frías, A. de los, M. Guauque Torres, P. del, Spectroscopic characterization and docking studies of ZnO nanoparticle modified with BSA. *Appl. Surf. Sci*., 412 (2017) 177-188.

[373] A.S. Abdelsattar, A. Dawoud, M.A. Helal, Interaction of nanoparticles with biological macromolecules: a review of molecular docking studies, *Nanotoxicology*, *15* (2020) 66-95.

[374] D.T. Huyen, T.Q. Bui, N.T. Si, Theoretical study of the binding mechanism between anticancerous drug mercaptopurine and gold nanoparticles using a cluster model. *J Mol Model*, 29 (2023**)** 307.

[375] M.A. Bakar, M. Sugiuchi, M. Iwasaki, Y. Shichibu, K. Konishi, Hydrogen bonds to Au atoms in coordinated gold clusters, *Nat. Commun*. 8 (2017) 576.

[376] F. Gao, J. Qu, Calculating the diffusivity of Cu and Sn in Cu_3Sn intermetallic by molecular dynamics simulations, *Mater. Lett.* 73 (2012) 92-94.

[377] V. Nikolova, D. Cheshmedzhieva, S. Ilieva, B. Galabov, Atomic Charges in Describing Properties of Aromatic Molecules, *J. Org. Chem*. 84 (2019) 1908-1915.

[378] S. Falsafi-zadeh, Z. Karimi, H. Galehdari, VMD DisRg: New user-friendly-implement for calculation distance and radius of gyration in VMD program. *Bioinformation,* 8 (2012) 341-343.

[379] D. Seeliger, B.L. de Groot, Conformational transitions upon ligand binding: Holo-structure prediction from apo conformations. *PLoS Comput. Biol*. 6 (2010) 1000634.

[380] P. Sneha, C.G Doss, Molecular Dynamics: New Frontier in Personalized Medicine, *Adv. Protein Chem. Struct. Biol*., 102 (2016) 181-224.

[381] J. Shang, T.A Ratnikova, S. Anttalainen, E. Salonen, P.C. Ke, H.T. Knap, Experimental and simulation studies of a real-time polymerase chain reaction in the presence of a fullerene derivative. *Nanotechnology*, 20 (2009) 415101.

[382] B. Kharazian, S.E. Lohse, F. Ghasemi, M. Raoufi, A.A. Saei, F. Hashemi, F. Farvadi, R. Alimohamadi, S.A. Jalali, M.A. Shokrgozar, N.L. Hadipour, M.R. Ejtehadi, M. Mahmoudi, Bare surface of gold nanoparticle induces infammation through unfolding of plasma fibrinogen, *Sci. Rep.*, 8 (2018) 12557.

[383] W.R. Li, X.B. Xie, Q.S. Shi, H.Y. Zeng, Y.S. Ou-Yang, Y.B. Chen. Antibacterial activity and mechanism of silver nanoparticles on Escherichia coli. *Appl. Microbiol. Biotechnol.* 85 (2010) 1115-1122.

[384] P. Mukherjee, A. Ahmad, D. Mandal, S. Senapati, S.R Sainkar, M.I. Khan, P. Renu, P.V. Ajaykumar, M. Alam, R. Kumar, Fungus-mediated synthesis of silver nanoparticles and their immobilization in the mycelial matrix: A novel biological approach to nanoparticle synthesis. *Nano Lett*. 1 (2001) 515-519.

[385] Z. Ferdous, A. Nemmar, Health Impact of Silver Nanoparticles: A Review of the Biodistribution and Toxicity Following Various Routes of Exposure. *Int. J. Mol. Sci,* 21 (2020) 2375.

[386] L. Pamela drake, J. Kyle Hazelwood, Exposure-Related Health Effects of Silver, and Silver Compounds: A Review, *Ann. occup. Hyg*., 49 (2005) 575.

[387] L.Y. Wei, J.R. Lu, H.Z. Xu, A. Patel, Z.S. Chen, G.F. Chen. Silver nanoparticles: Synthesis, properties, and therapeutic applications. *Drug Discov. Today*. 20 (2015) 595-601.

[388] M. Rycenga, C.M. Cobley, J. Zeng, W. Li, C.H. Moran, Q. Zhang, D. Qin, Y. Xia. Controlling the synthesis and assembly of silver nanostructures for plasmonic applications. *Chem. Rev*. 111 (2011) 3669-3712.

[389] W.P. Davey, Precision Measurements of the Lattice Constants of Twelve Common Metals. *Phys. Rev.* 25 (1925) 753-761.

[390] J.C. Azcárate, G. Corthey, E. Pensa, C. Vericat, M.H. Fonticelli, R.C. Salvarezza, P. Carro, Understanding the Surface Chemistry of Thiolate-Protected Metallic Nanoparticles. *J. Phys. Chem. Lett.*, 4 (2013) 3127-3138.

[391] N. Ivanova, V. Gugleva, M. Dobreva, I. Pehlivanov, S. Stefanov, V. Andonova, Silver Nanoparticles as Multi-Functional Drug Delivery Systems. *Nanomedicines* (2019) 71-92.

[392] D.P. Gnanadhas, M. Ben Thomas, R. Thomas, A.M. Raichur, D. Chakravortty, Interaction of Silver Nanoparticles with Serum Proteins Affects Their Antimicrobial ActivityIn Vivo. *Antimicrob. Agents. Chemother.*, 57 (2013) 4945-4955.

[393] P. Sarker, M.S.J. Sajib, X. Tao, T. Wei, Multiscale Simulation of Protein Corona Formation on Silver Nanoparticles: Study of Ovispirin-1 Peptide Adsorption, *J. Phys. Chem. B* 126 (2022) 601-608.

[394] N. Wasukan, M. Kuno, R. Maniratanachote, Molecular docking as a promising predictive model for silver nanoparticle-mediated inhibition of cytochrome P450 enzymes. *J. Chem. Inf. Model.* 59 (2019) 5126-5134.

[395] S. Chakroborty, E. Shakerzadeh, T. Yadav, In silico investigation on interaction of small Ag_6 nano-particle cluster with tyramine neurotransmitter. *Sci Rep* 13 (2023) 20200.

[396] S. Rattan, A. Leal, M. Sharma, S. Kumar, J.K. Goswamy, Comparative Study of Gold Nanoparticles Synthesized via Wet Chemical and Green Chemistry approach, IOP *Conf. Ser.: Mater. Sci. Eng.* 1033 (2021) 012051.

[397] K. Shameli, M.B. Ahmad, A. Zamanian, P. Sangpour, P. Shabanzadeh, Y. Abdollahi, M. Zargar., Green biosynthesis of silver nanoparticles using Curcuma longa tuber powder, *Int. J. Nanomedicine* 7 (2012) 5603-5610.

[398] L. Yang, Z. Wei, R. Tayebee, E. Koushki, H. Bai, Effects of laser penetration depth and temperature on the stability of afatinib-loaded gold nanoparticles: an optical limiting study, *J Nanopart Res*, 24 (2022) 147.

[399] J. Tian, Z. Shi, G. Wang, Thermodynamic and Kinetic Binding Behaviors of Human Serum Albumin to Silver Nanoparticles, *Materials*, 15 (2022) 4957.

[400] K. Ranoszek-Soliwoda, E. Tomaszewska, E. Socha, P. Krzyczmonik, A. Ignaczak, P. Orlowski, J. Grobelny, The role of tannic acid and sodium citrate in the synthesis of silver nanoparticles. *J. Nanoparticle Res*., 19 (2017) 273.

[401] S. Devi, B. Singh, A. K. Paula, S. Tyagi, Highly sensitive and selective detection of trinitrotoluene using cysteine-capped gold nanoparticles, *Anal. Methods*, 8 (2016) 4398-4405.

[402] R. Zong, X. Wang, S. Shi, Y. Zhu, Kinetically controlled seed-mediated growth of narrow dispersed silver nanoparticles up to 120 nm: secondary nucleation, size focusing, and Ostwald ripening. *Phys. Chem. Chem. Phys*, 16 (2014) 4236.

[403] J.P. Sylvestre, S. Poulin, A.V. Kabashin, E. Sacher, M. Meunier, and J.H.T. Luong, Surface Chemistry of Gold Nanoparticles Produced by Laser Ablation in Aqueous Media, *J. Phys. Chem. B* 108 (2004) 16864-16869.

[404] J.C. Mohan, G. Praveen, K.P. Chennazhi, R. Jayakumar, S.V. Nair, Functionalised gold nanoparticles for selective induction of in vitro apoptosis among human cancer cell lines, *J. Exp. Nanosci*., 8 (2013) 32-45.

[405] A.E. Segneanu, G. Vlase, A.T Lukinich-Gruia, D.D Herea, I. Grozescu, Untargeted Metabolomic Approach of Curcuma longa to Neurodegenerative Phytocarrier System Based on Silver Nanoparticles, *Antioxidants* (Basel), 11 (2022) 2261.

[406] S.F Braga, E. Trovatti, A.C Amaral, Bioactive Fibrin Scaffolds for Use in Musculoskeletal Regenerative Medicine, *Braz Arch Biol Technol*. 63 (2020) 1678-4324.

[407] S. Deepthi, A.A. Abdul Gafoor, A. Sivashanmugam, S.V. Nair, R. Jayakumar, Nanostrontium ranelate incorporated injectable hydrogel enhanced matrix production supporting chondrogenesis in vitro, *J. Mater. Chem. B*, 4 (2016) 4092-4103.

[408] M. Di Foggia, P. Taddei, A. Torreggiani, Self-assembling peptides for biomedical applications: IR and Raman spectroscopies for the study of secondary structure, *Proteomics Res J.*, 2 (2012) 231-272.

[409] H. Zhang, P. Wu, Z. Zhu, Y. Wang, Interaction γ-Fe_2O_3 nanoparticles with fibrinogen, *Spectrochim Acta A Mol and Biomol Spectrosc*., 151 (2015) 40-47.

[410] S. Kaur, N.K. Bari, S. Sinha, Varying protein architectures in 3-dimensions for scaffolding and modulating properties of catalytic gold nanoparticles, *Amino Acids.* 54 (2022) 441-454.

[411] M. Amini, M. R. Pourmand, R. Faridi-Majidi, M. Heiat, M. A. Mohammad Nezhady, M. Safari, F. Noorbakhsh, H. Baharifar, Optimising effective parameters to improve performance quality in lateral flow immunoassay for detection of PBP2a in methicillin-resistant Staphylococcus aureus (MRSA), *J. Exp. Nanosci*. 15 (2020) 266-279.

[412] G. Rutherford, B. Xiao, C. Carvajal, M. Farrell, K. Santiago, I. Cashwell, A. Pradhan, Photochemical Growth of Highly Densely Packed Gold Nanoparticle Films for Biomedical Diagnostics, *ECS J. Solid State Sci. Technol.* 4 (2015) 3071-3076.

[413] Y. Xu, J. Sherwood, Y. Qin, D. Crowley, M. Bonizzoni, Y. Bao, The role of protein characteristics in the formation and fluorescence of Au nanoclusters. *Nanoscale*, 6 (2014) 1515-1524.

[414] B. Chakraborty, R. Pal, M. Ali, L.M. Singh, D. Shahidur Rahman, S. Kumar Ghosh, M. Sengupta,. Immunomodulatory properties of silver nanoparticles contribute to anticancer strategy for murine fibrosarcoma. *Cell Mol Immunol,* 13 (2015) 191-205.

[415] Y.R Perera, J.X Xu, D.L. Amarasekara, A.C. Hughes, I. Abbood, N.C. Fitzkee, Understanding the Adsorption of Peptides and Proteins onto PEGylated Gold Nanoparticles, *Molecules*, 26 (2021) 5788.

[416] T. Mudalige, H. Qu, D. Van Haute, S.M. Ansar, A. Paredes, T. Ingle, Characterization of Nanomaterials. Nanomaterials for Food Applications, (2019) 313-353.

[417] M. Danaei, M. Dehghankhold, S. Ataei, F. Hasanzadeh Davarani, R. Javanmard, A. Dokhani, M. Mozafari, Impact of Particle Size and Polydispersity Index on the Clinical Applications of Lipidic Nanocarrier Systems. *Pharmaceutics,* 10 (2018) 57.

[418] S.L. D'souza, R.K. Pati, S.K. Kailasa, Ascorbic acid functionalized gold nanoparticles as a probe for colorimetric and visual read-out determination of dichlorvos in environmental samples. *Anal. Methods*, 6 (2014) 9007-9014.

[419] B. Halamoda-Kenzaoui, M. Ceridono, P. Urbán, A. Bogni, J. Ponti, S. Gioria, A. Kinsner-Ovaskainen, The agglomeration state of nanoparticles can influence the mechanism of their cellular internalisation. *J. Nanobiotechnology*, 15 (2017) 1-15.

[420] S. Murugadoss, F. Brassinne, N. Sebaihi, J. Petry, S,M, Cokic, K.L. Van Landuyt, S. van den Brule, Agglomeration of titanium dioxide nanoparticles increases toxicological responses in vitro and in vivo. *Part Fibre Toxicol.*, 17 (2020) 1-14.